Numerical investigation of Hydrogen-enriched Spark ignition Methanol engine

A thesis submitted in partial fulfillment of the requirements for the degree of Doctor of Philosophy (Ph.D.)

of the

Department of Mechanical and Aerospace,
Brunel University London

by

Subramanian Narayana Iyer

Principal Supervisor:	Prof Thanos Megaritis
Supervisor:	Prof Lionel Ganippa
Submission Date:	2024-11-14

Abstract

The majority of transportation and power generation depends on internal combustion engines, which primarily operate on fossil fuels and significantly contribute to greenhouse gas emissions.These engines release harmful pollutants such as carbon monoxide (CO), nitrogen oxides (NOx), and hydrocarbons (HC) through their exhaust,posing serious health and environmental risks.To mitigate these effects,the exploration of clean fuels for internal combustion engines is essential.Methanol,with its high knock resistance and latent heat of vaporization and hydrogen,with its high flame speed and superior energy content,present promising alternatives that can enhance efficiency and reduce environmental impact.This study explores detailed investigations using various strategies to reduce exhaust emissions and enhance engine performance by utilizing methanol in a spark-ignition engine. A detailed 1-dimensional and 3-dimensional computational fluid dynamics (CFD) model of a methanol spark-ignition engine was developed, incorporating varying proportions of hydrogen addition.Moreover, the combined effects of CO and hydrogen addition on the performance and emissions of the methanol spark-ignition engine were analyzed. The first part of the study was conducted using a 1-dimensional single-cylinder two-zone model to analyze methanol with varying proportions of hydrogen addition, employing both single and multi-Wiebe functions, validated against experimentally published data. The laminar flame correlation for methanol, developed by Xiaolong Liu et al, was incorporated into the single and multi-Wiebe models to simulate a 50-liter genset engine from the Ricardo WAVE engine database. The effects of boosting under low and high load conditions on a methanol spark-ignition engine with hydrogen enrichment were investigated. The results indicated that higher power operation with hydrogen addition reduced CO emissions and increased NOx emissions, along with higher in-cylinder pressure, heat release rate, and improved indicated thermal efficiency. Furthermore, increased boosting of methanol with hydrogen addition reduced both CO and NOx emissions, while also increasing the indicated thermal efficiency, maximum in-cylinder pressure, and heat release rate.

In the second part of the study, a 3-dimensional computational fluid dynamics (CFD) model of a single-cylinder methanol direct injection engine with hydrogen addition was developed using the Converge CFD solver. The SAGE solver, Reynolds-Averaged Navier Stokes (RANS) model with k- turbulence, and the O′Rourke and Amsden heat transfer sub-model were utilized to analyze in-cylinder behavior. The Extended Zeldovich mechanism and Hiroyasu-NSC model were applied to evaluate NOx and soot emissions, respectively. The effect of injection timing during the compression stroke was examined, revealing that retarded injection reduced indicated specific CO and soot emissions but

increased NOx emissions. Hydrogen enrichment further enhanced hydroxyl radical concentration, shortened combustion duration, and reduced CO and soot emissions, while increasing NOx emissions. Additionally, advancing methanol injection during the intake stroke with hydrogen addition caused an earlier rise in in-cylinder pressure, improved fuel-air mixing, and enhanced flame propagation, reducing combustion duration and lowering CO and soot emissions, though NOx emissions increased. Hydrogen enrichment also extended the lean burn limit, improved IMEP, and decreased specific CO, soot, and HC emissions compared to neat methanol, with shorter combustion duration and better fuel-air mixing near the spark plug. However, increasing hydrogen beyond 3% had little impact on combustion efficiency, though lean burn operation led to increased CO, HC, and soot emissions with reduced NOx emissions.

Lastly, the combined effect of a small proportion of CO and hydrogen addition under fixed load conditions was investigated. Results showed reductions in CO and NOx emissions and improved thermal efficiency compared to neat methanol. While hydrogen addition alone resulted in a greater reduction in CO emissions and higher thermal efficiency, it also led to increased NOx emissions compared to the combined CO and hydrogen addition.

Acknowledgments

I would like to express my deepest gratitude to my supervisors, Professor Thanos Megaritis and Professor Lionel Ganippa, for their unwavering motivation, guidance, and support throughout this journey. Their encouragement and insightful advice have been invaluable, and I am truly grateful for the stress-free environment they fostered during this research.

Thank you is not enough to convey my profound admiration for my parents, DR. Harish sarma Krishnamoorthy and my entire family. Your steadfast emotional and moral support has been my foundation through every challenge and triumph. Your belief in me has been a constant source of strength, guiding me forward and inspiring me to reach new heights. I am deeply grateful for your presence in my life; this achievement is as much yours as it is mine.

I would also like to extend special thanks to my teachers, friends, and fellow PhD colleagues for their camaraderie and encouragement, which helped me overcome the challenges along the way.

Finally, I would like to thank Convergent Science Company for sponsoring the licenses and providing technical support, which played a crucial role in the completion of my research.

List of Publications and Ongoing Research

Journal Articles

- Iyer, S. N., Rrustemi, D. N., Ganippa, L. C., and Megaritis, T., "Hydrogen enrichment in methanol SI engine at varying injection timing during compression stroke," *International Journal of Hydrogen Energy*, vol. 89, pp. 952–963, 2024. Elsevier.

Conference Proceedings

- Narayana Iyer, S., Megaritis, T., Ganippa, L., and Krishnamoorthy, H. S., "Methanol+ Hydrogen—A Prospective Alternate Fuel for Cleaner Offshore Power Generation," in *Proceedings of Offshore Technology Conference*, 2023, pp. D031S040R006. OTC.

Work in Progress

The following papers are currently in progress and will contribute to further advancements in the areas discussed within this thesis:

- Iyer, S. N., Rrustemi, D. N., Ganippa, L. C., and Megaritis, T., "Hydrogen enrichment in methanol SI engine at varying injection timing during intake stroke."
- Iyer, S. N., Ganippa, L. C.and Megaritis, T , "Combined Effects of carbon monoxide and hydrogen Enrichment in methanol-fueled SI engine".
- Iyer, S. N., Ganippa, L. C.and Megaritis, T , "Lean burn investigation of methanol SI engine with hydrogen addition"

Abbreviation

AFR	Air-Fuel Ratio
BMEP	Brake Mean Effective Pressure
bTDC	Before Top Dead Center (Crank Angle Position)
CA	Crank Angle
CFD	Computational Fluid Dynamics
CR	Compression Ratio
IMEP	Indicated Mean Effective Pressure
MAP	Manifold Absolute Pressure
RPM	Revolutions Per Minute
SI	Spark-Ignition
ST	Spark Timing
IT	injection timing
TDC	Top Dead Center
H_2	Hydrogen
CO	Carbon Monoxide
CO_2	Carbon Dioxide
HC	Hydrocarbons
NOX	Nitrogen Oxides
PM	Particulate Matter
SOOT	Soot Particulate Emissions
LHV	Lower Heating Value
ϕ	Equivalence Ratio
λ	Excess Air Ratio
OH	Hydroxyl Radical
DNS	Direct Numerical Simulation
LES	Large Eddy Simulation
RANS	Reynolds-Averaged Navier-Stokes
k-ϵ	Turbulence Model (Kinetic Energy and Dissipation)
k-ω	Turbulence Model (Specific Dissipation Rate)
η_{th}	Thermal Efficiency
$\dot{Q}$	Heat Transfer Rate
C_p	Specific Heat Capacity at Constant Pressure
C_v	Specific Heat Capacity at Constant Volume
γ	Ratio of Specific Heats (C_p/C_v)

Contents

List of Figures

List of Tables

Chapter 1

Introduction

Internal combustion engines (ICEs) play a crucial role in revolutionising power generation, industrial processes, construction, and transportation sectors worldwide engine are fundamental device that convert chemical energy into mechanical power. Presently, approximately 2 billion internal combustion engines (ICEs) are in operation worldwide, with 70% used for road transportation [60]. Governments in many nations are implementing policies to reduce dependency on fossil fuels, as their combustion is a major contributor to carbon emissions. Additionally, governments in many countries have called for shifting towards electrification for propulsion systems because during the operation electrical propulsion showed less emission compared to internal combustion engines. Previous studies have reported that emissions from electric propulsion are lower compared to internal combustion engines, provided that the electricity is generated from renewable resources. However, from Figure 1.1, the majority of electric power generation currently relies on coal, which produces 1.22 times more CO_2 emissions than oil and gas power generation. Therefore, with the widespread adoption of electrification, the overall carbon emissions could be comparable to those of internal combustion engines

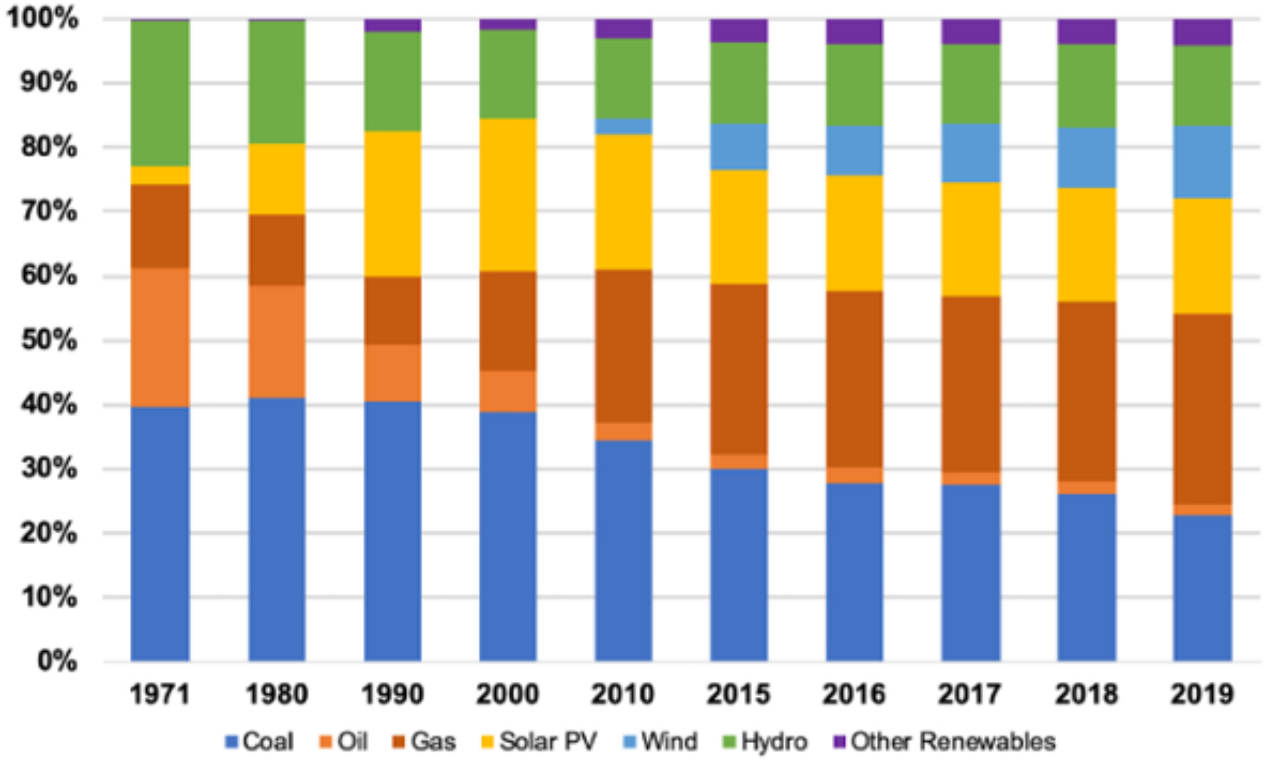

Figure 1.1: Electricity generation from various sector from the year 1971 to 2019[90]

Figure 1.2 shows Increasing global demand for energy and industrial infrastructure has been the driving force behind the consistent increase in greenhouse gas emissions over the past five decades, as reported by the JRC Science under the European Union. The power industry, which is the largest emitter of greenhouse gases, is experiencing an increase in emissions as a result of its major dependence on fossil fuels for the generation of electricity and heat. The transport sector has also experienced substantial growth in emissions, which is attributed to the persistent use of fossil fuels in vehicles and global mobility. The increase in emissions has also been influenced by the energy-intensive nature of industrial combustion processes. Furthermore, the extraction and refining of fossil fuels continue to be a consistent source of emissions. Despite the fact that agriculture, buildings, and waste sectors contribute lesser yet significant portions to overall emissions, these trends emphasize the critical role that internal combustion engines (ICEs) play in global emissions. Therefore, the necessity to investigate alternative fuels and technologies to reduce the environmental impact of ICEs and establish the foundation for more sustainable energy solutions.

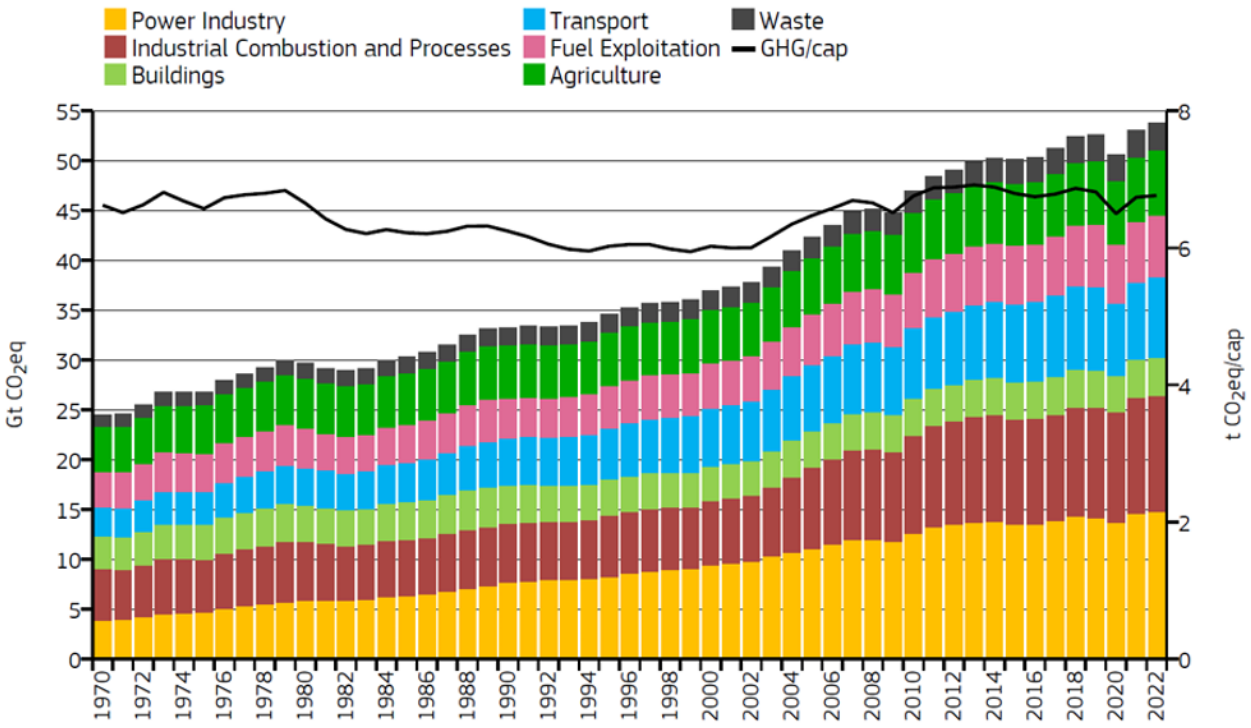

Figure 1.2: Global greenhouse gas emission in from 1970-2022 [8]

1.1 Strategy for optimizing engine performance

Enhancing the performance of spark-ignition engines requires the implementation of various strategies aimed at optimizing combustion efficiency, minimizing emissions, and maximizing overall engine efficiency. Some of the strategies is as follows:

Direct injection system

Direct injection of fuel into the combustion chamber enables a cooler intake charge, which helps reduce the tendency for knocking. This cooling effect not only supports a higher compression ratio, leading to improved engine efficiency but also enhances the quality of fuel and air mixing, resulting in optimal combustion and increased power output. Additionally, direct injection plays a crucial role in enhancing volumetric efficiency. However, some studies have reported that high-pressure direct injection and the resulting rich concentration of the fuel-air mixture can lead to an increase in particulate matter emissions [16, 54, 28, 79, 46, 36, 13, 81].

Spark timing optimisation

Studies indicate that the timing of spark ignition has a significant effect on important engine factors, including cylinder pressure, combustion duration, and thermal efficiency. Changing the ignition timing to be closer to top dead center (TDC) has the potential to enhance engine power and torque by increasing in-cylinder pressures. However, it is important to be aware that this adjustment also carries the risk of knocking and can result

in higher NOx emissions. For engines that utilize alternative fuels such as hydrogen or ethanol blends, the importance of ignition timing is greater. According to the study on ethanol-gasoline blends, it is important to adjust the spark timing to minimize ignition delay and avoid misfires. This adjustment helps improve brake thermal efficiency and reduce specific fuel consumption. Similarly, in engines that are enriched with hydrogen, the ideal ignition timing is influenced by the concentration of hydrogen present. This has an impact on both the combustion characteristics and the emissions produced. Although advanced ignition timing in engines can enhance thermal efficiency, it can also lead to higher NOx emissions. Thus, it is crucial to meticulously fine-tune the ignition timing in order to attain notable enhancements in engine efficiency and emissions regulation, all while minimizing the chances of engine knocking and increased pollutant emissions.

Boosting

Boosting in internal combustion engines increases intake air pressure, enhancing the engine's power output by allowing more air—and consequently more fuel—to enter the combustion chamber. This results in higher in-cylinder pressures and greater engine efficiency. Numerous studies have shown that increasing the boost ratio raises in-cylinder pressure during the compression stroke, leading to higher engine output. The increased intake manifold pressure also promotes more complete combustion due to the higher air density in the chamber, which reduces unburned hydrocarbon (HC) and carbon monoxide (CO) emissions. However, this increase in manifold pressure can also lead to higher thermal efficiency along with an increase in NOx emissions due to the elevated in-cylinder temperatures[113].

Injector angle calibration

Previous studies [53, 30]have reported that the injector angle at which fuel is injected into the engine cylinder plays a crucial role in engine performance and emissions. The injector angle directly influences the quality of fuel and air mixing before the combustion process. Optimizing the injector angle is essential to ensure that fuel droplets entering the cylinder are evenly distributed and mixed with the incoming air, thereby preventing the accumulation of a rich fuel mixture on the cylinder walls. Previous studies have shown that a wide injection angle can result in fuel droplet impingement on the cylinder wall due to poor atomization, leading to incomplete combustion. This poor mixing of fuel and air on the wall increases carbon monoxide and soot emissions. Furthermore, some studies have indicated that an improper injection angle can also contribute to engine knocking.

Injection timing optimisation

Optimizing injection timing is crucial for enhancing combustion efficiency. Injection of fuel-appropriate piston position before ignition timing ensures the fuel-air mixture quality, maximizing energy extraction and wall wetting. Many studies have proved that retarding or advancing the injection time can help achieve optimal combustion phasing. Thus, Optimal injection timing can increase indicated thermal efficiency and engine power out-

put. In addition to that optimal injection timing plays a key role in reducing nitrogen oxides (NOx), carbon monoxide (CO), and unburned hydrocarbon (HC), which is vital for meeting environmental regulations and reducing the engine's environmental impact. Moreover, aligning the injection timing with the engine's operating conditions, such as load and speed, contributes to smoother operation, reduced engine knocking, and overall improved performance.[44, 111, 45, 63, 14, 89, 116, 117]

Lean burn optimisation

Lean operation in the internal combustion is during the expansion stroke, the engine operates with a mixture containing a higher air content. This lean operation allows for more complete fuel combustion, resulting in higher indicated thermal efficiency and reduced emissions of unburned hydrocarbon and carbon monoxide. Additionally, operating the engine at a higher excess air ratio lowers the combustion temperature, leading to reduced nitrogen oxide emissions. Lean burn operation in spark-ignition engines can be achieved by using low-carbon or zero-carbon fuels, such as methanol, and hydrogen, which has been explored as a supporting fuel due to its fast flame speed compared to gasoline. Methanol fuel has also demonstrated the ability to achieve a leaner combustion of the fuel-air mixture compared to gasoline. However, the challenges of lean burn operation include combustion instability, primarily due to the difficulty in igniting the lean mixture. Furthermore, previous studies have shown that lean burn operation can lead to incomplete combustion, resulting in increased carbon monoxide and soot emissions. Extended lean burn operation can also reduce the indicated mean effective pressure.[11, 91, 47]

1.2 Alternative fuel for internal combustion engine

There has been considerable interest in the development of carbon-neutral fuels for internal combustion engines (ICEs) as a potential solution to the reduction of greenhouse gas (GHG) emissions in the transportation sector. The potential to replace conventional fossil fuels has been investigated for a variety of low-carbon and zero-carbon fuels, including hydrogen, ammonia, methanol, and synthetic fuels. According to the study, the methanol fuel has a reasonable volumetric density among the alternative fuel. Although hydrogen has less volumetric density compared to other fuelS. It has higher energy density, and using hydrogen as supporting fuel has been shown to improve the thermal efficiency of the internal combustion engine.

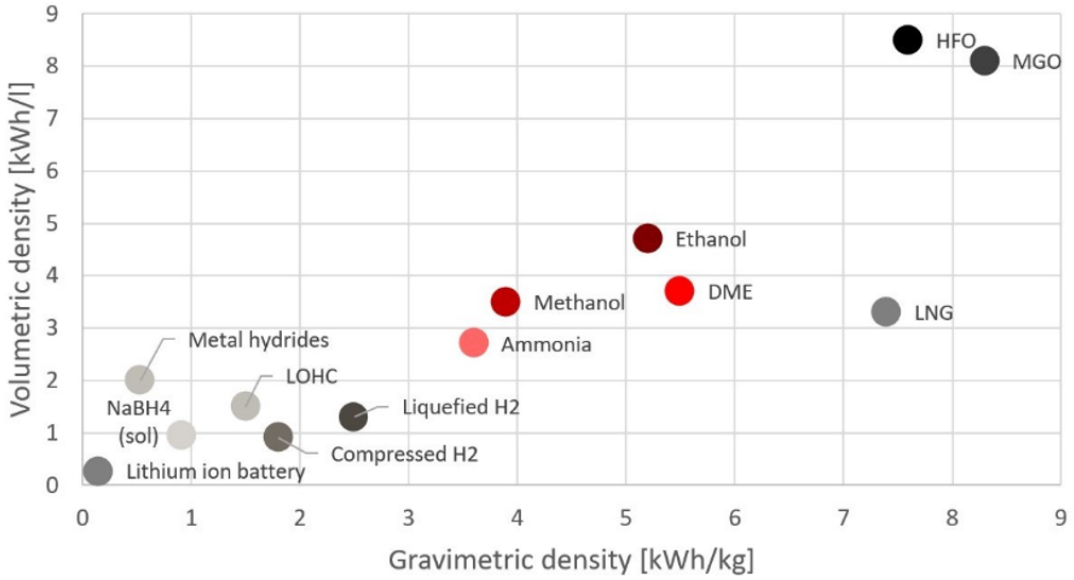

Figure 1.3: Volumetric and Gravimetric density of alternative fuels[88]

1.2.1 Methanol

Methanol (CH3OH) is a low-carbon, oxygenated liquid fuel which can be derived from natural gas, coal, and biomass. Although methanol has a lower gravimetric density compared to Liquefied Natural Gas (LNG), Heavy Fuel Oil (HFO), and Marine Gas Oil (MGO) as can be seen from the Figure 1.3, it is free from sulfur emissions and produces lower carbon and nitrogen oxide (NOx) emissions, making it a more advantageous fuel for heavy-duty operations.Potential benefit of methanol to achieve carbon neutrality, when methanol is produced from biohydrogen and atmospheric carbon dioxide (CO_2) using renewable energy resources through Power-to-X technology. As seen in Figure 1.3, the gravimetric density and volumetric density of methanol are positioned midway compared to various fuels.Methanol has a higher volumetric density compared to ammonia,compressed and liquefied hydrogen, making it a more beneficial option for onboard storage applications.Methanol has a very high heat of vaporization compared to more traditional fuels, such as gasoline and diesel. Because of its high heat of vaporization relative to its low heating value (LHV), methanol provides more effective energy utilization compared to traditional fuels. From Table 1.1, it can be observed that the hydrogen-to-carbon ratio of methanol fuel is similar to methane and higher than gasoline. Numerous studies have shown that using methanol as a fuel in internal combustion engines can reduce CO_2 emissions compared to gasoline. While hydrogen as a fuel results in zero carbon emissions, the overall "well-to-tank" carbon dioxide and other greenhouse gas emissions are higher when considering the entire lifecycle. Additionally, methanol's higher mass diffusivity compared to gasoline shown in Table 2,1 aids in better fuel-air mixing, enhancing combustion quality and further reducing emissions. Then compared

to gasoline density and viscosity of methanol are higher. However, the surface tension of gasoline and methanol are comparable. The fuel injection spray behaviour of methanol and gasoline is similar. The spray behavior is determined by Reynolds number and Wiebe member which will be discussed in the further session.The molecular mass contribution of a carbon atom is lower in methanol compared to gasoline.In addition to that, methanol has a lower molecular mass (32 g/mol) compared to alcohols such as ethanol (46 g/mol) and propane (60 g/mol), contributing to its high volatility, which causes the methanol spray to quickly vaporize.The OH (Hydroxyl) group present in the methanol makes it polar. The polarity of methanol also causes low vapour pressure. The knock limit of the methanol could be extended as the methanol has high latent heat of vaporisation which causes the in-cylinder temperature to drop. An increase in efficiency can be achieved in methanol as there is molecular expansion instead of contraction like the case of hydrogen combustion. Compared to gasoline combustion burned gas of methanol combustion has a higher ratio of a triatomic molecule such as CO_2 and H_2o to the diatomic molecule (N2 and O2).This is because methanol has a lower air-to-fuel ratio compared to gasoline, leading to a lower nitrogen concentration during the combustion process. Methanol has a closer flammability index than diesel fuel. Many studies have reported that methanol engines can be operated with a higher compression ratio than diesel engines. In addition to that methanol has greater potential for a hydrogen energy carrier. Methanol is used in the reforming process to generate hydrogen and carbon monoxide.

Table 1.1: Comparison of fuel properties of Methanol, Gasoline, Hydrogen, Methane, and Ethanol

Property	**Methanol**	**Gasoline**	**Hydrogen**	**Methane**	**Ethanol**
Chemical Formula	CH_3OH	-	H_2	CH_4	C_2H_5OH
Oxygen Content by mass [%]	49.93	-	0	0	34.8
Volumetric Energy Content [MJ/m^3]	15.87	-	14.20	32.50	21.29
Stoichiometric AFR [kg/kg]	6.50	14.70	34.20	17.65	9.00
Density (STP) [kg/m^3]	790	740	0.08	0.65	790
Vapour Density (STP) [kg/m^3]	1.42	3.88	0.08	0.65	0.79
Boiling Point at 1 bar [°C]	65	25-215	-253	-161.5	78
Heat of Vaporization [kJ/kg]	1100	180-350	461	510	838
Surface Tension (20 °C) [mN/m]	22.1	21.6	-	-	22.3
Dynamic Viscosity (20 °C) [mPa·s]	0.57	0.6	0.009	0.011	1.2
Autoignition Temperature [K]	738	465-743	858	813	698
Adiabatic Flame Temperature [K]	2143	2275	2093	2223	2138
Lower Heating Value [MJ/kg]	20.09	42.9	120.00	50.00	26.95
Higher Heating Value [MJ/kg]	22.88	48.00	142.00	55.00	29.85
Mass Diffusivity in Air [cm^2/s]	0.14	0.15	0.61	0.16	-

Methanol Production Methods

Table 1.2: Comparison of Methanol Production Methods

Production Method	**Carbon Emissions**	**Production Efficiency**	**Production Cost**
Fossil Fuel (Natural gas)[47, 104, 72]	High	Up to 62%	Low
Bio-Methanol from Biomass (Gasification process)[76, 34, 109]	Moderate	Up to 70%	High
Renewable Methanol (Electrolysis and CO_2 - carbon capture technique)[57]	Very low	Up to 52.9%	Very high
Renewable Methanol from CO_2 using solar-thermal energy[52]	Very low	7%	Very high

1.2.2 Hydrogen

Hydrogen (H_2) is a carbon-free energy carrier providing the potential to achieve a significant reduction of greenhouse gas (GHG) emissions and it is one of the solutions for climate change. Its extensive flammability range and high flame speed burnable under ultra-lean conditions raise thermal efficiency considerably in an internal combustion engine (ICE)[110]. However, significant challenges lie ahead that include carbon-free hydrogen production, storage, infrastructures for delivery, and volumetric energy density. Since hydrogen does not exist in natural reservoirs, it must be generated from other sources. Water is the most abundant, carbon-free source, but producing hydrogen from water does take a great deal of energy. If that is not from carbon-free sources like green electricity or nuclear power, then the (CO2) footprint for consuming hydrogen might be more significant than for conventional diesel or gasoline. Currently, the cheapest processes to manufacture hydrogen are from natural gas, coal, or biomass. But producing hydrogen from natural gas and coal Global greenhouse gas emission, whereas, from biomass (biohydrogen), the process can have a net-zero impact on Global greenhouse gas emission emissions[25, 4]. The volumetric energy density of hydrogen alone, however, is much smaller compared to the standard fuels—by around 3,000 times as low as compared to gasoline. Hydrogen has to be compressed at the pressure of about 700 bar or liquefied at -253°C to contain energy similar to other liquid fuels [100]. Both ways are costly, and most of all, they are potentially dangerous due to the high susceptibility to hydrogen leakages[12]. The generation of hydrogen by methanol reforming presents an effective

and feasible option for hydrogen storage, especially beneficial in applications necessitating secure, compact storage solutions. Methanol functions as a stable liquid carrier for hydrogen, facilitating on-demand production and simplifying transport relative to gaseous hydrogen[62, 73]. Utilizing this syngas as a supporting fuel offers significant advantages in mitigating backfire and preventing engine knocking.

1.2.3 Syngas

Syngas, primarily composed of hydrogen (H_2) and carbon monoxide (CO), is seen as an intermediate step toward transitioning from carbon-based to hydrogen-based fuels. The syngas gas can be produced from endothermic steam reforming of methanol to produce byproducts consisting of hydrogen and carbon monoxide. The equation for steam reforming,

$$CH3OH \rightarrow CO + 3H2 \tag{1.1}$$

Currently, on-board hydrogen generation is in the research and development stage. This technique involves integrating a reformer within the engine's exhaust system, where the reforming process utilizes hot exhaust gases to produce hydrogen gas from the fuel. The byproducts of the reformer, which contain hydrogen and carbon monoxide (syngas), are then directly fed into the engine cylinder to enhance combustion. Enrichment of syngas in internal combustion engines (ICEs) offers a way to reduce fossil fuel dependence while lowering emissions[5, 40].With its wide flammability range and high laminar flame speed, syngas is well-suited for lean combustion, enabling higher compression ratios and improved thermal efficiency. However, its lower heating value compared to traditional fuels can reduce engine power output and efficiency, though this can be mitigated through engine design optimizations like turbocharging. Syngas combustion typically results in lower CO_2 and unburned hydrocarbon(HC) emissions, but the high combustion temperatures can increase NOx emissions, requiring strategies like Exhaust Gas Recirculation (EGR) to manage these effectively. In dual-fuel configurations with diesel, syngas can significantly reduce diesel consumption by 50% to 90% and lower CO and HC emissions, especially under medium load conditions. However, challenges such as reduced volumetric efficiency and the need for precise combustion control to prevent knocking must be addressed for optimal performance.

1.3 Aims and objectives

The main aim of this thesis is to improve the performance characteristics and reduce emissions of a methanol-fuelled single-cylinder spark-ignition engine with hydrogen enrichment.
To reach this aim, the specific objectives are as follows, which will be evaluated via simulation analysis:

- To investigate the effect of direct injection timing of methanol with hydrogen enrichment during the compression and intake strokes on in-cylinder performance and emissions.
- To develop foundational knowledge of engine performance for methanol with hydrogen enrichment under lean burn conditions.
- To analyze the effect of boosting on emissions in a methanol engine operating with hydrogen enrichment.
- To examine the influence of carbon monoxide and hydrogen addition on emissions and engine performance in a methanol engine.

1.4 Research outline

Chapter 2:

This chapter presents current research on the use of methanol and hydrogen in internal combustion engines, emphasizing their impact on performance and emissions reduction. It covers studies on the influence of intake manifold pressure, injection timing and piston shapes on engine performance and emissions. Additionally, the chapter examines existing literature on the effects of carbon monoxide addition on engine combustion and previous research on hydrogen enrichment in methanol engines.

Chapter 3:

This chapter explains the three-dimensional and one-dimensional computational modelling methods used to compute engine performance and emissions. It covers a detailed explanation of the processes involved in solving combustion, including the chemical reactions, in-cylinder turbulence methods, and heat transfer techniques used for simulation. The chapter also discusses the computational methods employed to model methanol injection, as well as the mesh refinement techniques used to resolve boundary conditions. Additionally, it provides details on the boundary conditions applied in the modelling of

a single-cylinder engine and the validation of the three-dimensional modelling approach.

Chapter 4:

This chapter investigates the performance and emissions of a spark-ignition methanol engine with hydrogen enrichment using a 1-dimensional model in the Ricardo Wave solver. It covers the modelling approach, including the use of single and multi-Wiebe functions to represent methanol and methanol-hydrogen operations, and the calibration of these models using laminar flame speed correlations to overcome the solver's limitations in predicting combustion duration. The effects of hydrogen addition, boosting at different power levels, and variations in methanol injection timing are analyzed. Additionally, the chapter includes the validation of the 1-dimensional computational model.

Chapter 5:

This chapter explores the impact of varying in-cylinder methanol injection timings and hydrogen addition through the intake port using a CFD model. The study examines the effect of methanol injection timing during the compression stroke with various hydrogen concentrations analysing the effects on mixing, combustion, and emissions. Additionally, it investigates the late injection limits on mixing and combustion performance for neat methanol and hydrogen-enriched operations under different spark timings

Chapter 6:

This chapter extends the investigation of methanol injection timing with hydrogen addition using a CFD model, focusing on the intake stroke. The chapter provides a detailed analysis of in-cylinder mixing, hydroxyl radical formation, and flame propagation, while also exploring NOx, carbon monoxide, and soot emissions under both early and late injection conditions with varying proportions of hydrogen enrichment.

Chapter 7:

This chapter outlines the performance and emission characteristics of a methanol-fueled spark-ignition engine enriched with hydrogen under both stoichiometric and lean-burn conditions. The study investigates the effects of hydrogen addition, ranging from low to high proportions, on the performance of the methanol spark-ignition engine. Specifically, it examines in-cylinder pressure, combustion efficiency, and emissions, including CO, HC,

soot, and NOx, across stoichiometric to lean-burn operation modes

Chapter 8:

This chapter covers the impact of hydrogen enrichment and the combined effect of carbon monoxide and hydrogen with methanol at a fixed load. The study compares and analyzes in-cylinder mixing, specific carbon monoxide and NOx emissions, indicated thermal efficiency, and hydroxyl radical formation under three conditions: neat methanol, methanol with hydrogen enrichment, and the combination of carbon monoxide and hydrogen addition with methanol

Chapter 2

Literature review

This chapter explore review of how alternative fuels, engine parameters, and emission control strategies influence internal combustion engine performance. The experimental and numerical investigation of the properties of methanol and its applications in internal combustion engines (ICE), including its potential to improve combustion efficiency and reduce emissions such as CO, NOx, and particulate matter. The role of injection timing, impact boost pressure is discussed, with various studies highlighting its influence on thermal efficiency, combustion stability, and emissions control. In addition to that the currently conducted studies on the effects of enrichment hydrogen methanol-fuelled engines, focusing on their impact on engine performance and emissions. Furthermore, the chapter explores existing findings on the introduction of carbon monoxide (CO) into engine combustion characteristics and its impact on exhaust emissions

2.1 Effect of methanol in internal combustion engine

Extensive studies have been conducted on methanol as a fuel for internal combustion engines due to its potential benefits in emission reduction and efficiency improvement. The addition of methanol to internal combustion engines has been extensively investigated, showing notable improvements in combustion efficiency and reductions in emissions. According to S.Pandey et at[78] methanol blends with gasoline or diesel have been shown to improve overall thermal efficiency and brake-specific fuel consumption while lowering carbon monoxide (CO) and particulate matter (PM) emissions. Additional research has shown that adding methanol may increase combustion and flame propagation speed, both of which can lead to improved engine performance [98]. Ciniviz et al.[6] and Örs et al.[75] have noted that elevated in-cylinder temperatures may result in increased nitrogen oxide (NOx) emissions when there is a greater methanol concentration. Due to its high latent heat of vaporization, methanol has a cooling effect that may enhance engine efficiency and reduce engine knock in spark-ignition engines [41, 106, 65]. Based on previous stud-

ies by H.sharudin et al and J. Wei et al.[96, 101] methanol is considered a potentially useful substitute fuel that may enhance engine performance and lower hazardous exhaust emissions. This section reviews the numerical and experimental works conducted on methanol-fueled engines, highlighting different aspects of performance improvement and emission reduction.

The experimental study [24] on a naturally aspirated methanol engine, modified from a diesel engine, reported that using a high-energy multi-spark ignition system, compared to a single-spark ignition system, resulted in a 25% higher brake thermal efficiency under brake mean effective pressures (BMEP) between 0.11-0.29 MPa at an engine speed of 1600 RPM. Additionally, using the multi-spark system resulted in higher in-cylinder pressure and reduced combustion duration. Lowering the compression ratio from 16:1 to 14:1 at high-load operating conditions did not decisively affect brake thermal efficiency. However, at low-load operating conditions, it increased brake thermal efficiency. Despite these improvements, the brake thermal efficiency of the methanol engine under the same conditions was still 20% lower than that of the diesel engine.

Further investigations by Wouters et al.[103], a methanol-fuelled spark-ignition engine was explored using direct injection for a wide range of compression ratios: 10.8, 15.0, 17.7, and 20.6. Under a fixed load of IMEP = 18 bar, an increase in the compression ratio resulted in increased engine efficiency. Additionally, the highest indicated thermal efficiency was achieved with a compression ratio of 20.6. The increase in compression ratio resulted in higher in-cylinder pressure and reduced NOX emissions due to the drop in combustion temperature. However,hydrocarbon(HC) emissions were higher when the engine was tested at higher compression ratios. Furthermore, the lean burn limit extended from $\lambda = 1.7$ to $\lambda = 2.2$ with an increase in compression ratio from 10.8 to 17.7. When operated at the highest compression ratio of 20.6, the lean burn limit was limited to $\lambda = 1.9$ due to the maximum in-cylinder pressure limit.

An experimental study conducted by M. Crippa et at[8] on different engines showed that, compared to gasoline operation, a 10% increase in efficiency was obtained for methanol operation, and NOx emissions dropped by 5 to 10 g/kWh due to methanol's higher octane rating and higher latent heat of vaporization compared to gasoline . The tests were carried out in wide open throttle under lean burn conditions and wide-open throttle with exhaust gas recirculation (EGR). Both tests showed a 5% improvement in efficiency. Wide open throttle operation with EGR on a turbocharged engine at a high compression ratio resulted in achieving 42% efficiency, close to diesel engine operation, with negligible NOx emissions. In addition to that the study conducted by S.Liu et al. [68] on gasoline with methanol blend on spark ignition engine observed the during the cold start conditions and warming-up at 5-degree celsius, addition of methanol resulted above 50% and nearly 39% reduction inhydrocarbon(HC) emissions. Then enrichment of methanol to gasoline also resulted 20% reduction in carbon monoxide emission with increased exhaust

temperature enhancing the faster activation of two-way catalytic conversion.
The research was conducted by Ballapu Harshavardhan et al.[29], on the effect of the stroke-to-bore ratio on combustion efficiency and emissions in a spark-ignition engine using methanol and gasoline fuels. The tests were conducted with a compression ratio of 10.8 using gasoline and 15 using methanol. Similar efficiency gains were observed for gasoline operation at a compression ratio of 10.8 and methanol operation at a compression ratio of 15. The study found that a larger stroke improved tumble motion, mixture homogenization, and reduced combustion duration, while also reducing heat transfer losses. The lean limit was extended from $\lambda = 1.9$ to $\lambda = 2$ using methanol, achieving a maximum indicated thermal efficiency of 47%. Compared to gasoline operation, a 25% reduction in NOx emissions was obtained with methanol. Additionally, methanol operation resulted in reduced CO_2 emissions due to its higher charge cooling effect and better fuel oxidation process.
An experimental study [27] was conducted on a heavy-duty diesel engine modified to run on methanol. The engine was modified with port fuel injection and a spark plug. The test was conducted at 1800 RPM with a compression ratio of 13.8:1. The brake thermal efficiency was 44% higher than that of natural gas for the same 5-litre engine displacement. Engine knock was identified as the limiting factor for the achievable load, while pre-ignition was not found to be an issue even with extended burn distances in the combustion chamber. The engine was able to operate at an air/fuel ratio of up to 1.75. Higher combustion stability was obtained due to higher scavenging differential pressure and a reduced residual gas fraction.
A numerical study [118] was conducted to investigate the effects of exhaust gas recirculation (EGR) and spark timing on knock in a methanol-fuelled spark-ignition engine. The study was performed at a compression ratio of 17.5:1 on 1 litter engine. The tests were conducted under stoichiometric conditions. Occurrence of knock reduced by enrichment of the EGR rate from 10%-20% with significant reduction thermal efficiency and engine power. In addition to that it was noted that the combined effect of retarded spark timing and increased EGR percentage resulted in reduced knock occurrence and improved thermal efficiency.
A numerical study was conducted by C Gong et al.[23] on a methanol spark-ignition engine using a twin spark plug configuration. It was found that increasing the distance between the two spark plugs resulted in a reduction in in-cylinder pressure and temperature. This reduction occurred because the greater distance increased the time required for the flame fronts to propagate and meet each other, resulting in a slower combustion process as the flames took longer to burn through the air-fuel mixture. Additionally, placing the spark plugs too far apart increased heat transfer to the cylinder walls, further lowering in-cylinder pressure and temperature due to enhanced heat losses.

2.2 Effect of hydrogen addition to the internal combustion engine

Numerous studies have reported that integrating hydrogen with various fuels is the most effective approach to enhance engine efficiency and reduce carbon emissions. The incorporation of hydrogen into internal combustion engines has demonstrated a notable improvement in performance and a decrease in pollutants. Many researches have indicated that the addition of hydrogen enhances brake thermal efficiency and reduces emissions of carbon monoxide (CO), hydrocarbon(HC), and particulate matter (PM). This is because hydrogen's rapid flame speed and enhanced fuel and air mixing result in complete combustion [3, 49, 56]. On the other hand, improving the efficiency of combustion might result in an increase in nitrogen oxide (NOx) emissions, particularly under high-load operating conditions. This is because the addition of hydrogen causes the combustion temperatures to rise, which in turn leads to higher NOx emissions.[9, 42, 62]. Moreover, some studies have observed hydrogen enrichment have impact on specific energy consumption a despite the fact that it enhances combustion, NOx emissions must be carefully controlled[51, 58, 99, 119]. This section presents both existing numerical and experimental studies that explore the impact of hydrogen addition on engine performance and emissions under different operating conditions.

An experimental study by E.Porpatham et al.[83] was conducted on hydrogen addition to biogas on air-cooled single-cylinder diesel engine modified to spark ignition engine. The test was invested for 5%,10% and 15% volume of hydrogen addition to biogas at constant engine speed at 1500RPM for different equivalence ratios. It was observed from the study that hydrogen addition resulted in the improvement of the combustion rate as well as to extend the lead burn limit of biogas. Then for this tested operating condition optimal hydrogen addition was found to be 10% which resulted to enhancing the brake thermal efficiency and power output. In addition to that, an increase in the hydrogen addition of up to 15% to biogas facilitates the lean mixture performance. However, the addition of more than 10% hydrogen to biogas under richer operating conditions required retardation of spark timing to prevent the knocking. Furthermore, the addition of 10% hydrogen resulted in 57% reduction in hydrocarbon(HC) emissions under an equivalence ratio of 0.95. An increase in hydrogen addition resulted in reduced carbon monoxide emissions across all the equivalence ratios. But for rich burn condition, the carbon monoxide emission was slightly increased for higher hydrogen addition because of the dissociation of combustion products due to higher combustion temperature caused by higher hydrogen content.

The numerical study by X.Sun et al.[97] on the investigation of hydrogen addition to natural gas spark-ignition engine. The numeral computation fuel dynamic study was conducted using the SAGE combustion model. This study was validated in-cylinder pressure trace and heat reseal rate against with experimental data at engine speed of 1400RPM

for neat natural gas operating condition and natural gas with hydrogen addition operating condition. Results revealed that hydrogen addition to natural gas enhanced the initial spark kernel volume with more stable flame propagation which lead to improved combustion efficiency. This was because hydrogen addition to natural gas increased the reactive radical such as oxygen (O) and Hydroxide (OH) during the combustion period. However, hydrogen enrichment resulted in an increase in nitric oxide formation (NO) due to an increase in cylinder temperature. In addition to that hydrogen enrichment to natural gas also accelerated the turbulence inside the cylinder. Furthermore, hydrogen addition resulted in reducing the exhaust co,hydrocarbon and soot emission due to higher in-cylinder temperature and faster oxidation process.

Numerical 3-dimensional study on hydrogen addition with gasoline by N.Iafrate et al.[37] using extended coherent flame model and tabulated kinetic ignition combustion model. This study was investigated at an engine speed of 2000 RPM for a low load condition of 4 bar indicated mean effective pressure and engine speed of 3000 RPM for a medium load condition of 13 bar IMEP. All the operations were conducted at an excess air ratio of 2. For the both the load conditions, hydrogen addition to gasoline resulted in increase in the combustion speed and the flame front propagation was more isotropic which enabled combustion stability. For mid load condition addition of hydrogen to gasoline resulted in increase in the auto-ignition delay time, thus reducing the occurrence of knock.

Experimental study [61] on the effect of hydrogen addition to ammonia spark ignition engine at compression ratio of 10.5:1. The test was conducted at an engine speed of 1500 RPM, with manifold pressure of 1 and 1.2 bar and up to 60% hydrogen addition was investigated. The study observed that hydrogen addition to ammonia resulted in the improvement of the cyclic stability and misfire was avoided at higher engine load. An increase in the manifold presses from 1 to 1.2 bar resulted in a rise in the indicated mean effective pressure and fuel mean effective pressure. An increase in hydrogen blending with ammonia accelerates the combustion process during the initial stage due to the higher laminar burning velocity of hydrogen. In addition to that hydrogen enrichment to ammonia resulted in the reducing the unburned ammonia (NH3) . However, the NOx emissions increase with the increase in hydrogen addition to ammonia e due increase in the in-cylinder temperature.

2.3 Effects of boost pressure and exhaust Gas recirculation on performance and emissions in spark-ignition engines

Exhaust gas recirculation (EGR) and boost pressure have been critical research areas for enhancing the performance and reducing emissions in spark-ignition engines[77]. A higher air intake into the combustion chamber is facilitated by an increase in boost pressure, which leads to an increase in power output and an improvement in thermal efficiency as a consequence of improved air-fuel mixture and combustion conditions. Volumetric efficiency also increased as a result of the effect of an increase in the intake manifold pressure. However, an increase in engine manifold pressure can also result in higher in-cylinder temperatures. Studies have also shown that EGR dilution benefits NOx emission reduction by lowering cylinder temperature during the combustion process [70]. Abib Gürbüz[26] investigated the effect of the increasing the manifold press to hydrogen-fueled spark-ignition engine. The boost pressure was tested from 0.1 bar to 0.4 bar above the atmosphere on the engine with a displacement of 476.6 cm3 at an engine speed of 1600RPM of compression ratio 8.Compared to naturally aspirated conditions the 38% increase the IMEP was obtained for higher boost pressure. Increase in boost pressure also resulted in a 14% increase in thermal efficiency compared to naturally operated conditions. In addition to that 45% NOx emissions increased with an Increase in boost pressure due to an increase in the in-cylinder pressure and temperature. Furthermore, combustion duration was also obtained higher for higher boost pressure. The study also accounts for the optimisation of ignition timing is important under varying the boost pressure to obtain maximum brake torque.

Wei zeng investigated [113] the effect of the boosting by varying the intake manifold pressure between 100 and 160 Kpa . In addition to that the effect of the exhaust gas recirculation was studied by using nitrogen dilution through varying the intake oxygen model fraction between the 14% and 19% Test was investigated using the single and double injection strategies with a dwell time of 15°CA range .Then gasoline with ethanol blended fuel were used for this study at a blead of 30% ethanol with 705 gasoline. Double injection resulted in the reducing the soot emission compared to single injection. Thereafter the double injection improved the fuel distribution which allowed the increase in the combustion efficiency. Furthermore the addition of EGR resulted in significant NOx emissions and reducing the flame temperature. However, addition EGR resulted in the increase in soot emission. Moreover, increase in the intake manifold pressure reduce the soot emission and fuel impingement on the piston bowl.From the tested boosted condition of intake manifold pressure condition between 100 and 160 Kpa, intake manifold pressure of 130kpa was obtained to be best trade-off between NOx and soot emissions.

Xie et al.[48] conducted a study to explore the effects of air and exhaust gas recirculation (EGR) dilution on a high-compression ratio spark-ignition engine fuelled by methanol. The engine was operated under light load conditions, with a compression ratio of 13:1 and a speed of 1400 RPM. The study found that cooled EGR dilution lowered combustion temperatures, leading to a reduction in NOx emissions. In contrast, air dilution improved brake-specific fuel consumption and increased torque output, although it had less impact on reducing NOx emissions. Furthermore, the study also investigated the effects of hot EGR, which showed improvements in combustion efficiency and further increased torque output.

2.4 Effect of injection timing on engine performance

According to the study by Agarwal [1] found that shifting injection timings had a direct impact on the rate of heat release and brake thermal efficiency (BTE). However, it was also observed that this adjustment led to increased NOx emissions. In the same way study carried out by Li et al. [63]it was determined that optimizing injection timing had a beneficial effect on thermal efficiency and reduced cycle-by-cycle variations in spark-ignition methanol engines. Thereafter research conducted by [111] focused on reactivity-controlled compression ignition (RCCI) engines. Their findings indicated that advancing injection timing can lead to an increase in ignition delay. This, in turn, has the potential to improve combustion phasing and overall efficiency. Moreover, numerous studies have shown similar trends in the effects of injection timing across various fuel types and engine configurations, demonstrating the critical role of injection timing in optimizing engine performance and controlling emissions [111, 64, 95, 87, 1, 102, 85].
Experimental study by J.Li at al. [63] conducted on 2 litter methanol fuel spark ignition engine, modified from diesel engine. The test was carried out at compression ratio of 16:1 and engine speed of 1600 RPM. Injection timing was investigated from 15°CA to 39°CA bTDC. Advancing the injection timing from 15°CA to 39°CA bTDC resulted in reduce in maximum in-cylinder pressure and heat release rate due to leaner mixture concentration. Advancing the injection timing increased the NOx emission due to increase in combustion temperature and carbon monoxide emission was reduce. In addition to thathydrocarbonemission was obtained lowest at optimal injection timing of 39 °CA TDC.

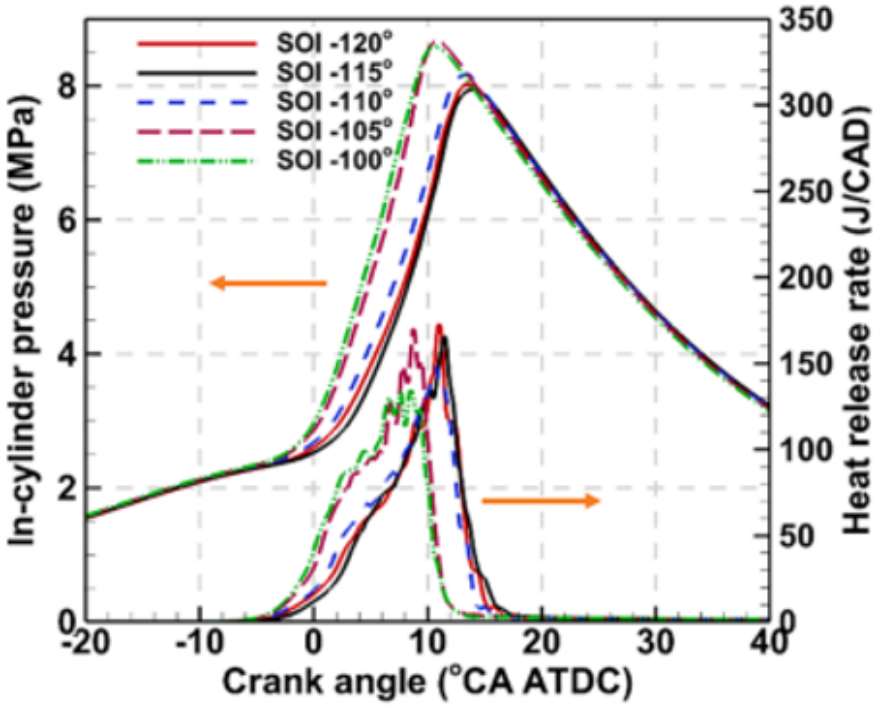

Figure 2.1: In cylinder pressure and heat release under different injection timing [89]

A numerical study [89] using SAGE combustion modelling was conducted on the direct injection of methanol at a compression ratio of 11:1 and a fixed engine speed of 2000 RPM. The injection timing was varied from -120° CA to -100° CA after top dead centre (ATDC). The study reported a slight decrease in in-cylinder pressure when the injection timing was retarded from -120° CA to -115° CA ATDC as shown in the figure 2.1. However, an increase in in-cylinder pressure was observed as the injection timing was further retarded from -115° CA to -105° CA ATDC, attributed to higher evaporation rates and improved fuel-air mixing. Subsequently, a drop in in-cylinder pressure was observed at -100° CA ATDC due to the shorter time available for mixing. Additionally, the study also found that retarding the injection timing shortened both the ignition delay and combustion duration trend.

Study [112] was conducted on direct -injection natural gas engine at injection timing from 150°CA bTDC to 210°CA bTDC. The test was conducted at engine speed of 1200 RPM and compression ratio 8 on spark ignition engine with displacement of 906 cm3.It was observed from the study that advancing the injection timing resulted in increase in overall equivalence ratio with decrease in the volumetric efficiency. Then advancing the injection timing from 150°CA bTDC to 180°CA bTDC resulted in increased engine performances such as engine power output, brake mean effective pressure and indicated thermal efficiency .But further advancing the injection timing from 180°CA bTDC to 210°CA bTDC

resulted slight decrease in engine performance, In addition to that investigation of the combustion characteristics showed highest in-cylinder pressure and heat release rate at 180°CA bTDC injection timing with short test combustion duration. Retarding and advancing the injection from 180°CA bTDC resulted in reducing the maximum in-cylinder pressure and lager combustion duration. Furthermore, reading the injection timing increased thehydrocarbonemission due to poor fuel and air mixing. Highest NOx emission was observed at 150°CA and 170°CA bTDC due to baster combustion and NOx emissions declined when further retarding the injection timing. Moreover, the injection timing did not show significant change in the carbon monoxide emissions.
A Study [64] was conducted on single-cylinder Scania D13 heavy-duty engine with a redesign of the engine head and piston crown to raise the compression ratio to 17.3:1. The test was carried medium load and speed (IMEP: 8 bar, 1200 RPM).Injection timing of methanol was investigated from -23°CA to -31°CA after top dead centre (ATDC) to investigate effect of in-cylinder turbulence and fuel/air mixing.. Advancing injection timing to -30°CA resulted in low peak in-cylinder pressure and slow flame front speed in the cylinder because of low turbulence, whereas when injection timing was retarded the fuel is better distributed and thus improved the combustion stability. In addition to that spray-included angle at 40°,50° and 60° was investigated. Small spray-included angle of 40 ° caused a high concentration of the fuel towards the piston bowl, resulted in enhancing the flame propagation thus leading to stable combustion. whereas the larger spray-included angle helped in achieving the more homogenous mixture but cause slow flame propagation if the mixture becomes too lean in certain regions. Moreover, the increased injection pressure resulted in better spray atomization and a reduction in particulate matter in emissions. Lower injection pressures result in increased flame speed and, thus an improved peak pressure; this is because they trap more fuel in the piston bowl. The spark timing that was found to be optimal was 4° CA ATDC, which had a trade-off related to fuel consumption, PPRR, and NOx emissions.

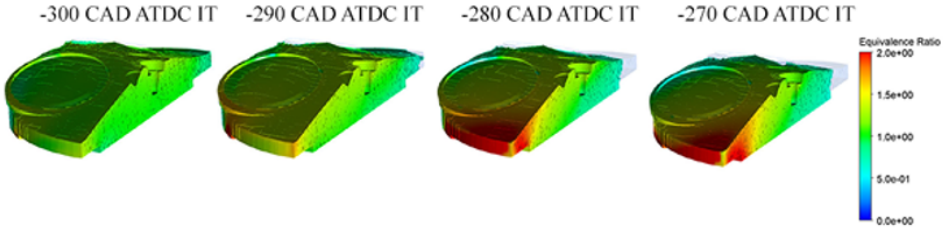

Figure 2.2: In cylinder pressure and heat release under different injection timing [116]

A numerical study by Y.Zhang et al.[116] was conducted on effect of injection timing during the compression stroke using gasoline direct injection. The test was conducted at 200 RPM at 10.1 compression ratio. The injection timing was varied from 270°CA

bTDC to 300°CA bTDC during the intake stroke to investigate the in-cylinder flow motion and its effect of emission. According to this study during the intake stroke the injected fuel droplets would interact with the air entering the cylinder and the velocity of the air decreases due to air friction at the droplets move through the cylinder. Then during the compression stroke during the upward motion of the piston the intake flow inertia contribute to the formation of counter clockwise tumble flow. Tumble flow is the rotation motion inside the cylinder which is effective flow pattern to enhance fuel-air mixture inside the chamber to obtained the effective combustion. Retarding the injection timing form 300°CA to 270°CA resulted in reducing the quality of fuel and air mixing. However, the varying the injection timing did not show significant effect in turbulent kinetic energy. In addition higher droplet wall impingement was obtained at advanced injection timing which resulted in larger Sauter Mean Diameter (SMD) due to droplet coalescence. Nevertheless, overall the droplet break up and atomization was obtained same at the end of the intake stroke. Delaying the injection timing from 300°CA bTDC to 270°CA bTDC reduced the timing was fuel and air to mix which caused reducing the in combustion efficiency and thermal efficiency as shown in the Figure 2.2.

The Numerical study [29]was conducted on investigation of effect of piston shapes on in cylinder flow and air-fuel mixture inside the cylinder. The test was carried out on spark ignition direct injection at engine speed of 1500 RPM using the RNG k- turbulence model. The study investigated the different piston shapes such as Flat piston (FP) ,Flat-with-centre-bowl piston Inclined piston (IP) and Inclined-with-centre-bowl piston (IBP). According the to that study the turbulent kinetic energy and tumble ration was observed higher for piston shapes with bowls compared to flat pistons. This increase in the turbulence kinetic energy and tumble ration resulted in enhancing air-fuel mixing leading efficiency combustion and reducing the emission. In addition to that bowl shaped piston facilitated the fuel evaporation rate and reduced wall wetting. The study also suggest that this increase in fuel evaporation rate results in drop in ambient temperature which could support higher compression ration and increase the engine efficiency. Therefore, study proves that flat with centre bowl piston was the optimal piston design.

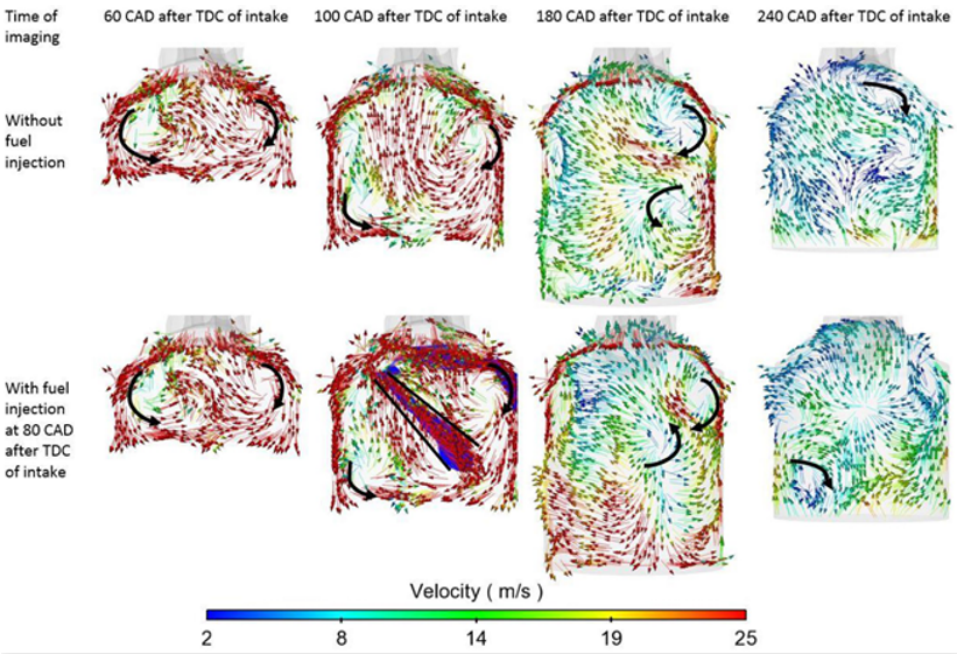

Figure 2.3: Effect of velocity field developed inside the cylinder due to the fuel injection [45]

Numerical [45] study conducted on the effect of direct injection of gasoline during the intake stroke on spark ignition using the flat crown piston using SAGE combustion modelling. The study was conducted at a compression ratio of 9.5 on the 200-cc engine displacement. at an engine speed of 300 RPM us. Injection timing was varied from 40°CA to 200°CA after the top dead centre (TDC). According to the study during the intake stroke high velocity of air flow as obtained near the valve curtain causing vortices below the valve area. Then these vortices are displaced during the downward motion of the piston. In addition to that compared effect in cylinder flow patterns without and with injection of fuel. It was observed from Figure 2.3 that without fuel injection spray high-velocity magnitudes were observed due to incoming air, Whereas when the fuel spray is present considerable changes in the air flow were observed. During the fuel injection, the increase the turbulent kinetic energy was obtained as the momentum of the injected fuel droplets is partially transferred to the surrounding air. But during the compression stroke turbulent kinetic energy decays which becomes comparable to the case without injection. It was also reported from the study that a higher turbulence level near the spark plug could help to enhance the flame propagation but if the intensity of turbulence is too high can cause the spark blowout. Furthermore, this study injection of fuel during the middle of the intake stroke could maintain the best balance between increased tumble ratio and obtained high turbulent kinetic energy in the vicinity of the spark plug for effect fuel and air mixing.

2.5 Effect of hydrogen addition to methanol engine

In this section, the main findings and tests from existing studies on hydrogen enrichment in methanol-fuelled spark-ignition engines are explored. Hydrogen enrichment with methanol offers stable combustion due to methanol's higher-octane rating and hydrogen's wide flammability limits, compared to hydrogen addition to gasoline or natural gas in spark-ignition engines. Additionally, hydrogen enrichment with methanol provides higher knock resistance compared to hydrogen enrichment in gasoline or natural gas engine operation [84].

According to the study by [84] neat methanol operating conditions demonstrated a brake thermal efficiency of 30.55% at an excess air ratio of 1.13 and an engine speed of 1400 RPM. However, at the same engine speed, the addition of 3% hydrogen to methanol resulted in an increased brake thermal efficiency of 31.9% under leaner operation with an excess air ratio of 1.25,. Methanol's high latent heat of vaporization and boiling point makes it difficult to evaporate at low temperatures, especially during cold starts. Adding hydrogen improves cold start performance by providing faster flame speed and requiring lower ignition energy than methanol. In cold start conditions, a 68.7% reduction in hydrocarbon emissions and a 75.2% reduction in carbon monoxide emissions were achieved with hydrogen addition to methanol. This is because less methanol is required for ignition, reducing the carbon content in the fuel mixture [115].

According to the experimental work [18] on the methanol spark ignition engine with 3% hydrogen addition. The test was conducted at engine speeds of 1200 and 1400 RPM with intake manifold pressures of 0.7 bar and 0.68 bar, respectively. The study observed that the lean operation of the methanol engine was extended from an excess air ratio of 1.6 to 2.2, leading to more efficient performance and a 90% reduction in brake-specific NOx emissions compared to stoichiometric conditions. In addition to that 3% hydrogen enrichment with methanol resulted 59% and 30% reduction of soot was observed at engine speed of 1200 RPM and 1800 RPM compared to neat methanol operation. Furthermore, under very lean condition 3% hydrogen enrichment with methanol resulted in the increase in carbon monoxide emission due to incomplete combustion.

The study by [18] explores the influence of ignition timing and hydrogen addition on the combustion performance and emissions characteristics of a methanol-fueled spark-ignition engine under lean-burn conditions with an excess air ratio of 1.4. The engine was tested at engine speeds 1200, 1800, and 2400 RPM. The research highlights that hydrogen addition significantly improves engine performance, particularly by increasing the indicated mean effective pressure (IMEP) and enhancing combustion efficiency at higher engine speeds[114]. However, a decrease in IMEP was observed at the lower engine speed of 1200 RPM compared to neat methanol operation, which was attributed to weak airflow motion entering the cylinder[18].

The study also suggests that increasing the hydrogen addition with methanol can reduce volumetric efficiency, resulting in a slower flame propagation speed [18, 43, 65]. Additionally, weak airflow motion in the cylinder contributed to increased carbon monoxide emissions when hydrogen was enriched with methanol[18]. Retarding the ignition timing of methanol with hydrogen led to an increase in IMEP and a reduction in both soot and NOx emissions at higher engine speeds. Furthermore, hydrogen addition with methanol resulted in increase in the soot emissions because the higher hydrogen addition because high concentration of H ion causes surface oxidation reaction of the soot. Hydrogen addition could slow prevent the soot oxidation due to the influence in the combustion temperature and chemical reaction. Enrichment of hydrogen can also slow down the formation polycyclic aromatic-hydrocarbon which would contribute to soot formation The study by Zhao et al. observed that hydrogen enrichment under stoichiometric fuel mixture can increase particular matter emission under high load operation in terms of total mass concentration

2.6 Effect of carbon monoxide addition to the internal combustion engine

Integrating carbon monoxide (CO) and hydrogen (H_2) into a natural gas engine has significantly enhanced its performance [31]. The presence of both carbon monoxide (CO) and hydrogen (H_2) increased maximum in-cylinder pressure and heat release rate. In addition to that, the combustion phase was advanced. Compared to a natural gas-air mixture, the carbon monoxide with hydrogen increases the laminar flame speed. According to the experimental study[67] on CO and H_2 addition on a natural gas engine, hydrogen plays a key role in enhancing one of the reactions involved in combustion, specifically the $OH + H_2 \rightarrow H + H_2O$ process. In contrast, CO addition primarily improves the $OH + CO \rightarrow H + CO_2$ reaction. With the increase of H_2 in H_2-CO blends, NO_x emissions also increase. Both hydrogen (H_2) and carbon monoxide (CO) play a role in decreasing total hydrocarbon(THC) emissions and enhancing engine effective thermal efficiency. At higher concentrations of hydrogen (H_2) in H_2-CO combinations, the emission levels of total hydrocarbon (THC) drop. Nevertheless, the impact of H_2 addition on CO emissions is minimal, but the addition of CO greatly raises CO emissions as a result of incomplete combustion, which is mainly caused by quenching and crevice effects. Both hydrogen (H_2) and carbon monoxide (CO) contribute to the increase in engine nitrogen oxide (NO_x) emissions, while also enhancing engine thermal efficiency[31].

Table 2.1: Properties of Hydrogen and Carbon Monoxide [31]

Properties	**H_2**	**CO**
Lower calorific value (MJ/Nm^3)	10.8	12.63
Flammability (% vol. of fuel in air)	4.1–75	12.5–74.6
Laminar flame speed (1 atm, 293.15 K, cm/s)	$\Phi = 1.00$: 207.04	16.54
	$\Phi = 0.73$: 153.49	14.04
Stoichiometric volume occupation in cylinder (%)	29.58	29.58
Stoichiometric mixture energy density (MJ/Nm^3)	3.19	3.74
Auto ignition temperature (K)	858	882
Adiabatic flame temperature (K)	2380	2383
Molecular weight(g/mole)	2.1015	26.01.
Density (Kg/m^3at 0 ^{o}C, 1 ATM)	0.71	0.90
Lower heating value (MJ/kg)	120	10.1
Lower heating value (MJ/m^3 at 0 ^{o}C)	10.1	12.63

A study was conducted on a reformer gas mixture consisting of hydrogen and carbon monoxide, along with an addition of nitrogen gas. This gas mixture was introduced into a diesel engine through the intake port for direct injection. The study shows that by incorporating N2 and reformer gas (H_2 + CO) to diesel, there is a notable decrease in NOx and soot emissions under various operating conditions. However, CO_2 emissions tend was observed when the carbon monoxide addition exceeds approximately 88%. In addition, the study suggests that when a flame is mixed with CO, it results to an overall higher production of smoke. In addition, the introduction of syngas and nitrogen into the intake air has been found to decrease the maximum pressure rise rate in the engine. The impact of load on this rate, however, varies depending on the engine speed. Lastly, the efficiency of the engine is higher on pure diesel operation compared to the reformer gas mixture. According to these findings, it seems that enhancing engine efficiency can be achieved by raising the engine load and speed with the inclusion of carbon monoxide and adjusting the engine speed.

2.7 Research gap

The literature review clearly demonstrated that hydrogen enrichment in a methanol spark-ignited engine resulted in lower exhaust gas emissions and improved combustion performance compared to the addition of hydrogen in a natural gas or gasoline spark-ignition engine. However, existing literature lacks a detailed analysis of in-cylinder characteristics concerning the effects of injection timing and lean combustion of methanol with hydrogen addition in spark-ignition engines, particularly regarding engine performance and the impact on exhaust emissions. Additionally, there is limited research on the combined effects of carbon monoxide and hydrogen addition to methanol in spark-ignition engines. Thus the current research work to address the existing gaps by comparing pure methanol with hydrogen-enriched methanol using both 1D and 3D computational fluid dynamics (CFD) models. The performance of methanol with hydrogen addition was evaluated under constant power conditions with varying levels of engine boosting. Additionally, the study examined the impact of varying injection timing of methanol with hydrogen addition in the intake and compression stroke of engine operation, thus analysing detailed in-cylinder characteristics and performance.Also, a comprehensive analysis of in-cylinder characteristics, engine performance, and emissions were conducted, covering combustion conditions ranging from rich to ultra-lean for both pure methanol and methanol with varying levels of hydrogen. Furthermore, the combined effects of methanol with carbon monoxide addition on engine performance and combustion characteristics were investigated and compared with those of neat methanol and methanol with hydrogen addition.Therefore, by conducting the aforementioned studies, the benefits and impact of hydrogen enrichment on methanol spark-ignited engine performance will be identified, while determining optimal operating conditions for reducing exhaust gas emissions without negatively affecting engine performance.

Chapter 3

Methodology

This chapter outlines the methodology used to analyze the performance and emissions of a single-cylinder methanol spark-ignition engine with varying levels of hydrogen addition, employing both 3-dimensional simulations in CONVERGE and 1-dimensional simulations in the Ricardo WAVE solver. The chapter covers the combustion process, solved using the SAGE combustion model, and details the turbulence modelling with the RANS method in the CFD solver. It also discusses the direct injection of methanol, modelled using the Kelvin-Helmholtz and Rayleigh-Taylor instability models in CONVERGE, along with the heat transfer analysis, solved using the O'Rourke and Amsden Heat Transfer Model. Additionally, the chapter describes the boundary conditions for the 3-dimensional single-cylinder methanol engine, including mesh generation and sensitivity testing. Then the chapter also discusses the validation of the methanol spark-ignition engine model with hydrogen addition using published experimental data. Further details include the Woschni heat transfer model used in Ricardo wave to simulate the single-cylinder direct injection methanol engine with port injection of hydrogen. In addition to that detail of SI Wiebe and multi-Wiebe combustion models to solve for neat methanol and methanol with hydrogen enrichment in the Ricardo WAVE solver.

3.1 Spray modelling

3.1.1 Kelvin-Helmholtz instability Model with Rayleigh-Taylor instability Model

In CONVERGE, to model direct injection of methanol, the Kelvin-Helmholtz (KH) intability model with the Rayleigh-Taylor (RT) instability model is used to simulate spray breakup.

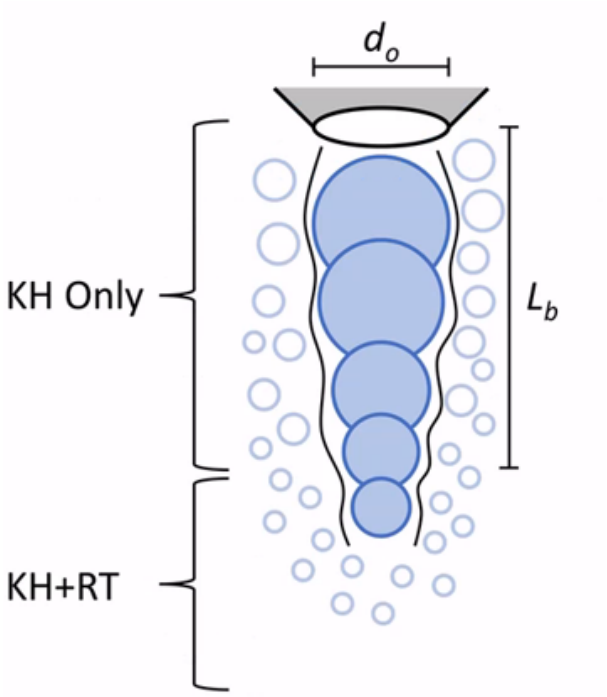

Figure 3.1: Schematic of the KH-RT instability spray breakup model[7]

In this model, L_b represents the distance of the methanol liquid before atomization, as shown in Figure 3.1. The constant C_{bl} is the empirical constant. The density ratio $\frac{\rho_l}{\rho_g}$ plays an important role in the stability of the droplet, where ρ_l and ρ_g are the densities of methanol and the surrounding air, respectively. d_0 represents the initial diameter of the liquid jet at the injection nozzle, and U is the relative velocity between the liquid jet and the surrounding gas.

The Rayleigh-Taylor intability breakup length L_b is given by:

$$L_b = C_{bl}\frac{\rho_l}{\rho_g}d_0 \tag{3.1}$$

The Kelvin-Helmholtz instability breakup length L_{KH}, as shown in Figure 3.1, is computed using:

$$L_{KH} = B_1 \frac{U}{\sqrt{\frac{\rho_l}{\rho_g}}} r_0 \tag{3.2}$$

Where B_1 is an empirical constant, and r_0 represents the initial radius of the liquid jet at the nozzle exit, which is $d_0/2$. article amsmath

3.2 Splash model

To simulate the behaviour of fuel parcels impacting the surface of the wall, O'Rourke's splash model was employed[74]. The forces and dynamics involved during the collision of droplets on the wall surface are described as follows.

The force balance equation is given by:

$$F - k_c \frac{dx}{dt} = m \frac{d^2x}{dt^2} \tag{3.3}$$

Where: - F is the force acting on the droplet, - k_c represents the damping force, - m is the mass of the fuel droplets, - $\frac{dx}{dt}$ is the velocity (first derivative of position), - $\frac{d^2x}{dt^2}$ is the acceleration of the droplets.

The force per unit mass on the droplet, F_m, is given by:

$$F_m = C_F \frac{\rho_g U_i^2}{\rho_l r_0} \tag{3.4}$$

Where: - C_F is a coefficient related to impact dynamics, - U_i is the impact velocity of the droplet, - ρ_g and ρ_l are the densities of gas and liquid, respectively, - r_0 is the initial droplet radius.

The stiffness-to-mass ratio, k_m, is given by:

$$k_m = C_k \frac{\sigma}{\rho_l r_0^3} \tag{3.5}$$

Where: - C_k is the coefficient, - σ is the surface tension, - r_0 is the initial droplet radius.

The damping-to-mass ratio, d_m, is given by:

$$d_m = C_d \frac{\mu}{\rho_l r_0^2} \tag{3.6}$$

Where: - C_d is the coefficient, - μ is the dynamic viscosity, - r_0 is the initial droplet radius. article amsmath

In order to predict whether a droplet will rebound or adhere to the wall, the amplitude of the droplet's oscillation is given by the equation:

Constant	Value
C_b	$\frac{1}{2}$
C_k	8
C_F	$\frac{1}{3}$
C_d	10

Table 3.1: Values of constants used in the model

$$A = \sqrt{(y - We_c)^2 + \left(\frac{y}{\omega}\right)^2} \tag{3.7}$$

Then predicting the droplet's behaviour under subsequent time steps inorder to predict splashing and spreading phenomena of the droplets. The evolution of the droplet position y_{n+1} in subsequent time steps is computed to predict splashing and spreading phenomena, which is given by:

$$y(t) = We_c + e^{-\frac{t}{t_d}} \left[(y(0) - We_c)\cos(\omega t) + \frac{1}{\omega}\left(\frac{dy}{dt}(0) + \frac{y(0) - We_c}{t_d}\right)\sin(\omega t) \right] \tag{3.8}$$

y_n is the initial droplet position, ωt represents the oscillatory behavior with respect to time.

$$We_g = \frac{\rho_g U^2 r_0}{\sigma}, \tag{3.9}$$

Where We_g is the drop weber number, a dimensionless parameter defined by the ratio of aerodynamic force to surface tension.

$$We_c = \frac{C_F}{C_k C_b} We_g, \tag{3.10}$$

$$\frac{1}{t_d} = \frac{C_d}{2}\frac{\mu_l}{\rho_l r_0^2}. \tag{3.11}$$

To determine the energy with which the droplet strikes the surface, the velocity component V_n is computed, which is given by:

$$V_n = 0.5 r_0 y \tag{3.12}$$

Then, the droplet's deformation during splashing is determined by the drop radius evolution r, which can be computed in the next equation (not provided in the current text).

The droplet's deformation during splashing is determined by the evolution of the drop radius r, which is given by:

$$r = r_0 \left(1 + \frac{8k_0^2 y^2 + \frac{\rho_l r_0^3}{\sigma y^2}}{6k - \frac{5120}{y}} \right) \tag{3.13}$$

r_0 is the initial drop radius, k_0 is a constant related to the droplet's properties,ρ_l is the density of the liquid,σ is the surface tension, y is the droplet displacement.

3.3 Combustion model

3.3.1 SAGE combustion model

In internal combustion engines, combustion is crucial because it involves chemical reactions between different species, heat transfer, and turbulence, all of which greatly influence the engine's performance. So, to predict the combustion process and to optimise combustion in cylinder performance it is essential to analyze the temperature, pressure distribution species concentrations, and pollutants inside the cylinder. The sage combustion model used in the Converge CFD solver can predict the detailed chemistry of different species that take part in the oxidation of mixtures which is applicable to premixed and non-premixed flames as well as for fuel blend composition in addition to that All elementary reaction rate and transport equation is computed using the SAGE combustion method. For this study, the reduced kinetic reaction mechanism for methanol developed by Christoffer.Pichler el al.[82] was utilized to solve the detailed chemistry. Different chemical reaction mechanisms used in the converge solver are as follows:

$$\sum_{m=1}^{M} \nu'_{m,i} \chi_m \rightleftharpoons \sum_{m=1}^{M} \nu''_{m,i} \chi_m \quad \text{for } i = 1, 2, \ldots, I \tag{3.14}$$

The stoichiometric coefficients of reactants and products are $v'^{\,i}_m$ and $v''^{\,i}_m$, respectively, where m represents species and i represents the reactions. The chemical symbol χ_m is used for species. I is the total number of reactions. The net production rate of species m is as follows:

$$\omega_m = \sum_{i=1}^{I} v_m^i q_i \quad \text{for} \quad m = 1, 2, 3, \ldots, M \tag{3.15}$$

Where M represents the total number of species, and:

$$v_m^i = v''^{\,i}_m - v'^{\,i}_m \tag{3.16}$$

q_i is the reaction rate progress of the i-th reaction, and X_m represents the molar concentration of species m. The forward and reverse reaction rates are denoted by k_{if} and k_{ir}, respectively.

$$q_i = k_{if} \prod_{m=1}^{M} X_m^{v_m^i} - k_{ir} \prod_{m=1}^{M} X_m^{v_m'' \, i} \tag{3.17}$$

The forward rate coefficient in Arrhenius form is expressed as:

$$k_{if} = A_i T^{\beta_i} \exp\left(-\frac{E_i}{RT}\right) \tag{3.18}$$

Where A_i is the pre-exponential factor, β_i is the temperature exponent, E_i is the activation energy (cal/mol), and R is the ideal gas constant. The reverse rate coefficient k_{ir} is computed using the equilibrium coefficient k_{ic} from the equation:

$$k_{ir} = \frac{k_{if}}{k_{ic}} \tag{3.19}$$

The equilibrium constant k_{ic} is calculated using thermodynamic properties as follows:

$$k_{ic} = k_{ip} P_{\text{atm}} \left(\frac{RT}{\prod_{m=1}^{M} v_m^i}\right) \tag{3.20}$$

Where P_{atm} represents atmospheric pressure, R is the ideal gas constant, and T is the temperature. The equilibrium constant k_{ip} is determined by:

$$k_{ip} = \exp\left(\frac{\Delta s_i^0}{R} - \frac{\Delta H_i^0}{RT}\right) \tag{3.21}$$

Δs_i^0 and ΔH_i^0 refer to the changes in entropy and enthalpy that occur in products from reactants in the i-th reaction, respectively:

$$\frac{\Delta s_i^0}{R} = \sum_{m=1}^{M} v_m^i \frac{S_m^0}{RT'} \tag{3.22}$$

$$\frac{\Delta H_i^0}{R} = \sum_{m=1}^{M} v_m^i \frac{H_m^0}{RT'} \tag{3.23}$$

In each computation cell, the governing equation for mass is computed by:

$$\frac{d[X_m]}{dt} = \omega_m \tag{3.24}$$

The energy in the governing equation is computed by:

$$\frac{dT}{dT} = \frac{dP}{dT} - \sum_m h_m \omega_m m([X_m] c_p^m) \tag{3.25}$$

Here, h_m and ω_m represent the molar specific enthalpy and the molar constant-pressure specific heat for species m. For constant volume combustion, it is computed by: The energy in the governing equation for constant volume combustion is computed by:

$$\frac{dT}{dT} = Q_{Vm} \sum_{m} h_m \omega_m m([X_m] c_p^m) \tag{3.26}$$

3.4 Turbulence modelling

Turbulence modelling is one of the important steps in computational fluid dynamics to resolve the turbulence eddy length scale in a discretized domain (grid). To find the solution for the Navier-Stokes equation, different methods are used depending on the information solved compared to those that are modeled. To predict turbulence convergence, three simulation methods are commonly used:

- **Large eddy simulation (LES):** In LES, the unsteady Navier-Stokes equations are solved directly for turbulent motions above a certain cut-off length scale, while the influence of smaller, subgrid-scale turbulence is modeled using a relatively simple eddy-viscosity model.
- **Direct numerical simulation (DNS):** DNS method resolves all turbulent scales of motion directly by solving the full Navier-Stokes equations without employing any turbulence models.But this method requires substantial computational resources, making it impractical for most engineering applications.
- **Reynolds-averaged Navier-Stokes equation (RANS):** In this method, the Navier-Stokes equation is solved using the time-averaging approach, which is one of the common simulation techniques used for CFD applications.

For this thesis, turbulence modelling is performed using the Reynolds-averaged Navier-Stokes equation (RANS). So, only the details of RANS will be explained in further sections.

3.4.1 RANS models

In the RANS turbulence model, the flow variable, instantaneous velocity u_i, is decomposed into an ensemble mean $\overline{u_i}$ and a fluctuation mean u_i':

$$u_i = \overline{u_i} + u_i' \tag{3.27}$$

The continuity equation is expressed as:

$$\frac{\partial \overline{\rho}}{\partial t} + \frac{\partial \overline{\rho} \tilde{u}_j}{\partial x_j} = 0 \tag{3.28}$$

The momentum equation is written as:

$$\frac{\partial \bar{\rho}\tilde{u}_i}{\partial t} + \frac{\partial \bar{\rho}\tilde{u}_i\tilde{u}_j}{\partial x_j} = -\frac{\partial \bar{P}}{\partial x_i} + \frac{\partial}{\partial x_j}\left[\mu\left(\frac{\partial \tilde{u}_i}{\partial x_j} + \frac{\partial \tilde{u}_j}{\partial x_i}\right) - \frac{2}{3}\mu\frac{\partial \tilde{u}_k}{\partial x_k}\delta_{ij}\right] + \frac{\partial}{\partial x_j}\left(-\rho\overline{u_i'u_j'}\right) \quad (3.29)$$

Where the Favre average $\tilde{u}_i$ is defined for velocity as:

$$\tilde{u}_i \equiv \frac{\overline{\rho u_i}}{\bar{\rho}}. \quad (3.30)$$

The Reynolds stress tensor is defined as:

$$\tau_{ij} = \overline{-\rho}\widetilde{u_i'u_j'}, \quad (3.31)$$

In the $k-\epsilon$ model:

$$l_e = c_\mu\left(\frac{k^{3/2}}{\epsilon}\right) \quad (3.32)$$

In the RNG $k-\epsilon$ model, the Reynolds stress is given by:

$$\tau_{ij} = \overline{-\rho}\widetilde{u_i'u_j'} = 2\mu_t S_{ij} - \frac{2}{3}\delta_{ij}\left(\rho k + \mu_t\frac{\partial \tilde{u}_i}{\partial x_i}\right) \quad (3.33)$$

The turbulent kinetic energy k is the trace of the stress tensor:

$$k = \frac{1}{2}\widetilde{u_i'u_i'} \quad (3.34)$$

The turbulent viscosity μ_t is defined by:

$$\mu_t = \rho C_\mu\frac{k^2}{\epsilon} \quad (3.35)$$

Where C_μ is a dimensionless parameter and ϵ is the dissipation of turbulent kinetic energy. The mean strain rate tensor s_{ij} is:

$$S_{ij} = \frac{1}{2}\left(\frac{\partial \tilde{u}_i}{\partial x_j} + \frac{\partial \tilde{u}_j}{\partial x_i}\right). \quad (3.36)$$

The models utilize terms for turbulent diffusion and turbulent conductivity to address the existence of turbulence in both mass and energy transport:

$$D_t = \frac{\mu_t}{\rho Sc_t} \quad (3.37)$$

Where D_t is the turbulent diffusion, Sc_t is the turbuent Schmidt number

$$k_t = \frac{\mu_t}{\rho Pr_t c_p'} \quad (3.38)$$

where Pr_t is the turbulent Prandtl number ,D_t is the turbulent diffusion and K_t is the turbulent conductivity. To obtain k^2 and ϵ the turbulent viscosity in equation (3.35).The turbulent kinetic energy transport equation is given by:

$$\frac{\partial \rho k}{\partial t} + \frac{\partial \rho \mu_i k}{\partial x_i} = \tau_{ij}\frac{\partial u_i}{\partial x_j} + \frac{\partial}{\partial x_j}\left(\mu + \frac{\mu_t}{Pr_k}\frac{\partial k}{\partial x_j}\right) - \rho\epsilon + \frac{c_s}{1.5}S_s \tag{3.39}$$

Factor 1.5 is the empirical constant. The transport equation for the dissipation of turbulent kinetic energy is given by:

$$\frac{\partial \rho \epsilon}{\partial t} + \frac{\partial \rho \mu_i \epsilon}{\partial x_i} = \frac{\partial}{\partial x_j}\left(\mu + \frac{\mu_t}{Pr_\epsilon}\frac{\partial \epsilon}{\partial x_j}\right) + C_{\epsilon 3}\rho\epsilon\frac{\partial u_i}{\partial x_i} + C_{\epsilon 1}\frac{\partial u_i}{\partial x_j}\tau_{ij} - C_{\epsilon 2}\rho\epsilon + C_s S_s\frac{\epsilon}{k} + S - \rho R_\epsilon \tag{3.40}$$

Table 3.2: Constants of the RNG $k-\epsilon$ turbulence model

Constant	**Value**
C_μ	0.0845
$C_{\epsilon 1}$	1.4200
$C_{\epsilon 2}$	1.6800
$C_{\epsilon 3}$	-1.000
η_0	4.3800
β	0.0120
ϵ	1.3900
Turbulent kinetic energy (TKE)	1.3900

3.5 Emission modelling

3.5.1 NOx emissions model

To predict the NOx formation in the Converge CFD solver, the extended Zeldovich method is used [32]. The mechanism involves the following reactions:

$$O + N2 <=> NO + N \tag{R1}$$

$$N + O2 <=> NO + O \tag{R2}$$

$$N + OH <=> NO + H \tag{R3}$$

For the above three forward and reverse reactions, the rate constants are given by:

$$k_{1f} = 7.6 \times 10^{13} \exp\left(\frac{-38000}{T}\right) \tag{3.41}$$

$$k_{1r} = 1.6 \times 10^{13} \tag{3.42}$$

$$k_{2f} = 6.4 \times 10^{9} T \exp\left(\frac{-3150}{T}\right) \tag{3.43}$$

$$k_{2r} = 1.5 \times 10^{9} T \exp\left(\frac{-19500}{T}\right) \tag{3.44}$$

$$k_{3f} = 4.1 \times 10^{13} \tag{3.45}$$

$$k_{3r} = 2.0 \times 10^{14} \exp\left(\frac{-23650}{T}\right) \tag{3.46}$$

Where: - f denotes the forward reaction, - r denotes the reverse reaction.

The rate of NO formation is given by:

$$\frac{d[NO]}{dt} = k_{1f}[O][N_2] - k_{1r}[NO][N] + k_{2f}[N][O_2] - k_{2r}[NO][O] + k_{3f}[N][OH] - k_{3r}[NO][H] \tag{3.47}$$

The rate of formation of N can be written as:

$$\frac{d[N]}{dt} = -k_{1f}[O][N_2] + k_{1r}[NO][N] + k_{2f}[N][O_2] + k_{2r}[NO][O] - k_{3f}[N][OH] + k_{3r}[NO][H] \tag{3.48}$$

article amsmath

3.5.2 Soot emission

Soot was predicted using the Hiroyasu empirical model to calculate soot formation and the Nagel Strickland-Constable (NSC) model to calculate soot oxidation [33]. The net soot formation rate M_s was determined by taking the single-step difference between the soot formation M_{sf} and soot oxidation M_{so}, as given by:

$$M_s = M_{sf} - M_{so} \tag{3.49}$$

The soot formation and oxidation rates are given by:

$$M_{sf} = SF \cdot M_{\text{form}} \tag{3.50}$$

$$M_{so} = SO \cdot M_s \tag{3.51}$$

Where: - M_{form} is the fuel vapor mass, - M_s is the total soot particle mass.

More detailed soot emission model information can be found in [33].

3.6 Heat transfer model

For this study, the spark-ignition engine used the O'Rourke and Amsden Heat Transfer Model to accurately predict the thermal behavior of the engine. The model predicts heat transfer between the engine in the fluid domain and solid boundaries, which include the piston, cylinder liner, and cylinder head. The O'Rourke and Amsden wall heat transfer equation is given by:

$$K\frac{\partial T}{\partial x_i} = \mu_m c_p F(T_f - T_w)\frac{Pr_m}{y_n} \tag{3.52}$$

Where: - K is the molecular conductivity, - T_f is the fluid temperature, - T_w is the wall temperature, - μ_m represents the shear speed, - c_p is the specific heat at constant pressure, - y_n is the distance from the wall.

The function F is defined as:

$$F = \begin{cases} 1.0 & \text{if } y^+ < 11.05 \\ \frac{Pr_m}{Pr_t}\left(\frac{1}{k}\ln(y^+) + B + \frac{11.05}{Pr_m/Pr_t} - 1\right) & \text{if } y^+ > 11.05 \end{cases}$$

Where: - $y^+ = \frac{\rho u_\tau y}{\mu_m}$, - k is the von Karman constant (0.42), - B is the law of the wall parameter (5.5), - Pr_m is the molecular Prandtl number, - Pr_t is the turbulent Prandtl number, - u_τ is the shear velocity. article amsmath graphicx booktabs

3.7 3-dimensional computational case set-up

A computational fluid dynamic study on a spark-ignition engine was conducted using the commercial code of the Converge CFD solver. The time-dependent unsteady RANS equation was used to model turbulent flow. The time-dependent unsteady RANS equations were applied to simulate the turbulent flow in the numerical simulation carried out with the Converge CFD code. Since the RNG $k-\epsilon$ model is especially well-suited for investigating internal combustion engines, it was used for turbulence modelling.

3.7.1 Assigning regions to the boundary

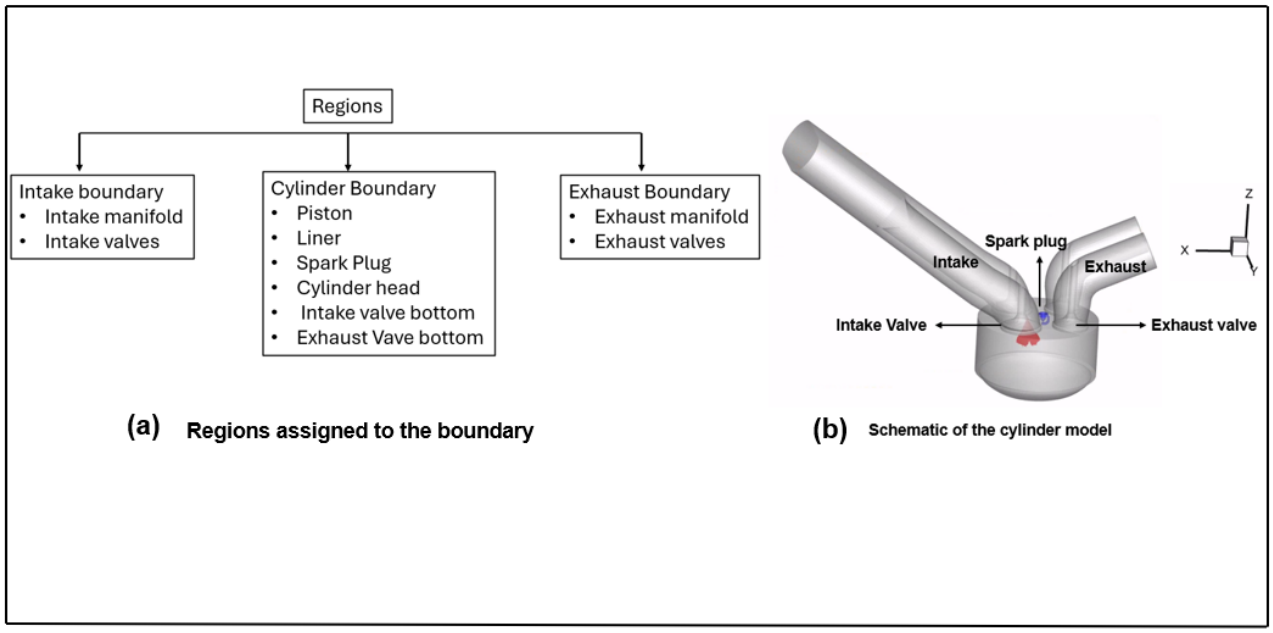

Figure 3.2: Regions assigned to the boundary and schematic of cylinder model

In this simulation study of an SI engine, boundary conditions were assigned to accurately represent the physical environment of the engine. Initial boundary conditions were specified in the Converge CFD solver to define the fluid state at the start of the simulation. The initial temperatures assigned to each boundary are shown in table 3.3.

To conduct the engine operation simulation, three regions were created: intake, cylinder, and exhaust. The intake region consists of the intake manifold and intake valves. The intake manifold plays a crucial role in supplying air to the engine cylinders. In this study, the intake manifold pressure was defined by assigning the pressure to the intake region. The species mass fractions of air, consisting of nitrogen (N_2) and oxygen (O_2), were assigned to the inflow boundary region.

All the temperatures of the boundary conditions were assigned to the walls, as shown in table 3.3. The O'Rourke and Amsden model was assigned to the boundary to predict heat transfer between the boundaries and the combustion gases. The species mass fractions of combustion products from methanol were assigned to the cylinder region. The exhaust region consists of the exhaust manifold and exhaust valve, with the mass fractions of the combustion products from methanol.

Table 3.3: Boundary Conditions

Boundary	**Temperature (K)**
Piston wall	450
Cylinder head	450
Liner	450
Exhaust port (wall)	500
Intake port (wall)	425
Intake (inflow)	363
Exhaust (outflow)	800
Exhaust valve (wall)	525
Intake valve (wall)	480

Boundary conditions

For this simulation study, the manifold pressure is assigned using the inflow boundary setting in the CFD solver. The pressure of the manifold is computed using the Dirichlet method where p_{total} is imposed on the solver. The solver calculates the static pressure using the compressible flow equations provided by:

$$P_{static} = P_{total}\left[1 + \frac{\gamma - 1}{2}\frac{\mu_i^2}{\gamma RT} - \gamma\frac{\gamma - 1}{\rho gh}\right] \tag{3.53}$$

where ρ is the density of air, h is the height above gravity g, γ is the ratio of specific heat, R is the ideal gas constant, and μ_i is the mass flow velocity boundary.
Then from the total pressure p_{total}, the static temperature is computed from the initial boundary condition of the intake (inflow) T_{total} as shown by the equation:

$$T_{static} = T_{total}\left[1 + \frac{\gamma - 1}{2}\frac{\mu_i^2}{\gamma RT} - \gamma\frac{\gamma - 1}{\rho gh}\right] \tag{3.54}$$

where γ is the ratio of specific heat, R represents the ideal gas constant, and μ_i is the mass flow velocity boundary.

For this CFD simulation, the mass fractions of the species at the inflow boundary are determined by solving the combustion stoichiometric equation for methanol at different excess air ratios. To assign the species composition of the air for various excess air ratios, the stoichiometric equation of methanol combustion is balanced, and the mass fractions of the reactants involved in air, such as oxygen and nitrogen, are computed.

The mass fractions of nitrogen and oxygen are computed for different excess air ratios using the stoichiometric equation of methanol given by:

$$CH3OH + 1.5 \cdot \left(O2 + \frac{79}{21}N2\right) \rightarrow CO2 + 2 \cdot H2O + 1.5 \cdot \frac{79}{21} \cdot N2 \tag{3.55}$$

stoichiometric equation of methanol at excess air ratio is given by :

$$CH3OH + E \cdot 1.5 \cdot \left(O2 + \frac{79}{21} \cdot N2\right) \rightarrow CO2 + 2 \cdot H2O + E \cdot \frac{79}{21} \cdot 1.5 \cdot N2 + \left(\frac{3}{2} \cdot (1 - E)\right) \cdot O2 \quad (3.56)$$

Where E is the excess air ratio

3.7.2 Intake valve and exhaust Valve

The exhaust and intake valves were modelled as moving boundaries by assigning the valve lift profiles. The O'Rourke and Amsden heat transfer model was assigned to the bottom of the valves to accurately predict thermal interactions.

The valve timing diagram (figure 3.3) provides a detailed representation of the valve lift profiles for both the intake and exhaust valves with respect to crank angle. Valves' opening and closing times are modelled as follows:

- Exhaust valve opening (EVO) at -585° CA
- Exhaust valve closing (EVC) at -321° CA
- Intake valve opening (IVO) at -380° CA
- Intake valve closing (IVC) at 124° CA

These events were carefully modeled and incorporated into the simulation to accurately capture the dynamic operation of the valves. The intake valve lift profile and the exhaust valve lift profile depict the precise timing and amount of valve lift, ensuring that the simulation accurately reflects the real-world behavior of the engine's valve mechanism.

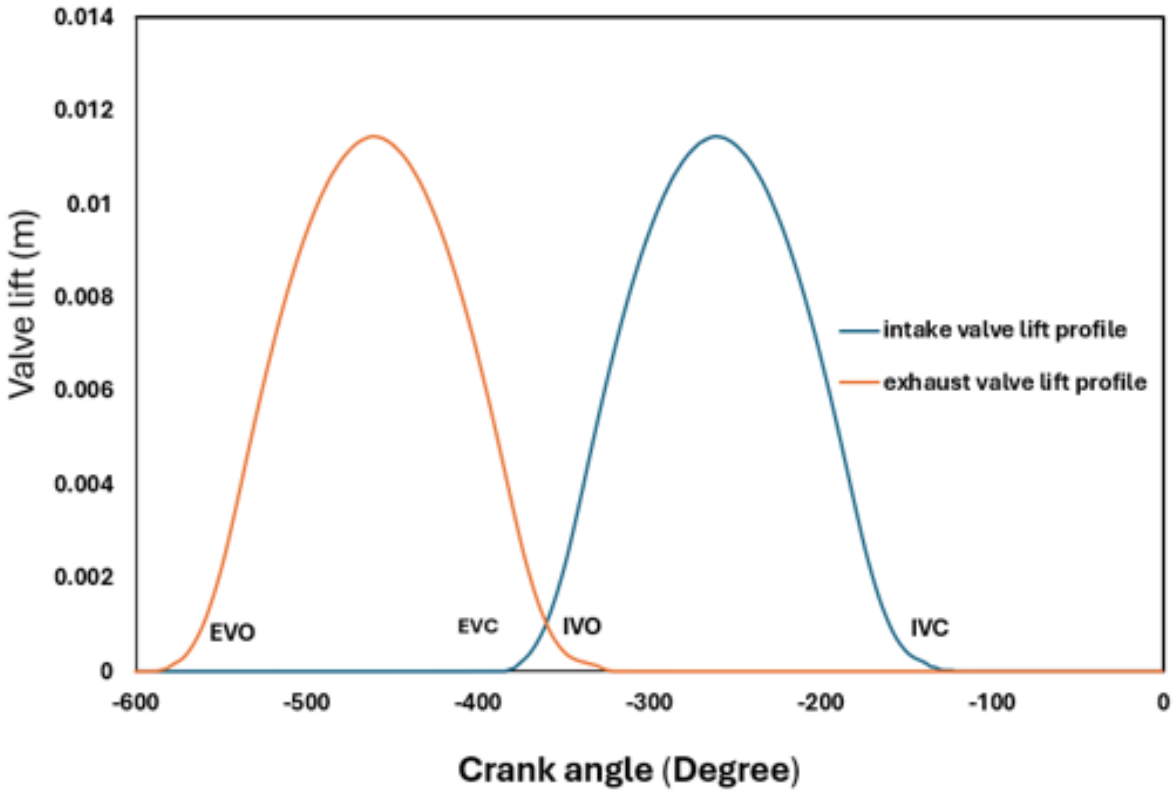

Figure 3.3: Value lift profile of the single cylinder methanol fuelled spark ignition engine model

Piston

The piston was modelled as a translating moving boundary based on the engine's compression ratio. The O'Rourke and Amsden model was utilized to solve the heat transfer equation between the combustion gases and the piston. The temperature of the piston was assigned as detailed in Table 3.3.

Liner and cylinder head

The liner and cylinder head were modelled as fixed wall boundaries. The temperature of the liner was assigned as shown in Table 3.3. Similar to the piston, the O'Rourke and Amsden model was applied to solve the heat transfer equations to accurately predict the temperature distribution and heat flux in critical regions.

Spark plug

In the converge solver, two distinct energy sources were assigned to replicate the ignition process, as shown in Figure 3.4. To replicate the breakdown phase, source 1 was modelled

for a 0.5° CA duration (short duration). Then, source 2 was assigned for an 8° CA duration to replicate the arc and glow phase discharge duration. Additionally, the radius of the spark was assigned in the solver to fit the gap between the two electrodes of the engine model.

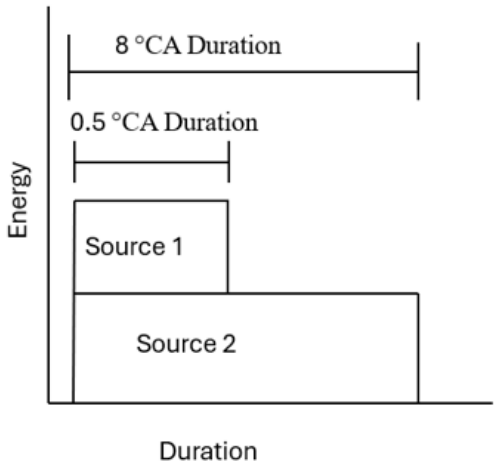

Figure 3.4: Schematic of the spark model of single cylinder 3-D CFD model

3.7.3 Mesh generation and refinement

Mesh plays a crucial role in the accuracy of computational fluid dynamic (CFD) simulations. The Converge CFD solver uses a hybrid meshing strategy to balance computational accuracy and efficiency. For this study, the meshing method involves the following:

Base grid mesh

To cover the entire computational domain, a structured mesh was created using grid scaling. By defining the grid scale parameter n, the base grid size can be changed during the simulation at a specified time:

$$dx_{\text{scaled}} = \frac{dx_{\text{base}}}{2^n} \tag{3.57}$$

Where dx_{base} is the base grid size, and dx_{scaled} is the scaled grid size.

Fixed embedding

This feature allows refining the grid in a specific domain location by specifying an embedding scale n:

$$dx_{\text{embedding}} = \frac{dx_{\text{base}}}{2^n} \tag{3.58}$$

Adaptive mesh refinement

Adaptive mesh refinement allows grid refinement without increasing computational time. The grid is refined based on fluctuating and moving variables, such as species velocity and temperature. The magnitude of the sub-grid fields is estimated to determine where the grid needs refinement.

$$\phi' = \phi - \bar{\phi} \tag{3.59}$$

$$\phi' = -\alpha_k \frac{\partial^2 \phi'}{\partial x_s \partial x_k} + \frac{1}{2!}\alpha_k \alpha_l \frac{\partial^4 \phi'}{\partial x_s \partial x_k \partial x_m \partial x_l} - \frac{1}{3!}\alpha_k \alpha_l \alpha_m \frac{\partial^6 \phi'}{\partial x_s \partial x_k \partial x_m \partial x_l \partial x_p \partial x_t} + \dots \tag{3.60}$$

For rectangular cells, α_k is:

$$\alpha_k = \frac{dx_k^2}{24} \tag{3.61}$$

In order to handle the entire series, the second-order term is utilized, that is:

$$\phi' \approx -\alpha_k \frac{\partial^2 \phi'}{\partial x_s \partial x_k} \tag{3.62}$$

Where ϕ' is the sub-grid scalar, ϕ is the actual scalar field, and $\bar{\phi}$ is the resolved scalar field.

The refinement of the cell takes place if the absolute value of the sub-grid cell is above the specified value. In the other case, the cell will be generated if the absolute value is below $\frac{1}{5}$ of the specified value.

3.7.4 Mesh sensitivity analysis

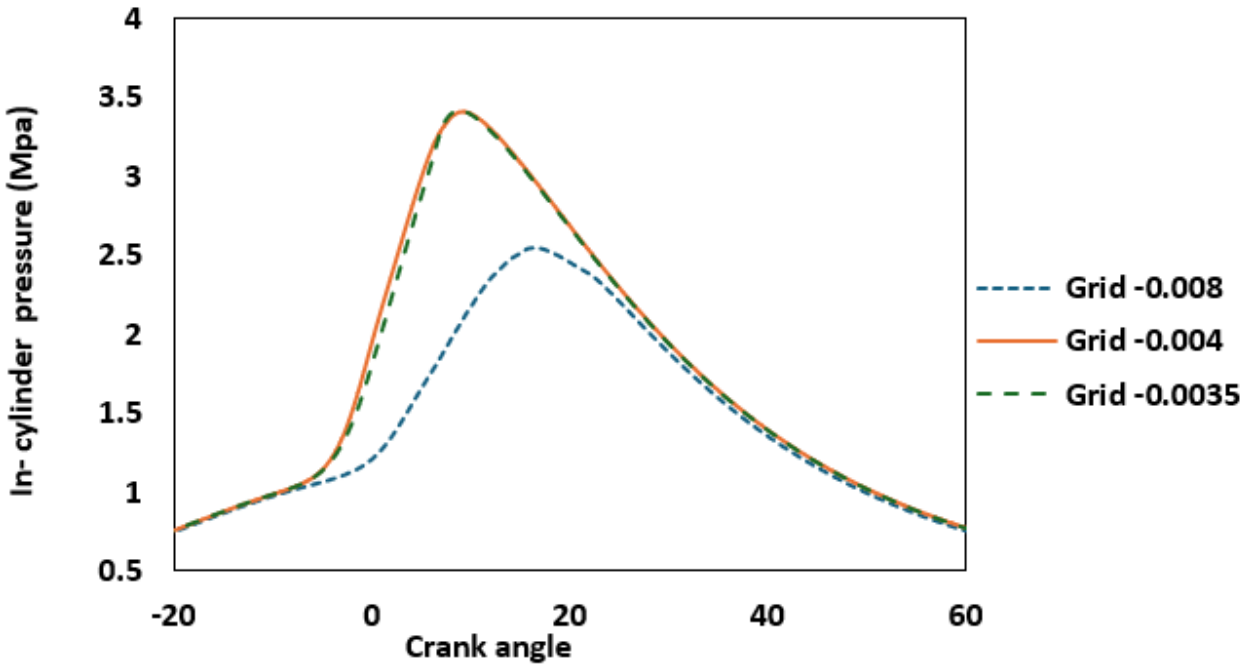

Figure 3.5: Mesh sensitivity analysis of in cylinder pressure with respect to crank of single cylinder 3-D CFD methanol fueled spark ignition engine model

To investigate the influence of mesh refinement on predicting engine performance, the accuracy differences between various grid sizes were analyzed.Figure 3.5 represents a mesh refinement analysis performed using the Converge CFD solver, comparing in-cylinder pressure curves for various sizes of mesh during a combustion simulation in a single-cylinder methanol spark-ignition engine enriched with 6% hydrogen under excess air ratio of 1.4. The particular setup is based on published experimental research conducted by Gong [21], the details of the engine operating condition will be covered in detail later in the validation section. Mesh sizes ranging from 0.008 m to 0.0035 m were used to predict in-cylinder pressure, as shown in Figure 3.4. The coarse mesh (0.008 m and 0.006 m) performed resulted in less accuracy in predicting pressure rise and expansion strokes but required less computational time. To improve accuracy, the mesh was refined to 0.0035 m. However, the difference in results between the 0.004 m and 0.0035 m grids was less than 5%, showing a minor improvement. For the simulation investigation in this work, a grid size of 0.004 m was chosen to strike a balance between computational time and accuracy

3.8 Validation of 3-dimensional CFD model

To investigate engine combustion performance and exhaust emissions, the in-cylinder pressure versus crank angle plays a crucial role in providing a detailed representation of the pressure changes during the intake, compression, combustion, and exhaust strokes using the 3-dimensional CFD model. The in-cylinder pressure with respect to the crank angle of the 3-dimensional CFD model was validated against experimental data published by C.Gong [22] on the effect of hydrogen addition to methanol in a spark-ignition engine. The engine specifications shown in the table were used for this validation. This validated engine specification is used for the investigations in Chapters 5, 6, 7, and 8 of this study.

The engine model was validated with experiments under different operating conditions to accurately predict spark timing, hydrogen addition, and lean operation scenarios. The validation process included the neat methanol operating condition and the effect of hydrogen addition to methanol from stoichiometric to lean operation. All the validations involved different combustion conditions, including varying spark timings and fuel mixtures, which implies that the CFD model can predict the combustion process more accurately. This comprehensive validation ensures the model's robustness and reliability in simulating various combustion performance characteristics of the engine.

The experimental work [22] utilized methanol as a direct injection fuel and hydrogen using port injection. To replicate this setup, a CAD model of the engine was created, incorporating methanol direct injection. The computation of methanol liquid spray modelling was conducted using the Kelvin-Helmholtz model as discussed in Section 3.3. For modelling hydrogen addition via port injection, the hydrogen mass fraction was assigned to the intake manifold boundary region along with the share of air. The mass fraction of hydrogen addition was computed by balancing the stoichiometric equation of methanol with hydrogen under different excess air ratios.

The percentage of hydrogen addition was calculated using the formula:

$$\alpha = \frac{V_{H_2}}{V_{\text{air}} + V_{H_2}} \tag{3.63}$$

where V_{H_2} and V_{air} are the volumetric flow rates of hydrogen and air, respectively.

The excess air ratio for different combustion processes for neat methanol and methanol with different hydrogen additions was computed as follows:

$$\lambda = \frac{m_{\text{air}}}{m_{H_2}\text{AF}_{H_2\,st} + m_{\text{CH}_3\text{OH}}\text{AF}_{\text{CH}_3\text{OH}\,st}} \tag{3.64}$$

Where $m_{\text{air}}, m_{H_2}, m_{\text{CH}_3\text{OH}}$ are the masses of air, hydrogen, and methanol, respectively. $\text{AF}_{H_2\,st}$ and $\text{AF}_{\text{CH}_3\text{OH}\,st}$ are the stoichiometric ratios, defined as values of 32 and 6.5, respectively.

The spark timing for the validation of different conditions was performed using the

source modelling approach, as discussed in Section 3.4. Figure 3.5 (a), (b), and (c) represent the validation of in-cylinder pressure traces during the compression to expansion process.

- **Figure 3.6 (a)** shows the validation for neat methanol under lean operation with an excess air ratio of $\lambda = 1.2$ at a spark timing of -28°CA bTDC.
- **Figure 3.6 (b)** presents the validation for 3% hydrogen addition to methanol under lean operation with an excess air ratio of $\lambda = 1.2$ at a spark timing of -28°CA bTDC.
- **Figure 3.6 (c)** shows the validation for 6% hydrogen addition to methanol under lean operation with an excess air ratio of $\lambda = 1.4$ at a spark timing of -4°CA bTDC.

The simulated in-cylinder pressure curves (red line) closely match the experimental pressure curves (blue line) from [22] throughout the combustion cycle, showing strong agreement at the peak pressure and during the expansion stroke, with less than 2% error compared to the experimental data. This close alignment confirms the model's ability to accurately capture the effects of both hydrogen enrichment and lean combustion conditions.

Furthermore, the validation of in-cylinder pressure traces for methanol with different hydrogen additions showed a maximum error of 2%, which falls within the cycle-to-cycle variation of the experimental data[22]. This demonstrates the accuracy and reliability of the CFD model in predicting the combustion process under various operating conditions.

Table 3.4: Engine specifictation

Characteristics	**Values**
Bore x stroke [m]	0.0825 x 0.0842
Displacement volume [m^3]	0.0001798
Compression ratio [-]	9.6
Speed [RPM]	1200

3.9 1-Dimensional computational fluid dynamics set-up

A 1-dimensional computational fluid dynamics (CFD) analysis of an ignited methanol engine with hydrogen addition was conducted using the Ricardo WAVE solver.

3.9.1 Combustion modelling

To compute the combustion process, a single Wiebe combustion model was used for neat methanol as a single fuel in the Ricardo solver, while a multi-Wiebe combustion model

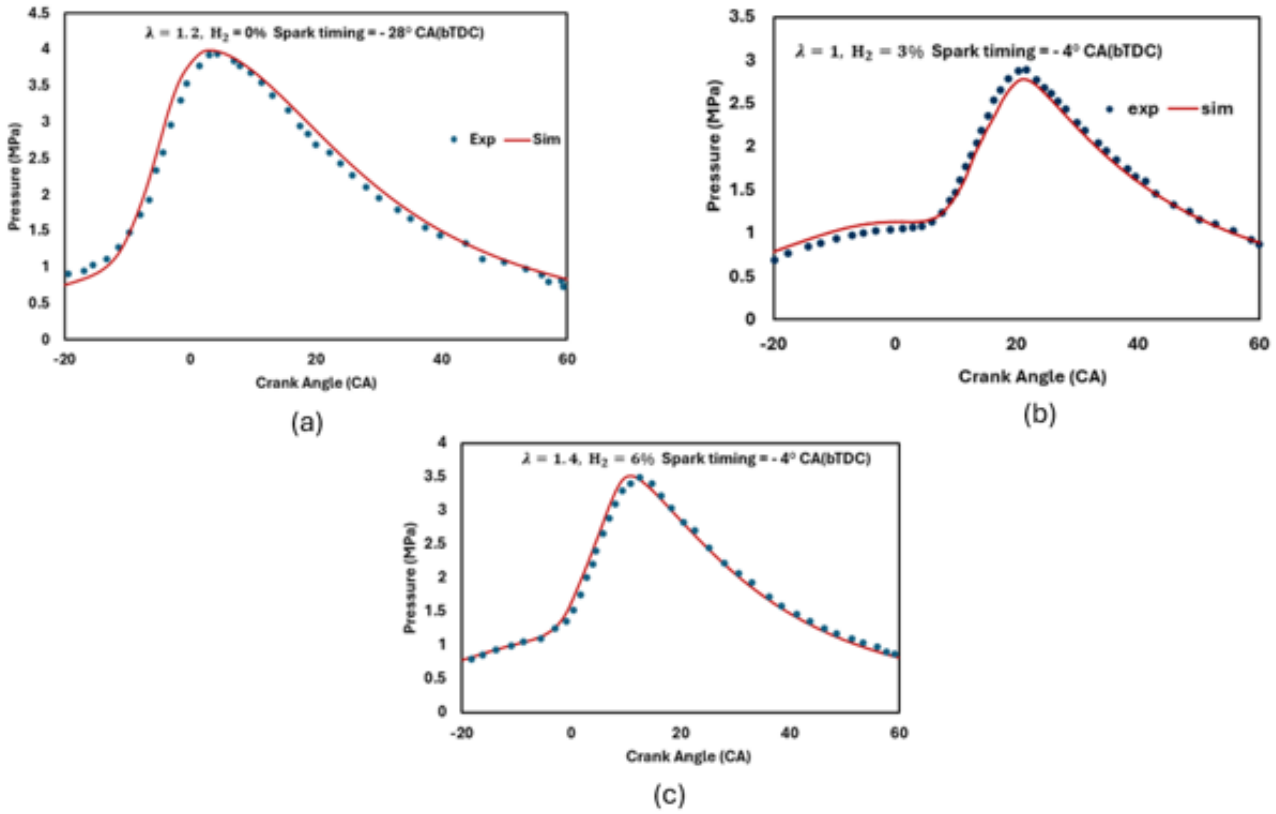

Figure 3.6: validation in cylinder pressure trace with respect to crank angle form neath methanol and methanol with different level hydrogen addition under stoichiometric to lean conditions

was employed for methanol with hydrogen enrichment in the Ricardo WAVE solver to handle dual fuel combustion. Both models utilized a mathematical representation of the mass fraction burned during the combustion process using the Wiebe function, given by:

$$W_n = 1 - \exp\left(-a\left(\frac{\theta_t - \theta_0}{b} + 1\right)\right)$$

Where θ_0 is the start of combustion, b is the Wiebe exponent, and a is the shape factor.

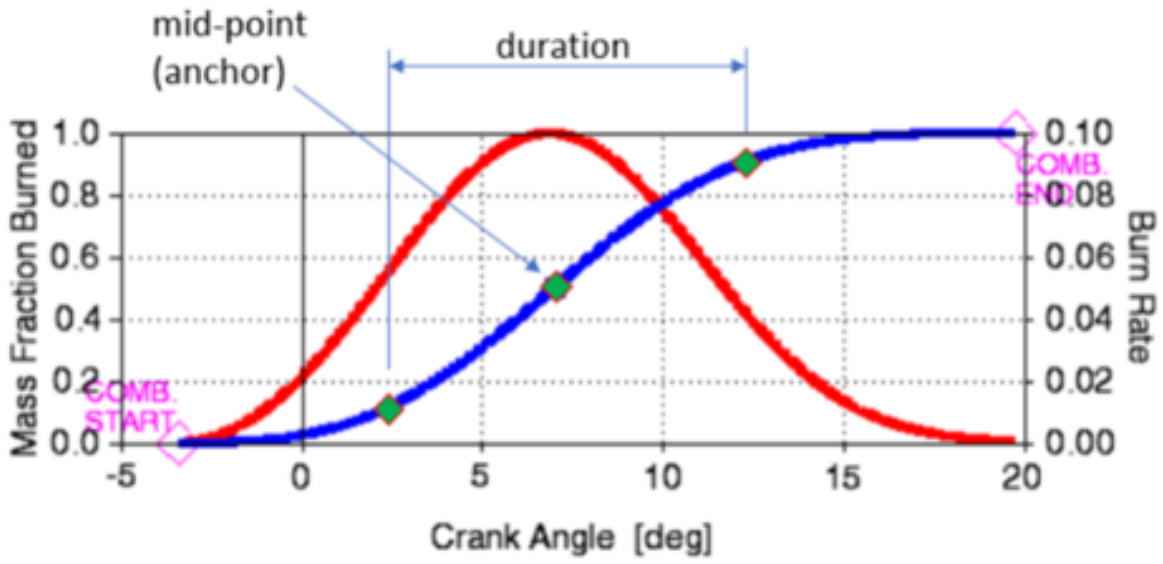

Figure 3.7: Wiebe curve (blue curve) and the burn rate (red curve)

The shape factor a and the Wiebe exponent are assigned to the solver to fit the characteristics of the curve. To compute the combustion process, the 50% combustion point (CA50) and combustion duration (CA10-90) are assigned to the Ricardo WAVE solver. The green diamond shapes on the Wiebe curve indicate the three anchor points, with the midpoint (anchor) defining the CA50 location, and the distance between the first and third anchors defining CA10-90. article amsmath

3.9.2 Heat transfer model

To compute the heat transfer in the Ricardo WAVE solver, the Woschni heat transfer model was utilized. Woschni's heat transfer model computes the heat transfer to and from the cylinder charge. In this model, the heat flow coefficient and velocity are assumed to be uniform on all cylinder surfaces. The heat transfer coefficient is given by:

$$h_g = 0.0128 D^{-0.20} p^{0.80} T^{-0.53} v_c^{0.8} C_{enht}$$

Where:

- D is the cylinder bore,
- p is the in-cylinder pressure,
- T is the cylinder temperature,
- v_c is the characteristic velocity.

The characteristic velocity v_c is given by:

$$v_c = C_1 v_m + C_2 \frac{V_D T_r}{p_r V_r}(P - P_{\text{mot}})$$

Where:

- v_m is the mean piston speed,
- V_D is the cylinder displacement,
- T_r is the reference temperature,
- p_r is the reference pressure,
- P is the cylinder pressure,
- P_{mot} is the motoring pressure.

The coefficient C_1 is given by:

$$C_1 = 6.18 + 0.417 \frac{v_s}{v_m}$$

During the combustion process, the coefficient C_2 is given by:

$$C_2 = 2.28 + 0.308 \frac{v_s}{v_m}$$

Where v_s is the swirl velocity. In this study, the swirl ratio v_s is assumed to be zero. Before combustion and during scavenging, the coefficient C_2 is:

$$C_2 = 0$$

3.10 Modeling setup for 3D investigation of methanol spark-ignition engine investigation

This section outlines the common modelling methodology used in the 3D simulation studies conducted in Chapters 5, 6, 7, and 8. The basic grid size for the 3D model was

set to 4 mm through careful investigation of mesh refinement, as discussed in the earlier session, with the in-cylinder region refined to a mesh size of 1 mm during the combustion and gas exchange processes. Additionally, a finer mesh of 0.5 mm was applied around the injector and spark plug to accurately capture flame characteristics such as kernel formation, growth, and development, as detailed in the previous section of this chapter.

The spark timing and energy were modelled using a source/sink approach, replicating the arc phase and glow phase of the spark with durations of 0.5° CA for the arc phase and 8° CA for the glow phase, as mentioned in Chapter 3. Adaptive Mesh Refinement (AMR) was automatically applied by the solver, refining the mesh based on l°CA gradients in temperature and velocity, as discussed in the previous section of this chapter.

The computational fluid dynamics (CFD) solver Converge [7] was employed to solve the three-dimensional Reynolds-Averaged Navier-Stokes (RANS) equations with turbulence inside the combustion chamber simulated using the k-ϵ model [59]. The O'Rourke and Amsden heat transfer sub-model was applied, and for combustion investigations, the SAGE detailed chemistry solver was used to calculate the reaction rates of all elementary reactions in the methanol/hydrogen combustion mechanism [82], which consists of 20 elementary reversible reactions validated across a wide range of experimental data.

Chapter 4

Effects of boosting on methanol spark-ignition engine with hydrogen addition using 1-dimensional computational modelling

This chapter investigates the performance of a spark-ignition methanol engine and the effect of hydrogen enrichment using a 1-dimensional model in the Ricardo Wave solver. The methanol spark-ignition engine is modelled using both single Wiebe and multi-Wiebe functions to represent methanol and methanol with hydrogen addition under various operating conditions. These models are validated against published experimental works [22, 19], addressing the limitations of the Ricardo Wave solver in predicting combustion duration under different operating conditions. To overcome these limitations, the laminar flame speed correlation study conducted by [69] for methanol and methanol with hydrogen addition was utilized to calibrate the Wiebe combustion curve. Using this approach, the effect of boosting at a constant power of 30 kW (low power rating) and 110 kW (high power rating) on neat methanol and methanol with 2% to 9% hydrogen addition was investigated. Additionally, the variation in injection timing of methanol was examined. This investigation is carried out on a 50-liter genset diesel engine using the Ricardo engine database, modified to a spark-ignition methanol-fueled single-cylinder engine. This work was published in the Offshore Technology Conference, titled "Methanol + Hydrogen - Prospective Alternative Fuel for Cleaner Offshore Power Generation

4.1 Validation of 1-dimensional single cylinder methanol spark ignition engine model

The objective of this section is to understand the precision of 1-dimensional analysis software in relation to experimental setups for analyzing engine performance. Neat methanol and methanol with various levels of hydrogen enrichment were evaluated for different excess air ratios based on the published experimental work by C.Gong [19]. Additionally, the in-cylinder pressure trace was validated against the experimental work by [18] for different spark timings for neat methanol and methanol with varying levels of hydrogen addition. The article published by C.Gong [18, 19] utilized an EA888 HPI + MDI engine to conduct experiments. The two published experimental works employed direct injection of methanol and hydrogen using port injection.

4.1.1 Modelling procedure for validation

To validate the neat methanol and methanol with hydrogen addition, two models were created in Ricardo Wave Solver. For modelling neat methanol operation, a single-cylinder direct injection methanol fuel engine model was created in the Ricardo solver, as shown in Figure 4.1. The combustion model was developed using the SI Wiebe combustion model and the Wochni heat transfer model. A mass flow rate injector type was used for methanol injection and an injection timing of 80°CA bTDC was assigned to the solver.

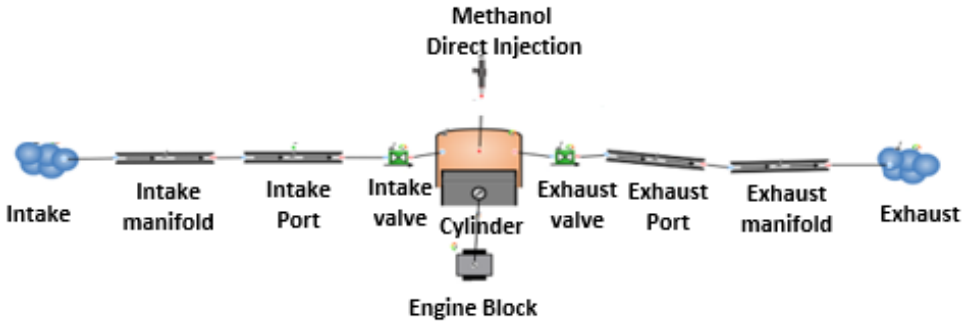

Figure 4.1: validated 1-dimensional model of single cylinder direct injection of methanol using single Wiebe combustion

Then to model methanol with hydrogen addition, the mass flow rate injector was used to simulate methanol direct injection. To replicate the port injection of the hydrogen from the experiment [22, 19] periodic flow rate injector was utilised and connected to the duct 2 of the single-cylinder methanol spark ignition engine model as shown in figure 4.2. Then muti-Wiebe function was selected for combustion modeling and the Wochni heat transfer model. Combustion models, the SI Wiebe and multi-wiebe models utilized the Wiebe function mode as discussed in the previous section.

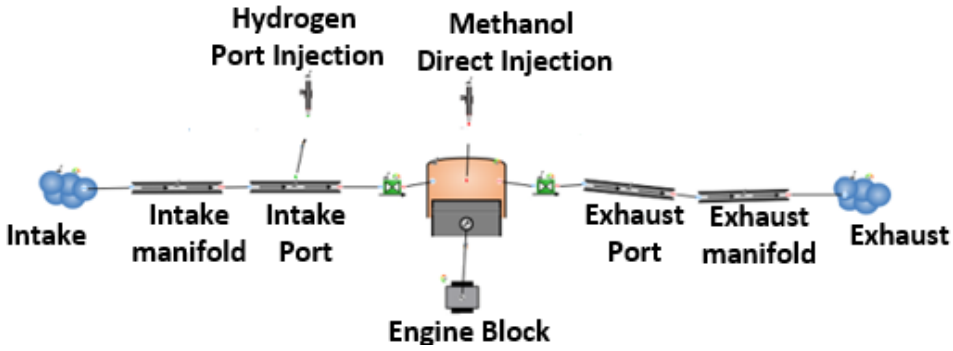

Figure 4.2: validation of 1-dimentional model single cylinder direct injection of methanol and hydrogen using port injection using Multi-Wiebe combustion

Percentage of the hydrogen addition:

The injection rate of the hydrogen for different proportions is computed using from mass flow rate of air. The mass flow rate of air is computed for the 4-stroke form engine speed and engine specification such as bore and stroke given by

$$\text{mass flow rate}_{\text{air}} = \frac{\pi}{4} \times (\text{bore})^2 \times \text{Stroke} \times \frac{\text{engine speed}}{2} \tag{4.1}$$

The percentage of hydrogen addition is calculated as previously discussed in Equation 3.60

Excess air ratio

To investigate different excess air ratio fuel injection rates of methanol adjusted for different proportions of hydrogen addition, the excess air ratio for neat methanol and methanol with hydrogen addition is computed by:

$$\lambda = \frac{\text{mass flow rate}_{\text{air}}}{\text{mass flow rate}_{H_2} \times \text{AF}_{H_2 st} + \text{mass flow rate}_{\text{CH}_3\text{OH}} \times \text{AF}_{\text{CH}_3\text{OH}st}} \tag{4.2}$$

Where $AF_{H_2,\text{st}}$ and $AF_{\text{CH}_3\text{OH},\text{st}}$ are the stoichiometric ratios of hydrogen and methanol, respectively. Then,mass flow rate_{air}, mass flow rate_{H_2}, and mass flow $\text{rate}_{\text{CH}_3\text{OH}}$ represent the mass flow rates (kg/hr) of air, hydrogen, and methanol, respectively.

Spark timing

Spark timing for methanol combustion with different percentages of hydrogen is determined by providing the start of combustion (SOC) to the Ricardo Wave solver. The start of combustion is defined in the Ricardo Wave solver using the Wiebe function. The Wiebe function is an empirical model used in internal combustion engine simulations to represent the mass fraction burned during the combustion process. This method involves

fitting the combustion curve to the Wiebe function parameters. The combustion curve fitting is calibrated using the combustion duration, the crank angle at which 50% of combustion takes place (CA50), and the shape factor of the Wiebe function. To validate different operating conditions, CA50 and combustion duration are assigned to the solver from the experimental results.

4.2 Validation results of 1 dimensional model

1-dimentional simulation model validation of Indicated men effective pressure

To quantify engine performance, Indicated Mean Effective Pressure (IMEP) was chosen to validate one-dimensional single-cylinder methanol spark ignition engine model with hydrogen enrichment under various excess air ratios. The validation of IMEP enabled the 1-dimensional numerical model to accurately predict the average pressure within the cylinder throughout the entire engine cycle, providing a direct correlation to engine efficiency and output. Validating IMEP at different excess air ratios enabled the determination of the accuracy of the Wiebe combustion curve fit function as shown in Figure 3.7 used in the one-dimensional model in Ricardo wave solver to capture the combustion process under different operating conditions.

Table 4.1: Engine Operating Condition

Parameter	**Value**
Engine speed	1200
Spark timing CA (bTDC)	20
Start of injection of methanol (CA bTDC)	80
Start of injection of Hydrogen (CA bTDC)	210
Bore (mm)	82.5
Compression ratio	9.6
Stroke (mm)	84.2

For the validation IMEP under various excess air ratio, the engine operating conditions presented in the table 4.1, based on the experimental work by Changming Gong, were utilized [19]. Experimental results [19] on the effect of IMEP for neat methanol and methanol with a 3% hydrogen addition under stoichiometric to lean operation, with excess air ratios ranging from λ=1 to λ=1.6, at manifold pressure of 0.7 bar were chosen to validate the one-dimensional simulation model. Validation was performed by assigning the CA50 data from C.Gong[19] experimental results of excess air ratios from λ=1 to λ=1.6 into the Wiebe function for combustion curve fitting. The excess air ratio in the one-dimensional Ricardo solver was obtained by adjusting the methanol injection rate for neat methanol operating conditions. For the 3% hydrogen addition operating condition,

the excess air ratio from λ=1 to λ=1.6 was simulated by fixing the injection rate of hydrogen and by adjusting methanol injection rate. The validation under-predicts the experimental result with less than 2% error shown in Figure 4.3

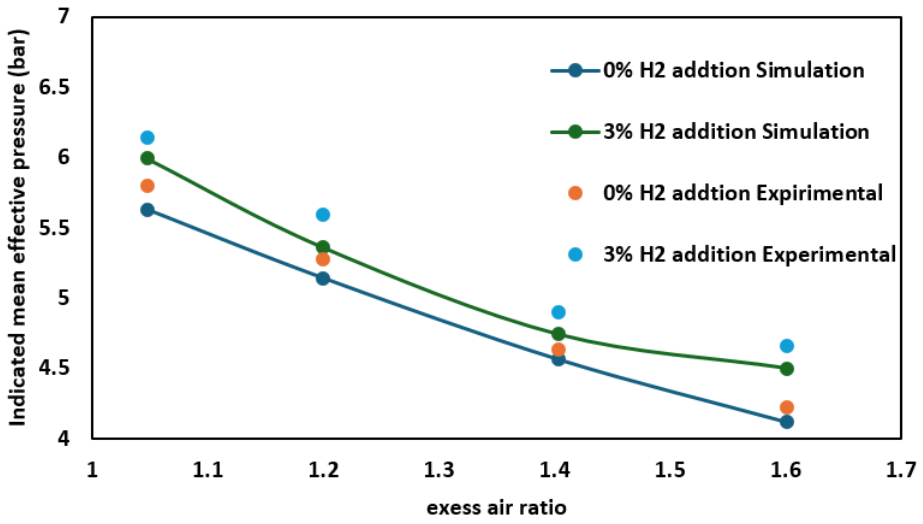

Figure 4.3: validation of the indicated mean effective pressure under different of methanol and methanol with 3% hydrogen addition

Validation of in-cylinder pressure

To investigate engine combustion performance and exhaust emissions, the in-cylinder pressure versus crank angle provides a detailed representation of pressure changes during the intake, compression, combustion, and exhaust strokes [39]. In order to enhance the accuracy of the combustion model and boundary conditions in Ricardo Wave, the in-cylinder pressure with respect to crank angle for different spark timings was chosen for validation. For the evaluation of in-cylinder pressure with respect to crank angle, the CA50 data from the experimental work [22] for each case was replicated into the Ricardo Wave solver, and the Wiebe combustion function was modelled accordingly. For validation, spark timings of 4, 12, 20, and 28 °CA bTDC for 6% hydrogen addition with methanol were selected based on the experimental work conducted by C Gong [18], with the operating conditions shown in the table at excess air ratio λ=1.4 and manifold pressure of 0.9 bar. The validation was performed using the multi-Wiebe combustion model in Ricardo Wave. The multi-Wiebe combustion model fitting was calibrated using the experimental data [18] for CA50 at the specified spark timings. The simulation results underpredicted the experimental results [22] with less than 2% error as shown in Figure 4.4

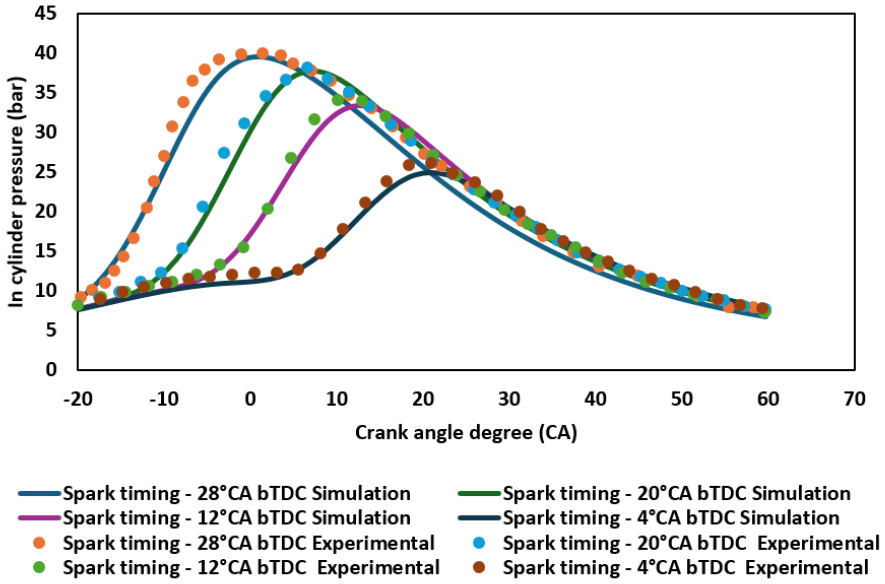

Figure 4.4: validation of In-cylinder pressure at spark timing 4°CA, 12°CA, 28 °CA 6% bTDC of 6% hydrogen addition with methanol

4.3 Effect of boosting of methanol spark ignition engine with hydrogen addition using 1-dimensional analysis

4.3.1 Operating conditions

To analyze the engine performance, Ricardo Wave 1-d solver is used. Ricardo wave solvers utilize Naiver-Strokes equations for analyzing the mass, momentum, and energy to solve compressible gas flow equation. A Genset 16-cylinder engine model from the Ricardo engine database was considered. Investigation is carried out by remodeling the 16- cylinder genset engine to single-cylinder engine operating conditions for simplicity of analysis, as shown in Figures 4.1 and 4.2. The engine's test conditions are shown in the flow diagram Figure 4.5 and its design parameters are shown in Table 4.2. To conduct engine operation with pure methanol as fuel, a single-cylinder direct injection model is created separately using a single Wiebe combustion model in the Ricado wave solver, as shown in Figure 4.1. Then to carry out the study on the combustion of methanol with hydrogen addition, a model for direct injected methanol with port injected hydrogen is created using the multi-Wiebe solver in Ricardo wave tool, which is shown in figure 4.2

Test matrix

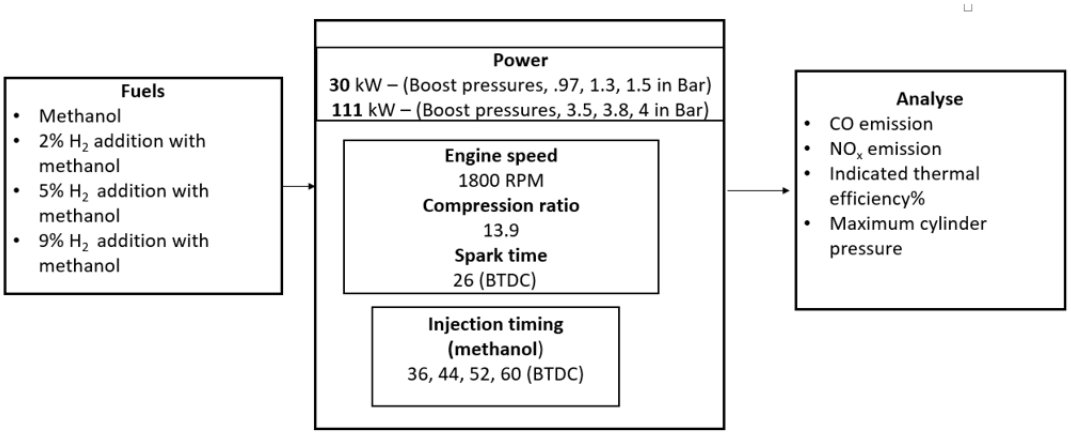

Figure 4.5: Test matrix

Table 4.2: Engine Specification

Parameter	**Value**
Type	50 liter Genset engine
Cylinder bore (mm)	159
Cylinder stroke (mm)	159
Engine compression ratio	13.9
Connection rod length (mm)	289.6

The study was carried out at an engine speed of 1800 RPM and the engine was simulated at the boost pressure conditions of 0.97, 1.3, 1.5 bar for fixed power 30 kW and 3.5, 3.8, 4.0 bar for fixed power of 111 kW. These power levels are considered in this study because for comparing the pure methanol combustion and that of the hydrogen-methanol blend, the data to calculate the laminar flame speed correlation for methanol-hydrogen combustion are only available between the equivalence ratios of 0.6 and 1.7, and the power levels are estimated using these values based on [69]. Then, the indicated thermal efficiencies, and CO/NOx emissions are investigated for each injection timing shown in Figure 4.5 (36, 44, 52, 60 °CA bTDC) under the directly injected fuel scenario from late to early 'start of injection' time before the combustion. In addition, constant power is maintained for each injection timing condition by altering the fuel flow rate (kg/hr) and injection duration (°CA). After that, to conduct a numerical study of pure methanol and hydrogen-methanol blend, spark ignition method is adopted to the genset engine model. The spark timing is fixed at 26 °CA bTDC. For the operating scenarios of pure methanol and methanol-hydrogen blend, a single Wiebe function and a multi-Wiebe function, two zone combustion models, respectively, are used on the Ricardo wave solver to determine

the start of combustion. The inputs for the single and multi-Wiebe functions are determined by using the laminar flame speed correlation function of methanol-hydrogen blends developed in [69] and by understanding the SI combustion model's laminar burning velocity correlation function developed in [11]. The solution of the laminar flame speed correlation function includes a 42-coefficient fit to determine the laminar flame speed for a given excess air ratio.

$$\theta_{50} = \theta_0 + \left(\frac{\ln(1-0.5)}{\ln 0.001}\right)^{\frac{1}{m+1}} \Delta\theta \tag{4.3}$$

where $\Delta\theta$ is the combustion duration and θ_{50} represents the crank angle at which 50% of the fuel is burned

$$DUR_{10-90} = \Delta\theta \left(\left(\frac{\ln(1-0.9)}{\ln 0.001}\right)^{\frac{1}{m+1}} - \left(\frac{\ln(1-0.1)}{\ln 0.001}\right)^{\frac{1}{m+1}} \right) \tag{4.4}$$

Then, the start of combustion θ_0 was computed by imputing the values of the crank angle position at 50% combustion (CA50) and the combustion durations (10%-90%) to the Ricardo wave solver [66].

$$w = 1 - \exp\left(-a\frac{\theta_t - \theta_0}{b} + 1\right) \tag{4.5}$$

θ_0 is the crank angle at the start of combustion, θ_t is the crank angle under consideration, 'a' (defines the end of combustion) and exponent 'b' (represents the shape of the combustion profile) are constants. Then, the scenarios of 2%, 5%, 9% H_2 addition are simulated by adjusting the fuel flow rate of H_2 as per the air flow rate [21, 22] and adjusting the methanol fuel flow rate to achieve the required power. The proportion of H_2 is determined by using eq(4.2)

The NOx emission is computed using the Ricardo wave solver and Zelkovas mechanism. The CO emission is computed by evaluating the unburned and burned zones derived from thermodynamic equilibrium. In addition to that, passive scalar values for NOx and CO are assigned to the solver, which then assist the solver in understanding the specific molecular weight and computing the targeted emissions.

4.4 Results and discussions

4.4.1 Carbon monoxide emissions

In this section discusses the carbon monoxide (CO) emissions observed during the investigation of a spark-ignition methanol engine with varying hydrogen enrichment. The

results were analyzed under two different power conditions (30 kW and 111 kW) with different injection timings and boost pressures, as illustrated in Figures 4.8 and 4.9 Figure 4.8 illustrates the CO emissions (ppm) when the engine is operated at a constant power of 30 kW under various boost pressures and hydrogen enrichment levels. Compared to neat methanol operation, hydrogen addition resulted in a decrease in CO emissions under all operating conditions. Additionally, varying the start of injection of methanol from 30°CA bTDC to 60°CA bTDC resulted in a decline in CO emissions across all scenarios. Focusing on the CO emissions at 60°CA bTDC injection timing, which proved to be the most effective, compared to neat methanol operation increase in hydrogen enrichment the results are as follows:

- At a boost pressure of 0.91 bar, compared to neat methanol, CO emissions were reduced by 52.5%, 60.5%, and 71.2% for 2%, 5%, and 9% hydrogen addition, respectively.
- At a boost pressure of 1.3 bar, CO emissions were reduced by 29.5%, 36%, and 86.4% for 2%, 5%, and 9% hydrogen addition, respectively, compared to neat methanol.
- At a boost pressure of 1.5 bar, CO emissions decreased by 6.9%, 28.8%, and 83.1% for 2%, 5%, and 9% hydrogen addition, respectively, compared to neat methanol.

Furthermore, an increase in boost pressure from 0.97 to 1.3 bar resulted in a 63.5%, 45.8%, 40.8%, and 82.7% decrease in CO emissions for neat methanol, 2%, 5%, and 9% hydrogen addition with methanol, respectively. Additionally, an increase in boost pressure from 0.97 to 1.5 bar resulted in a 75.1%, 51.1%, 55.1%, and 85.4% decrease in CO emissions for neat methanol, 2%, 5%, and 9% hydrogen addition with methanol, respectively. These results highlight the significant impact of hydrogen enrichment and optimized injection timing on reducing CO emissions in methanol-fueled engines.
Figure 4.9 illustrates the CO emissions for the engine operating at a constant power of 111 kW under various boost pressures and hydrogen enrichment levels. Compared to neat methanol operation, hydrogen addition resulted in a decrease in CO emissions under all operating conditions. Additionally, varying the start of injection of methanol from 30°CA bTDC to 60°CA bTDC resulted in a decline in CO emissions across all scenarios. Focusing on the CO emissions at 60°CA bTDC injection timing, which proved to be the most effective, the results compared to neat methanol operation addition of hydrogen are as follows:

- At a boost pressure of 3.5 bar, compared to neat methanol, CO emissions were reduced by 32.1%, 61%, and 68.3% for 2%, 5%, and 9% hydrogen addition, respectively.

- At a boost pressure of 3.8 bar, CO emissions were reduced by 23.6%, 61.6%, and 80.4% for 2%, 5%, and 9% hydrogen addition, respectively, compared to neat methanol.
- At a boost pressure of 4 bar, CO emissions decreased by 9.3%, 58.5%, and 81.1% for 2%, 5%, and 9% hydrogen addition, respectively, compared to neat methanol.

Furthermore, an increase in boost pressure from 3.5 to 3.8 bar resulted in a 28.7%, 19.8%, 29.9%, and 56.0% decrease in CO emissions for neat methanol, 2%, 5%, and 9% hydrogen addition with methanol, respectively. Additionally, an increase in boost pressure from 3.5 to 4 bar resulted in a 47.2%, 29.4%, 43.8%, and 68.5% decrease in CO emissions for neat methanol, 2%, 5%, and 9% hydrogen addition with methanol, respectively.

Higher boost pressures generally resulted in lower CO emissions for both power levels (30 kW and 111 kW). This reduction is attributed to better air-fuel mixing and more complete combustion. Overall, CO emissions were higher in naturally aspirated mode (0.97 bar boost pressure) due to the rich air-fuel mixture required to operate the engine. At 111 kW power, CO emissions were reduced compared to the 30 kW power scenario it is because the engine was able to operate at a lean mixture at higher power level of 111 kw. CO emissions were further reduced when the start of methanol injection was varied from late to early timings (35 °CA to 60 °CA bTDC). Early injection timing accelerates the fuel evaporation process during ignition, resulting in more efficient combustion. Furthermore, CO emissions are reduced when the start of injection of methanol is varied from late to early timings (35 °CA to 60 °CA bTDC) for all the test conditions. This is because the early injection timing speeds up the evaporation process of fuels during injection [93, 2].

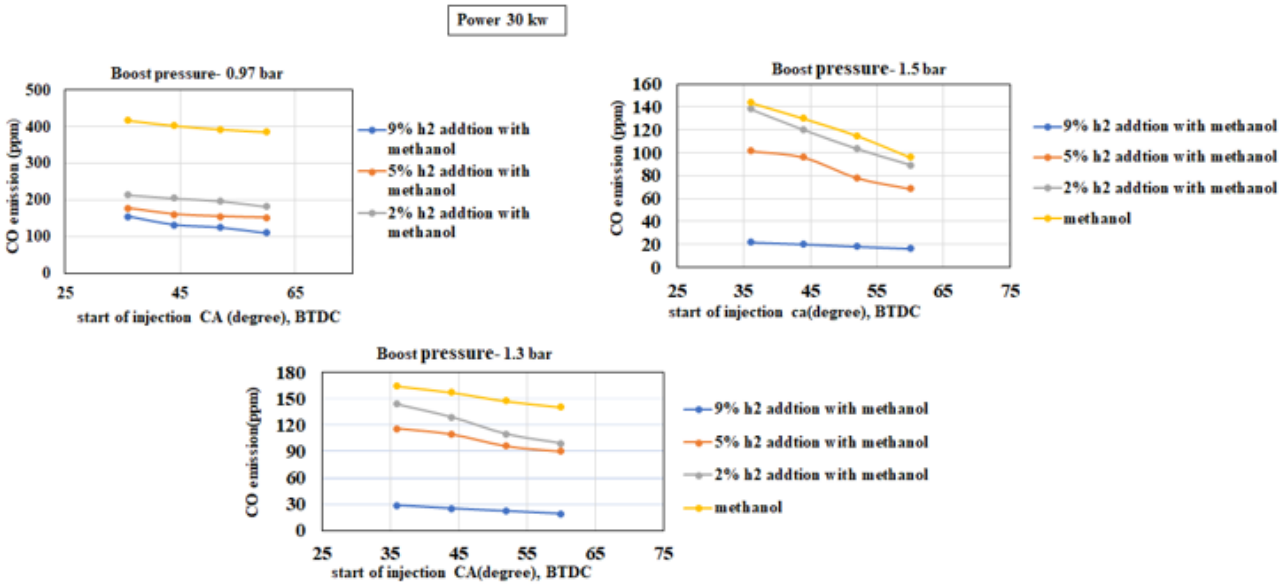

Figure 4.6: Carbon monoxide emissions when the engine is operated at 30 kW power

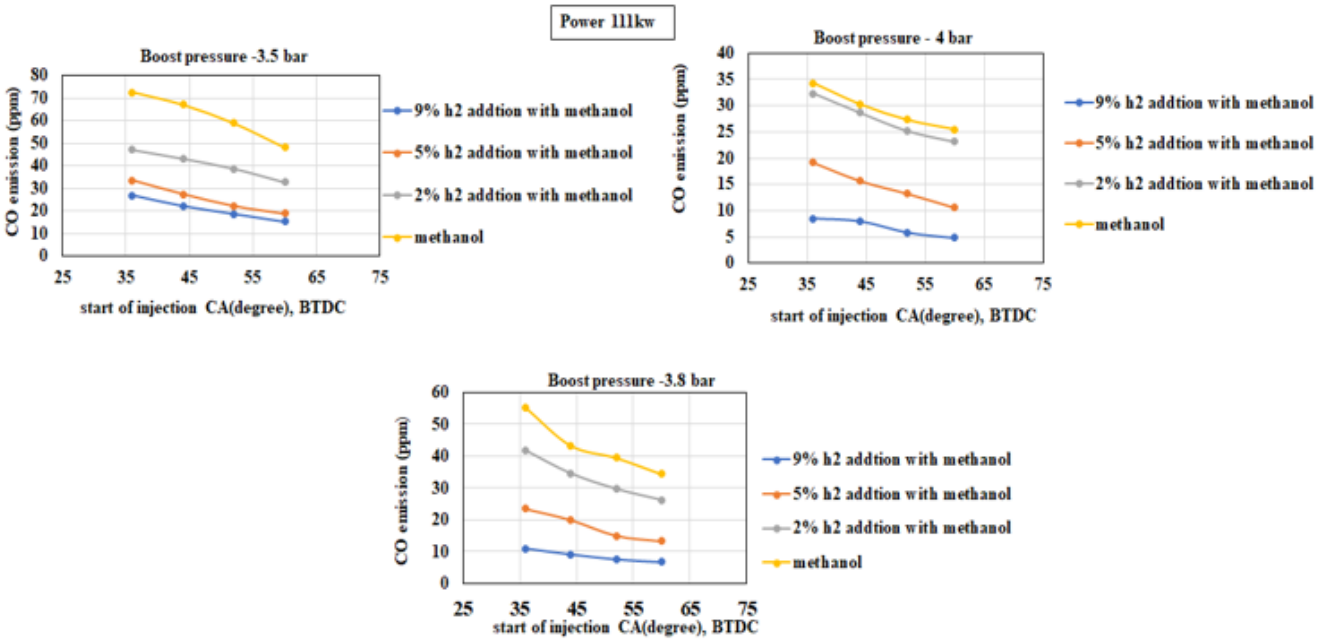

Figure 4.7: Cabon monoxide emissions when the engine is operated at 111 kW

4.4.2 NOx emissions

In this section discusses the nitric oxide (NOX) emissions observed during the investigation of a spark-ignition methanol engine with varying hydrogen enrichment. The results were analysed under two different power conditions (30 kW and 111 kW) with different injection timings and boost pressures, as illustrated in Figures 4.10 and 4.11. Figure 4.10 illustrates the NOx emissions when the engine is operated at a constant power of 30 kW under various boost pressures and hydrogen enrichment levels. Compared to neat methanol operation, hydrogen addition resulted in increased NOx emissions under all operating conditions. Additionally, varying the start of injection of methanol from 30°CA bTDC to 60°CA bTDC resulted in a decline in NOx emissions across all scenarios. Focusing on the NOx emissions at 60°CA bTDC injection timing, which proved to be the most effective, compared to neat methanol operation increase in hydrogen enrichment the results are as follows:

- At a boost pressure of 0.91 bar, compared to neat methanol, NOX emissions increased by 68.5%, 155.3% and 693.8% for 2%, 5%, and 9% hydrogen addition, respectively.
- At a boost pressure of 1.3 bar, NOx emissions increased by 4.0%, 87.4% and 177.9% for 2%, 5%, and 9% hydrogen addition, respectively, compared to neat methanol.
- At a boost pressure of 1.5 bar, NOx emissions incresed by 2.4%, 16.2% and 29.0% for 2%, 5%, and 9% hydrogen addition, respectively, compared to neat methanol.

Furthermore, an increase in boost pressure from 0.97 to 1.3 bar resulted in 83.0%, 89.5%,87.6% and 94.1% decrease in NOX emissions for neat methanol, 2%, 5%, and 9% hydrogen addition with methanol, respectively. Additionally, an increase in boost pressure from 0.97 to 1.5 bar resulted in 86.5%, 91.8%, 93.8% and 97.8% decrease in NOX emissions for neat methanol, 2%, 5%, and 9% hydrogen addition with methanol, respectively.
Figure 4.11 illustrates the NOX emissions for the engine operating at a constant power of 111 kW under various boost pressures and hydrogen enrichment levels. Compared to neat methanol operation, hydrogen addition resulted in an increase in NOX emissions under all operating conditions.Additionally, varying the start of injection of methanol from 30°CA bTDC to 60°CA bTDC resulted in a decline in NOX emissions across all scenarios. Focusing on the NOX emissions at 60°CA bTDC injection timing, which proved to be the most effective, the results compared to neat methanol operation addition of hydrogen are as follows:

- At a boost pressure of 3.5 bar, compared to neat methanol, NOX emission increase by 32.1%, 61%, and 68.3% for 2%, 5%, and 9% hydrogen addition, respectively.
- At a boost pressure of 3.8 bar, NOX emissions increased by 23.6%, 61.6%, and 80.4% for 2%, 5%, and 9% hydrogen addition, respectively, compared to neat methanol.
- At a boost pressure of 4 bar, NOX emissions increased by 9.3%, 58.5%, and 81.1% for 2%, 5%, and 9% hydrogen addition, respectively, compared to neat methanol.

Furthermore, an increase in boost pressure from 3.5 to 3.8 bar resulted in a 28.7%, 19.8%, 29.9%, and 56.0% decrease in NOX emissions for neat methanol, 2%, 5%, and 9% hydrogen addition with methanol, respectively. Additionally, an increase in boost pressure from 3.5 to 4 bar resulted in a 47.2%, 29.4%, 43.8%, and 68.5% decrease in NOX emissions for neat methanol, 2%, 5%, and 9% hydrogen addition with methanol, respectively. From the results observed for low power 30 kw and 111 kw power increase hydrogen addition resulted in increase in NOx emission. This could be because hydrogen has higher flame propagation properties and its adiabatic flame temperature compared to methanol [86]. An increase in the higher hydrogen addition resulted in cylinder temperature which would increase NOX emission. Then at fixed power of 30kw and 111kw, the increase in boost pressure resulted in a decrease in NOx emissions this could be because the increase in the boost pressure for the fixed power operation resulted increase in the charge motion inside the cylinder which enhanced the lean combustion of fuel and air mixture. Furthermore retarding the injection time from 30°CA bTDC to 60°CA bTDC resulted in a decline in NOx emissions this could be fuel and air mixing quality is improved which could help to reduce the cylinder temperature for the fixed power operation scenarios.

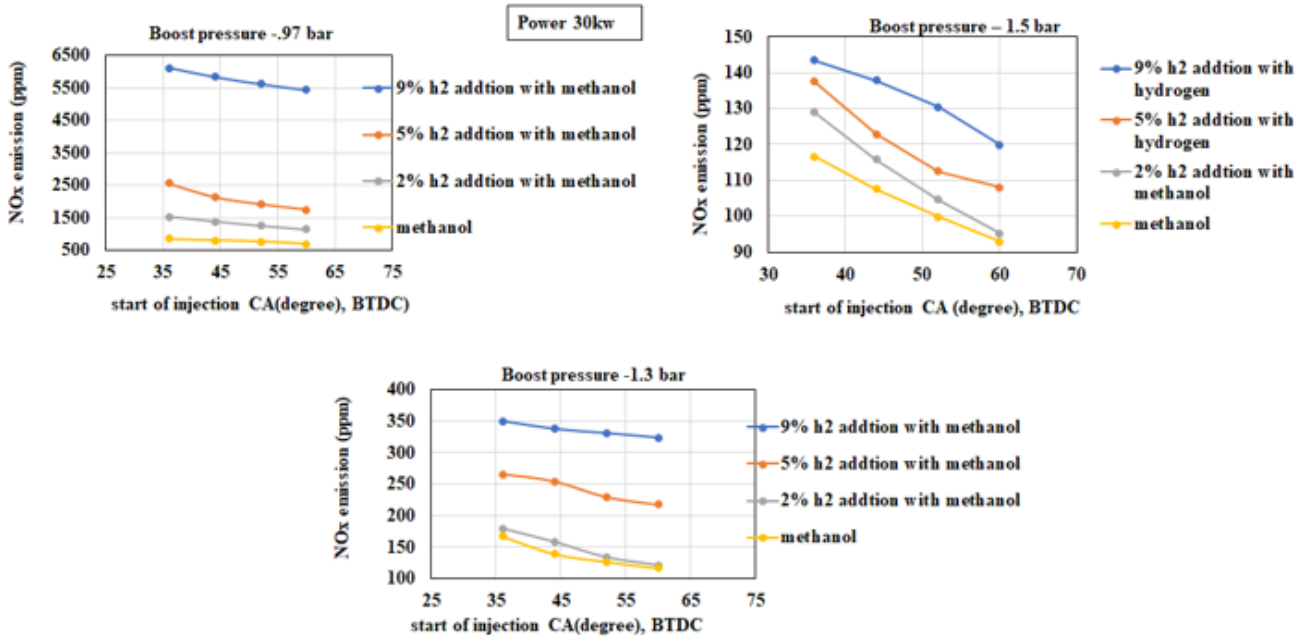

Figure 4.8: NOx emissions when the engine is operated at 30 kW power

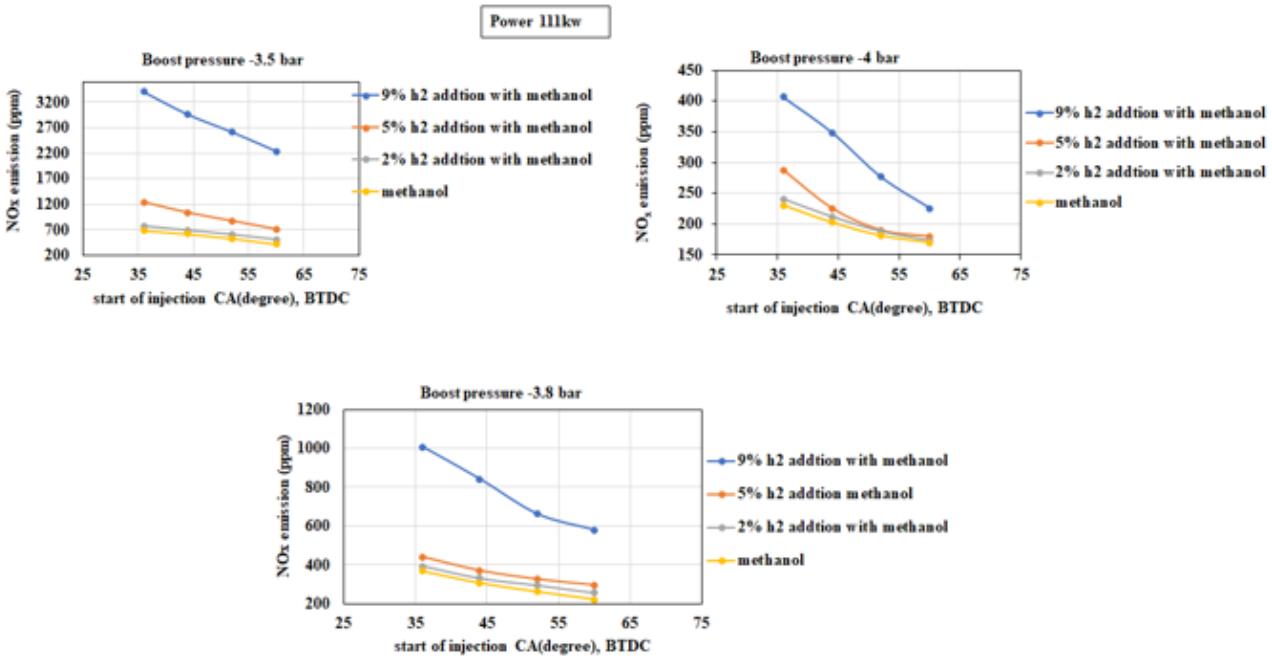

Figure 4.9: NOx emissions when the engine is operated at 111 kW power

4.4.3 Indicated thermal Efficiency

Figure 4.11 illustrates the indicated thermal efficiency of the engine under two different power conditions: high power (111 kW) with a high boost pressure of 4 bar, and low power (30 kW) with a high boost pressure of 1.5 bar. The results show significant improvements in thermal efficiency with the addition of hydrogen to methanol across various injection timings. For the low power condition of 30 kW and boost pressure of 1.5 bar, the addition of hydrogen resulted in notable increases in indicated thermal efficiency. Specifically, a 2% hydrogen addition led to a 12.5% increase, 5% addition resulted in a 14.2% increase, and 9% addition yielded a 20.4% increase in thermal efficiency. These improvements are primarily attributed to the higher calorific value of hydrogen compared to methanol, which facilitates leaner combustion and enhances thermal efficiency. At the high power condition of 111 kW and a boost pressure of 4 bar, similar trends were observed. The inclusion of 2% hydrogen resulted in a 6.2% increase in indicated thermal efficiency, 5% hydrogen led to a 12.6% increase, and 9% hydrogen produced a 13.1% increase. The higher power levels and increased manifold pressure contribute to more efficient combustion due to the greater density of the air-fuel mixture entering the combustion chamber, thus boosting thermal efficiency. Overall, the indicated thermal efficiency improved with an earlier start of injection for all test conditions, highlighting the combined benefits of hydrogen enrichment and optimized injection timing on engine performance. At the higher power level of 111 kW and higher manifold pressure, lean air-fuel combustion was achieved due to the increased density of the air-fuel mixture, further enhancing thermal efficiency.

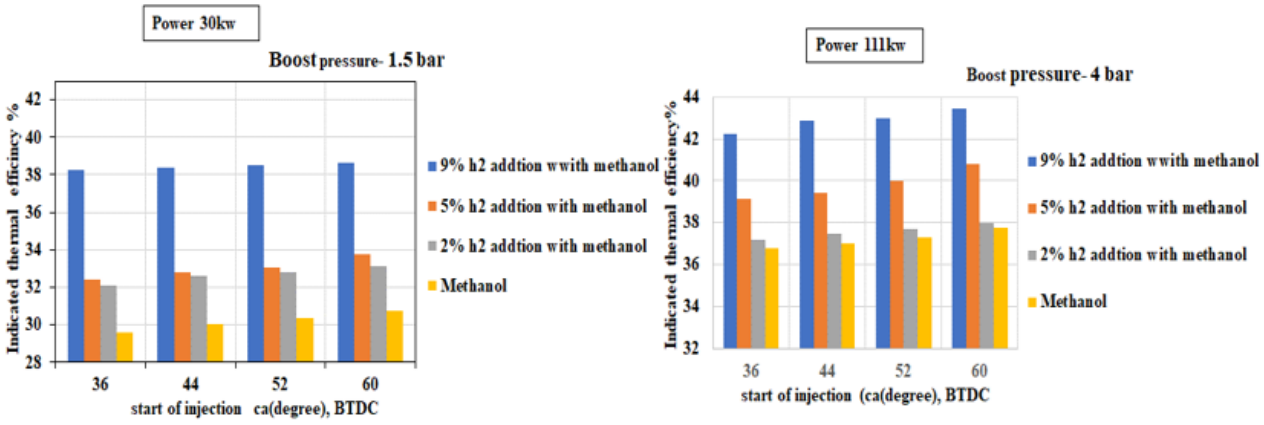

Figure 4.10: Indicated thermal efficiency under 30kW and 111kw power at high boost pressure(1.5 bar and 4 bar)

4.4.4 Combustion characteristics

Maximum cylinder pressure and heat release rate

Figure 4.13 illustrates the maximum cylinder pressure and heat release rate comparison for the two power conditions 30 kW and 111 kW at high boost pressures (1.5 bar and 4 bar). Higher engine power (111 kW) operation increases the cylinder pressure and heat release rate for all the test conditions. Moreover, heat release rate and in-cylinder pressure are increased in 3%,5% and 9% hydrogen with methanol. Specifically compared to the neat methanol operation under 30 kw and 111 kw power increase in the 3%,5%,9% hydrogen addition resulted in the 18%,26% and 72% increase in the maximum in-cylinder pressure and heat release rate. This is due to the faster flame propagation behaviour of hydrogen and an increase in the excess air ratio. Therefore, the addition of hydrogen speeds up the fuel-air mixing during combustion [86, 20].

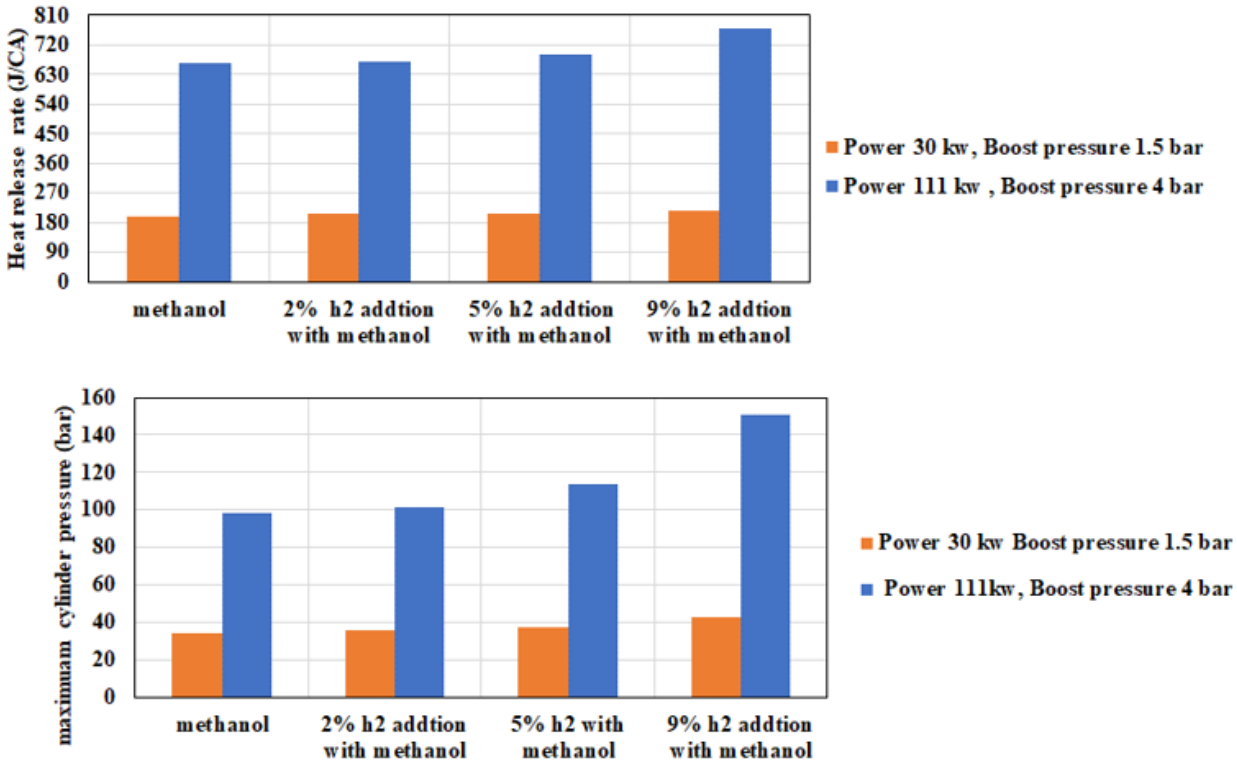

Figure 4.11: Maximum cylinder pressure and heat release rates at engine operation of 30 kW and 111 kW at high boost pressures (1.5 bar and 4 bar))

4.5 Summary

Validation of 1-Dimensional single cylinder model

The validation aimed to understand the accuracy of 1-dimensional analysis software using the Wiebe function in relation to experimental setups for analyzing engine performance.The effect of indicated mean effective pressure for neat methanol and methanol with various levels of hydrogen enrichment was evaluated for different excess air ratios based on published experimental works [19]. The in-cylinder pressure trace was validated against experimental results [22] under different spark timings of neat methanol and methanol with varying levels of hydrogen addition operating conditions. The validation showed that the 1-dimensional simulation results underpredicted the experimental results with less than 2% error.

Effect of Boosting at High and Low Load Conditions

Engine performance was analyzed using the Ricardo Wave 1-D solver under fixed power levels of 30 kW and 111 kW with varying boost pressures and injection timings. The indicated thermal efficiencies and CO/NOx emissions were investigated for each condition as follows:

- **CO Emissions:** CO emissions were significantly reduced with hydrogen injection compared to neat methanol operation. Higher boost pressures resulted in lower CO emissions due to better air-fuel mixing and more complete combustion.
- **NOx Emissions::** NOx emissions increased with higher hydrogen enrichment due to hydrogen's higher flame propagation properties. However, increasing boost pressure resulted in a decrease in NOx emissions due to enhanced lean combustion. Retarding the injection timing also led to a decline in NOx emissions.
- **Indicated Thermal Efficiency:** Indicated thermal efficiency improved with hydrogen addition and optimized injection timing. Higher power levels and increased manifold pressure contributed to more efficient combustion.
- **Combustion Characteristics:** Higher engine power operation increased the cylinder pressure and heat release rate for all test conditions. Hydrogen addition further increased these parameters due to faster flame propagation.

To overcome the limitations of the Ricardo Wave solver in predicting the combustion process for methanol and methanol with hydrogen addition, the laminar flame speed correlation for methanol and methanol with hydrogen addition was superimposed into the SI and multi-Wiebe functions in the Ricardo Wave solver under different operating conditions. From this study, limitations in the Ricardo Wave solver's ability to predict

combustion duration, in-cylinder mixing, and flame propagation were noted. Due to these limitations, a detailed study of the combustion process was conducted using a 3-dimensional numerical modelling approach in the further chapters.

Chapter 5

Hydrogen enrichment in methanol SI engine at varying injection timing during compression stroke

In this chapter the computational fluid dynamics (CFD) model explores the impact of varying the in-cylinder injection timings of methanol for different amounts of hydrogen addition through the intake port. This study examines the effect of methanol injection at 150, 120, 80, and 60 °CA bTDC during the compression stroke when the hydrogen concentration in the engine was varied from 0 to 12%. Then late injection limit on mixing and combustion performance of neat methanol as well as hydrogen enrichment operation have been considered for different spark timing. This study explores salient parameters such as in-cylinder mixing, combustion characteristics, and formation of gaseous and soot emissions for the above-mentioned operating conditions.The study explored in this chapter is published in the International Journal of hydrogen[38].

5.1 Operating condition

The operating conditions for the methanol-fueled spark-ignition engine were tested using methanol direct injection at 150°, 120°, and 80° CA bTDC during the compression stroke, with hydrogen concentrations varied at 3%, 9%, and 12%. The tests were conducted with fixed parameters, including an injection pressure of 110 bar, an equivalence ratio of 0.71, a manifold air pressure of 90 kPa, a compression ratio of 9.6, and an engine speed of 1200 RPM. The engine was operated with a fixed spark timing of 20° CA TDC. The analysis focused on in-cylinder mixing, and combustion characteristics, and indicated specific CO and NOx emissions, and soot emissions under these conditions. Additionally, to explore the late injection limits of methanol, the study investigated the effects of late methanol injection at 60° CA bTDC, with spark timings of 20°, 15°, 10°, and 4° CA. The impact of

hydrogen enrichment (ranging from 3% to 12%) on in-cylinder fuel and air mixing was also examined for methanol injection at 60° CA bTDC.

Table 5.1: Simulation Conditions

Injection timing [°CA bTDC]	150	120	80	60
Spark timing [°CA bTDC]	20	20	20	20 – 4
Hydrogen addition [increments of 3%]	0 – 12	0 – 12	0 – 12	0 – 12

Model setup

The computational simulation of methanol direct injection was conducted using the K-H model with the Rayleigh-Taylor mechanism. The extended Zeldovich mechanism was incorporated into the CFD model to compute NO emissions, and the Hiroyasu-NSC soot model was employed to assess soot at different equivalence ratios, spark timings, and hydrogen addition as mentioned in chapter 3.

Hydrogen addition

The 3%, 9%, and 12% hydrogen addition was simulated using port injection. The hydrogen was added to methanol as a volume fraction of the intake air as mentioned in equations 3.60 and 3.61.

Excess air combustion equation of the methanol with hydrogen addition

$$\begin{aligned} &CH3OH + x \cdot H2 + \left(E \cdot 1.5 \cdot \frac{(2 + 2 \cdot (1 + x/2)) - 1}{3}\right) \cdot \left(O2 + \frac{79}{21} N2\right) \\ &\rightarrow CO2 + \left(2 \cdot \left(1 + \frac{x}{2}\right)\right) H2O \\ &\quad + \left(1.5 \cdot \frac{((2 + 2 \cdot (1 + x/2)) - 1)}{3} \cdot E \cdot \frac{79}{21}\right) N2 \\ &\quad + \left(\left(E \cdot 1.5 \cdot \frac{(2 + 2 \cdot (1 + x/2)) - 1}{3}\right) - 0.5 - \left(\frac{2 \cdot (1 + x/2)}{2}\right)\right) O2 \end{aligned} \tag{5.1}$$

where E is the excess air ratio and x is % of hydrogen addition.

In the simulation, the boundary conditions were set up to accurately reflect the chemical composition of the inflowing mixture. The mass fractions of the species were calculated based on the excess air ratio combustion equation to ensure the correct proportions of fuel and oxidizer. To simulate hydrogen addition using port injection, the mass fractions of hydrogen for the required proportion were applied to the intake port using inflow boundary conditions, along with the appropriate mass fractions of oxygen and nitrogen.This approach ensures that the inflowing mixture entering the combustion chamber represents

the stoichiometric balance required for optimal combustion, thereby providing realistic conditions for the simulation.

5.2 Results and discussion

5.2.1 In-cylinder characteristics

In-cylinder pressure

The injection timing effect on the in-cylinder pressure variations for neat methanol SI engine at an injection timing of 150, 110 and 80 °CA bTDC are presented in Figure 5.1. It can be observed that the in-cylinder pressure did not vary significantly for methanol injection timing between 80 and 110 °CA bTDC, where the magnitudes of in-cylinder peak pressures were 5.38 MPa and 5.28 MPa, respectively. But, with the advancement of injection to 150 °CA bTDC, the peak pressure reduced by 17% compared to the case when methanol was injected at 80 °CA bTDC. This was due to the accumulation of rich stratified regions of fuel-air mixture within the chamber during compression which also causes a drop in OH concentration during the combustion process that will later be discussed in Figures. 5.4-9.

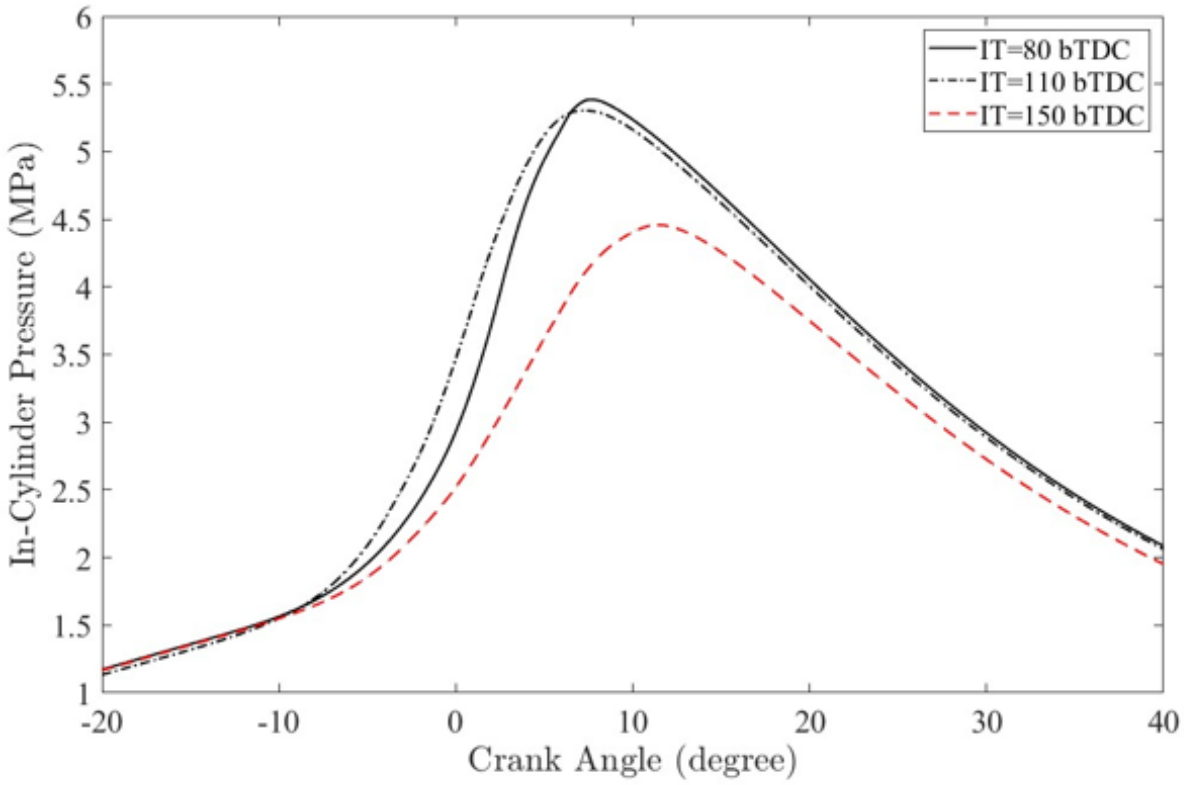

Figure 5.1: Results for in-cylinder pressure of neat methanol at injection timings of 150, 110 and 80 °CA bTDC.

Figure 5.2 represents the variation of in-cylinder pressure for varying percentages of hydrogen addition (0-12%) at an injection timing of 80 °CA bTDC when maintained at an equivalence ratio of 0.71. It can be seen that by increasing the hydrogen addition up to 9% the combustion rate was enhanced due to higher flame speeds of hydrogen and its adiabatic flame temperature compared to neat methanol, similar effects were also observed in [86]. The in-cylinder pressure rise can be related to the advancement of the position of peak cylinder pressure by 5 °CA with 3% hydrogen and by 6 °CA with 9% hydrogen compared to 0% hydrogen addition. Meanwhile, the peak in-cylinder pressure increased by 6.7% and 7.0% for 3% hydrogen addition and 9% hydrogen addition respectively compared to pure methanol operation. The benefit of hydrogen enrichment on the combustion characteristics was not observed for 12% hydrogen addition. Where the peak in-cylinder pressure reduced compared to 9% hydrogen addition. This may be associated with lower volumetric energy density of hydrogen which at higher percentages could result in lower overall energy content of the mixture inside the cylinder which was also noticed in [20].

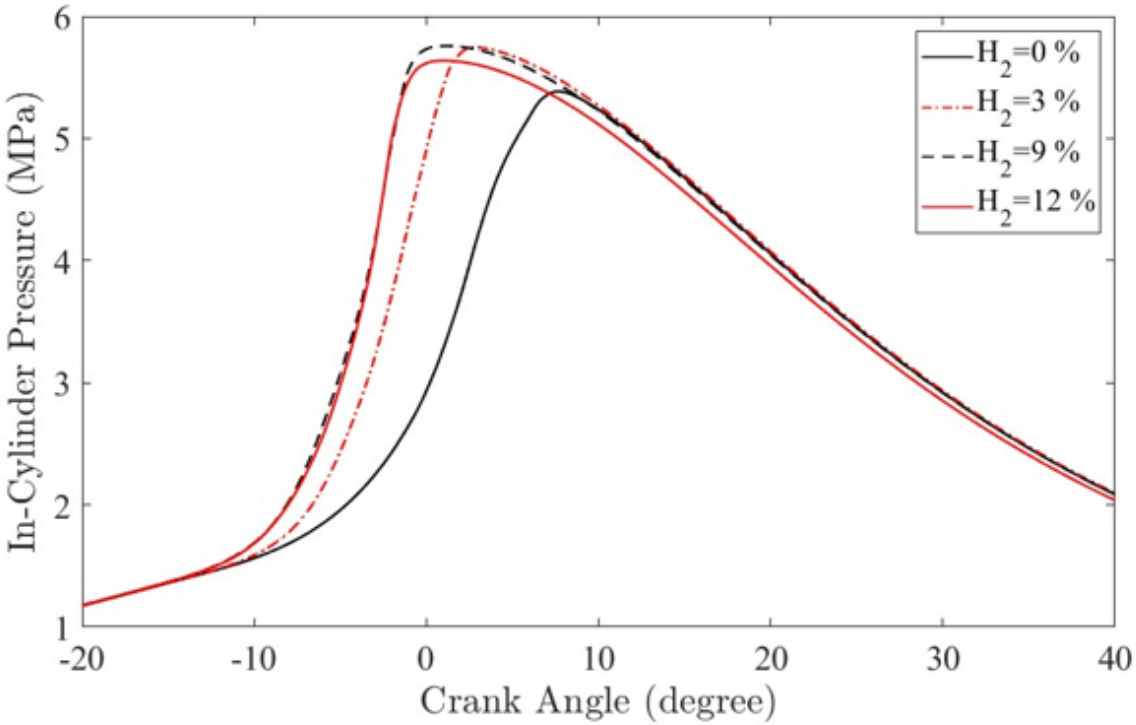

Figure 5.2: Results for in-cylinder pressure with various hydrogen additions of 0%, 3%, 9% and 12% at fixed injection timing of 80 °CA bTDC,at a spark timing of 20 °CA bTDC (ϕ=0.71,CR=9.6,MAP=90kPa,N=1200 RPM)

Figure 5.3 presents the simulated peak in-cylinder pressure values at different injection timings, with hydrogen additions ranging from 0 to 12%, at a fixed spark timing of 20°CA bTDC. The peak pressure was highest when methanol was injected at 80°CA bTDC, while the peak cylinder pressure was relatively lower at 150°CA for various levels of hydrogen addition (0%, 3%, 9%, 12%) with methanol. As can be seen from Figs. 3 and 5, the injection timing of 110°CA and 80 °CA bTDC did not have much impact on peak in-cylinder pressure for neat methanol as well as for 3%, 9% and 12% hydrogen addition, the difference was in the order of 1.5% greater for injection timing of 80 °CA bTDC. The data presented in Fig. 5 reveal that for the considered injection timings of 150, 110 and 80 °CA bTDC, the peak cylinder pressure increased with hydrogen addition and thereafter tends to decrease with 12% hydrogen injection. But when methanol was injected late at 60 °CA bTDC, the peak pressure was observed to be higher for 12% hydrogen addition when compared to 9% hydrogen addition. The mixing time was significantly reduced, no combustion occurred for neat methanol and for 3% hydrogen addition but combustion was initiated with the addition of 9% hydrogen. The peak pressure was observed to be higher for 12% hydrogen addition when compared to 9% and this could be due to hydro-

gen having faster flame propagation that enhanced combustion, particularly during late injection when the mixing time was relatively inadequate compared to earlier injection events.

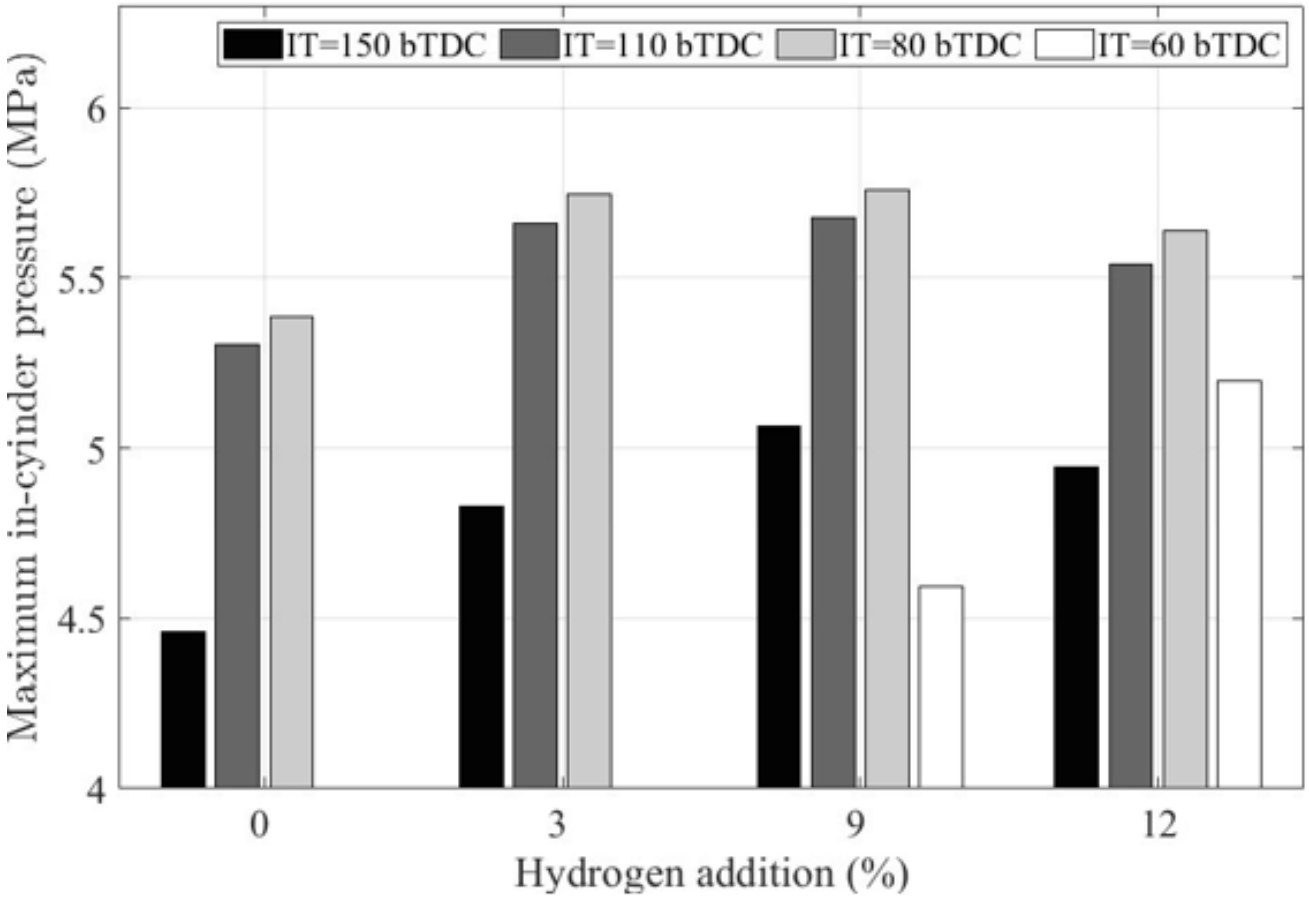

Figure 5.3: Maximum in-cylinder pressure values for different hydrogen additions at different injection timings (ST=20 °CA bTDC, =0.71, CR=9.6, MAP=90kPa, N=1200 RPM).

In-cylinder mixing

Injection timing is a crucial parameter that controls in-cylinder mixing and combustion, the impact of early and late injection timings on the local equivalence ratio of the charge in the cylinder just before the occurrence of spark at 20 °CA bTDC is presented in Figure. 5.4 for various injection timing of 150, 110, 80, and 60 °CA bTDC. The injection of methanol at 150 °CA bTDC resulted in an accumulation of fuel on one side of the cylinder as shown in Figure 5.4. The presence of relatively higher fuel concentration on the piston crown and cylinder wall towards the side of the intake valve was noticed in the x-z and x-y plane, which suggests the occurrence of fuel impingement on the cylinder

wall due to the location of injector, and the associated spray-air interactions. During the compression process the tumble motion caused the fuel droplets to be transported to one side of the cylinder.This leads to an asymetric distribution of a richer mixture at the later stages of the compression stroke, similar kinds of fuel distribution patterns have been observed in [117]. When the start of injection was delayed from 150 to 110 or 80 °CA bTDC, a reduction in the uneven distribution of fuel-air mixture at the later stages of the compression stroke was observed for neat methanol and also for cases with hydrogen addition. Injecting methanol later than 80 °CA bTDC resulted in very ultra-lean mixtures in the regions surrounding the spark plug as can be seen in Figure 5.4 for injection at 60 °CA bTDC case. The differences in fuel-air mixture distribution in the chamber closer to the initiation of spark for early and later injection timings could be due to maintaining the same magnitude of 110 bar injection pressure. This led to wall impingement, fuel film formation that affects evaporation and mixing for early injection timing of 150 °CA, whilst this effect was minimised for later injection timings and similar observations have been reported in [108, 71, 55]. The effect of in-cylinder flow field on mixing and transport of injected fuel spays during the compression stroke for different injection timings (150 °CA bTDC, 110 °CA bTDC and 80 °CA bTDC) of neat methanol and 9% hydrogen addition are presented in Figure.5.5 The simulation analysis revealed that during the early stages of the compression process, two counter-rotating vortices were observed, one on either sides of the cylinder when viewed in the x-y plane. This is in line with [63]. When methanol was injected at 150 °CA bTDC, it could be observed that during the compression stroke at 69 °CA bTDC, the velocity field at the left side of the cylinder transports the fuel-air fuel mixture towards the wall and to the cylinder head as can be seen at 57 °CA bTDC. Subsequently, at a later phase of the compression stroke at 20 °CA bTDC a rich fuel-air mixture accumulated below the intake valve region in the cylinder head as shown both in Figure 5.4 and 5.5. When the injection time was retarded to 110 °CA bTDC, the accumilation of a rich concentration of fuel-air mixture that was observed at 150 °CA bTDC injection timing towards the left side of the cylinder wall was reduced significantly at 69 °CA bTDC, 57 °CA bTDC and 20 °CA bTDC due to relatively improved evaporation and mixing. Also, in Figure 5.5, a thin film of rich fuel mixture was formed at 69 °CA bTDC on the right side of piston crown, which was subsequently vaporised and mixed by the counter rotating vortices. Furthermore, when the methanol injection timing was retarded further to 80 °CA bTDC, a rich mixture was observed at the center of the piston bowl during upward motion at 69 °CA bTDC due to spray tip impingement on the piston. Later at 57 °CA bTDC, the fuel-rich regions were transported by the counter-rotating vortices towards the left side of the piston bowl to mix further and to form a uniform mixture in the vicinity of the spark plug. Retarding the fuel injection timing to 80 °CA bTDC in comparison to injection timings at 150 °CA bTDC and 110 °CA bTDC resulted in a favourable interaction between the injected

methanol sprays and charge motion, which resulted in a uniform distribution of mixture at the time of initiation of spark. The addition of hydrogen to methanol resulted in a decrease in the accumulation of rich fuel-air mixture on the left side of the cylinder wall, compared to pure methanol. Specifically, at injection timings 150 °CA bTDC and 110 °CA bTDC, as can be seen in Figure. 5.5.During the compression process at 69 °CA bTDC, 57 °CA bTDC, and 20 °CA bTDC an enhanced uniformity of fuel-air mixing was observed for 9% of hydrogen addition, this improved mixing may be attributed to [92]. Inorder to maintain a global equivalence ratio of 0.71, therefore the quantity of methanol fuel droplets had to be reduced when hydrogen was added. Reducing the amount of fuel droplets may also reduce the fuel film formation. Additionally, the presence of hydrogen also contributes to enhanced mixing and combustion [92, 105].

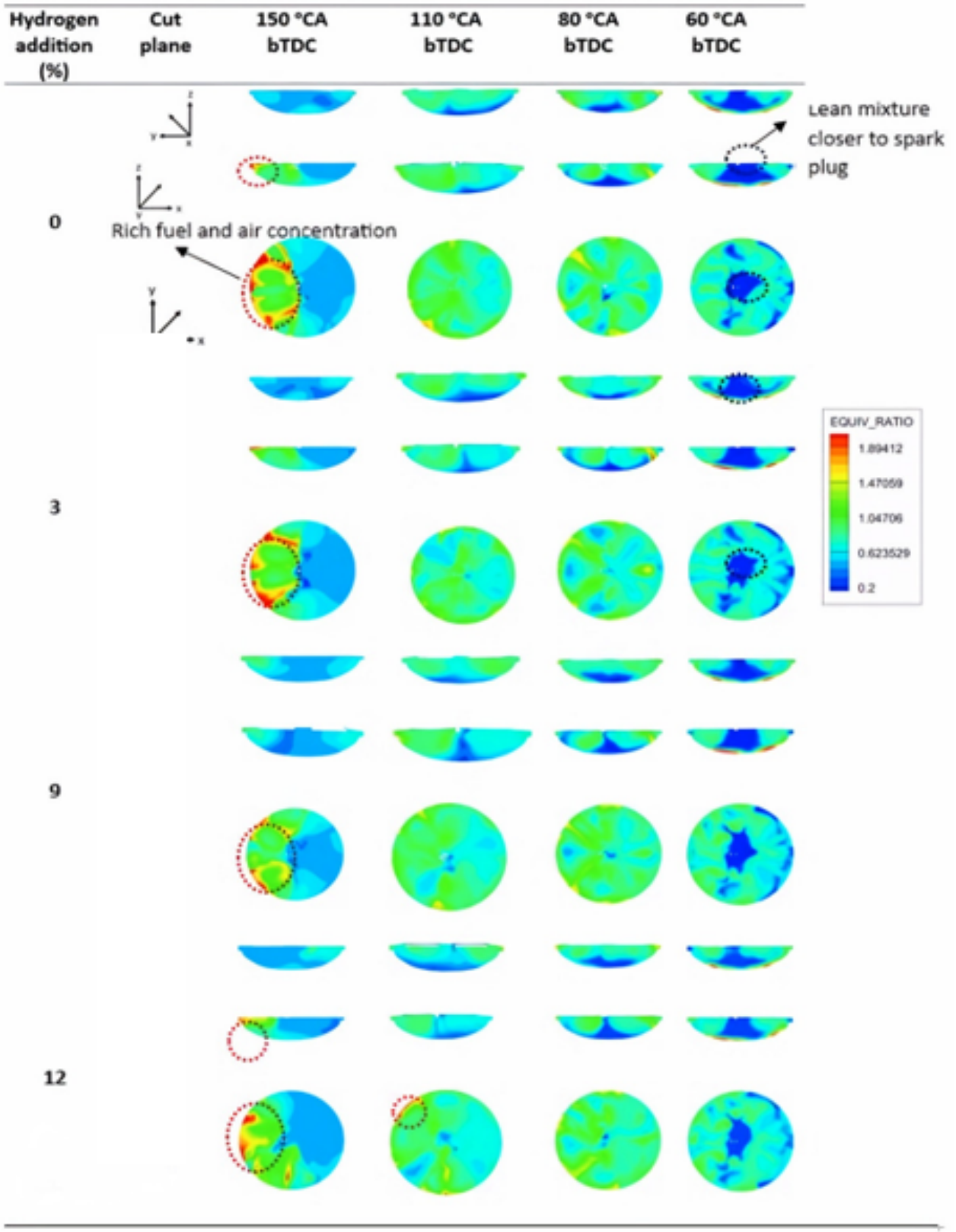

Figure 5.4: Comparison of in-cylinder mixing for various hydrogen additions (0, 3, 9 and 12%) and injection timings (150, 120, 80 and 60°CA bTDC) just before the initiation of spark at 20 °CA bTDC.

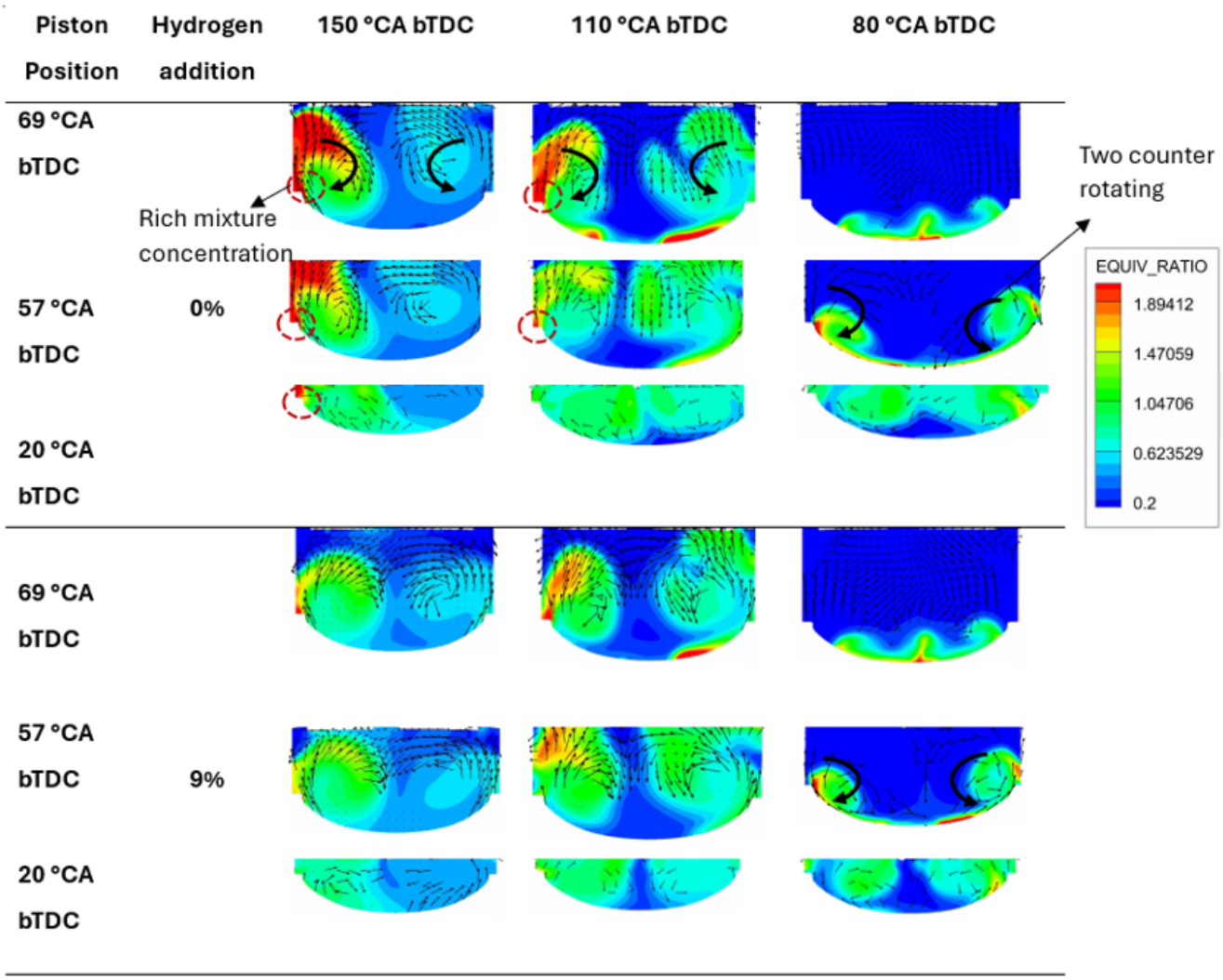

Figure 5.5: Effect of velocity field distribution associated to in-cylinder mixing during the compression process for neat methanol and 9% hydrogen additions at injection timings (150, 110, 80 °CA bTDC).

For the later injection timing of 60 °CA bTDC, combustion did not initiate for neat methanol and also for 3% hydrogen addition, this was mainly due to an inadequate time to form a reactive mixture in the region surrounding the spark plug as seen in Figure 5.6. But, when the hydrogen addition was increased to 9% and 12%, the charge was ignited for the late methanol injection timing of 60 °CA bTDC. The increase in hydrogen addition contributed to the development of a flamable mixture near the spark plug that initiated flame due to its wider flammability and higher flame speed compared to methanol. To explore the residence time effects on mixing during late injection, simulations were conducted for neat methanol operation at the 60 °CA bTDC injection timing by retarding the spark timing from 20 °CA bTDC to 4 °CA bTDC as shown in Figure. 5.6 The mixture distribution of methanol with air in the cylinder just before the initiation

of the spark showed that by delaying the spark timing from 20 to 4 °CA bTDC promoted mixing that led to a mixture homogeneity near the spark plug and initiation of flame. However increasing the amount of hydrogen also enhanced ignition and combustion performance by extending the injection timing limits which could eventually increase the stability of ignition, and combustion and improved thermal efficiency of and improved methanol/hydrogen SI engine [20].

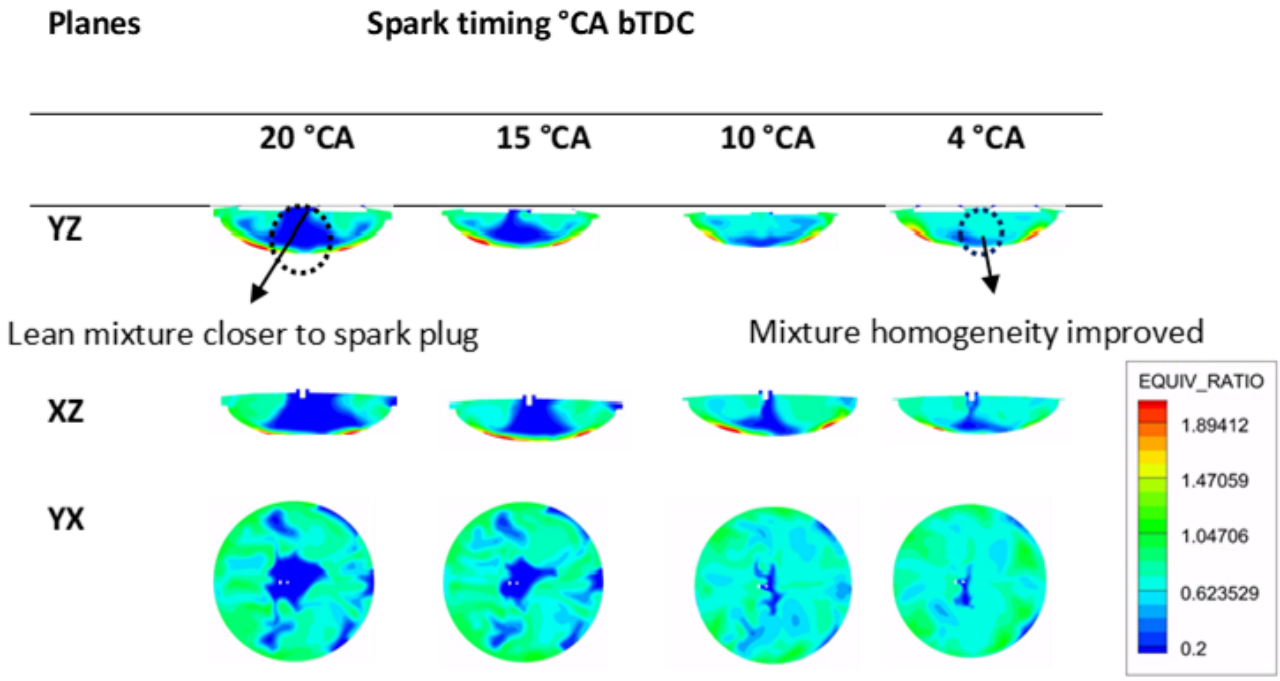

Figure 5.6: In-cylinder mixing around the spark plug for different spark timing for pure methanol for 60 °CA bTDC injection timing

Hydroxl radical

Hydrogen addition to methanol helps to promote the generation rate of radicals such as O, H and OH during the oxidation process of methanol [89]. The hydroxyl radicals play a crucial role in influencing the speed of the chemical reaction and the corresponding increase of the in-cylinder temperature. In Figure. 5.7, the OH radical formation was explored with respect to crank angle for different injection timings (150 °CA, 110 °CA, and 80 °CA bTDC) and various hydrogen addition levels (0%, 3%, 9%, 12%) for a constant spark timing of 20 °CA bTDC. The results showed that the effect of retarding the fuel injection timing from 150 °CA bTDC to 110 °CA bTDC and 80 °CA bTDC for neat methanol caused the peak value of OH to occur about 4 °CA earlier, with an associated increase in the peak OH concentration of 135.25% and 165% compared to injection of

methanol at 150 °CA bTDC due to increase in homogeneity of charge discussed Figure 5.4-5.7. The presence of rich stratified regions of fuel-air mixture at the vicinity of spark at 150°CA bTDC could have reduced the intensity of combustion as seen by delaying the formation of OH radical during the combustion process. The difference between the initiation of OH formation and its peak are consistent with the combustion duration shown in Figure. 5.7. Moreover, for the case of hydrogen addition greater than 3%, the value of peak OH occurred 4 °CA and 8 °CA earlier for an injection timing of 110 °CA and 80 °CA bTDC compared to 150 °CA bTDC. For 9% and 12% hydrogen addition, retarding the injection timing form 150 °CA to 110 °CA and 80 °CA led to a 65.28% and 81.94% increase in peak OH formation. Then OH was initiated quicker by retarding the injection timing at higher hydrogen addition, due to better quality mixing. For the case of 3% hydrogen addition, compared, retarding the injection timing to 150 °CA bTDC resulted in an increase of up to 82.11% and 88.36% in the peak value of OH for 110 °CA and 80 °CA bTDC, respectively. Increasing hydrogen addition also resulted in an increase in peak OH formation during the combustion process. This is due to hydrogen having higher flame speed that helps in fast oxidation process leading to an increase in OH radical concentration in the high temperature flame front and the associated high activation energy during combustion.

Combustion duration

The combustion duration is defined as the crank angle interval required to burn the methanol and hydrogen mixture, from the start of flame development at CA10 to the end of flame propagation at CA90. Figure. 5.8 represents the combustion duration (CA10-90) for the injection timings of 150 °CA, 110 °CA and 80 °CA bTDC of methanol with 0%, 3%, 9% and 12% hydrogen addition. Combustion duration was reduced when the injection timing was retarded from 150 °CA bTDC to 80 °CA bTDC under all conditions. Delaying the injection timing of methanol from 150 °CA bTDC to 110 °CA bTDC resulted in a decrease in combustion duration by 6.29% for pure methanol, a reduction of 39.03%, 32.08%, and 27.93% was observed for methanol with 3%, 9%, and 12% hydrogen addition, respectively. Subsequently, further delaying the injection timing of methanol from 150 °CA to 80 °CA bTDC led to a decrease in combustion duration of 13.11% for pure methanol and a reduction by 54.11%, 43.51%, and 42.45% for methanol with 3%, 9%, and 12% hydrogen addition respectively. Shortest combustion duration was obtained when methanol was injected at 80°CA bTDC, this could relate to better evaporation and mixing before the start of ignition when compared to earlier injection timings of 150°CA and 110°CA bTDC of methanol as shown in the figure. 5.8. In addition to that it can be seen that by increasing hydrogen by 3%, 9% and 12%, the combustion duration (CA10-90) effectively reduces when compared to neat methanol for all the injection timing presented

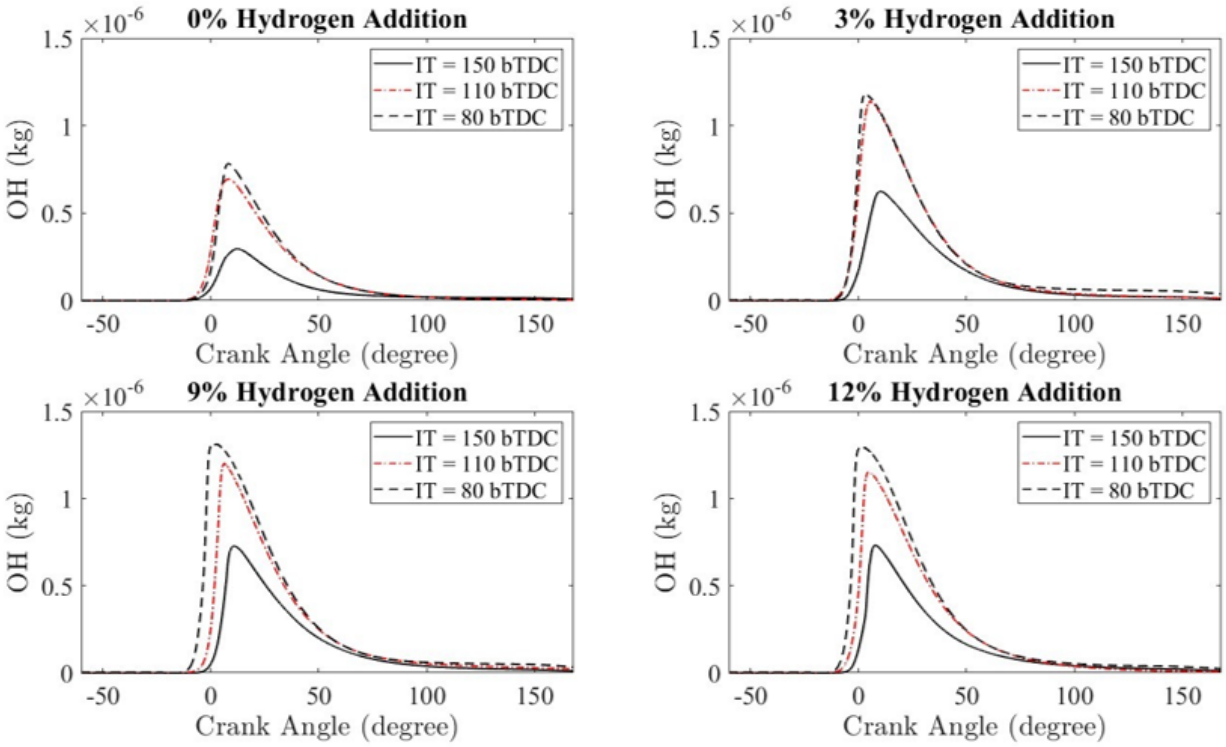

Figure 5.7: The OH formation at different injection timings and hydrogen additions with respect to crank angle (ST=20 °CA bTDC, =0.71, CR=9.6, MAP=90kPa, N=1200 RPM).

in this study. At an injection timing of 150 °CA bTDC, combustion duration decreased by 9.74%, 39.64%, and 36.98% for 3%, 9%, and 12% hydrogen addition compared to pure methanol, respectively. Similarly, at an injection timing of 110 °CA bTDC, combustion duration decreases by 41.50%, 56.42%, and 51.73% for 3%, 9%, and 12% hydrogen addition compared to pure methanol, respectively. Moreover, at an injection timing of 80 °CA bTDC, combustion duration decreases by 52.68%, 60.75%, and 58.26% for 3%, 9%, and 12% hydrogen addition compared to pure methanol. The observed variation is due to higher diffusivity of hydrogen that significantly enhances the formation of a favourable reactive mixture and the associated higher flame speed of hydrogen that fastens combustion. Figure. 5.8 also illustrates that for hydrogen addition beyond 9% resulted in an increase in combustion duration by 4.40%, 10.77% and 6.34% for retarded injection timing of 150 °CA bTDC, 110 °CA bTDC and 80 °CA bTDC respectively. This was mainly due to the partial replacement of air under higher percentages of hydrogen addition that resulted in reducing the volumetric efficiency and flame propagation rate, similar kinds of results were also observed in the experimental study [49].

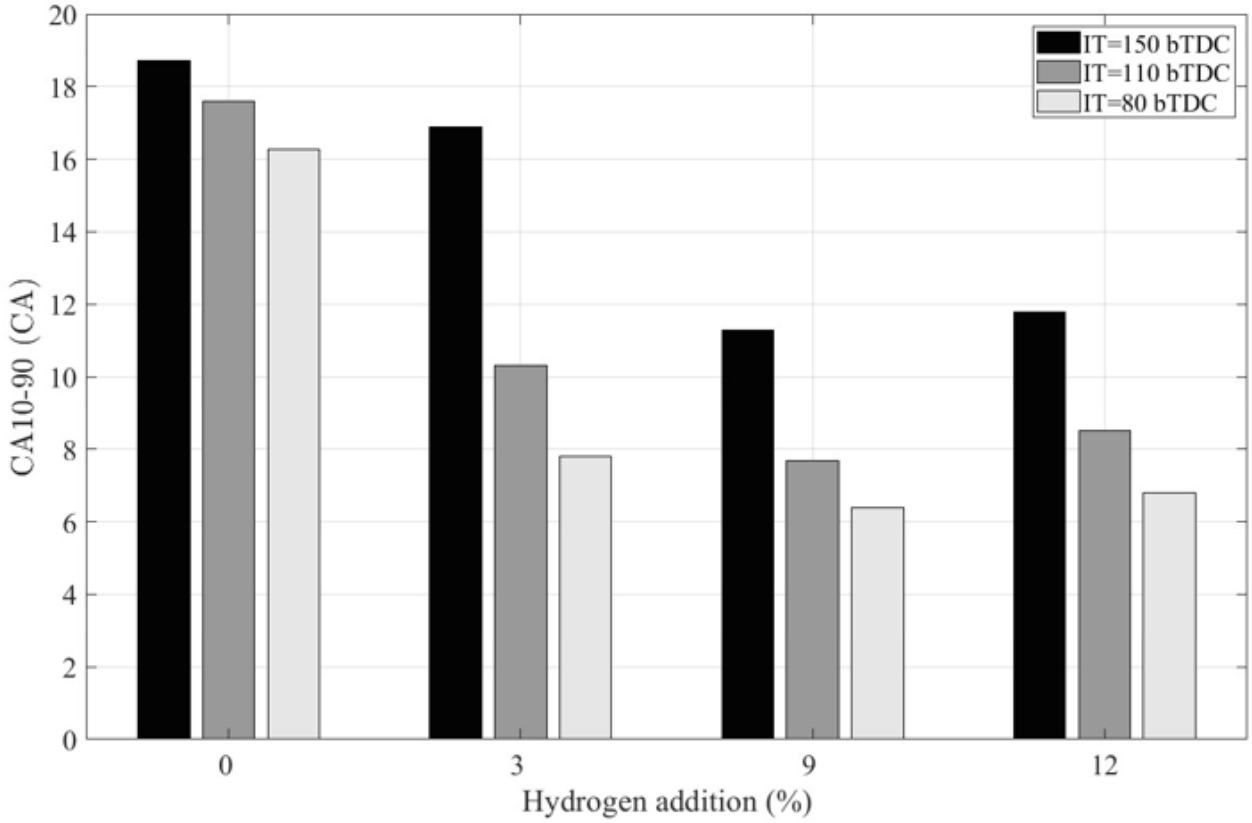

Figure 5.8: combustion duration CA10-90 at different injection timings and hydrogen additions (ST=20 °CA bTDC, =0.71, CR=9.6, MAP=90kPa, N=1200 RPM)

5.2.2 Emissions

The simulated results for NOx, Soot, and CO emissions from hydrogen-enriched methanol SI engine are discussed at different timings of methanol injection for varying percentages of hydrogen addition.

Indicated specific NOx emissions

Several studies have shown that enriching SI engines with hydrogen can lead to higher NOx emissions [81]. Figure. 5.9 shows the variation of NOx emission for 0%, 3%, 9% and 12% hydrogen addition at different injection timing of 150°CA, 120°CA and 80°CA bTDC, it can be seen that NOx emission increases respectively for the chosen conditions mentioned above. For neat methanol operating conditions, retarding the injection timing from 150 to 110 °CA bTDC resulted in the 161.37% increase in indicated specific NOx emission. Injection of methanol at 150 °CA bTDC resulted in a non-uniform mixture due to poor evaporation and wall film formation. Figure.5.9 shows a reduction in the OH radical concentration and a reduction in the global combustion temperature contributing to lower NOx emissions, similar observations have also been reported in [80]. At an injection timing of 150°CA bTDC, the addition of 3%, 9%, and 12% hydrogen with methanol resulted in an increase in the magnitude of NOx emission by 149.13%, 164.90%, and 164.56%, respectively, compared to pure methanol.For the retarded injection timing of 110°CA bTDC, the addition of 3%, 9%, and 12% hydrogen resulted in an increase in NOx emission by 81.17%, 84.45%, and 83.41%, respectively, compared to pure methanol. Retarding the injection timing to 80°CA bTDC, resulted in an increase in NOx emission by 105.13%, 146.28%, and 145.06% for 3%, 9%, and 12% hydrogen addition, respectively, compared to pure methanol, as illustrated in Figure. 5.9.This is due to faster flame speed and higher adiabatic temperatures of hydrogen which also increases the in-cylinder temperature [35]. For methanol with 3%, 9% and 12% hydrogen addition under retarded injection timings of 150°CA bTDC to 110°CA bTDC resulted in 90%, 81.00% and 81.2% increase of NOx emissions. Retarding the injection timing further from 150°CA bTDC to 80°CA bTDC on methanol for 3%,9% and 12% hydrogen addition resulted in an increase in NOx emissions by 114.62%, 142.3% and 141.445% respectively. This was due to an increase in the peak in-cylinder pressure as shown in Figure 5.4 which eventually leads to an increase in the in-cylinder temperature which increases NOx emissions. Additionally, the combustion duration was observed to decrease with hydrogen addition under all tested conditions, as depicted in Figure 5.8. This reduction in combustion duration indicates a clear trade-off, as rapid combustion could potentially contribute to the enhancement of thermal NO [50].For 12% hydrogen addition there was a small reduction in NOx emission compared to 9% hydrogen for the injection timing of 150 °CA, 110 °CA and 80 °CA bTDC by 0.13%, 0.56% and 0.49%, respectively. This is due to a reduction in

lower oxygen concentration inside the cylinder due to a higher percentage of hydrogen displacing air, similar effects were reported experimentally in [71].

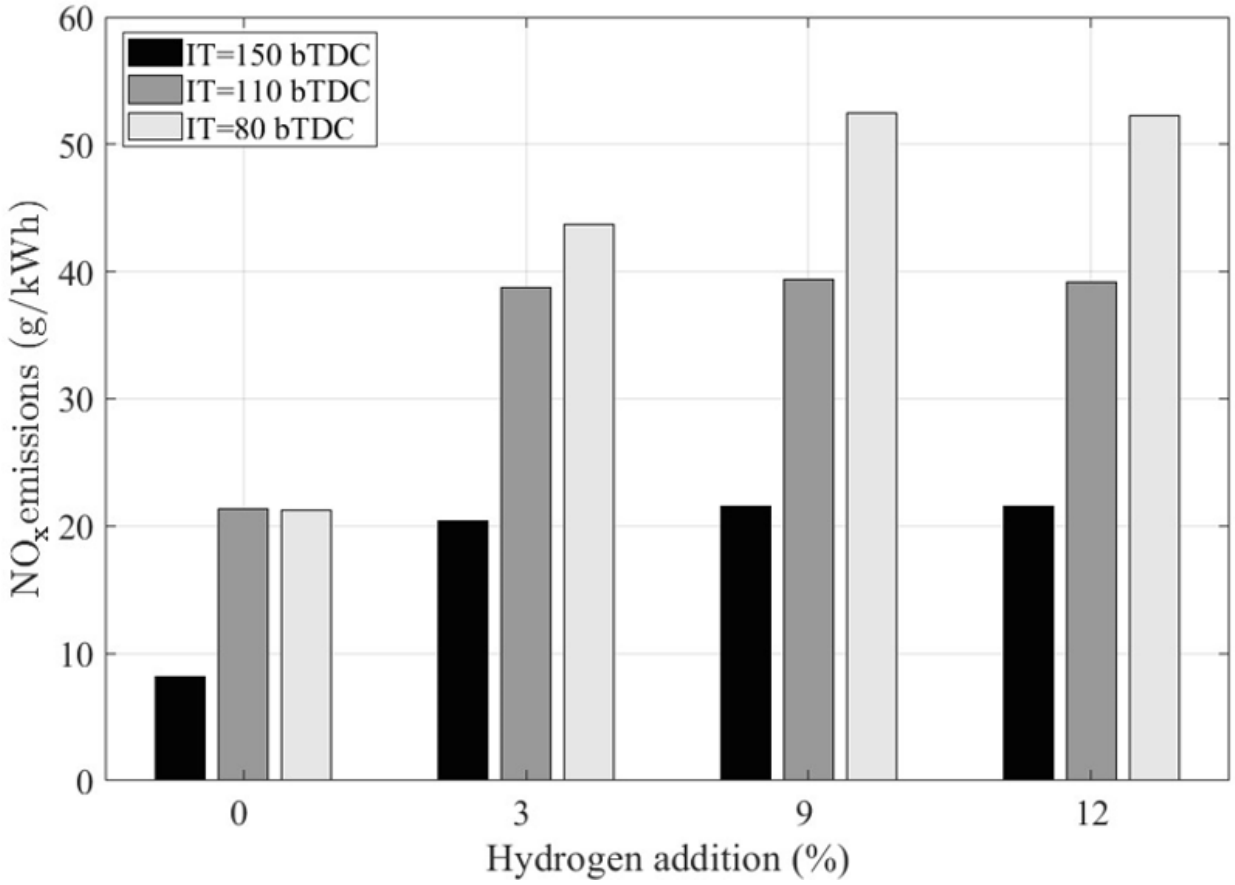

Figure 5.9: Results for NOx emission for hydrogen addition ranging from 0 to 12% and injection timings from 150 to 80 °CA bTDC at a fixed spark timing (=0.71, CR=9.6, MAP=90kPa, N=1200 RPM).

Indicated specific Soot emissions

Figure. 5.10 shows the indicated specific soot emission of neat methanol and methanol with 3%, 9% and 12% hydrogen addition for injection timings of methanol at 150 °CA bTDC ,110 °CA bTDC and 80 °CA bTDC at a fixed spark timing of 20 °CA bTDC. The addition of hydrogen to methanol consistently reduced soot emissions at various injection timings compared to neat methanol. Figure. 5.10 illustrates a decrease in indicated specific soot emissions when injection timing was retarded from 150 °CA bTDC to 110 °CA bTDC a considerable decrease of up to 93%, 97%, 98% and 94% was observed for corresponding hydrogen addition levels of 0%, 3%, 9% and 12% respectively. Similarly, Figure 5.10 also demonstrates a decrease in indicated specific soot emissions with the retardation of injection timing from 150 °CA bTDC to 80 °CA bTDC, with the soot

emissions following a declining pattern of 98%, 98%, 98%, 99% for corresponding hydrogen addition levels of 0%, 3%, 9% and 12% respectively. Specifically, at an injection timing of 150 °CA bTDC a reduction of 63.4%, 76.9%, and 61.90% of soot was observed of 3%, 9% and 12% hydrogen when compared to neat methanol. At 110 °CA bTDC, reduction of indicated soot emission obtained for 3%, 9% and 12% hydrogen addition of methanol was 84.24%, 93.55%, and 64.4%, and at 80 °CA bTDC, reductions were 67%, 82.4%, and 78.9%, respectively, compared to neat methanol. This reduction in soot could be related to higher OH radical concentration with hydrogen addition in methanol compared to neat methanol as can be seen in Figure 5.7 The OH radical plays a crucial role in enhancing the soot oxidation process during combustion [109]. In addition, it was also observed that from Figure 5.10 the indicated specific NOx emission was higher for methanol with hydrogen addition compared to neat methanol, and the trend is contrary for soot which is the clear trade-off, The addition of hydrogen facilitates and rapid due to higher burning flame speed [77]. Since there is no carbon-carbon chain and lack of any aromatic content the overall amount of soot produced from methanol combustion is negligible. The presence of hydroxyl group also favours oxidation through a maximum reduction of up to 99% has been obtained the actual magnitude variations between the operating conditions are insignificant therefore a semi-log scale was used to highlight the differences. Hydrogen addition greater than 9% resulted in a rise in soot emissions for all injection timings because of the depletion of oxygen content in the cylinder.

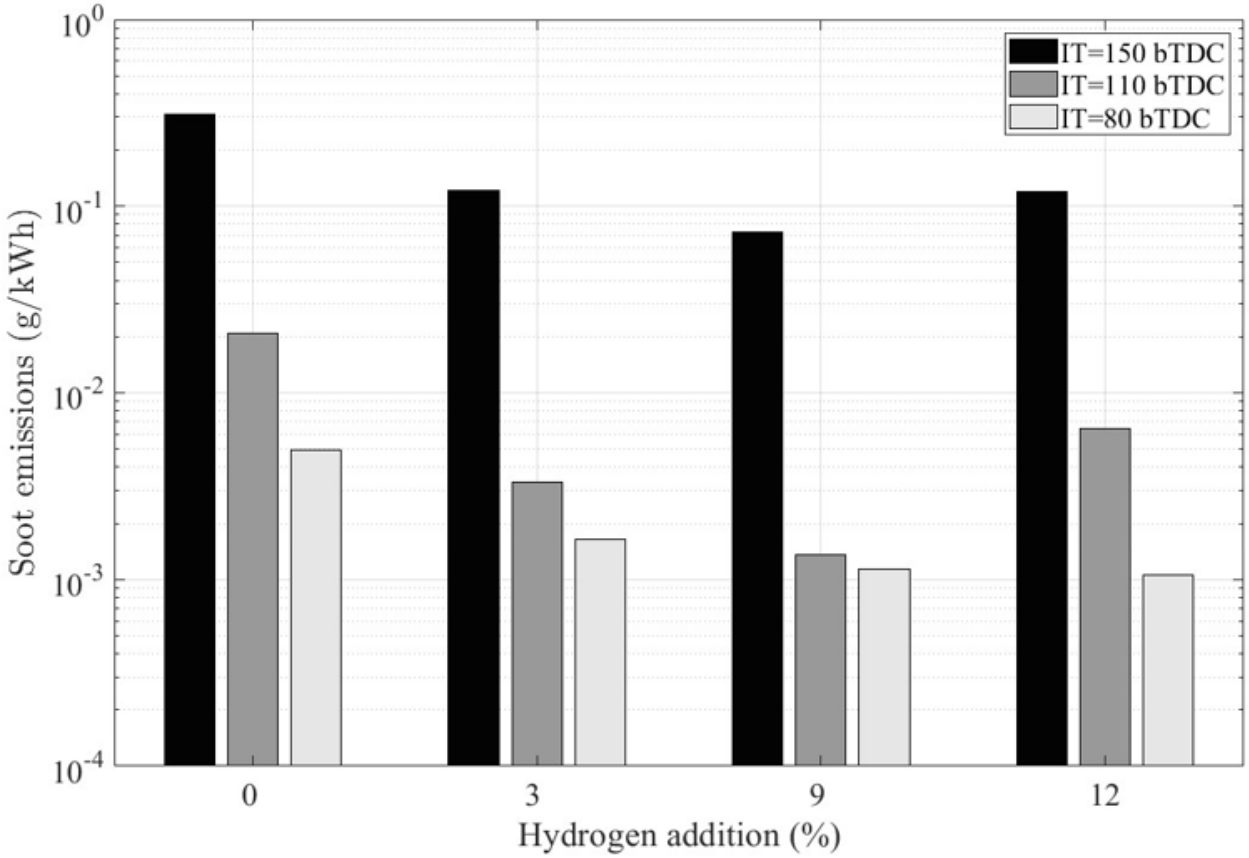

Figure 5.10: Indicated specific soot emission for hydrogen addition ranging from 0 to 12% and injection timings from 150 °CA to 80 °CA bTDC at a fixed spark timing (=0.71, CR=9.6, MAP=90kPa, N=1200 RPM)

Indicated specific carbon monoxide emissions

Indicated specific CO emissions' results represent incomplete combustion's effect [17,19,28,60]. Figure 5.11 shows the indicated specific CO emission for methanol combustion for varying percentages of hydrogen addition to methanol for different injection timings at 150°CA, 110°CA and 80 °CA bTDC at fixed spark timing of 20 °CA bTDC. High indicated specific CO emission was observed when methanol was injected at 150 °CA bTDC under all concentrations of hydrogen additions with methanol compared to injection timing of 110 °CA bTDC and 80 °CA bTDC. This could be due to poor evaporation leading to the formation of liquid film on the piston crown and the accumulation of rich fuel-air mixture as discussed in Figure. 5.4-5 also leads to an increase in CO emission. Through the amount of methanol injection was reduced with hydrogen addition the above-mentioned effect was still present for 150° CA bTDC compared to retarded injection timing. In addition to that it was also evident that the formation of OH radical at 150 °CA bTDC injection timing was lower compared to 110 °CA and 80 °CA bTDC which resulted in

partial oxidation of fuel. It was also observed that retarding the injection timing from 150 °CA bTDC to 110°CA bTDC and 80°CA bTDC for (0%, 3%, 9% and 12%) hydrogen additions to methanol caused the indicated specific CO emission to decrease significantly hence they are presented on a semi-log plot in Figure. 5.11. The addition of hydrogen to methanol at various concentrations resulted in a consistent reduction in specific CO emissions compared to using pure methanol across different injection timings. For the injection timing of 150 °CA bTDC, the addition of 3%, 9%, and 12% hydrogen lowered CO emissions to 41.78%, 58.21%, and 28.59%, respectively, compared to neat methanol. Significant reductions were observed at injection timings of 110 °CA bTDC and 80 °CA bTDC. Furthermore, compared to 9% hydrogen addition with methanol, the addition of 12% hydrogen with methanol resulted in 41.48%, 95.72%, and 58.10% rise in indicated specific CO emissions for injection timings of 150, 110, and 80 °CA bTDC. This could be due to fixed global equivalence ratio operation, so any further addition of hydrogen beyond 9% lowers the oxidation potential of the in-cylinder mixture during combustion which also affects the volumetric efficiency. The outcomes of CO emission from this simulation work are in agreement with experimental findings presented in [11].

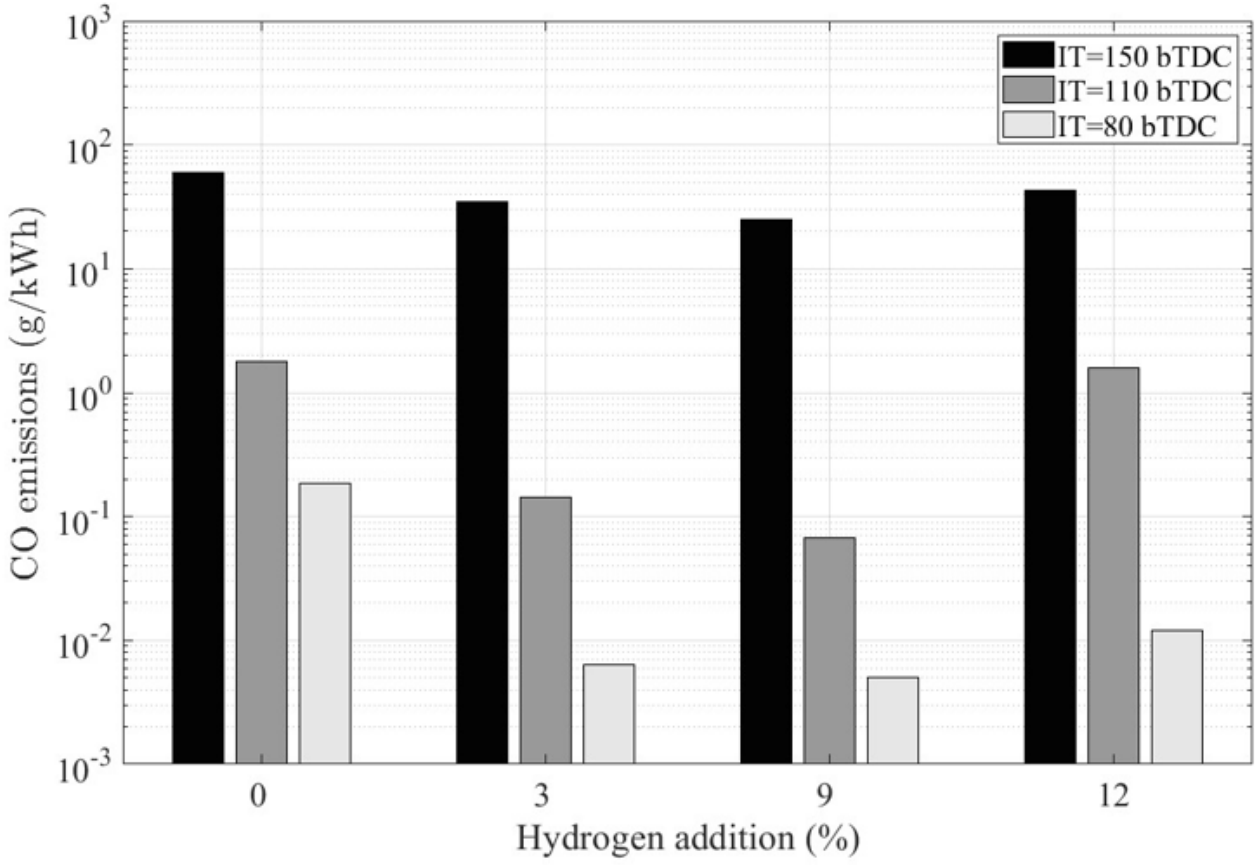

Figure 5.11: Results for CO emission for hydrogen addition ranging from 0 to 12 % and injection timings from 150 to 80 °CA bTDC at a fixed spark timing (=0.71, CR=9.6, MAP=90kPa, N=1200 RPM)

5.3 Summary

In this study, the effect of injection timing on the performance and emissions of a hydrogen-enriched methanol SI engine was done by using the three-dimensional computational fuel dynamics model. SAGE solver, Reynolds-Averaged Navier Stokes (RANS) Ring k- model, and O'Rourke and Amsden heat transfer sub-model were utilized to analyse in-cylinder characteristics. The extended Zeldovich mechanism and the Hiroyasu-NSC model were used for analysing NOx and soot emissions, respectively. The important results when retarding injection timing from 150 °CA bTDC to 80 °CA bTDC are summarised as follows:

- Led to a reduction of the maximum in-cylinder pressure for both neat methanol and methanol with hydrogen addition. There was no significant variation in maximum in-cylinder pressure between the injection timings of 110 °CA bTDC and 80 °CA

bTDC. Increasing the enrichment percentage of hydrogen resulted in an earlier rise of in-cylinder pressure as well as increased the maximum in-cylinder pressure compared to neat methanol operation.

- Improved the quality of fuel and air mixing around the spark plug. In addition to that by increasing hydrogen addition also enhanced the mixing quality.

- Increased the hydroxide radical (OH) formation for neat methanol and for hydrogen addition conditions. Then compared to neat methanol addition of 3%, 9% and 12% hydrogen with methanol also resulted in enhancing the OH formation for all the injection timing.

- Decreased the soot emissions for neat methanol and for all hydrogen addition conditions. Compared to the operation using neat methanol, the addition of hydrogen with methanol resulted in a reduction of soot emissions by up to 99%. It was also observed an increase in soot emissions for 12% hydrogen addition compared to 9% hydrogen addition with methanol for all the injection timing.

- The Indicated specific NOx emissions increased for the scenarios involving neat methanol and methanol plus different hydrogen addition percentages listed earlier. In addition to that increase in 3%, 9% and 12% hydrogen addition with methanol resulted in increasing Brake specific NOx emission compared to neat methanol. Then NOx emissions drop for 12% hydrogen addition compared to 9% hydrogen addition for all the injection timing.

- Combustion duration dropped for neat methanol and for methanol with all hydrogen addition conditions Compared to neat methanol increase in 3%, 9% and 12% hydrogen addition with methanol resulted in reducing the combustion duration. Furthermore, it found that combustion duration increases for 12 % hydrogen addition with methanol compared to 9% hydrogen addition.
  Additionally, combustion did not initiate for methanol and with greater than 9% hydrogen addition for late injection of methanol at 60 °CA bTDC due to the formation of the lean mixture closer to the spark plug caused by insufficient mixing time. In addition to that the increase of the hydrogen addition with methanol expanded the late injection limit of the neat methanol. Moreover, combustion did not initiate for methanol and with less hydrogen addition with under late injection of methanol due to the formation of the lean mixture closer to the spark plug caused by insufficient mixing time. In addition to the increase in hydrogen addition with methanol expanded the late injection limit of the neat methanol.

Chapter 6

Hydrogen enrichment in methanol spark ignition engine engine at varying injection timing during intake stroke

This chapter investigates the effect of methanol injection timing during the intake stroke, with varying levels of hydrogen addition. The research focuses on methanol injection at 240°, 260°, and 290° CA bTDC, with hydrogen concentrations ranging from 0% to 9%. A detailed investigation is carried out for early and late methanol injection during the intake stroke. Key parameters examined include in-cylinder mixing, hydroxyl radical formation, flame propagation characteristics after spark timing, and indicated specific emissions of NOx, carbon monoxide, and soot under the specified operating conditions.

6.1 Operating condition

Table 6.1: Simulation condition

Injection timing [°CA bTDC]	240	260	290
Spark timing [°CA bTDC]	20	20	20
Hydrogen addition[%]	0 – 9	0 – 9	0 – 9

The operating conditions for the methanol-fuelled spark-ignition engine were tested using methanol injection at 240°, 260°, and 290° CA bTDC, with hydrogen concentrations varied at 3% and 9%. The tests were conducted with fixed parameters, including a manifold pressure of 0.9 bar, an engine speed of 1200 RPM, an injection pressure of methanol 110 bar a compression ratio of 9.6, and an equivalence ratio of 0.71. The engine was operated with a fixed spark timing of -20° CA. The analysis focused on in-cylinder fuel/air mixing, cylinder pressure, OH radical formation, flame propagation, and combustion duration, and indicated specific CO and NOx emissions under these conditions.

Model setup

The computational simulation of methanol direct injection was conducted using the K-H model with the Rayleigh-Taylor mechanism. The extended Zeldovich mechanism was incorporated into the CFD model to compute NO emissions, and the Hiroyasu-NSC soot model was employed to assess soot at different equivalence ratios, spark timings, and hydrogen addition as mentioned in chapter 3.

Hydrogen addition:

The 3% and 9% hydrogen addition was simulated by using port injection. The hydrogen was added to methanol as a volume fraction of the intake air, as defined in the previous chapter. The excess air ratio of the dual-fuel methanol/hydrogen is defined in the previous chapter. Furthermore, the chemical composition for the boundary condition used in the port injection of hydrogen, as well as the boundary condition for hydrogen addition with methanol, is the same as described in Chapter 5.

Tumble ratio:

$$\text{Tumble ratio} = \frac{\omega}{\omega_{\text{crank shaft}}}$$

Where ω and $\omega_{\text{crank shaft}}$ is the angular speed of the flow inside the cycle and angular speed of the crankshaft structure

6.2 Results and discussion

6.2.1 In-cylinder characteristics

In-cylinder pressure

In this simulation study presented in Figure 6.1, the influence of injection timing on the maximum in-cylinder pressure variations in a methanol-fuelled spark ignition (SI) engine is examined at three different injection timing (240°CA, 260°CA, and 290°CA bTDC) at fixed spark timing 20°CA bTDC. The simulated study reveals that the highest peak in-cylinder pressure of 5.68 MPA magnitude was obtained at 290°CA injection timing. Advancing injection timing from 240°CA bTDC to 260°CA bTDC and 290°CA bTDC leads to a notable increase in maximum in-cylinder pressures. Subsequently, it was noted that by advancing the injection timing to 260°CA and 290°CA bTDC, the maximum in-cylinder pressure shifted to occur 19°CA and 24°CA earlier, respectively, when compared to the maximum in-cylinder pressure at 240°CA bTDC injection timing. This could be attributed to the lean mixture concentration before the spark timing when methanol is injected at 240°CA bTDC, as depicted in Figure 6.4. This condition results in a delayed initiation of the flame, as seen in the figure 6.5.

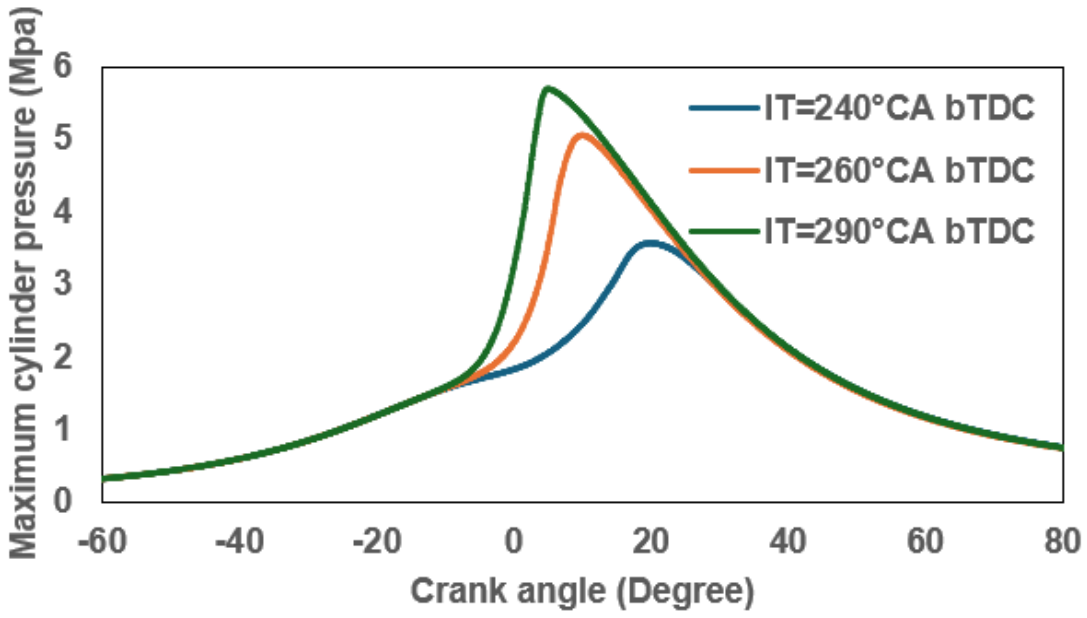

Figure 6.1: : Results for in-cylinder pressure of neat methanol at injection timings of 240, 260 and 290 °CA bTDC.

Figure 6.2 illustrates the in-cylinder pressure at different crank angles when the methanol is injected at 290°CA bTDC under neat methanol and hydrogen-enriched operating conditions. Enrichment of hydrogen increased the in-cylinder pressure and earlier occurrence of the maximum in-cylinder pressure. Compared to neat methanol 3% and 9% hydrogen addition resulted in the 4°and 7° earlier maximum in-cylinder pressure. This could be because hydrogen has higher flame propagation properties which facilitates the initiation of flame after spark timing as shown in Figure 5 Figure 6.4 illustrates the simulated peak in-cylinder pressure at different

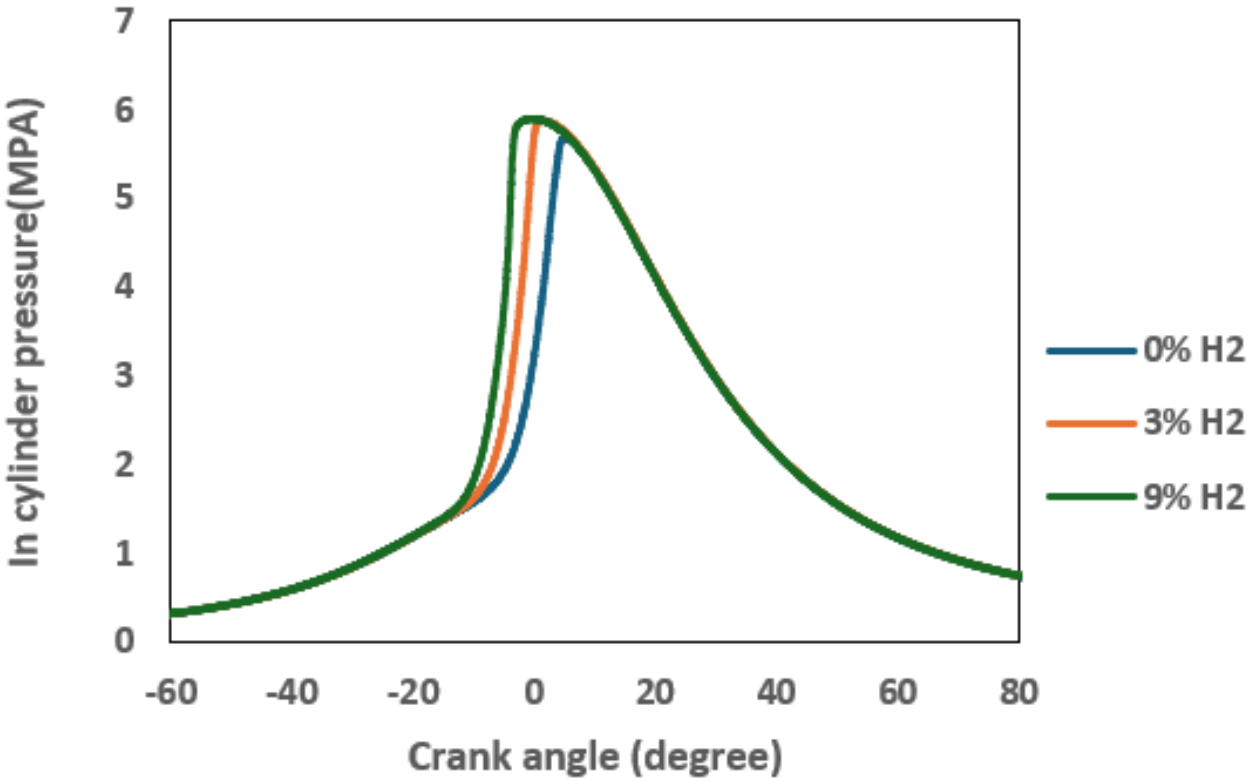

Figure 6.2: Results for in-cylinder pressure with various hydrogen additions of 0%, 3%, 9% and 12% at fixed injection timing of 80 °CA bTDC

injection timings, with hydrogen enrichment ranging from 0 to 9%, at a fixed spark timing of 20°CA bTDC. The highest peak pressure was achieved when methanol was injected at 290°CA bTDC, while the lowest peak cylinder pressure was observed at 240°CA for different levels of hydrogen enrichment (0%, 3%, 9%) with methanol. Advancing the injection timing from 240°CA to 260°CA bTDC for neat methanol, 3% and 9% hydrogen enrichment resulted in 29.44%,39.44% and 8.23% increase in the maximum in-cylinder pressure. Further advancing the injection timing from 240°CA bTDC to 290°CA bTDC for neat methanol, 3% and 9% hydrogen

enrichment resulted in 59%,46.98% and 11.35%. Then it can be also observed from Figure 6.4 that compared to neat methanol operating conditions enrichment of 3% and 9% hydrogen additions increased the maximum in-cylinder pressure for various injection timing. Specifically, at 240°CA bTDC injection enrichment of 3% and 9% hydrogen addition resulted in 12.21% and 117.46% compared to neat methanol operation conditions. Then an injection of methanol at 260°CA resulted in enriching 3% and 9 hydrogen addition resulting in 11.33% and 14.2%. Then an injection of methanol at 290°CA bTDC enriching 3% and 9% hydrogen addition resulted in 3.31% and 3.61% compared to neat methanol operating conditions. This could be because hydrogen has high flame propagation properties compared to methanol would enhance the oxidation process during the combustion as seen in Figure 6.7.

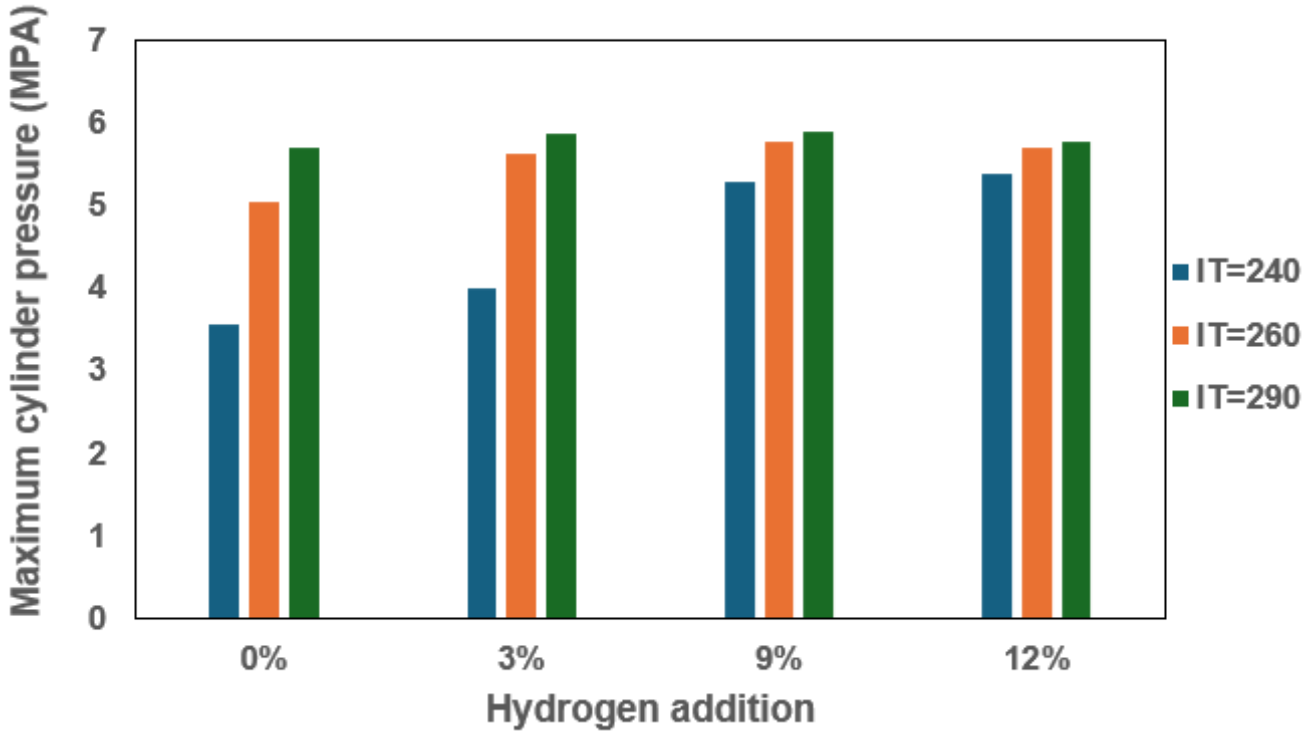

Figure 6.3: Maximum in-cylinder pressure values for different hydrogen additions (0%,3% and 9%) at different injection timings (240,260 and 290°CA bTDC)

In -cylinder fuel-air mixing

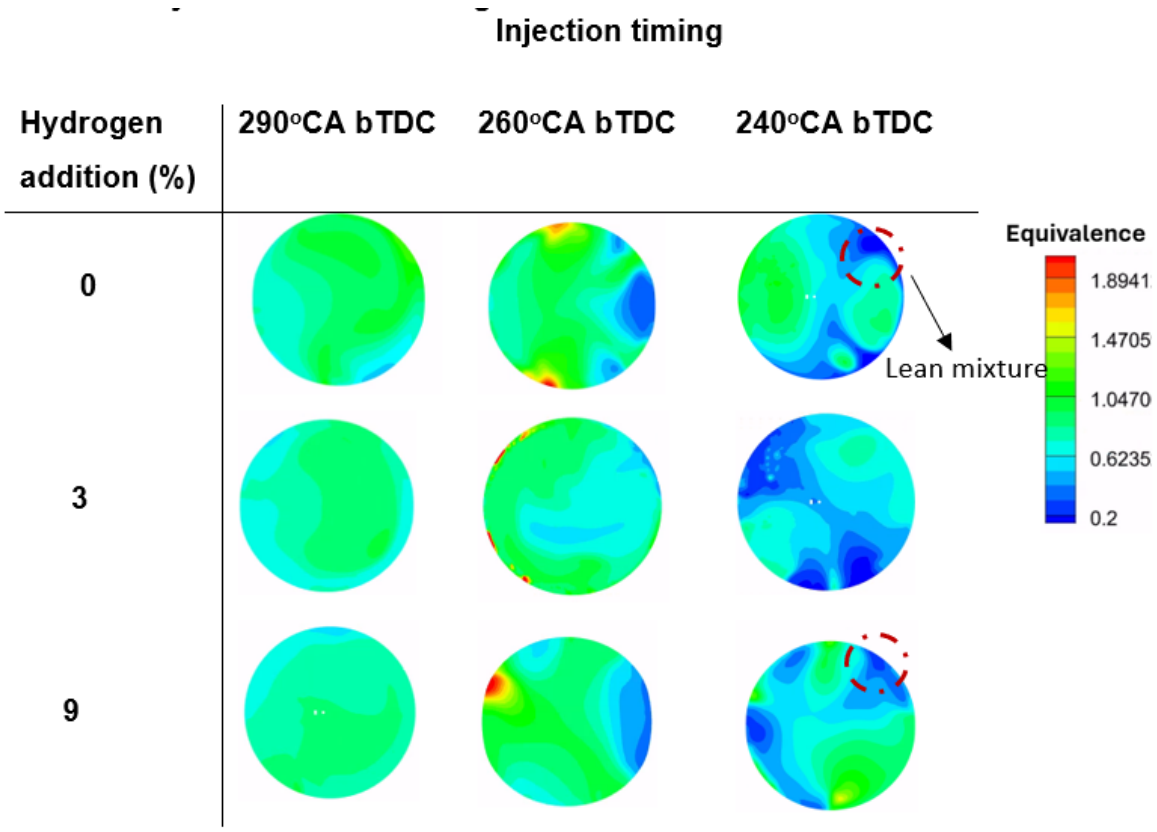

Figure 6.4: Comparison of in-cylinder mixing for various hydrogen additions (0, 3, and 12%) and injection timings (240, 260 and 290 °CA bTDC) just before the initiation of spark at 20 °CA bTDC.

The injection timing is a important parameter that influence in-cylinder mixing and combustion processes [10]. Figure 6.4 represents in-cylinder mixing obtained just before the spark timing (20°CA bTDC) of methanol injection at 240°CA, 260°CA bTDC, and 290°CA bTDC, under both neat methanol and conditions with 3% and 9% hydrogen addition. As it can be seen from Figure 6.4 , injection of methanol at 240°CA bTDC resulted in lean mixture concentration around the spark plug. This could be because of the impinged fuel mixture on the piston crown at the piston crown during the late stage of compression stroke as shown in Figure 6.5(c). Additionally, when the injection timing was advanced to 290°CA bTDC, improved fuel and air mixing was obtained around the spark plug location. This was because, under the 290°CA bTDC injection timing conditions, the fuel had been completely injected into the cylinder before the maximum lift of the intake valve. This maximum valve lift, occurring after the fuel injection, allowed for a higher charge motion

of air to enter the cylinder. This higher air charge motion may have enhanced the mixing quality of the impinged fuel droplets from the piston surfaces seen in Figure 6.5 (a) from the injection of fuel from 290°CA bTDC.Therefore improving the quality of mixing just before the spark timing. Then higher tumble ratio is obtained during the compression stroke for 290°CA bTDC injection timing compared to the retarded injection timing condition (240°CA bTDC) as can be seen from Figure 6.5 In addition, enrichment of 3% and 9% hydrogen addition with methanol quality of fuel and air mixing is improved for all injection timing of methanol compared to neat methanol operating conditions. This could be cause hydrogen has a better diffusive coefficient in air which enhances the fuel and air mixing inside the chamber.Furthermore Figure 6.5 (a),(b),(c) detailed study on the air-fuel mixing was conducted after the injection of fuel for different injection timings (290°CA bTDC and 240°CA bTDC) for neat methanol operating condition.

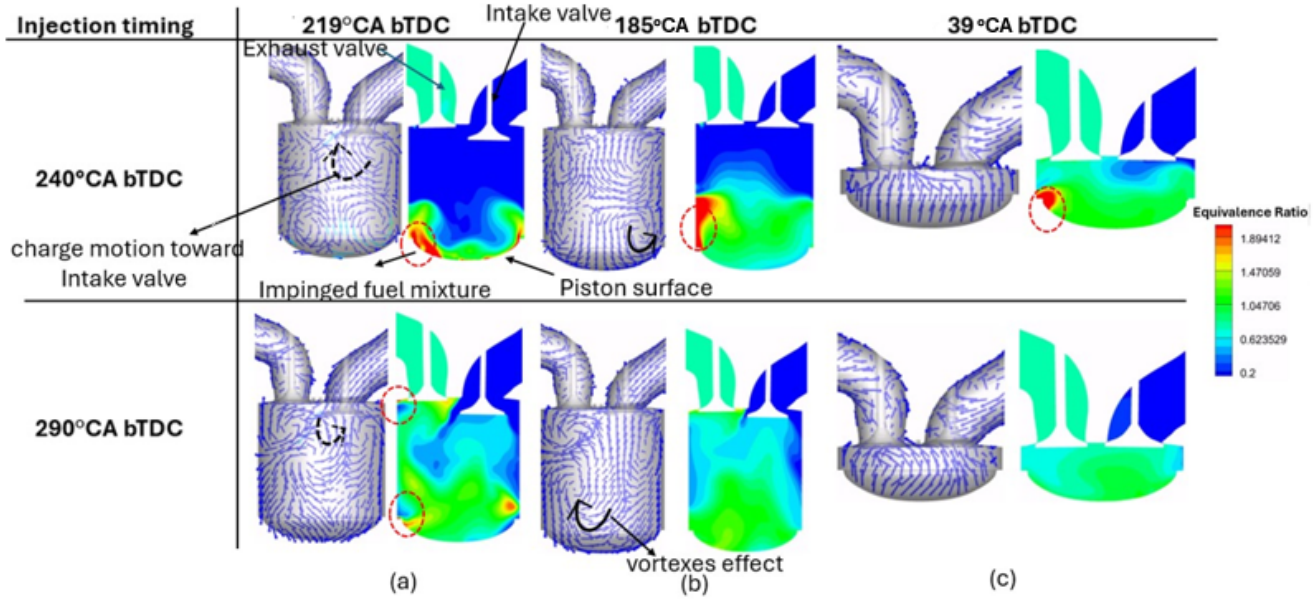

Figure 6.5: (a),(b),(c) Detailed study of air-fuel mixing after fuel injection for neat methanol at injection timings (290°CA bTDC and 240°CA bTDC)

As depicted in Figure 6.5(a), at 219°CA bTDC during the late stage of the intake stroke, the charge motion of air was towards the intake valve. In the case of late injection at 240°CA, fuel began to impinge on the piston surface at this crank angle, whereas with advanced injection timing at 290°CA bTDC, the fuel that had impinged on the piston surface started to mix throughout the chamber, leading to a noticeable accumulation of a rich fuel mixture towards the exhaust valve side. This accumulation was driven by the charge motion towards the intake valve, as shown

in Figure 6.5 (a).
Figure 6.5(b) illustrates that at 185°CA bTDC, during the beginning of the compression stroke, a vortex charge was generated from the piston surface due to the upward motion of the piston. With late injection timing at 240°CA bTDC, the impinged fuel mixture from the piston surface was pushed towards the piston crown and cylinder wall. In contrast, for advanced injection timing at 290°CA bTDC, the fuel-air mixture began to spread evenly across the piston surface, and the concentrated fuel near the exhaust valve started to distribute more evenly throughout the chamber due to vortexes effect, as seen in the figure.
Figure 6.5 (c) then demonstrates that during the late stage of the compression stroke at 39°CA bTDC, with late injection timing at 240°CA bTDC, a rich fuel mixture gathered on the piston crown surface. This resulted in lean mixture concentration near the spark timing, as depicted in Figure 6.4. In contrast, with advanced injection timing, the fuel mixture was evenly distributed, achieving homogeneous mixing at the time of ignition. This may be because for the advance injection timing condition the fuel was injection was before maximum lift period of the intake valve. In addition to that higher intensity of the charge motion is generated during maximum lift of the intake valve. Then during the compression stroke better vortexes effect is generated from the piston surface and from the Figure 6.6 during the compression stoke higher tumble ratio intensity was achieved compared to 240°CA bTDC injection timing condition this enhances fuel-air mixture to evenly distributed across the combustion chamber [108].

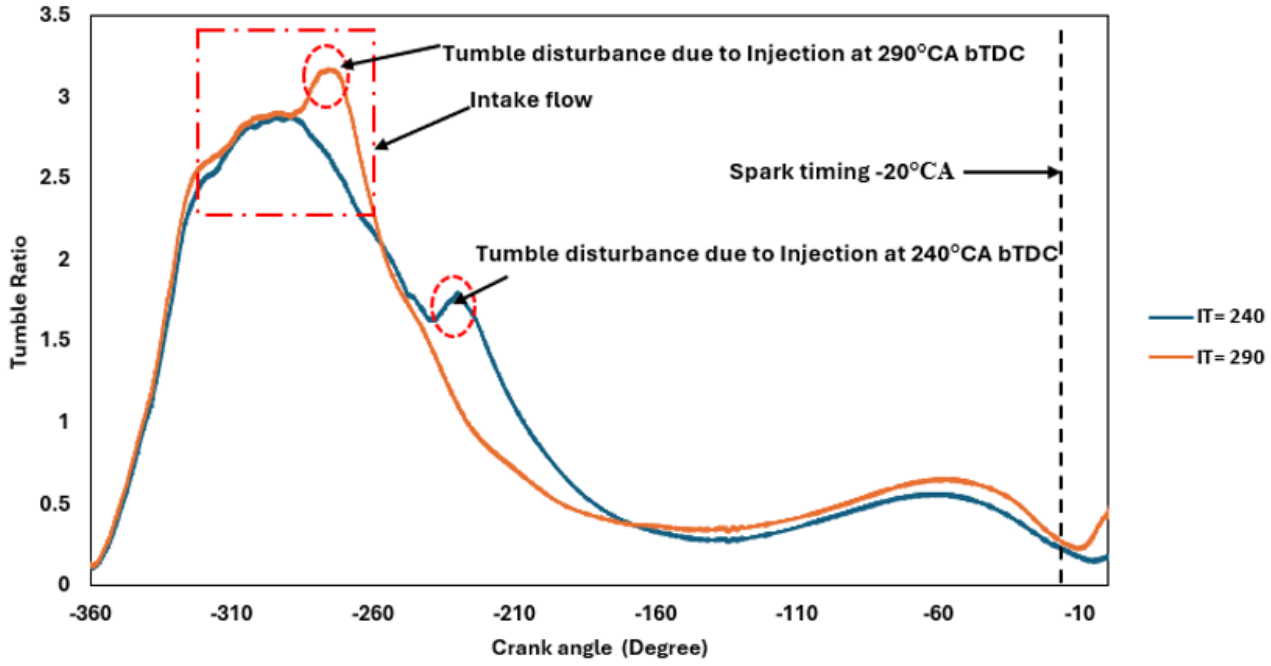

Figure 6.6: Effect of In cylinder tumble ratio for the injection timing 240°CA bTDC and 290° CA bTDC

Figure 6.6 illustrates the detailed study on the tumble ratio of in-cylinder flow to investigate the intensity of tumble ratio at different injection timings of methanol (240°CA bTDC and 290°CA bTDC) for neat methanol operating conditions. As shown in Figure 6.6 the tumble ratio is higher during the intake flow. It is also observed that a disturbance in the tumble ratio occurs during injection, leading to a decrease in the tumble ratio. However, later tumble ratio was intensified from -180°CA during the upward motion of the piston during the compression stroke under all the injection timing conditions.In addition to that for the 290°CA bTDC injection timing condition, the tumble ratio declined earlier compared to 240°CA bTDC injection timing. But during the compression stroke tumble ratio was initiated earlier for 290°CA injection timing compared 240°CA bTDC injection timing. From Figure 6.6 it can be also noted that compared to retarded injection timing of 240°CA bTDC 25% higher tumble ratio is obtained during the compression stroke from -180°CA for 290°CA bTDC injection timing condition. This increase in tumble ratio during the compression ratio may result in an even distribution of fuel and air mixture just before the spark timing for 290°CA bTDC injection timing condition as shown in Figure 6.4

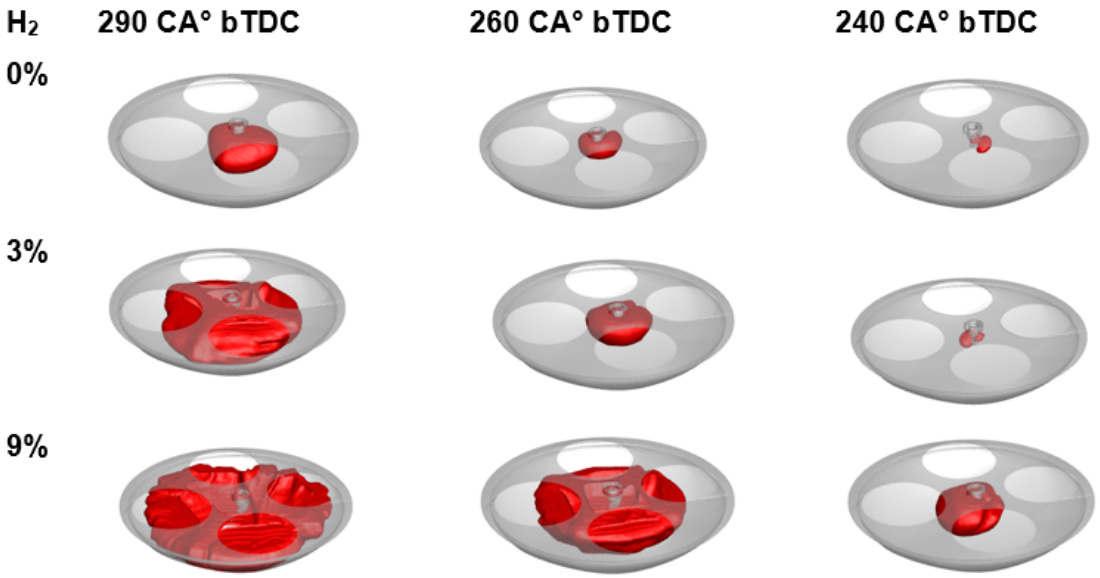

Figure 6.7: Flame Propagation at 15°CA after the spark timing of neath methanol and methanol with 3%,9% hydrogen addition for the injection timings 240°CA bTDC, 260°CA bTDC and 290°CA bTDC

Flame propagation is an important parameter that influences an engine's operation stability and engine efficiency. Figure 6.7 shows the snapshot of flame propagation within the chamber captured at 15°CA after spark timing (20°CA bTDC) for neat methanol and with 3%,9% hydrogen enrichment at injection timings 240°CA,260°CA and 290°CA bTDC of methanol. It can be observed form Figure 6.7 that advancing the injection timing from 240 CA° bTDC to 290°CA bTDC resulted in the enhancement of the propagation for neat methanol and methanol with 3% and 9% hydrogen enrichment. This could be due to the better quality of the fuel and air mixing obtained before the spark timing as seen in Figure 6.4. In addition to that increase in 3% and 9% hydrogen addition resulted in faster flame propagation when compared to neat methanol operating conditions. This could be because hydrogen has a better diffusive coefficient in air which promotes fast fuel and air mixing before combustion. In addition, the hydrogen has higher adiabatic temperature properties compared to methanol.

Hydroxyl radical formation

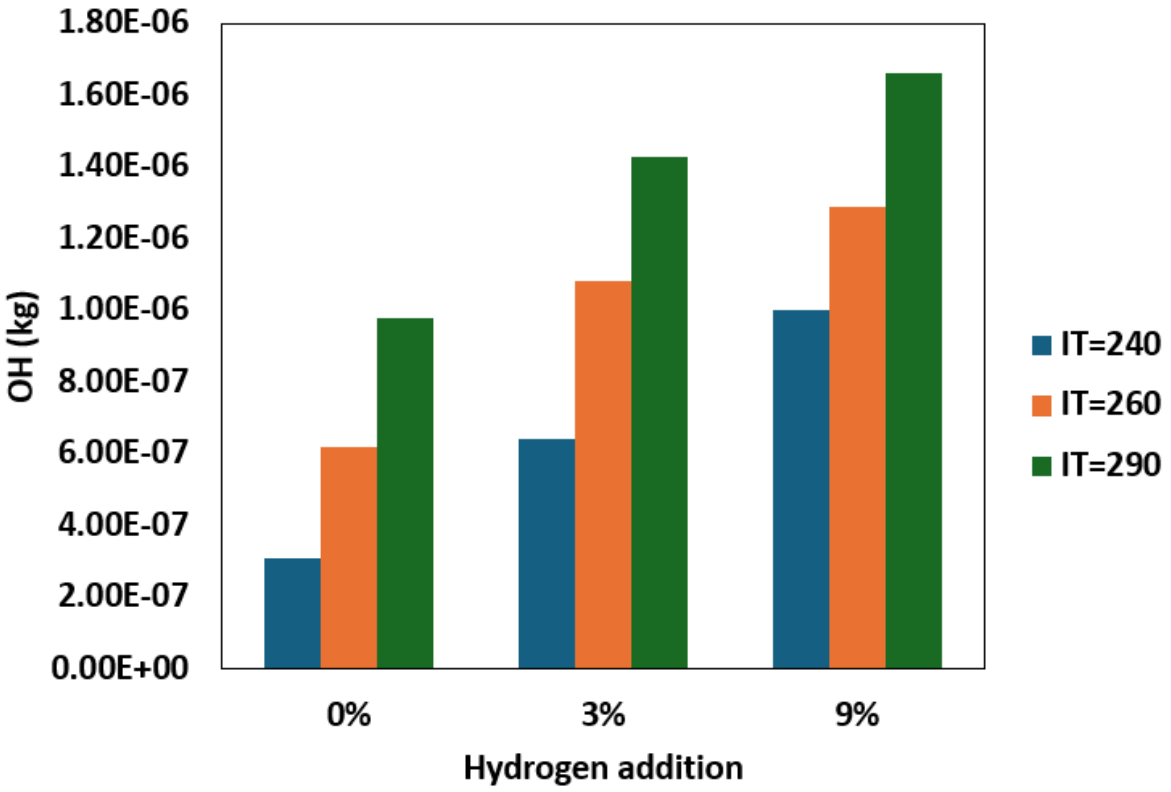

Figure 6.8: The peak OH formation at different injection timings and (0%, 3% and 9%) hydrogen additions with methanol

Adding hydrogen to methanol promotes the generation rate of O, H, and OH radicals during methanol oxidation. OH radicals play a crucial role in this process, influencing reaction speed and in-cylinder temperature. Figure 6.8 illustrates the maximum concentration of OH radical formation for different methanol injection timings (240, 260, and 290 CA° bTDC) with neat methanol and varying hydrogen enrichment levels (3%, 9%) at a fixed spark timing of 20 °CA bTDC. Advancing injection timing from 240° to 260°CA bTDC resulted in a 101.01%, 89.21%, and 28.48% increase in peak OH concentration for neat methanol, 3%, and 9% hydrogen-enriched conditions, respectively. Further retarding injection timing from 240° to 290°CA bTDC resulted in a 216.56%, 122.99%, and 65.80% increase in peak OH radical concentration. This is because at 240°CA bTDC, the fuel and air mixture concentration lean just before the spark timing, as shown in figure 6.4. Compared to neat methanol, hydrogen enrichment (3% and 9%) resulted in higher OH radical concentrations for all injection timings. Specifically, at an injection timing of 240 °CA bTDC, 3% and 9% hydrogen addition resulted in a 107.68% and 224.69% rise in peak OH radical formation, respectively. At 260 °CA bTDC, the increase

was 74.82% and 107.53%, and at 290 °CA bTDC, it was 46.29% and 70.06%, respectively. This can be attributed to hydrogen's higher flame speed, facilitating faster oxidation during combustion. Hydrogen enrichment enhances OH radical concentration by promoting diffusion from the hot flame zone, providing high activation energy due to high combustion temperature, thereby promoting methanol oxidation.

6.2.2 Emissions

Indicated specific CO emission

The indicated specific carbon monoxide emissions directly reflect incomplete combustion during the engine combustion[17, 18]. Figure 6.9, illustrates indicated specific CO emissions for neat methanol and hydrogen enrichment (3% and 9%) with methanol operating conditions, at injection timings of 240°CA, 260°CA, and 290°CA bTDC, maintaining a fixed spark timing of 20°CA bTDC. Increased levels of indicated specific CO emissions were observed when methanol was injected at 240°CA bTDC, both for neat methanol and hydrogen addition conditions, in comparison to injection timings of 260°CA bTDC and 290°CA bTDC. Under neat methanol operating conditions, the advancing injection timing from 240°CA to 260°CA and 290°CAbTDC resulted in 15.07% and 99.30% decrease in indicated specific CO emission. Then hydrogen enriched conditions, advancing the injection timing from 240°CA to 260°CA bTDC for methanol with 3% and 9% hydrogen reduced CO emissions by 83.03% and 84.07%, respectively, and further advancing to 290°CA bTDC achieved reductions of 99.66% and 99.78%. This reduction may be attributed to improved mixing of fuel and air just before ignition, as illustrated in Figure 6.4. Additionally, advancing the injection from 240°CA to 290°CA bTDC greater flame propagation area was observed at 15°CA after spark timing, this may accelerate oxidation, as shown in Figure 6.7. The addition of hydrogen to methanol at various concentrations (3% and 9%) resulted in a reduction indicated specific CO emissions compared to neat methanol across different injection timing. Injection of methanol at 240°CA indicated specific co-emission dropped to 53.78% and 90.62%, at 260° CA bTDC injection timing co emission reduced to 88.63% and 94.81%, and further advancing the injection timing 290°CA bTDC indicated specific co emission dropped to 78 and 91.50% compared to neat methanol neat methanol operating condition. This may be because the addition of hydrogen results in higher flame propagation as seen in figure 6.7 due to its adiabatic properties.

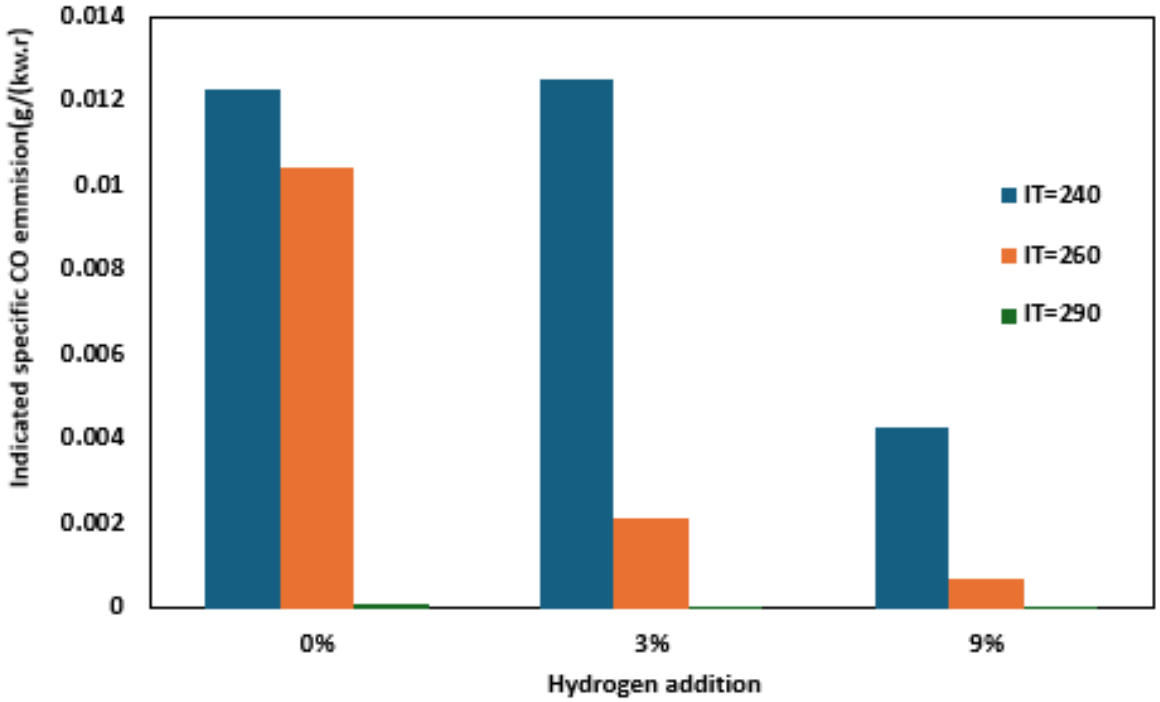

Figure 6.9: Results for Indicated specific CO emission for hydrogen addition ranging from 0 to 12% and injection timings from 240 to 290 °CA bTDC at a fixed spark timing

Indicated specific NOx emission

The formation of thermal NO was simulated using the extended Zeldovich mechanism in the Converge CFD solver. It has been noted from previous studies that enriching spark ignition (SI) engines with hydrogen leads to increased NO emission [80]. Figure. 6.10 shows the NOx emission for the neat methanol and 3%,9% hydrogen addition for the injection timings of 240°CA,260°CA and 290°CA bTDC in increased in NOx emission under all the conditions. For neat methanol operating conditions, advancing the injection timing from 240°CA bTDC to 260° and 290°CA bTDC led to increases in specific NOx emissions of 453.78% and 937.25%, respectively. With the addition of 3% and 9% hydrogen to methanol, advancing the timing from 240°CA bTDC to 260°CA bTDC resulted in NOx emission increases of 195.12% and 57.18%, respectively. Further, retarding the timing from 240°CA bTDC to 290°CA bTDC for these hydrogen-enriched mixes led to increases of 353.31% and 128.94%, respectively. These increases were attributed to higher in-cylinder pressures, as depicted in Figure 6.1, which in turn raised in-cylinder temperatures and consequently NOx emissions. Injecting methanol at 240°CA bTDC creates a lean mixture around the spark plug as shown in Figure 6.4, delaying flame propagation as depicted in Figure 6.7. This delay also decreases OH radical con-

centrations during combustion, which lowers the overall combustion temperature, thereby reducing NOx emissions, as also noted in [39]. When 3% and 9% hydrogen are added to methanol at 240°CA bTDC injection timing, NOx emissions increase by 286.21% and 873.88%, respectively, compared to pure methanol. At 260°CA bTDC, adding 3%, 9%, and 12% hydrogen to methanol results in NOx increases of 105.82% and 176.42%, respectively. Moreover, at 290°CA bTDC, adding 3% and 9% hydrogen boosts NOx emissions by 68.79% and 114.95%, respectively, as shown in Figure 6.9. These increases may be attributed to the accelerated flame speed and higher adiabatic temperatures from hydrogen, which raise in-cylinder temperatures as per [48]. Additionally, flames ignite more rapidly post-spark timing than with neat methanol, as illustrated in Figure 6.7. This quick flame propagation suggests a trade-off, where rapid combustion could enhance thermal NOx production via the Zeldovich mechanisms. [93].

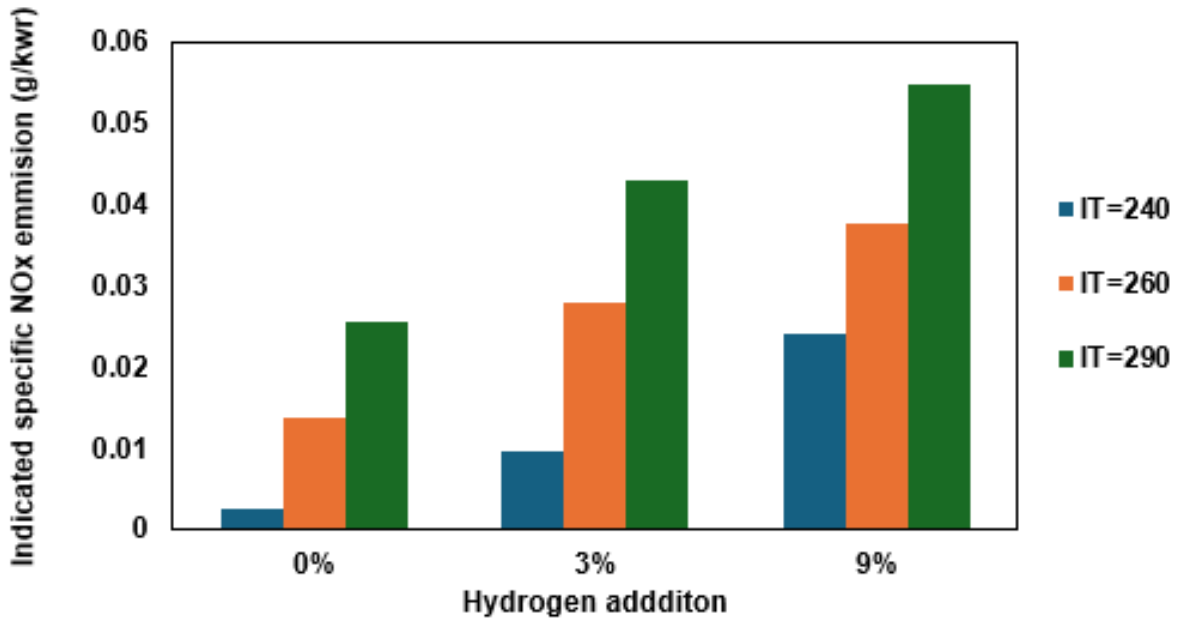

Figure 6.10: Results for Indicated specific co emission for hydrogen addition ranging from 0 to 12% and injection timings from 240 to 290 °CA bTDC at a fixed spark timing

Indicated specific soot emission

Soot formation was analysed using the Hiroyasu model, and soot oxidation was simulated using the NSG model [37]. Figure 6.10 illustrates the Indicated specific soot emissions for neat methanol and methanol enriched with 3% and 9% hydrogen at methanol injection timings of 240°CA bTDC, 260°CA bTDC, and 290°CA bTDC, with a constant spark timing of 20°CA bTDC. A notable decrease in the Indicated

specific soot emissions was observed as injection timing advanced from 240°CA bTDC to 260°CA bTDC, with reductions of 55.67% for neat methanol, 13.69%, and 30.76% for 3%, and 9% hydrogen enrichment levels, respectively. Similarly, Figure 6.10 illustrates a decrease in indicated specific soot emissions as injection timing was delayed from 240°CA bTDC to 290°CA bTDC, representing a reduction of 98.42%, 98.7 and 95.23% for neat methanol and 3% and 9% hydrogen enrichment levels. The Enrichment of 3% and 9% hydrogen to methanol lowered soot emissions across all injection timings compared to neat methanol operating conditions. Specifically, at 240°CA bTDC, the addition of 3% and 9% hydrogen led to soot emission reductions of 53.78% and 90.62%. At 260°CA bTDC, the reductions were 88.63% and 94.81%, and at 290°CA bTDC, they were 56.77% and 71.75%, respectively. This reduction in soot could be due to higher OH radical concentrations during combustion with hydrogen-enriched methanol, as shown in figure 6.6, which significantly enhances the soot oxidation process [117]. Additionally, Figure 6.9 indicates that specific NOx emissions were higher for methanol with hydrogen addition compared to neat methanol, reflecting a clear trade-off: the reduction in specific soot emissions with increased hydrogen addition, likely due to the faster flame speeds as shown in figure 6.7 and shorter flame development angles associated with hydrogen, promoting more complete combustion [53].

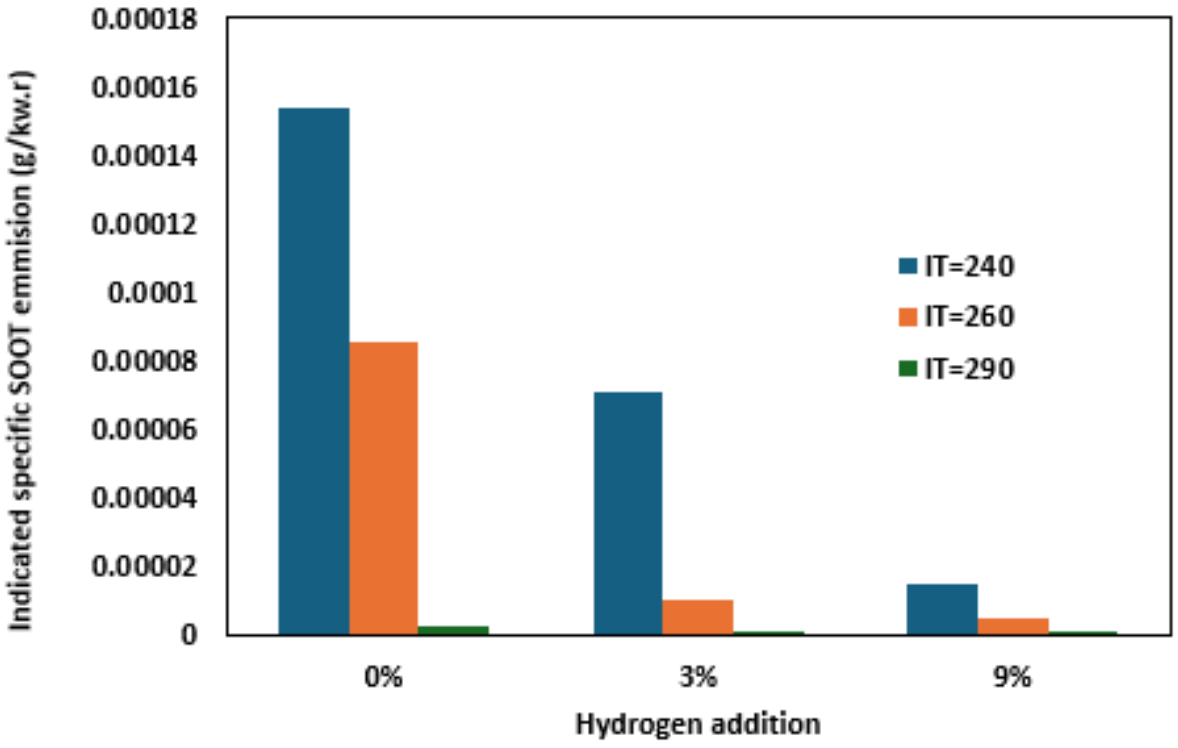

Figure 6.11: Results for indicated specific SOOT emission for hydrogen addition ranging from 0 to 12% and injection timings from 240 to 290 °CA bTDC at a fixed spark timing

6.3 Summary

In this study, the effect of varying injection timing of methanol during intake stroke with hydrogen enrichment on the performance and emissions. The results obtained on advancing injection timing from 240°CA bTDC to 290°CA bTDC are summarised as follows:

- Increase in the maximum in-cylinder pressure for both neat methanol and methanol with hydrogen addition. In addition to that earlier shift in the in-cylinder pressure for for neath methanol operating and methanol with hydrogen addition. Furthermore, Increasing the enrichment percentage of hydrogen resulted in an earlier rise of in-cylinder pressure as well as increased the maximum in-cylinder pressure compared to neat methanol operation.
- Improved the quality of fuel and air mixing around the spark plug. In addition to that by increasing hydrogen addition also enhanced the mixing quality.
- Increased the hydroxide radical (OH) formation for neat methanol and for hydrogen addition conditions. Then compared to neat methanol addition of 3%, and 9% hydrogen with methanol also resulted in enhancing the OH formation for all the injection timing.
- Faster flame propagation was obtained after the spark for neat methanol and for hydrogen addition conditions. Then compared to neat methanol addition of 3%, and 9%hydrogen with methanol also resulted in enhancing initiation of flame propagation for all the injection timing.
- Decreased the soot emissions for neat methanol and for all hydrogen addition conditions. Compared to the operation using neat methanol, the addition of hydrogen with methanol

- The Indicated specific NOx emissions increased for the scenarios involving neat methanol and methanol plus different hydrogen addition percentages listed earlier. In addition to that increase in 3% and 9% hydrogen addition with methanol resulted in increasing indicated specific NOx emission compared to neat methanol.
- Combustion duration dropped for neat methanol and for methanol with all hydrogen addition conditions Compared to neat methanol increase in hydrogen addition with methanol resulted in a decrease in the combustion duration.

Chapter 7

Lean burn investigation of methanol spark ignition engine with hydrogen addition

This chapter provides a detailed analysis of methanol-fuelled combustion in a spark-ignition engine with hydrogen additions ranging from 3% to 50%, under both stoichiometric and lean conditions. The lean burn limit and performance of a methanol-fueled spark-ignition engine are investigated with hydrogen enrichment. The detailed investigation of In-cylinder characteristics, such as in-cylinder pressure, indicated mean effective pressure (IMEP), and maximum in-cylinder temperature, are examined. In addition to the formation of hydroxyl radicals during the combustion process and detailed investigation of the quality of in-cylinder fuel and air mixing before spark timing is analysed. Furthermore, the chapter analyses emissions, including NOx, hydrocarbons (HC), carbon monoxide (CO), and soot, as well as combustion efficiency and duration. The impact of hydrogen enrichment indicated specific emissions (CO, NOx, HC, and soot) as hydrogen levels increase, from stoichiometric conditions (λ=1) to ultra-lean conditions λ=3.3.

7.1 Operating condition

As shown in the figure 7.1 the simulation was performed by maintaining a manifold pressure of 0.9 bar and fixing the spark timing at -20 degrees CA (crank angle) before top dead centre (bTDC), with the engine speed set at a constant 1200 RPM. The simulation utilized direct injection of methanol and port injection of hydrogen, as described in the previous chapter. Under stoichiometric conditions with an excess air ratio of λ=1, the simulation was conducted for neat methanol and

methanol with 3% and 9% hydrogen enrichment. For leaner conditions with an excess air ratio of λ=1.4, the study investigated neat methanol and methanol with 0% to 12% hydrogen enrichment. To explore very lean conditions, the excess air ratio was set to λ=2.2, and methanol with 0% to 12% hydrogen addition was examined. Under ultra-lean conditions (λ=3.3), higher hydrogen concentrations of 12% and 50% were tested. The analysis focused on several critical parameters, including indicated specific NOx, soot, and hydrocarbon (HC) emissions, in-cylinder equivalence ratio, cylinder pressure, hydroxyl radical (OH) formation, indicated mean effective pressure (IMEP), and carbon monoxide (CO) emissions. These operating conditions were selected to provide a comprehensive understanding of how hydrogen enrichment affects methanol combustion, particularly under varying air-fuel mixtures, and its impact on engine performance and emission characteristics.

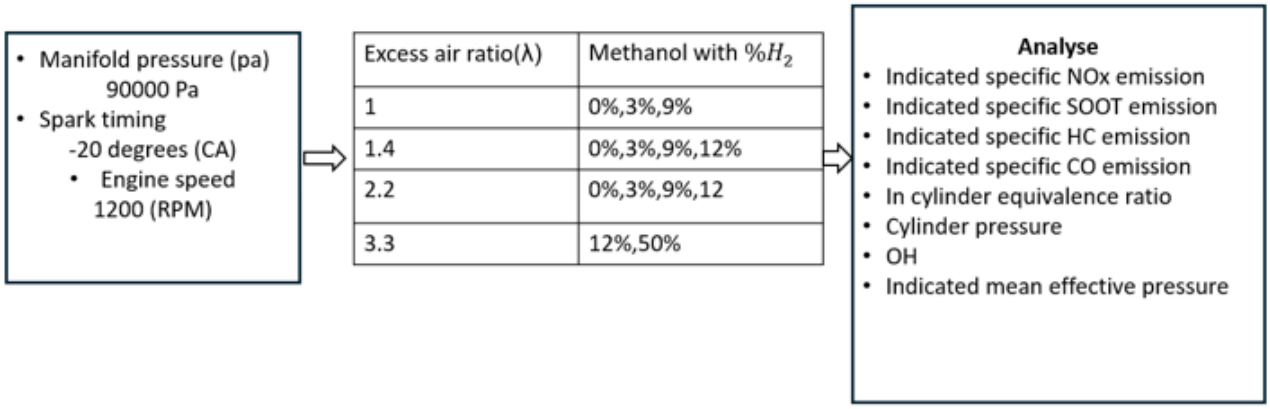

Figure 7.1: Test matrix

Model set up

To perform the above operating conditions, the validated 3D model described in Chapters 3 and 5 was utilized. The same direct injection model of methanol, as outlined in Chapters 5 and 6, was employed. Hydrogen addition, ranging from 3% to 50%, was simulated with methanol under various excess air ratios, using the methods detailed in Chapters 5 and 6. Furthermore, NOx and soot emissions were computed using the extended Zeldovich mechanism and the Hiroyasu-NSC soot model in Converge CFD, as previously

Combustion Efficiency

The combustion efficiency (%) can be calculated as:

$$\text{Combustion efficiency } (\%) = \frac{\text{Total heat release rate}}{m_{CH_3OH} \cdot \text{LHV}_{CH_3OH} + m_{H_2} \cdot \text{LHV}_{H_2}} \times 100 \quad (7.1)$$

Where: - m_{CH_3OH} and m_{H_2} (kg)are the masses of methanol and hydrogen, respectively, - LHV_{H_2} and LHV_{CH_3OH} (MJ/kg) represent the lower heating values of hydrogen and methanol, respectively.

7.2 Result and discussion

7.2.1 In cylinder characteristics

In cylinder pressure

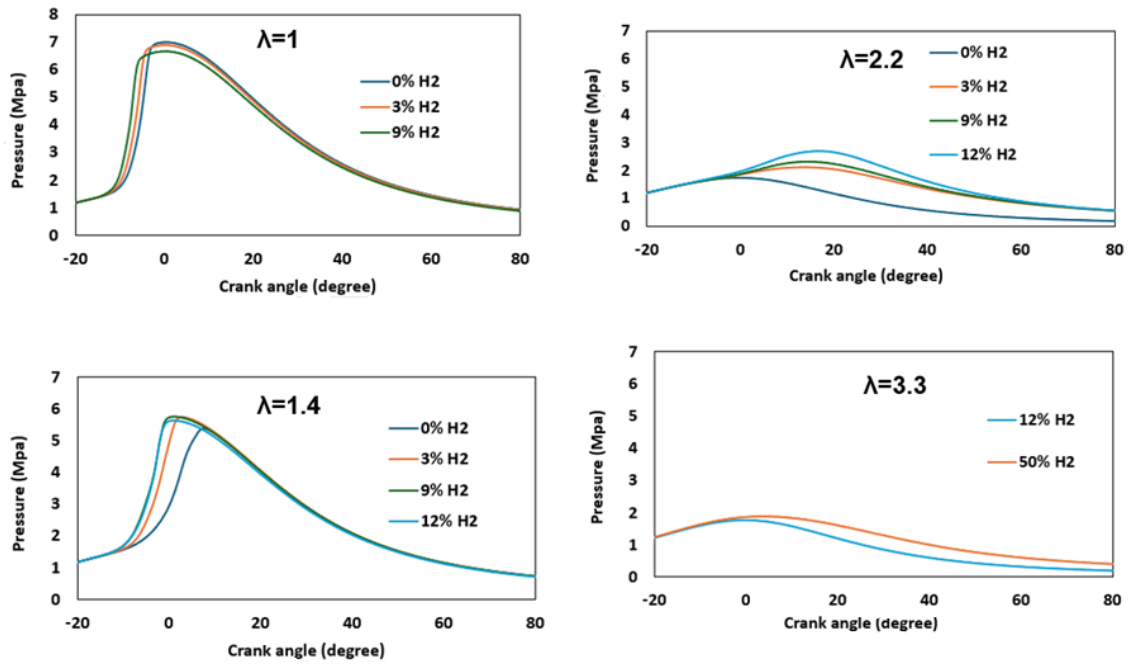

Figure 7.2: In cylinder pressure profiles at different crank angles for a methanol fuelled spark-ignition and varying levels of hydrogen addition (0% to 50%) under different excess air ratios (λ = 1, 1.4, 2.2, and 3.3)

Figure 7.2 illustrates the in-cylinder pressure obtained with respect to the crank angle for neat methanol and methanol with varying levels of hydrogen addition, under stoichiometric and lean operating conditions For stoichiometric operating conditions (λ = 1), the maximum in-cylinder pressure, reaching a peak magnitude

of 7 bar, was obtained with neat methanol. The addition of 3% and 9% hydrogen caused the in-cylinder pressure peaks to occur 1.47° and 2.87° CA earlier, respectively, compared to neat methanol.

Under lean operating conditions ($\lambda = 1.4$), the highest in-cylinder pressure was observed with 9% hydrogen addition to methanol. Compared to neat methanol, the addition of 3%, 9%, and 12% hydrogen resulted in the peak in-cylinder pressure rising 5° and 6° CA earlier. Additionally, the peak in-cylinder pressure increased by 6.7% and 7.0% with the addition of 3% and 9% hydrogen, respectively, compared to pure methanol operation.

Under very lean conditions ($\lambda = 2.2$), the peak in-cylinder pressure for neat methanol occurred at 0° CA at top dead centre, indicating that combustion did not initiate. In these very lean conditions, the highest peak in-cylinder pressure of 2.6 bar was achieved with 12% hydrogen addition to methanol. Moreover, increasing hydrogen addition from 3% to 9% and 12% resulted in the in-cylinder pressure rising 1° CA and 3° CA earlier, respectively. Compared to 3% hydrogen addition, 9% and 12% hydrogen addition led to a 13% and 24% increase in peak in-cylinder pressure, respectively.

Under ultra-lean conditions (=3.3), a peak in-cylinder pressure of less than 1.9 bar was observed for 12% hydrogen addition with methanol at 0° crank angle, as shown in Figure 7.2. This indicates that combustion did not initiate, possibly due to low fuel–air concentration near the spark plug, as illustrated in Figure 7.5. In contrast, with a 50% hydrogen addition to methanol, a peak in-cylinder pressure of 2 bar was observed at 4°CA.

Indicated mean effective pressure

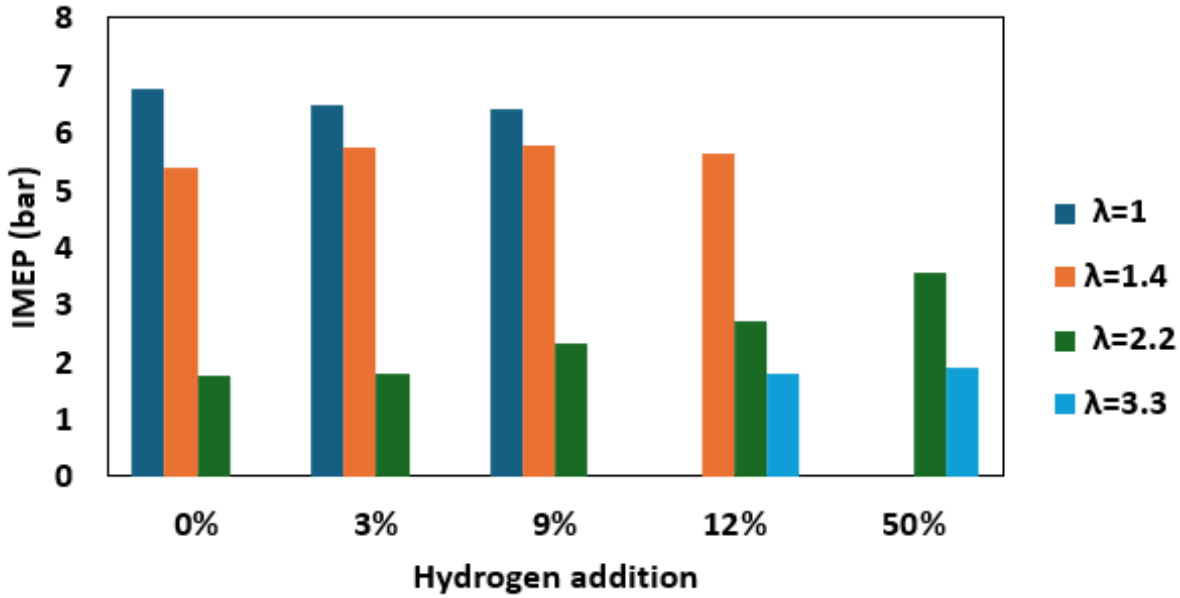

Figure 7.3: Indicated mean effective pressure (IMEP) for a spark-ignition engine fuelled with methanol and various levels of hydrogen addition (0% to 50%) under different excess air ratios (λ=, 1.4, 2.2, and 3.3)

. Figure 7.3 illustrates the effect of indicated mean effective pressure (IMEP) on a spark-ignition engine using neat methanol and methanol with varying levels of hydrogen addition, across a range of operating conditions from stoichiometric to lean. As shown in the figure, the highest IMEP of 11 bar was achieved under stoichiometric conditions ($\lambda = 1$). Additionally, the IMEP did not vary significantly between neat methanol and methanol with different levels of hydrogen addition under both stoichiometric and lean conditions ($\lambda = 1.4$). However, compared to stoichiometric operation, there was a 42% drop in IMEP under the leaner condition of $\lambda = 1.4$. Furthermore, compared to stoichiometric operation, the IMEP decreased by approximately 60% and 84% under very lean conditions at $\lambda = 2.2$ and ultra-lean conditions at $\lambda = 3.3$, respectively.

Under lean conditions with an excess air ratio (λ) of 2.2, IMEP was not achieved with neat methanol due to the failure of combustion. However, increasing hydrogen addition led to an increase in IMEP under these conditions. Specifically, increasing hydrogen addition from 3% to 9% and 12% resulted in a 123% and 158% increase in IMEP, respectively. Under ultra-lean conditions with an excess air ratio (λ) of 3.3, combustion did not occur with 12% hydrogen addition, but an IMEP of 1.9 bar was achieved with 50% hydrogen addition. These results demonstrate that hydro-

gen addition significantly influences the IMEP of methanol under various operating conditions, with the impact varying depending on the air-fuel ratio and the percentage of hydrogen added.

Mean flame temperature

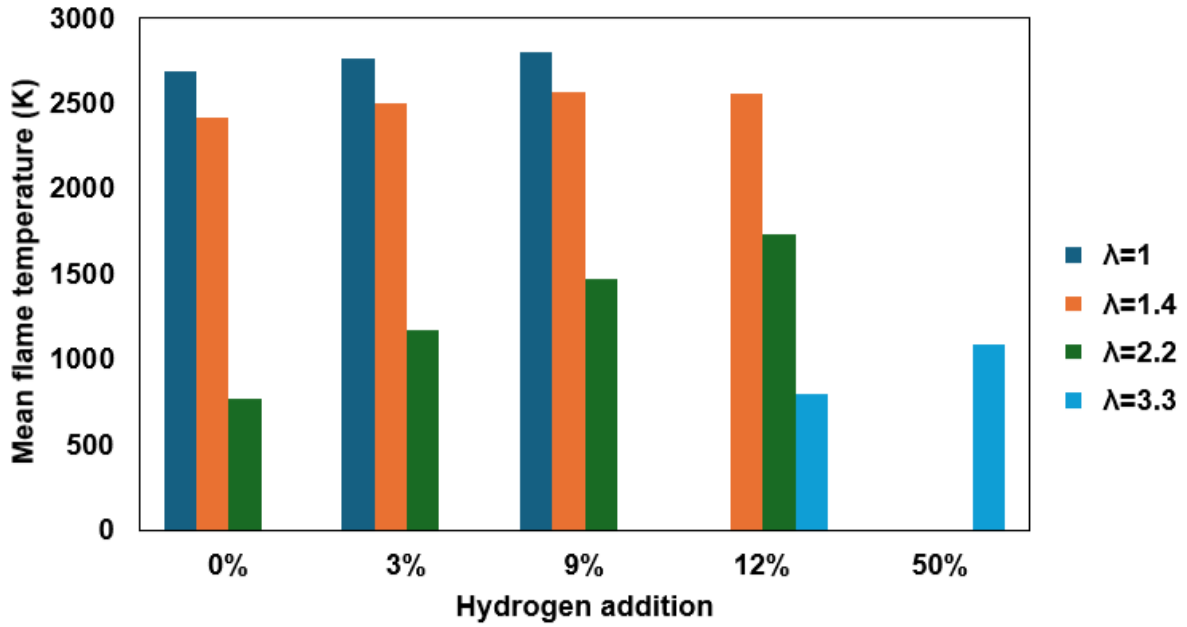

Figure 7.4: Mean flame temperature for a spark-ignition engine fuelled with methanol and various levels of hydrogen addition (0% to 50%) under different excess air ratios (λ = 1, 1.4, 2.2, and 3.3)

Figure 7.4 represents the mean flame temperature obtained under stoichiometric and lean operating conditions. The highest temperature was obtained for neat methanol and methanol with hydrogen addition under stoichiometric operating conditions compared to lean operating conditions.

Under stoichiometric operating conditions, the highest men flame temperature was obtained with 12% hydrogen addition to methanol. Compared to neat methanol, the maximum mean flame temperature increased by 2.5% with 3% hydrogen addition and by 4.2% with 9% hydrogen addition.

Under leaner conditions with an excess air ratio (λ) of 1.4, the highest mean flame temperature was obtained with 9% hydrogen addition to methanol. Compared to neat methanol, the addition of 3% hydrogen resulted in a 4% increase in mean flame temperature, while 9% and 12% hydrogen addition resulted in a 6% increase in mean flame temperature.

Under very leaner conditions (λ = 2.2), the addition of 3%, 9%, 12%, and 50% hydrogen to methanol resulted in an increase in mean flame temperature, as illustrated in Figure 7.4. This can be attributed to hydrogen's high diffusivity and rapid burning velocity, which enhance the reaction rate of methanol under lean conditions, leading to an increase in mean flame temperature. Less than 800 K was obtained for neat methanol during the expansion stroke, as combustion did not initiate under this excess air ratio condition. Compared to 3% hydrogen addition, increases of 9% and 12% hydrogen addition to methanol resulted in 26% and 48% increases in meanflame temperature, respectively.

Furthermore, methanol with 12% and 50% hydrogen addition was studied under very lean conditions with an excess air ratio (λ) of 3.3. The mean flame temperature obtained for 12% hydrogen addition was less than 800 K, indicating that combustion did not initiate under this condition. However, 50% hydrogen addition to methanol under λ = 3.3 resulted in a mean flame temperature of less than 1000 K.

In cylinder fuel and air mixing

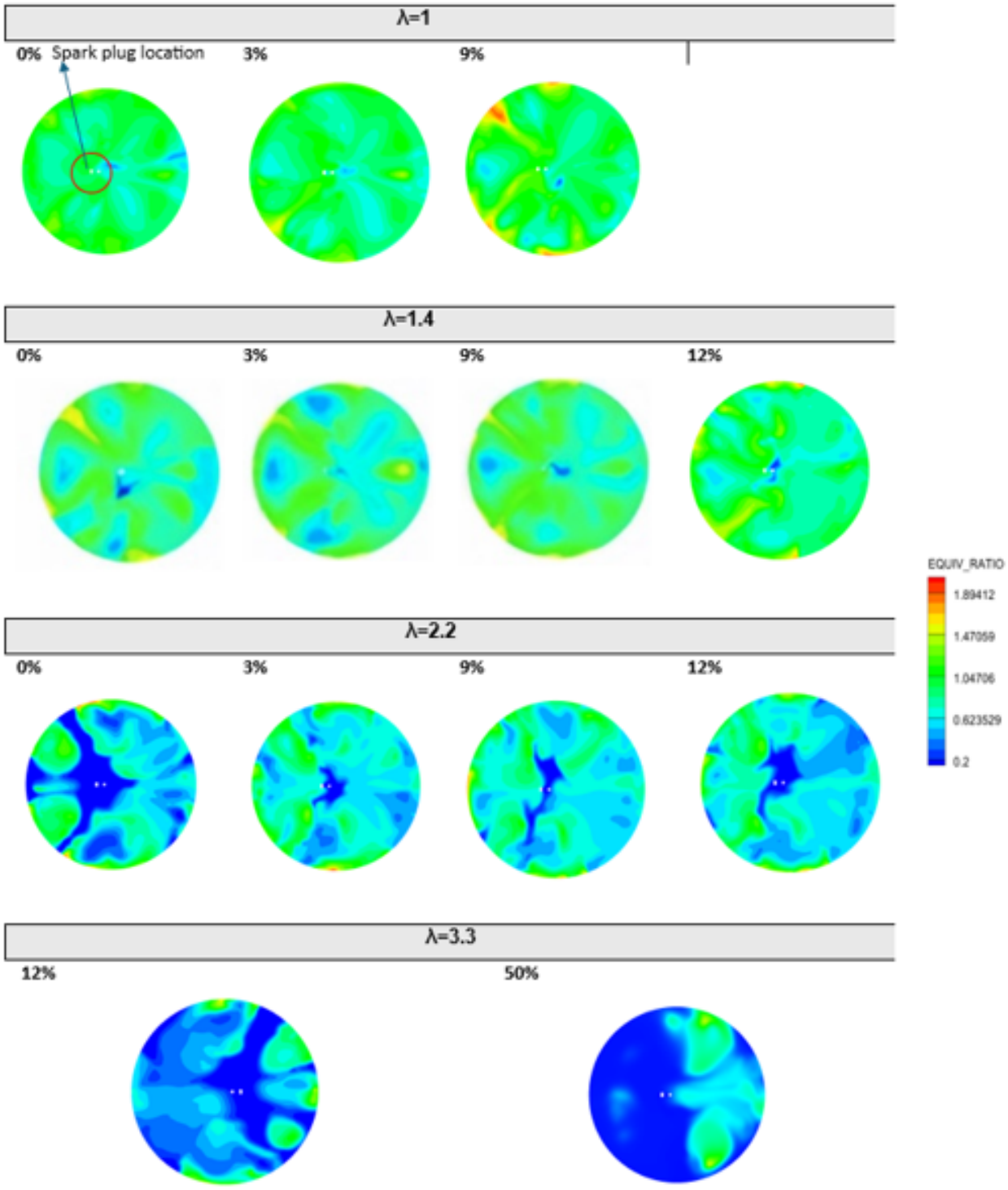

Figure 7.5: Comparison of in-cylinder mixing for various hydrogen additions (0, 3, 9 and 12%) and under stoichiometric and lean operating conditions (=1,1.4,2.2. and 3.3) just before the initiation of spark at 20°CA bTDC

Figure 7.5 illustrates the fuel and air mixing before spark timing at 20° CA bTDC for neat methanol and methanol with varying levels of hydrogen addition under stoichiometric (λ=1) and lean operating conditions. As seen in the figure 7.5, a richer fuel and air concentration is obtained around the spark plug before ignition under stoichiometric conditions compared to leaner operations, for both neat methanol and methanol with different levels of hydrogen addition. Across all operating conditions, increasing hydrogen addition improves the quality of fuel and air mixing by reducing the leaner areas, which are denoted by the blue regions in the contour plots.

Under stoichiometric operating conditions (λ=1), a richer fuel and air mixture was observed closer to and around the spark plug, as indicated by the green contours for neat methanol. The addition of 3% and 9% hydrogen to methanol further increased the fuel concentration around spark plug, enhancing the mixture's richness, as denoted by the yellow and red regions, while simultaneously reducing the leaner areas, indicated by the blue regions.

Operating under lean conditions (λ=1.4), uniform fuel and air mixing was achieved around the region close to the spark plug for both neat methanol and methanol with 3%, 9%, and 12% hydrogen addition. This is indicated by the yellow and green regions, with fewer lean areas denoted by blue. In addition to that increase in 3%,9% and 12% hydrogen addition resulted in a higher concentration of fuel air mixing closer and area round the spark plug compared to neat methanol operation.

Under very lean operation at λ=2.2, a larger area of leaner mixture concentration was observed for neat methanol, as indicated by the blue regions. This could potentially result in the failure to initiate combustion during the expansion stroke for neat methanol. However, increasing hydrogen addition from 3% to 12% reduced the leaner mixture concentration near the spark plug, as shown by the reduction of blue regions in the contour plot.

Furthermore, under ultra-lean operation at λ=2.2, combustion did not initiate for 12% hydrogen addition with methanol due to the higher concentration of lean mixture surrounding the spark plug. In contrast, increasing hydrogen addition to 50% with methanol resulted in the formation of a slightly richer fuel-air mixture closer to the spark plug, which allowed combustion to initiate.

Hydroxide radical

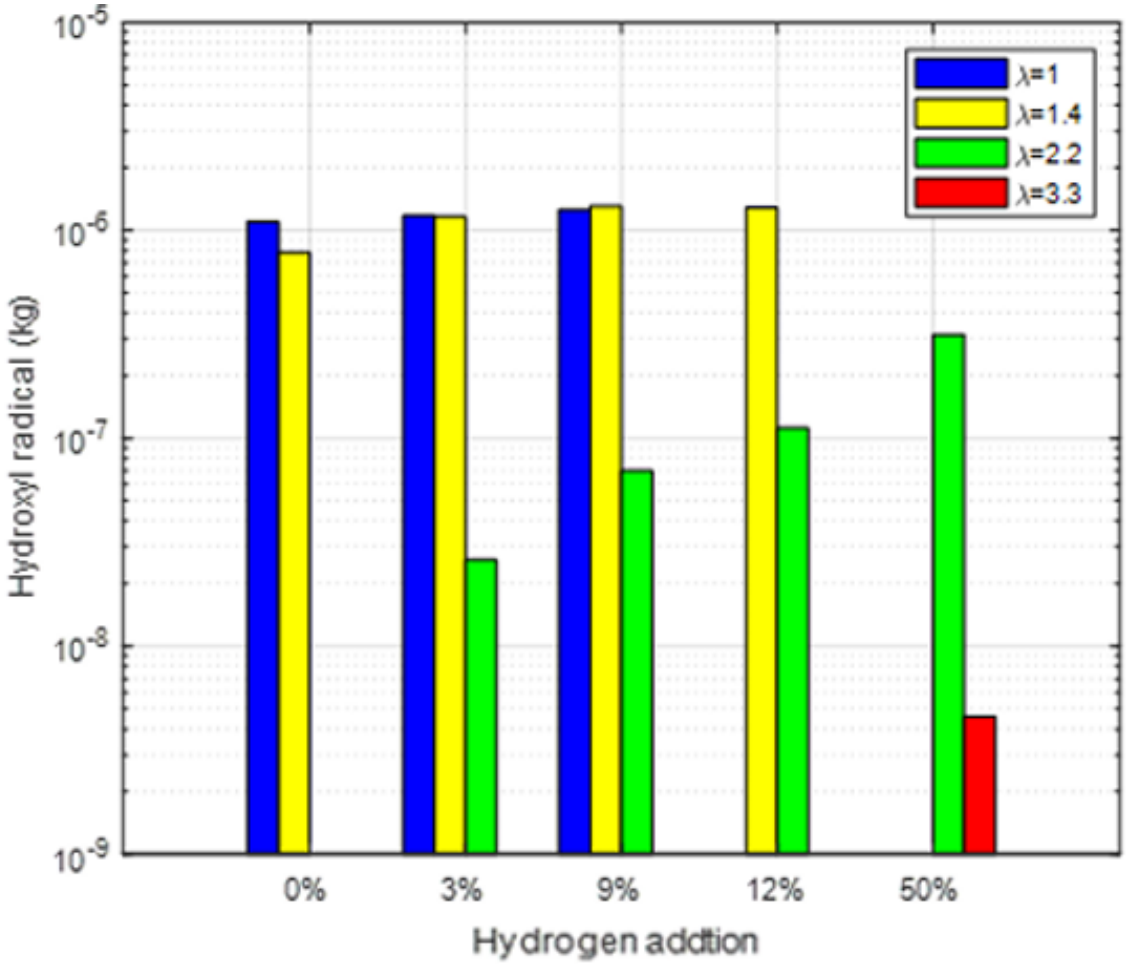

Figure 7.6: The peak hydroxyl radical formation for different level of (0, 3, 9 and 12%) hydrogen enrichment with methanol and under stoichiometric and lean operating conditions (λ=1,1.4,2.2. and 3.3) just before the initiation of spark at 20° CA bTDC

Figure 7.6 illustrates the Hydroxy radical formation during the combustion for neat methanol and methanol with different levels of hydrogen addition under stoichiometric and leaner operating conditions. Compared to leaner operating conditions during the combustion process highest Hydroxide radical was obtained for leaner operating condition λ=1.4 for 9% hydrogen addition with methanol.

Under stoichiometric operating conditions during combustion highest OH radical was obtained for 9% hydrogen addition with methanol compared to neat methanol and methanol with 3% hydrogen addition. The addition of 3% and 9% hydrogen addition under stoichiometric conditions resulted in a 7.2% and 13% rise in peak Hydroxide radical concentration during combustion process compared to neat methanol.

Under lean operation conditions, λ=1.4 highest OH radical concentration during the combustion process was obtained for methanol with 9% hydrogen addition with methanol. Compared to neat methanol addition of the 3%,9% and 12% hydrogen addition with methanol resulted in a 50%, 68%, and 65% increase in Hydroxide radical concentration during the combustion process. Then it was also noticed the addition of 12% hydrogen resulted in less than 1% reduction in the indicated specific NOx emission compared to 9% hydrogen addition.

Under very lean conditions of λ=2.2 Hydroxide concentration was not formed for neat methanol because combustion did not initiate. Formation of hydroxide ratio concentration during combustion was investigated for 3%,9% and 12% hydrogen addition under λ=2.2 very lean operating conditions. It was found that compared to 3% hydrogen addition with methanol 9% and 12% hydrogen addition increased by 168% and 331% of peak Hydroxide formation respectively. The extreme lean condition of λ= 3.3 Hydroxide concentration was investigated for 50 % hydrogen with methanol, indicated specific NOx emission was obtained lowest compared to stoichiometric and other leaner operating conditions

Hydroxyl formation at CA50

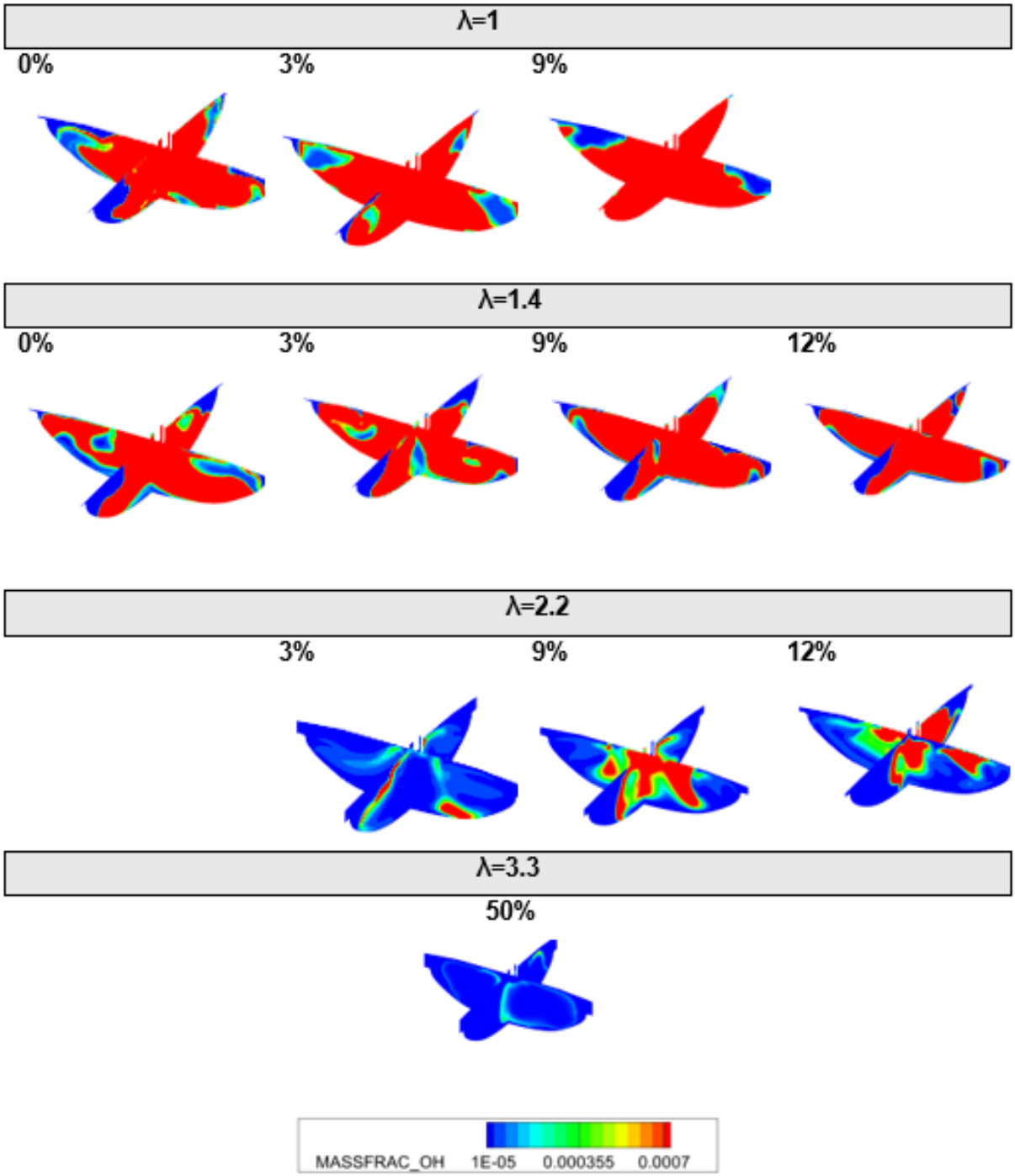

Figure 7.7: Hydroxyl radical formation at CA50 under stoichiometric to lean operating conditions for neat methanol and methanol with different levels of hydrogen addition.

Figure 7.7 illustrates the hydroxyl radical (OH) formation at CA50 (the crank angle at which 50% of the fuel has burned) during the combustion of neat methanol and

methanol with varying levels of hydrogen addition under stoichiometric (λ=1) and leaner operating conditions (λ=1.4, λ=2.2, and λ=3.3). The contour plots represent the distribution and intensity of hydroxyl radical formation that occurs with different hydrogen additions under each operating condition. As seen in the figure, shown by read areas in the contour plot the highest intensity of OH radicals at the CA50 point across the combustion chamber occurs under stoichiometric conditions, both for neat methanol and with varying levels of hydrogen addition. The formation of OH radicals decreases progressively under leaner conditions, from λ=1.4 to λ=3.3, for both neat methanol and methanol with different levels of hydrogen addition.

Under stoichiometric operating conditions at the CA50 location, the OH radical distribution exhibited a higher area of intense formation in the cylinder, as indicated by the extensive red regions, with fewer blue areas, suggesting consistent OH radical formation during the combustion process. Additionally, the 3% and 9% hydrogen addition led to an increase in the intensity of OH radical distribution, while reducing the presence of blue and green regions.

Under the lean operating condition of λ=1.4 at the CA50 location, the OH radical distribution was observed to be uniform across the chamber for both neat methanol and hydrogen addition conditions. Compared to neat methanol, the addition of 3%, 9%, and 12% hydrogen increased the intensity of OH radical distribution, reducing the less intense regions, as indicated by the green areas.

Under the lean operating condition of λ=2.2 at the CA50 location, the intensity of hydroxyl formation was concentrated in smaller regions during the combustion process, as indicated by the red areas in the figure. Less intense OH radical formation, denoted by the green regions in the contour covering the chamber, was observed for the 3%, 9%, and 12% hydrogen addition operating conditions. Additionally, increasing the hydrogen addition from 3% to 12% resulted in an expansion of OH intensity radical formation across the chamber at the CA50 point during the combustion process.

Furthermore, under the extremely lean operating condition of λ=3.3 with 50% hydrogen addition to methanol, a less intense OH radical formation was observed at the CA50 location during the combustion process, as indicated by the green regions in the contour, along with larger area of blue in the contour

Combustion duration

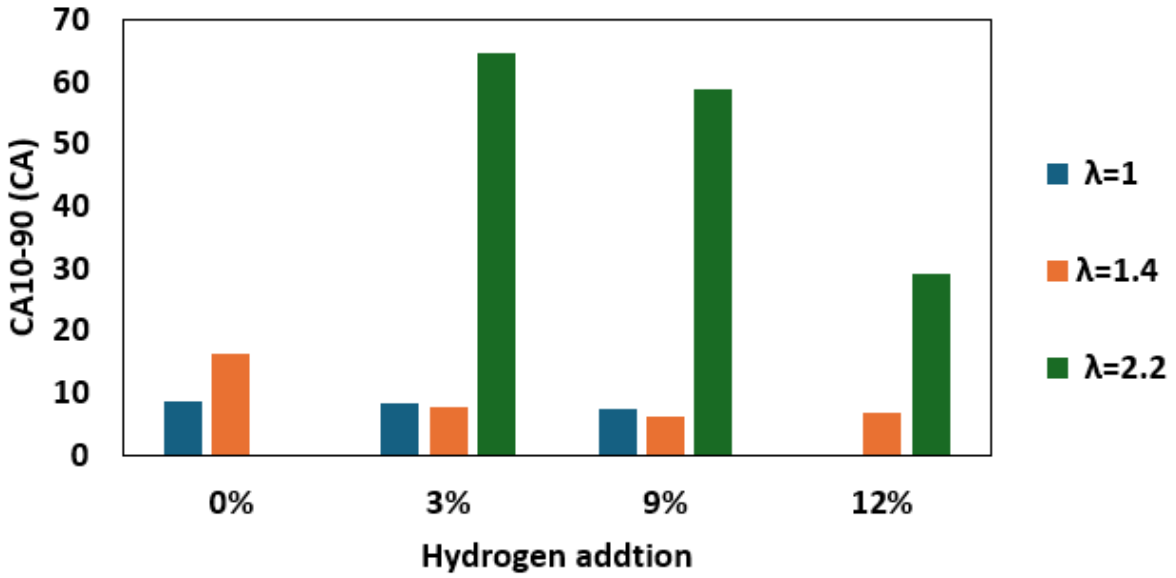

Figure 7.8: combustion duration of neat methanol and methanol with different levels of hydrogen addition stoichiometric (λ=1) and lean operating conditions(λ=1.4,λ=2.2)

Figure 7.8 represents combustion duration for different operating conditions of methanol combustion with varying levels of hydrogen addition under stoichiometric (λ=1) and leaner conditions (λ=1.4 and λ=2.2) The combustion duration is defined as the crank angle interval required to burn the methanol and hydrogen mixture, from the start of flame development at CA10 to the end of flame propagation at CA90.As can be seen from figure 7.8 the highest combustion duration as obtained under very lean operating conditions of λ=2.2, suggesting a slower combustion process

As can be seen from Figure 7.8 for stoichiometric operating condition (λ=1) highest combustion duration was obtained for neat methanol. The addition of 3% and 9% hydrogen addition under stoichiometric conditions resulted in a 2% and 12% reduction in combustion duration compared to neat methanol. Under lean operation conditions, λ=1.4 highest combustion duration was observed for neat methanol operation. Compared to neat methanol addition of the 3%,9% and 12% hydrogen addition with methanol resulted in 53%,61% and 59% reduction in combustion duration.

Under very lean conditions of λ=2.2, where combustion did not initiate with neat methanol, the lean operation was analysed by enriching the mixture with hydrogen from 3% to 9% in a methanol-operated spark-ignition engine. An increase in

hydrogen addition from 3% to 12% resulted in a decrease in the combustion duration. Specifically increase in hydrogen addition from 3% to 9% and 3% to 12% with methanol resulted in 9% and 55% reduction in combustion duration.

7.2.2 Emission

Indicated specific NOx emission

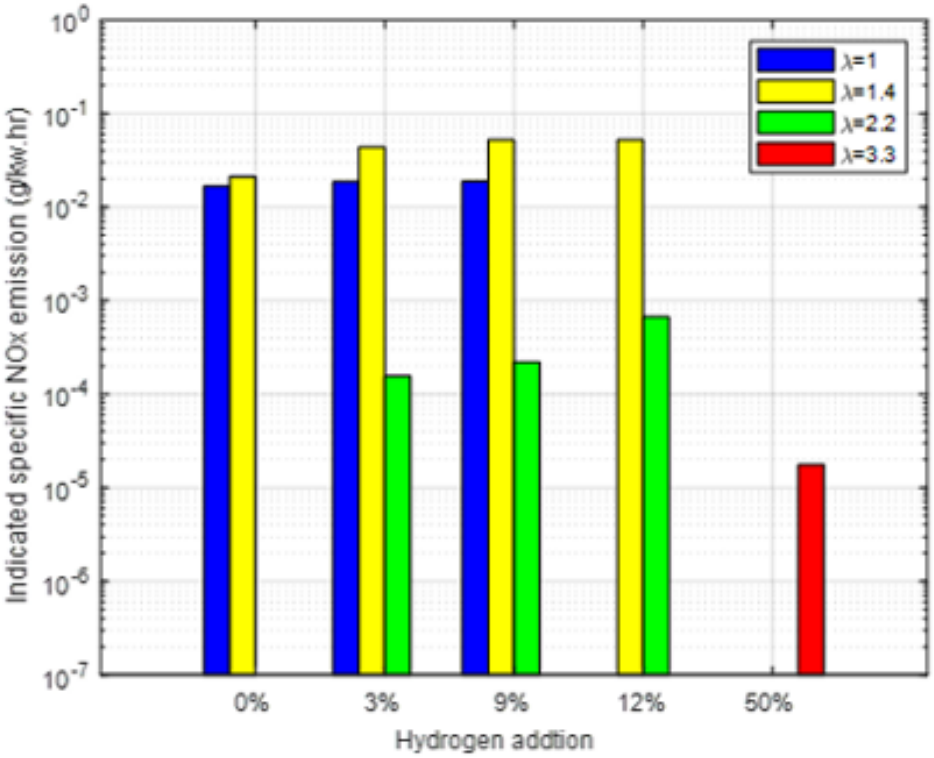

Figure 7.9: Indicated specific NOx emissions (g/kW.hr) for a spark-ignition engine fuelled with methanol and varying levels of hydrogen addition (0% to 50%) under different excess air ratios (λ = 1, 1.4, 2.2, and 3.3)

Indicated specific NOx emissions (g/kW.hr) for a spark-ignition engine fuelled with methanol and varying levels of hydrogen addition (0% to 50%) under different excess air ratios (λ = 1, 1.4, 2.2, and 3.3) Figure 7.9 represents the indicated specific NOx emissions obtained from neat methanol and methanol with different levels of hydrogen addition under stoichiometric to lean operating conditions. The highest indicated specific NOx emission was observed with 9% hydrogen addition to methanol under an excess air ratio (λ) of 1.4, compared to stoichiometric and other lean operating conditions.

As can be seen from Figure 7.9 for stoichiometric operating condition (λ=2.2) highest indicated NOx emission was obtained during the methanol with 12% hydrogen addition operation compared to methanol with different levels (3%,9%) of hydrogen addition. The addition of 3% and 9% hydrogen addition under stoichiometric conditions resulted in a 1.4% and 7.9% increase in indicated specific NOX emission compared to neat methanol

Under lean operation conditions, λ=1.4 highest NOx emission was obtained for methanol with 9% hydrogen addition with methanol.Compared to neat methanol addition of the 3%,9% and 12% hydrogen addition with methanol resulted in 105.13%, 146.28%, and 145.06% increase in indicated specific NOx emission. Then it was also noticed the addition of 125 hydrogen resulted in less than 1% reduction in the indicated specific NOx emission compared to 9% hydrogen addition.

Under very lean conditions of λ=2.2 NOx emission was not obtained for neat methanol because combustion did not initiate. Indicated specific NOx emission was investigated with the addition of 3%,9%,12% and 50% hydrogen addition under λ=2.2 very lean condition. It was found that compared to 3% hydrogen addition with methanol 9% and 12% hydrogen addition increased by 41% and 303% of indicated specific NOx emission respectively. The extreme lean condition indicated specific NOX emission was investigated for 50 % hydrogen with methanol 1.76e-5 indicated specific NOx emission was obtained.

Indicated specific hydrocarbon emission

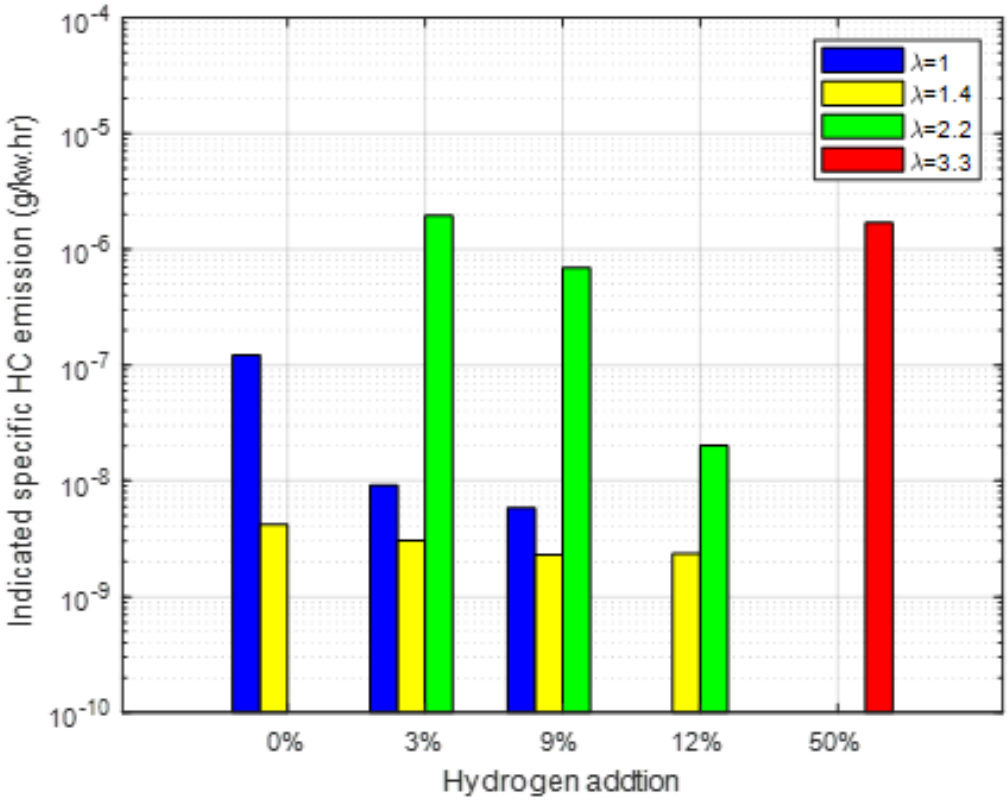

Figure 7.10: Indicated specific HC emissions (g/kW.hr) for a spark-ignition engine fuelled with methanol and varying levels of hydrogen addition (0% to 50%) under different excess air ratios (λ = 1, 1.4, 2.2, and 3.3)

Figure 7.10 represents the indicated specific hydrocarbon emissions obtained for neat methanol and methanol with different levels of hydrogen addition under stoichiometric to lean operating conditions. The highest indicated specific hydrocarbon emission was observed with 3% hydrogen addition to methanol under an excess air ratio (λ) of 2.2, compared to stoichiometric and other lean operating conditions.
As can be seen from Figure 7.11, under stoichiometric operating conditions (λ=1), the highest indicated specific hydrocarbon emission was obtained with neat methanol compared to methanol with 3% and 9% of hydrogen addition. The addition of 3% and 9% hydrogen under stoichiometric conditions resulted in a 92% and 95% drop in indicated specific hydrocarbon emissions compared to neat methanol.
Under lean operating conditions (λ=1.4), the highest hydrocarbon emission was obtained for neat methanol operation. An increase in hydrogen addition with methanol resulted in a drop in indicated specific hydrocarbon emissions. Compared to neat methanol, the addition of 3%, 9%, and 12% hydrogen resulted in a 27%, 45%, and 43% decrease in indicated specific hydrocarbon emissions, respec-

tively.

Under very lean conditions (λ=2.3), the indicated specific hydrocarbon emission study was conducted for methanol with 3%, 9%, 12%, and 50% hydrogen addition. The highest indicated specific hydrocarbon emission was obtained with 3% hydrogen addition to methanol. It was also noted that, compared to 3% hydrogen addition, indicated specific hydrocarbon emissions dropped by 14% with 9% hydrogen addition and then further increased with 12% and 50% hydrogen addition, showing a 100% decrease in indicated specific hydrocarbon emission. Under extreme lean conditions, the indicated specific hydrocarbon emission for 50% hydrogen addition was higher than under stoichiometric and lean operating conditions (λ=1.4).

Indicated specific carbon monoxide emission

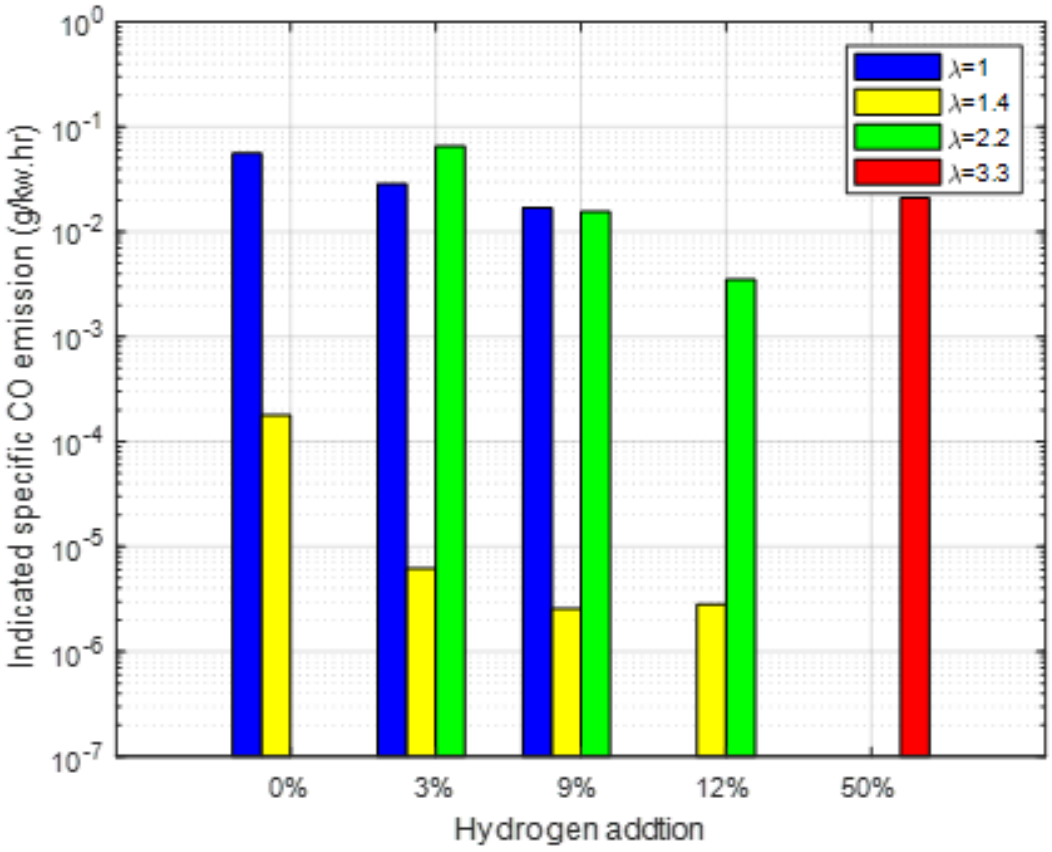

Figure 7.11: Indicated specific carbon monoxide emissions (g/kW.hr) for a spark-ignition engine fuelled with methanol and varying levels of hydrogen addition (0% to 50%) under different excess air ratios (λ = 1, 1.4, 2.2, and 3.3).

Figure 7.11 represents the indicated specific co-emission obtained for neat methanol and methanol with different levels of hydrogen addition under stoichiometric and lean-operated conditions. As can be seen from the figure lowest indicated specific

CO emission was obtained when neat methanol and methanol with different levels of the hydrogen addition is operated at λ= 1.4 excess air ratio compared to stoichiometric and other lean operating conditions (λ=2.2 and λ=3.3).

Under stoichiometric operating conditions, the highest indicated co-emission is obtained for neat methanol. Then compared to neat methanol, 112% and 50% reduction in indicated specific co-emission was obtained for 9% and 12% hydrogen addition with methanol under stoichiometric operating conditions. It was also noticed that increasing the level of hydrogen by more than 3% under stoichiometric operating conditions resulted in reducing the indicated specific co-emission. In addition to that increasing hydrogen addition to 12% with methanol resulted in a 78% decrease in the indicated specific co-emission compared to neat methanol.

Under lean operating condition of λ=1.4 lower co emission was obtained for 9% hydrogen addition with methanol. Compared to neat methanol operating conditions indicated specific co-emission dropped to 97%, 99% and 98.5% on 3%,9% and 12% hydrogen enrichment. It was noticed that compared to 9% hydrogen addition with methanol resulted in a less 1% increase in the indicated specific co-emission for 12% hydrogen enrichment under λ=1.4 operating conditions.

Under more lean operating condition of (λ=2.2) highest indicated specific co-emission was obtained for 3% hydrogen addition with methanol. Then indicated specific co-emissions were not obtained It was also noticed that an increase in the level of the hydrogen addition resulted in reducing the indicated specific co-emissions under lean operating condition of the λ=2.2. Compared to 3% hydrogen addition with methanol indicated specific co-emission dropped to 71%,94% and 100% on 9%,12% and 50% hydrogen enrichment with methanol. Furthermore, extreme lean operating condition (λ=3.3) indicated specific co-emission studied for 50% hydrogen addition with methanol which was found higher compared to lean burn operating conditions of neat methanol and methanol with different levels of hydrogen addition λ=1.4)as well as very higher levels of hydrogen addition (9% ,12%) with methanol under very lean operation of λ=2.2

Indicated specific soot emission

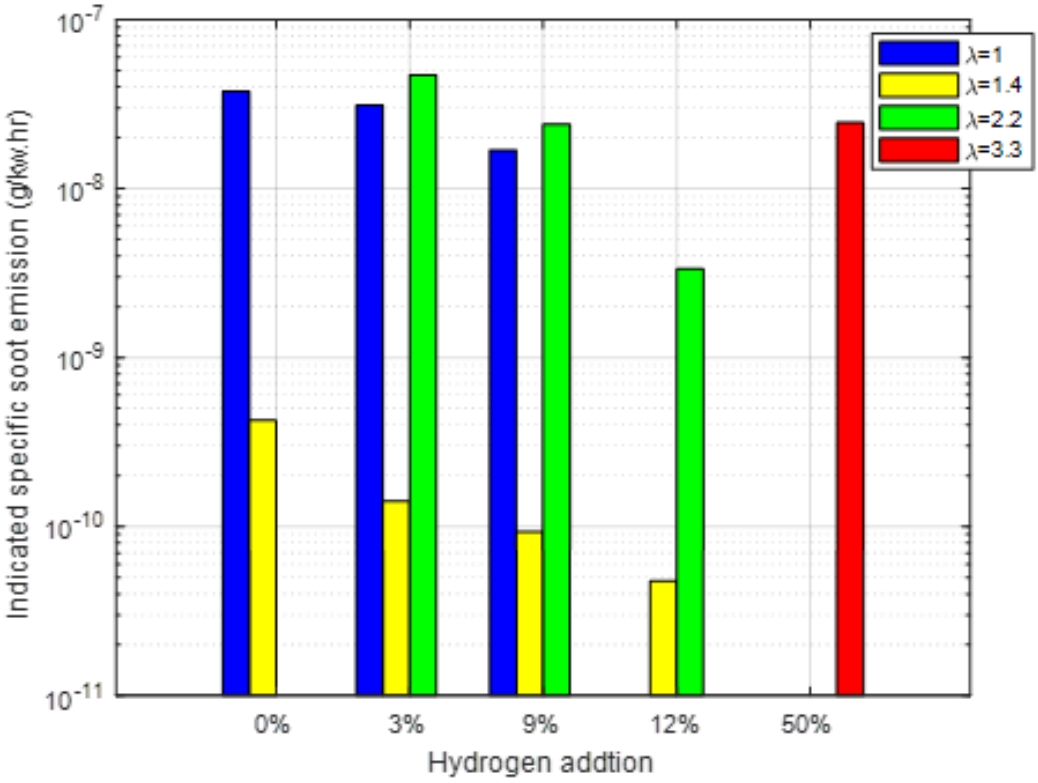

Figure 7.12: Indicated specific soot emissions (g/kW.hr) for a spark-ignition engine fuelled with methanol and varying levels of hydrogen addition (0% to 50%) under different excess air ratios (λ = 1, 1.4, 2.2,3.3)

Figure 7.12 illustrates the indicated specific soot emissions obtained for neat methanol and methanol with different levels of hydrogen addition under stoichiometric and lean operating conditions. As can be seen from the figure, the highest indicated specific soot emission was obtained for λ=2.2 compared to stoichiometric and other lean operating conditions. Under stoichiometric operating conditions, 3% and 9% hydrogen addition to methanol resulted in a 15% and 51% reduction in indicated specific soot emissions compared to neat methanol, respectively.

Under operating conditions of λ = 1.4, the indicated specific soot emissions were close to zero for neat methanol as well as for methanol with 3%, 9%, and 12% hydrogen addition. Compared to neat methanol, indicated specific soot emissions dropped by 67.0%, 82.4%, and 78.9% for methanol with 3%, 9%, and 12% hydrogen addition, respectively.

When operating under leaner conditions (λ=2.2), the highest indicated soot emission was obtained with 3% hydrogen addition to methanol. Increasing the hydrogen

enrichment to more than 3% resulted in a decrease in indicated specific soot emissions. Compared to 3% hydrogen addition to methanol, indicated specific soot emissions decreased by 76% and 97% with 9% and 12%, hydrogen addition, respectively.

Furthermore, under extremely lean operating conditions (λ=3.3), the indicated specific soot emission was studied for 50% hydrogen addition to methanol and was found to be higher compared to other lean burn operating conditions with neat methanol and methanol with different levels of hydrogen addition (λ=1.4 and λ=2.2).

7.2.3 Combustion efficiency

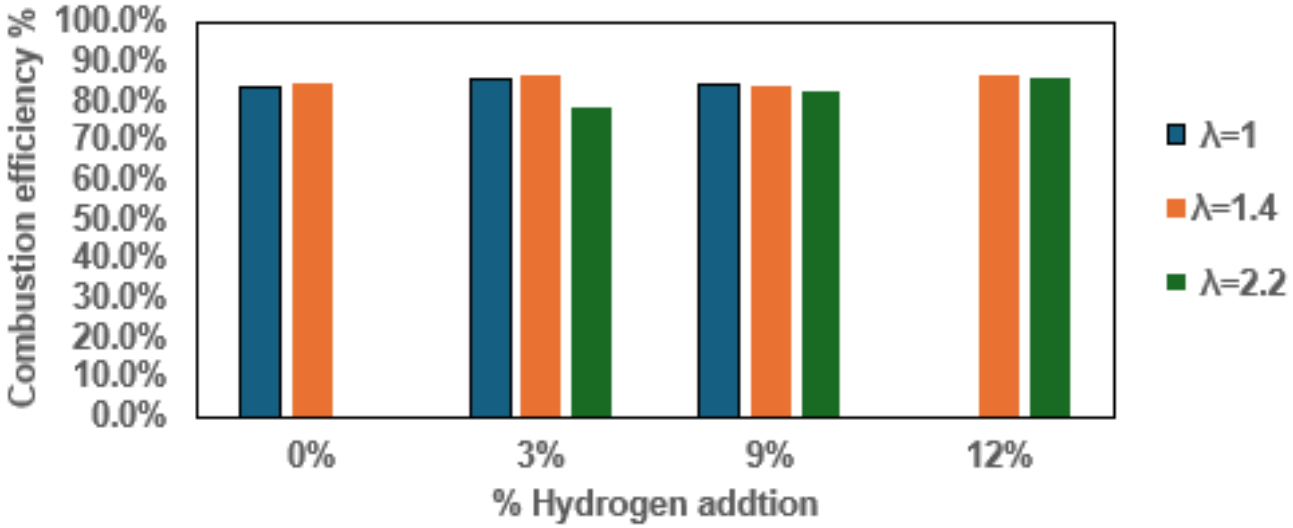

Figure 7.13: Combustion efficiency (%) for a spark-ignition engine fuelled with methanol and varying levels of hydrogen addition (0% to 12%) under different excess air ratios (λ = 1, 1.4, and 2.2)

Combustion efficiency is a crucial parameter in alaysisng the effectiveness of fuel energy conversion during combustion, directly impacting engine performance, fuel consumption, and emissions. Figure 7.13 represents a comparison of combustion efficiency for different operating conditions of methanol combustion with varying levels of hydrogen addition under stoichiometric (λ=1) and leaner conditions (λ=1.4 and λ=2.2). As shown in the figure 7.13, the highest combustion efficiency was obtained with 3% hydrogen addition to methanol under the leaner operating condition of λ=1.4. For the stoichiometric operating condition (λ=1), the highest combustion

efficiency was observed for 3% hydrogen addition to methanol, compared to neat methanol and 9% hydrogen addition. Specifically, a 2% increase in combustion efficiency was achieved with 3% hydrogen addition compared to neat methanol. However, it was noted that higher hydrogen addition of 9% with methanol resulted in more than a 5% drop in combustion efficiency compared to the 3% hydrogen addition. Under lean operating conditions (λ=1.4), combustion efficiency was also analysed for methanol with 9% hydrogen addition. Compared to neat methanol, the addition of 3%, 9%, and 12% hydrogen to methanol resulted in 2.5%, 4%, and 3.5% increases in indicated specific NOx emissions, respectively. Additionally, it was observed that 12% hydrogen addition led to a reduction of more than 1% in combustion efficiency compared to the 9% hydrogen addition. Under very lean conditions (λ=2.2), combustion efficiency was analysed for methanol with 3%, 9%, and 12% hydrogen addition. As shown in the figure, under the very lean operating condition of λ=2.2, higher combustion efficiency was achieved with 12% hydrogen addition to methanol. Specifically, compared to 3% and 9% hydrogen addition, the 12% hydrogen addition resulted in 9% and 4% increases in combustion efficiency, respectively.

7.3 Summary

In this study the performance and emission of the methanol-fueled spark ignition engine under stoichiometry to lean burn operating conditions with different levels of hydrogen enrichment with methanol. The results obtained under stoichiometric to lean burn conditions are summarised as follows:

- For stoichiometric conditions (λ=1), neat methanol produced the highest in-cylinder pressure, with hydrogen addition causing the pressure peaks to occur earlier. Under lean conditions (λ=1.4), 9% hydrogen addition resulted in the highest pressure, with an earlier rise in peak pressure. Under very lean conditions (λ=2.2), combustion initiation was delayed with neat methanol,but the addition of 12% hydrogen produced the highest in-cylinder pressure, with earlier and higher pressure peaks as hydrogen levels increased.
- The highest indicated mean effective pressure (IMEP) was obtained under stoichiometric conditions with neat methanol and various levels of hydrogen addition. IMEP was not significantly affected under both stoichiometric and lean operating conditions (λ=1.4) with hydrogen enrichment. However, increasing hydrogen addition significantly improved IMEP under very lean (λ=2.2) and ultra-lean (λ=3.3) operating conditions.

- The analysis revealed that the highest in-cylinder temperatures were achieved under stoichiometric conditions for both neat methanol and methanol with varying levels of hydrogen addition, compared to leaner operating conditions with excess air ratios ranging from λ=1.4 to λ=3.3. Across all operating conditions, increasing hydrogen addition led to an increase in maximum cylinder temperature. Temperatures below 800 K were observed for neat methanol under very lean conditions λ=2.2 and for 12% hydrogen addition under ultra-lean conditions λ=3.3.
- The analysis shows that under stoichiometric conditions (λ=1), a richer fuel and air mixture was obtained near the spark plug with hydrogen enrichment in methanol. In leaner operating conditions with an excess air ratio of λ=1.4, a more uniform fuel-air mixture was obtained around the spark plug. Under very lean (λ=2.2) and ultra-lean conditions, higher hydrogen levels reduced lean areas around the spark plug, helping to initiate combustion.
- The analysis of indicated specific emissions under stoichiometric to leaner operating conditions revealed that hydrogen addition to methanol led to a significant increase in indicated specific NOx emissions and a significant reduction in indicated specific hydrocarbon(HC), carbon monoxide (CO), and soot emissions. The highest indicated specific NOx emissions were observed under lean conditions (λ=1.4) for both neat methanol and methanol with varying levels of hydrogen addition, compared to stoichiometric and more extended lean conditions (λ=2.2). Additionally, higher indicated specific hydrocarbon and soot emissions were obtained under very lean conditions (λ=2.2) and ultra-lean conditions (λ=3.3) compared to stoichiometric and moderately lean operations (λ=1.4). The lowest indicated specific carbon monoxide emissions were achieved under lean operation (λ=1.4) for both neat methanol and methanol with varying levels of hydrogen addition.
- The highest combustion efficiency was achieved under lean operation with an excess air ratio of λ=1.4 with 3% hydrogen addition to methanol. In addition to that 3% hydrogen addition also resulted in the highest combustion efficiency under both stoichiometric (λ=1) and lean conditions (λ=1.4), compared to neat methanol and higher levels of hydrogen addition (9% and 12%). Under very lean conditions (λ=2.2) and ultra-lean conditions (λ=3.3), higher levels of hydrogen addition led to an increase in combustion efficiency.
- Shorter combustion duration was achieved under stoichiometric conditions compared to leaner operating conditions with excess air ratios from λ=1.4 to λ=3.3 for both neat methanol and methanol with increasing levels of hydrogen addition. Increasing hydrogen addition to methanol resulted in reduced

combustion duration across all operating conditions.

Chapter 8

Combined effects of carbon monoxide and hydrogen enrichment in methanol-fueled spark ignition engine

This chapter presents a simulation study conducted on a spark-ignition methanol-fuelled engine, focusing on the effects of carbon monoxide combined with hydrogen addition. The study evaluates the effect of hydrogen enriched with methanol and the combined effect of carbon monoxide along with hydrogen addition with methanol at a fixed load of 11 bar indicated mean effective pressure.This study analysed in-cylinder mixing, indicated specific carbon monoxide, and NOx emissions, Indicated thermal efficiency, Hydroxy radical formation and under the operating conditions mentioned above.

8.1 Operating condition

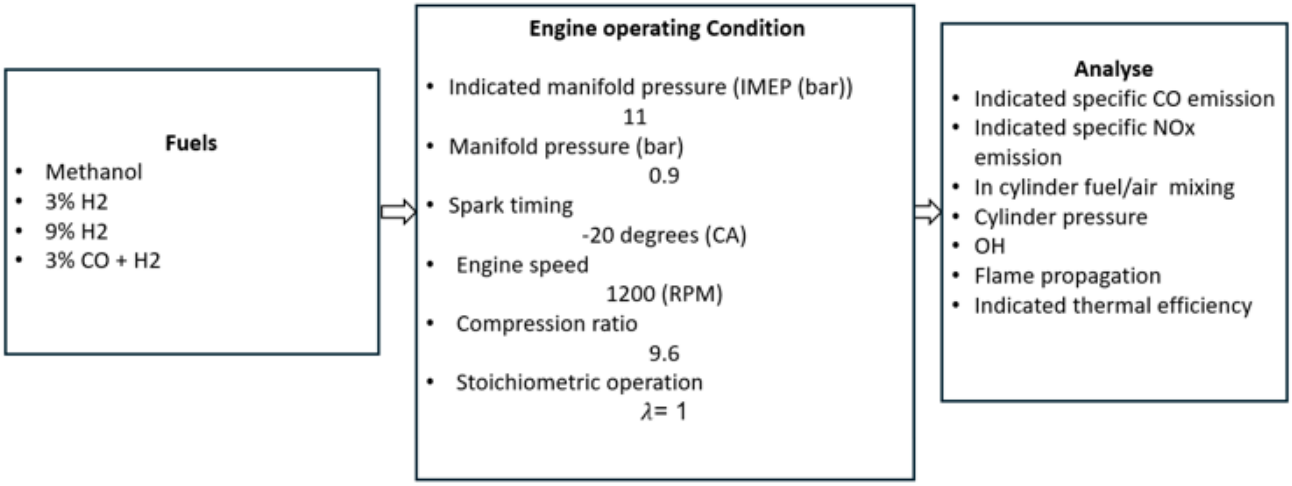

Figure 8.1: Test matrix

Figure 8.1 test matrix The operating conditions for the methanol-fuelled spark-ignition engine were tested using neat methanol as a baseline, along with methanol enriched with 3% and 9% hydrogen (H_2), and methanol combined with 3% hydrogen (H_2) and carbon monoxide (CO). The tests were conducted by maintaining an Indicated Mean Effective Pressure (IMEP) of 11 bar, with fixed parameters including a manifold pressure of 0.9 bar and an engine speed of 1200 RPM. The engine was operated under stoichiometric conditions with an air-fuel equivalence ratio(ϕ) of 1. The analysis focused on indicated specific CO and NOx emissions indicated thermal efficiency, and in-cylinder characteristics such as pressure, OH radical formation, and flame propagation.

Model setup

To perform the above-mentioned operating conditions, a three-dimensional model of direct methanol injection was created. Methanol was injected at 80° CA bTDC with an injection pressure of 110 bar. The computational simulation of methanol direct injection was conducted using the K-H model with the Rayleigh-Taylor mechanism as mentioned in chapter 3.

Hydrogen addition

The 3%,9% hydrogen addition was simulated using port injection. The hydrogen was added to methanol as a volume fraction of the intake air. The % of hydrogen addition is calculated based the on equation 3.60 in Chapter 3

Carbon monoxide and Hydrogen addition

The 3% CO + 3% H_2 addition was simulated using port injection. The hydrogen was added to methanol as a volume fraction of the intake air, defined as:

$$y = \frac{V_{\mathrm{CO}}}{V_{\mathrm{air}} + V_{\mathrm{H_2}} + V_{\mathrm{CO}}} \tag{8.1}$$

Where $V_{\mathrm{H_2}}$ and V_{CO} are the volumetric flow rates of hydrogen and carbon monoxide, respectively. The excess air ratio for methanol with carbon monoxide and Hydrogen addition is calculated by:

$$\lambda = \frac{m_{\mathrm{air}}}{m_{H_2} \cdot AF_{H_2 st} + m_{\mathrm{CH_3OH}} \cdot AF_{\mathrm{CH_3OH}st} + m_{\mathrm{CO}} \cdot AF_{\mathrm{CO}st}} \tag{8.2}$$

Excess air combustion equation of methanol with hydrogen and carbon monoxide addition

$$\begin{aligned} CH3OH + x\,H2 + y\,CO + E \cdot 1.5 \cdot e \cdot \left(O2 + \frac{79}{21} N2\right) \\ \rightarrow (1+y) \cdot CO2 + \left(2 \cdot \left(1 + \frac{x}{2}\right)\right) H2O \\ + \left(E \cdot 1.5 \cdot e \cdot \frac{79}{21}\right) \cdot N2 \\ + \left(c - \frac{(a+b)}{2}\right) \cdot O2 \end{aligned}$$

Variables

$$\begin{aligned} a &= 2 \cdot (1+y) \\ b &= \frac{2 \cdot (2+x)}{2} \\ e &= \frac{(2 \cdot (1+y) + ((2 \cdot (2+x))/2) - 1)}{3} \\ c &= (1 + y + (((E \cdot 1.5) \cdot e) \cdot 2)) \end{aligned}$$

where x and y are the % of hydrogen and carbon monoxide addition

In this simulation, the boundary conditions were set up to accurately reflect the chemical composition of the inflowing mixture. The mass fractions of the species were calculated based on stoichiometric equations to ensure the correct proportions of fuel and oxidizer. For the CO + H_2 addition operating condition, the computed

mass fractions of hydrogen and carbon monoxide were applied to the inflow boundary, while for the hydrogen addition operating condition, only the computed mass fractions of hydrogen were applied. In both cases, these were applied along with the appropriate proportions of oxygen and nitrogen. This approach ensures that the inflowing mixture entering the combustion chamber represents the stoichiometric balance required for optimal combustion, thereby providing realistic conditions for the simulation.

The test performed at the basic grid size for the 3D model was 4mm. The in-cylinder region was refined to a mesh size of 1 mm during the combustion and gas exchange process. Finally, a finer embedding of 0.5 mm was applied around the injector and the spark plug to capture the flame characteristics such as: kernel formation its growth, and developments mentioned in chapter 3. The spark timing and spark energy were replicated by the source/sink modelling. This approach was used to replicate the arc phase and glow phase of the spark, with a duration of 0.5 °CA for the arc phase and a duration of 8 °CA for the spark as mentioned in Chapter 3. The adaptive mesh refinement (AMR) was applied automatically by the solver, and the mesh was refined based on the l°CA gradient of temperature and velocity as mentioned in Chapter 3. The computational fluid dynamics (CFD) solver, Converge [107, 7], to solve the three-dimensional Reynolds-Averaged Navier Stokes (RANS) equations and the turbulence inside the combustion chamber was simulated using k- model [99]. The O'Rourke and Amsden heat transfer sub-model was applied and for combustion investigations, SAGE a detailed chemistry solver was used to calculate the reaction rates of all elementary reactions of the methanol/hydrogen combustion mechanism [82, 94]. This mechanism [82] consists of 20 elementary reversible reactions, which have been validated across a wide range of experimental data.

8.2 Results and discussion

8.2.1 In-cylinder characteristics

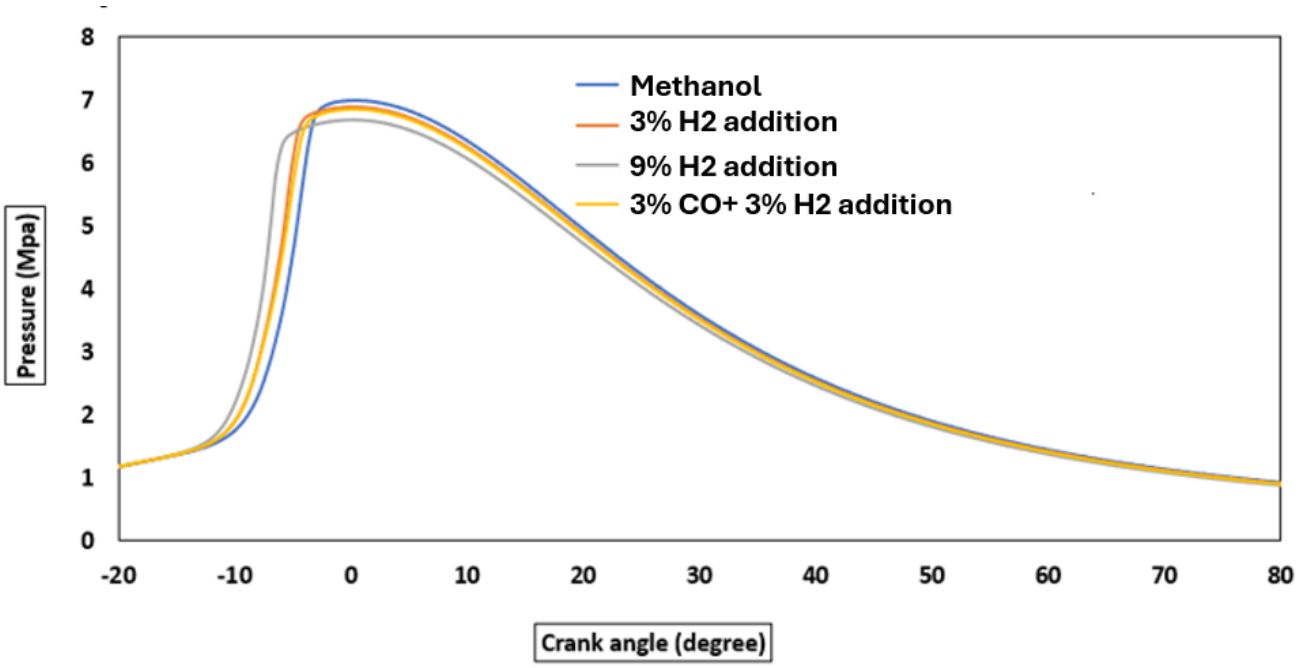

Figure 8.2: In-cylinder of methanol spark-ignition engine with (3%, 9%) hydrogen addition and 3% CO + 3% H_2 addition

Figure 8.2 illustrates the effects of 3% and 9% hydrogen enrichment, as well as a 3% CO + 3% H_2 addition, on in-cylinder pressure variations at different crank angles in a methanol-fueled spark ignition engine with fixed spark timing of 20° CA bTDC. The simulation reveals that the highest peak in-cylinder pressure of 7 MPa was achieved under neat methanol operation. The addition of 3% and 9% hydrogen, as well as 3% CO + 3% H_2 addition with methanol, resulted in less than a 1% drop in maximum in-cylinder pressure compared to neat methanol operation. Furthermore, the in-cylinder pressure peaks occurred 1.47° and 2.87° CA earlier with 3% and 9% hydrogen addition, and with 3% CO + 3% H_2 addition peak in-cylinder pressure occurred 1.35°CA earlier compared to neat methanol operation respectively. This shift can be attributed to the higher adiabatic properties of hydrogen and carbon monoxide compared to methanol, as well as hydrogen's higher laminar flame speed compared to methanol as mentioned in table 1.1.[86]

In-cylinder mixing

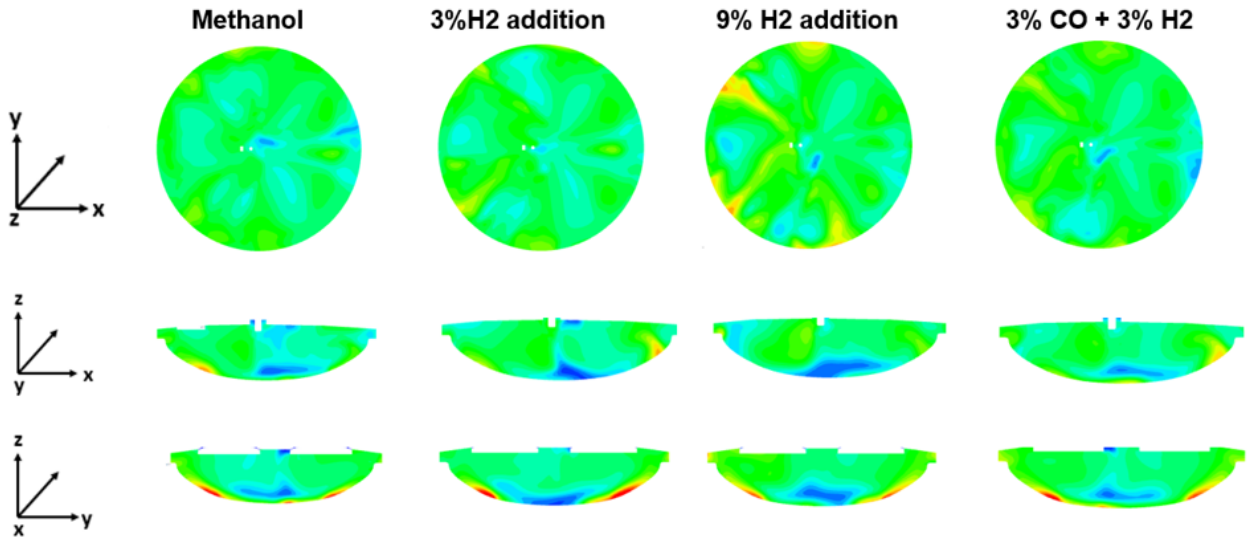

Figure 8.3: In-cylinder mixing for (3%,9%) hydrogen addition with methanol and (3% carbon monoxide + 3% hydrogen addition) with methanol before 20°CA bTDC

Figure 8.3 illustrates the in-cylinder fuel and air mixing just before spark timing (20°CA bTDC) for various fuel compositions: neat methanol, methanol with 3% hydrogen, methanol with 9% hydrogen, and methanol with a 3% CO + 3% H_2 blend. In the top view (XY plane) of Figure 8.3, it is evident that adding 3% and 9% hydrogen results in a richer fuel-air mixture concentrated closer to the spark plug, as indicated by the red and yellow regions. Additionally, increasing 3% and 9% hydrogen addition reduced the accumulation of a rich mixture on the piston crown surface, as shown in the side views (ZX and ZY planes) compared to neat methanol. This improvement in mixture distribution may be attributed to hydrogen's high diffusivity in air, which enhances the overall quality of the mixing process. Furthermore, compared to neat methanol, the addition of 3% CO + 3% H_2 improved fuel-air mixing quality, likely due to the presence of hydrogen gas. However, the mixing process for the 3% CO + 3% H_2 blend with methanol was slower than that of 3% and 9% hydrogen alone with methanol, as shown in Figure 8.3. This difference may be because carbon monoxide has a higher density and molecular weight than hydrogen, which can slow down the mixing process.

Flame propagation

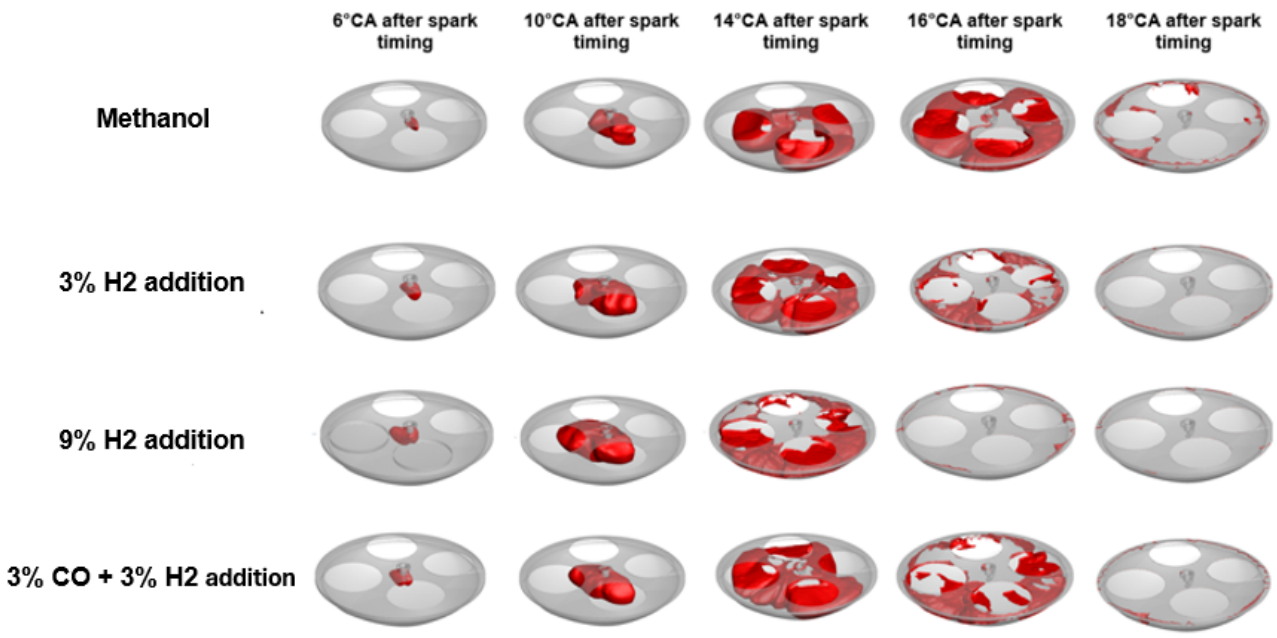

Figure 8.4: Flame propagation in a methanol-fuelled engine with various hydrogen addition and CO+H_2 addition concentrations at different crank angles after spark timing

The red regions in Figure 8.4 illustrates a comparison on the effect of flame propagation at various crank angles (6°, 10°, 14°, 16°, 18° CA) after the spark timing (20°CA bTDC), under the effect of 3%, 9% H_2 addition and 3% CO + 3% H_2 additive concentration. As can be seen from Figure 8.4 under neat methanol operation the extent of the flame propagation expands from 6° to 18° CA after the spark timing as the combustion starts with a small localised flame and gradually spreads by 18° CA after the spark timing. Then under 3% hydrogen addition with methanol operation compared to neat methanol operation the flame propagation spread rapidly across the from 6° to 16°CA after spark timing across the chamber. Furthermore, under 9% hydrogen addition, the flame propagation is even more widespread, extending quickly from 6° to 14°CA, as shown in Figure 8.4. This enhanced flame propagation with hydrogen-enriched methanol is likely due to hydrogen's higher laminar flame speed than methanol. In addition to that 3% and 9% hydrogen enrichment, compared to neat methanol, initiates hydroxide radicals earlier, as seen in Figures 8.5 and 8.6. The proximity of the rich mixture to the spark plug, as depicted in Figure 8.3, may further enhance flame initiation and propagation, as seen in Figure 8.4.

Additionally, with 3% CO + 3% H_2 added to methanol, the flame propagation

spreads earlier across the chamber (from 6° to 16°CA after spark timing) than with neat methanol. However, the 3% CO + 3% H_2 blend does not accelerate flame propagation as significantly as 3% and 9% hydrogen addition alone. This suggests that the presence of CO may moderate hydrogen's effect, likely due to its influence on flame temperature and reaction kinetics.

OH radical

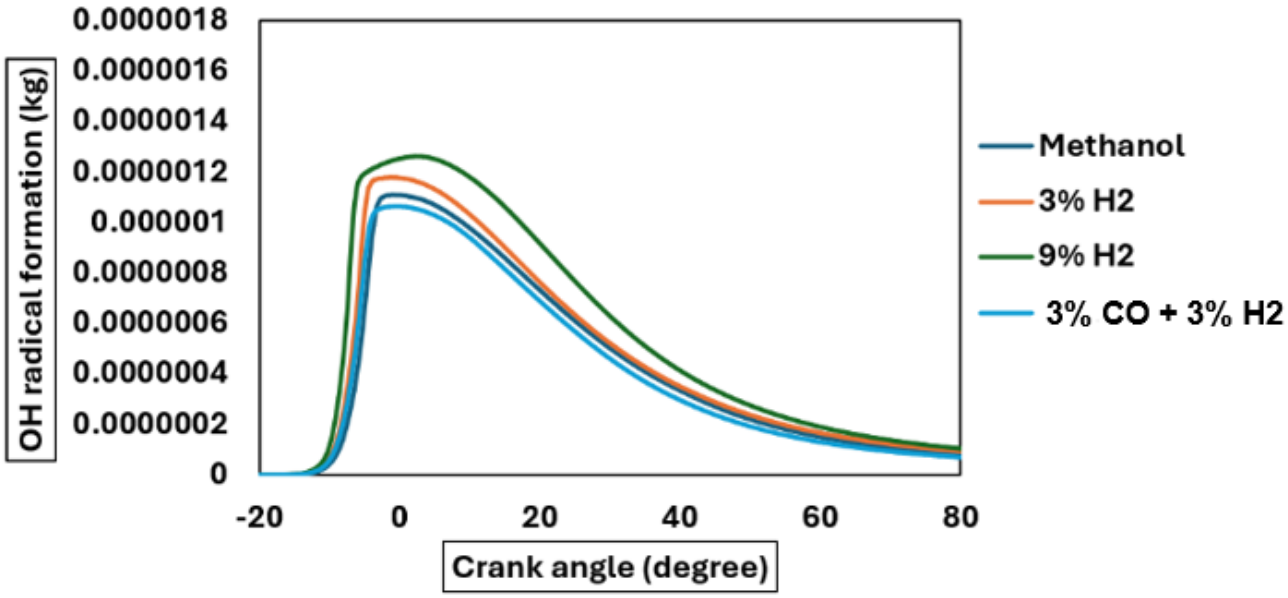

Figure 8.5: Hydroxyl radical formation with respect to crank angle under different operating conditions: neat methanol, methanol with 3% hydrogen addition, methanol with 9% hydrogen addition, and methanol with 3% CO + 3% H_2 addition

The hydroxyl radical (OH) is a crucial reactive species that plays a vital role in breaking down fuel molecules during the combustion process. Figure 8.5 illustrates the effect of OH radical formation at various crank angles under different operating conditions: neat methanol, methanol with 3% hydrogen enrichment, methanol with 9% hydrogen enrichment, and methanol with addition of 3% CO + 3% H_2. As shown in Figure 8.5, compared to neat methanol, enriching the fuel with 3% and 9% hydrogen resulted in a 6.3% and 12.6% increase in peak OH radical formation, respectively, during combustion. Additionally, these hydrogen enrichments led to OH radical formation occurring 0.8° CA and 1.71° CA earlier, respectively. This shift is likely due to the increased hydrogen content, which promotes the formation of H radicals and consequently enhances OH radical production. Furthermore, the

addition of 3% CO + 3% H_2 to methanol led to a 4% decrease in peak OH radical formation compared to neat methanol, while causing OH radical formation to occur 0.6° CA earlier. This earlier formation of OH radicals in the 3% CO + 3% H_2 addition could be attributed to the presence of hydrogen. However, the reduction in peak OH radical formation is likely due to the presence of carbon monoxide, which reacts with OH to form CO, reducing the availability of OH radicals for further reactions. Consequently reducing the OH formation.[15].

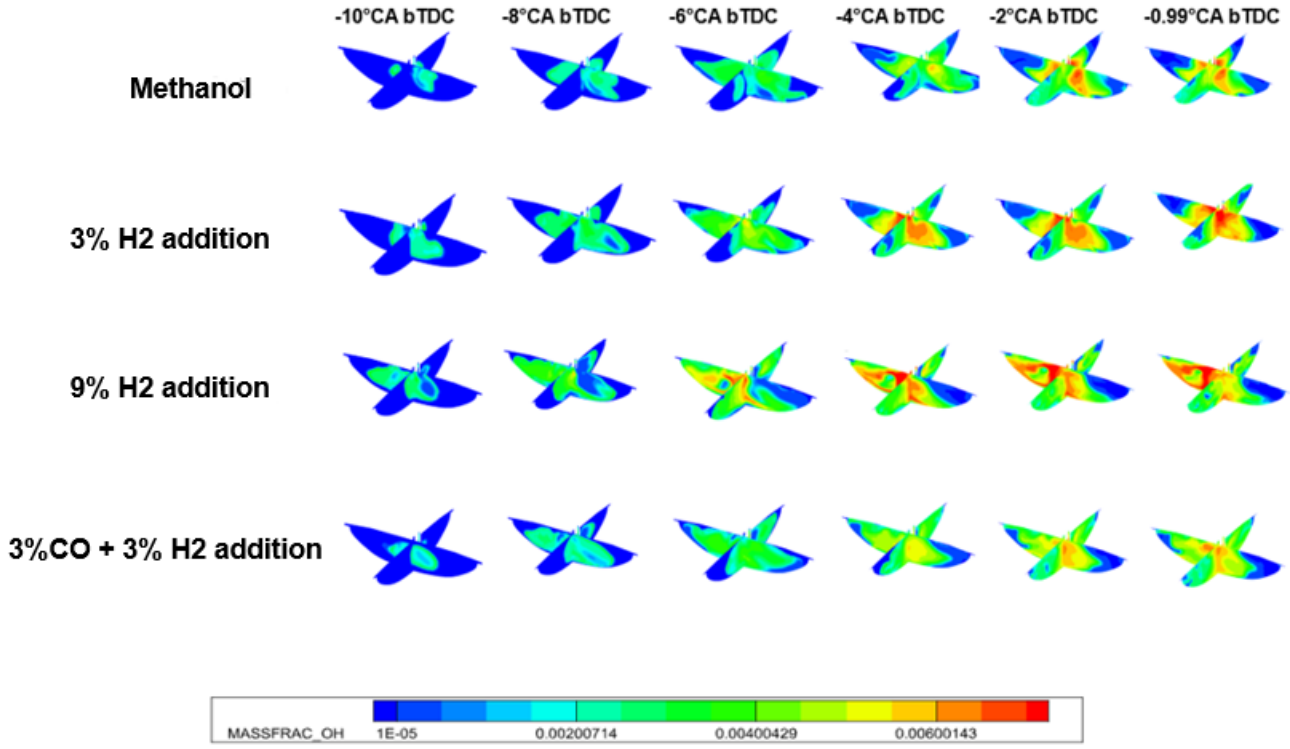

Figure 8.6: Hydroxyl radical concentration and distribution across the chamber at various crank angles for different hydrogen

Figure 8.6 illustrates the distribution of hydroxyl radical (OH) formation during the combustion process at crank angles ranging from -10° to -0.9° CA bTDC, under different conditions: 3% and 9% hydrogen addition to methanol, and 3% CO + 3% H_2 addition to methanol.

As shown in figure 8.6, with 3% hydrogen addition to methanol, OH formation begins earlier, at -10° CA bTDC, compared to neat methanol. A higher concentration of OH is observed intensifying from -4° CA bTDC, indicating an earlier and more widespread distribution of OH. With 9% hydrogen enrichment, the intensity of OH formation increases further compared to neat methanol, with a high concentration

of OH starting to spread across the chamber from -6° CA bTDC. This intense OH distribution, represented by the red and yellow regions, is prominent up to -0.9° CA bTDC.

Furthermore as shown in figure 8.6 for methanol with 3% CO + 3% H_2 addition, a high intensity of OH formation is observed earlier in the combustion process, from -10° to -6° CA bTDC, likely due to the presence of hydrogen. However, in the later stages of combustion (from -4° to -0.9° CA bTDC), the intensity of OH formation decreases compared to neat methanol. This reduction in OH concentration is likely due to the presence of carbon monoxide, which reacts with oxygen and reduces the availability of OH radicals.

Combustion duration

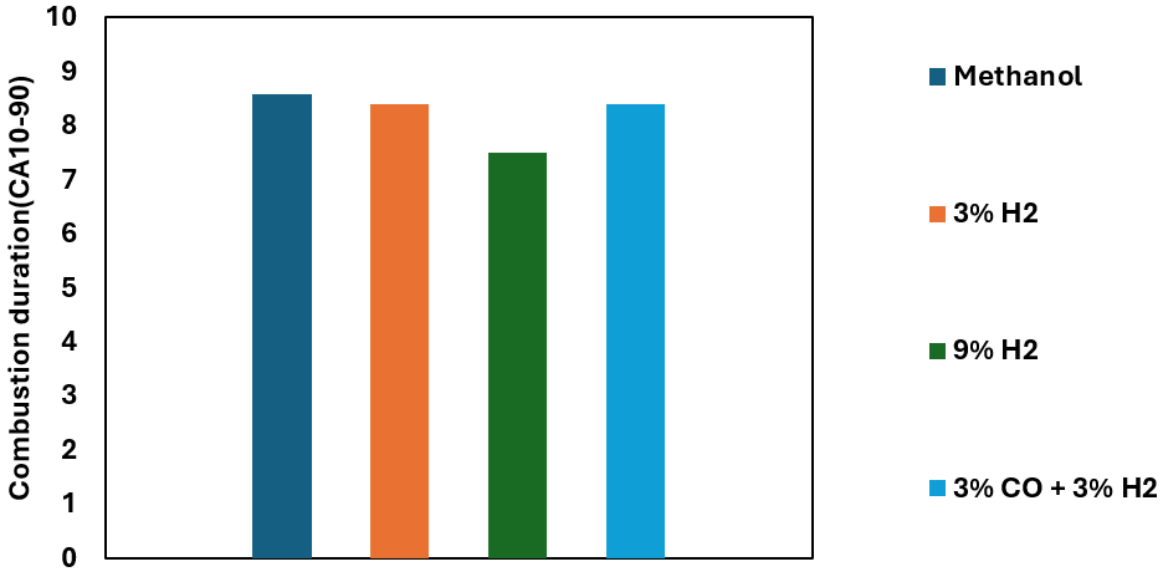

Figure 8.7: Combustion duration in a methanol-fuelled engine with various hydrogen addition and 3% CO + 3% H_2 additive concentrations

Figure 8.7 compares the combustion duration for neat methanol, methanol with 3% and 9% hydrogen addition, and methanol with 3% CO + 3% H_2 addition. As can be seen from figure 8.7, 3% and 9% hydrogen enrichment reduced the combustion duration by 2% and 12%, respectively, compared to neat methanol operation. The reduction in combustion duration with increased hydrogen addition can be attributed to hydrogen's higher laminar flame speed, which accelerates the flame propagation process and improves the quality of fuel and air mixing, as seen in Figures 8.3–8.6. Furthermore, the addition of 3% CO + 3% H_2 resulted in a 2%

decrease in combustion duration compared to neat methanol. This effect can be explained by the increased flame speed resulting from the hydrogen content, as shown in Figure 8.4. The higher diffusivity properties of both CO and H_2 also contribute to better fuel and air mixing compared to neat methanol operation as can be seen from figure 8.3 combustion.[15]

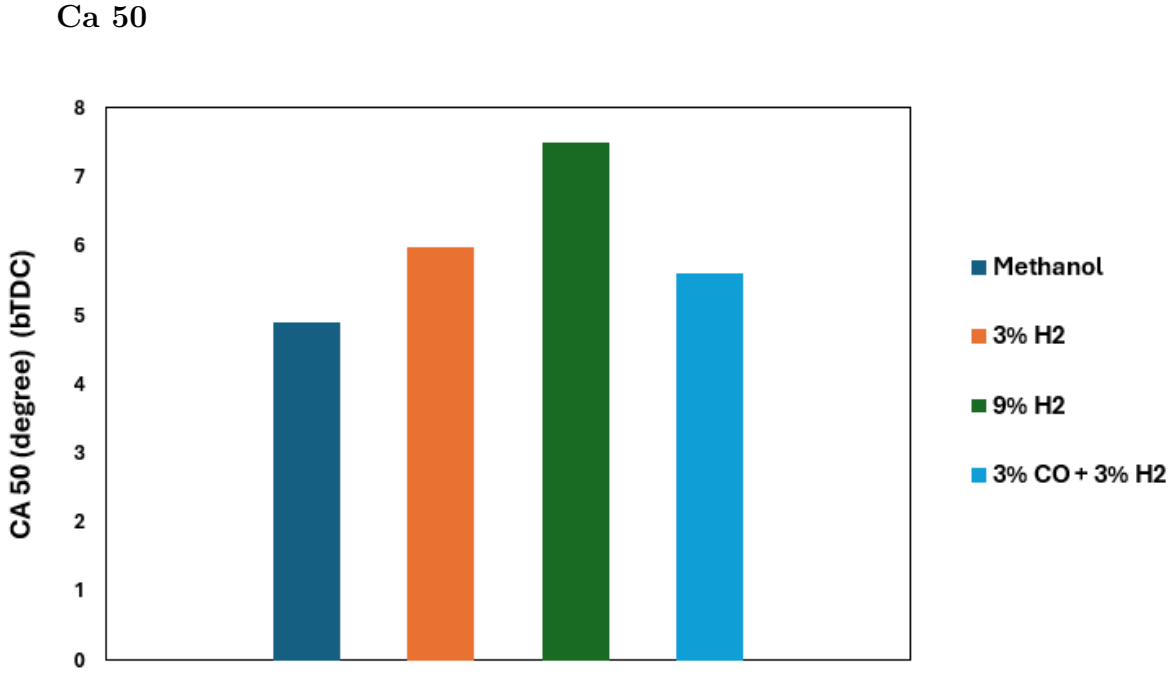

Figure 8.8: crank angle location of 50% mass fraction burn for methanol, 3% hydrogen addition, 9% hydrogen addition, and 3% CO + 3% H_2 addition

Figure 8.8 illustrates the position of the crank angle at which 50% of the fuel mass is burned under various operating conditions: neat methanol, methanol with 3% hydrogen addition, methanol with 9% hydrogen addition, and methanol with 3% CO + 3% H_2 addition. As can be seen from the Figure. 8.8 that for neat methanol operation, the crank angle at which 50% of the fuel mass is burned (CA 50° bTDC) occurs at 4.8°CA before the top dead centre (bTDC). On 3% and 9% hydrogen is added to methanol, and 50% of the fuel mass is burned earlier to around 6° and 7.5 bTDC, indicating that the presence of hydrogen accelerates the combustion process. This can be attributed to figures 8.4 and 8.5 the increase in the hydrogen addition results in the rapid flame propagation across the chamber as well as an increase in the formation of hydroxyl radical formation enhancing the oxidation process during the combustion. Furthermore, compared to neat methanol operation 50% mass

fraction occurred earlier around 5.8° CA bTDC for 3% CO + 3% H_2 addition with methanol.

8.2.2 Emissions

Indicated specific NOx emmision

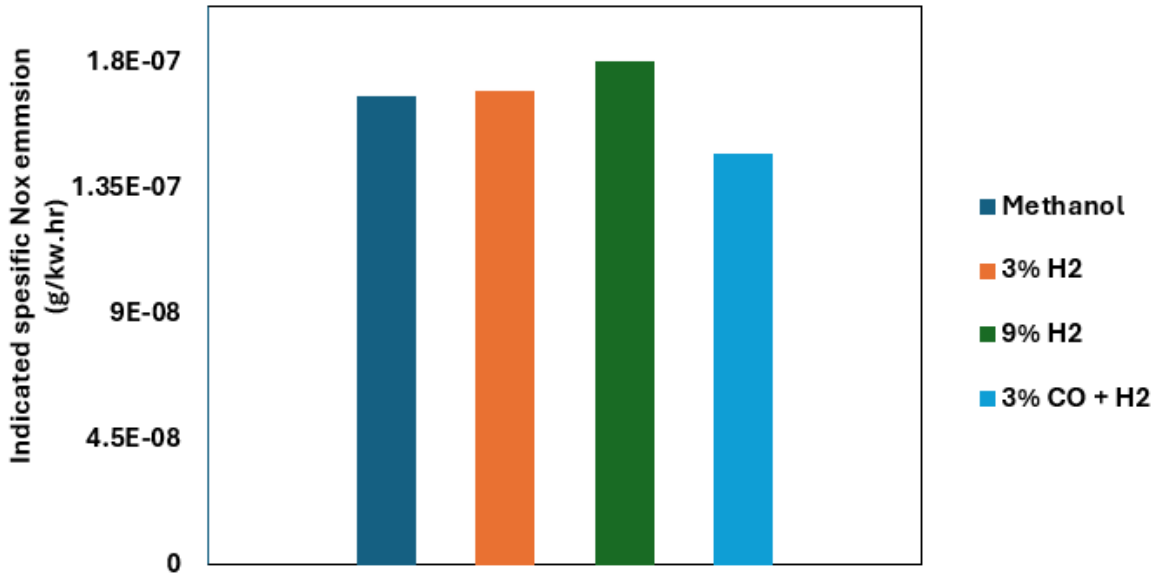

Figure 8.9: Indicated specific NOx emissions associated with neat methanol, 3% hydrogen addition, 9% hydrogen addition, and3% CO + 3% H_2 addition.

The NOx emissions for neat methanol serve as the baseline in this comparison. Methanol, being an oxygenated fuel, typically burns at a lower temperature compared to conventional fossil fuels, resulting in relatively moderate NOx emissions. Figure 8.9 illustrates the comparison of indicated specific NOx emissions for neat methanol, methanol with 3% and 9% hydrogen addition, and methanol with a 3% CO + 3% H_2 addition. It shows that, compared to neat methanol, the 3% and 9% hydrogen additions result in increases of 1.4% and 7.9% in NOx emissions, respectively.This increase can be attributed to the rise in maximum in-cylinder temperature due to hydrogen enrichment. Additionally, hydrogen has a higher adiabatic flame temperature compared to methanol, which can further contribute to the increase in NOx emissions.Conversely, the addition of 3% CO + 3% H_2 to methanol results in a 12% reduction in indicated specific NOx emissions compared to neat methanol.This reduction could be due to the presence of carbon monoxide, which enhances the formation of carbon dioxide in the combustion process of methanol, leading to a decrease in in-cylinder temperature[15].

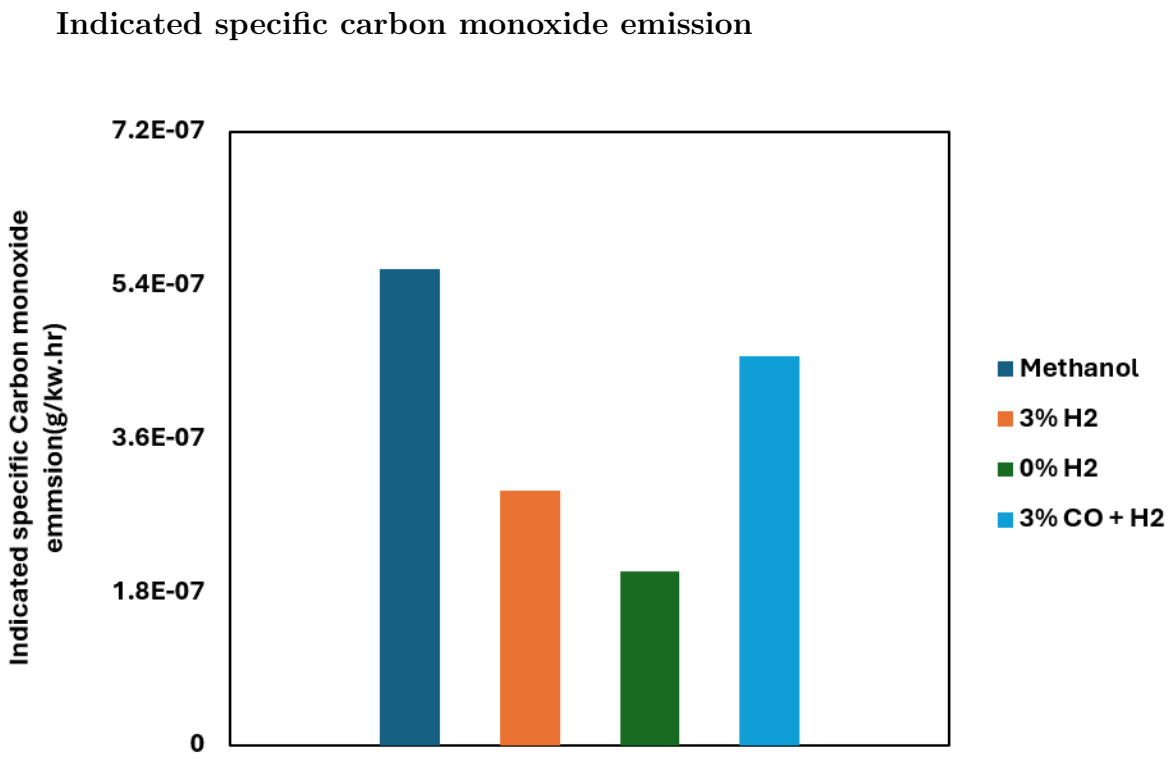

Figure 8.10: Indicated specific CO emissions associated with neat methanol, 3% hydrogen addition, 9% hydrogen addition, and 3% CO + 3% H_2 addition

Figure 8.10 illustrates the comparison of indicated specific carbon monoxide emissions for neat methanol, methanol with 3% and 9% hydrogen addition, and methanol with a 3% CO + 3% H_2 addition.Figure 8.10 shows that, compared to neat methanol, the 3% and 9% hydrogen additions result in decreases of 47% and 64% in CO emissions, respectively. This can be attributed to Figure 8.10 increase in 3% and 9% hydrogen addition with methanol resulting in higher OH radical concentration during the combustion as shown in Figures 8.5 and 8.6. Additionally, the increased hydrogen content leads to faster flame propagation across the chamber after spark timing, as shown in Figure 8.4. However, adding 3% CO + 3% H_2 leads to an increase in CO emissions compared to the 3% and 9% hydrogen additions. Despite this, the 3% CO + 3% H_2 mixture still results in an 18% reduction in indicated specific CO emissions compared to neat methanol. This suggests that the hydrogen present in the mixture continues to promote better combustion efficiency.

Indicated thermal efficiency

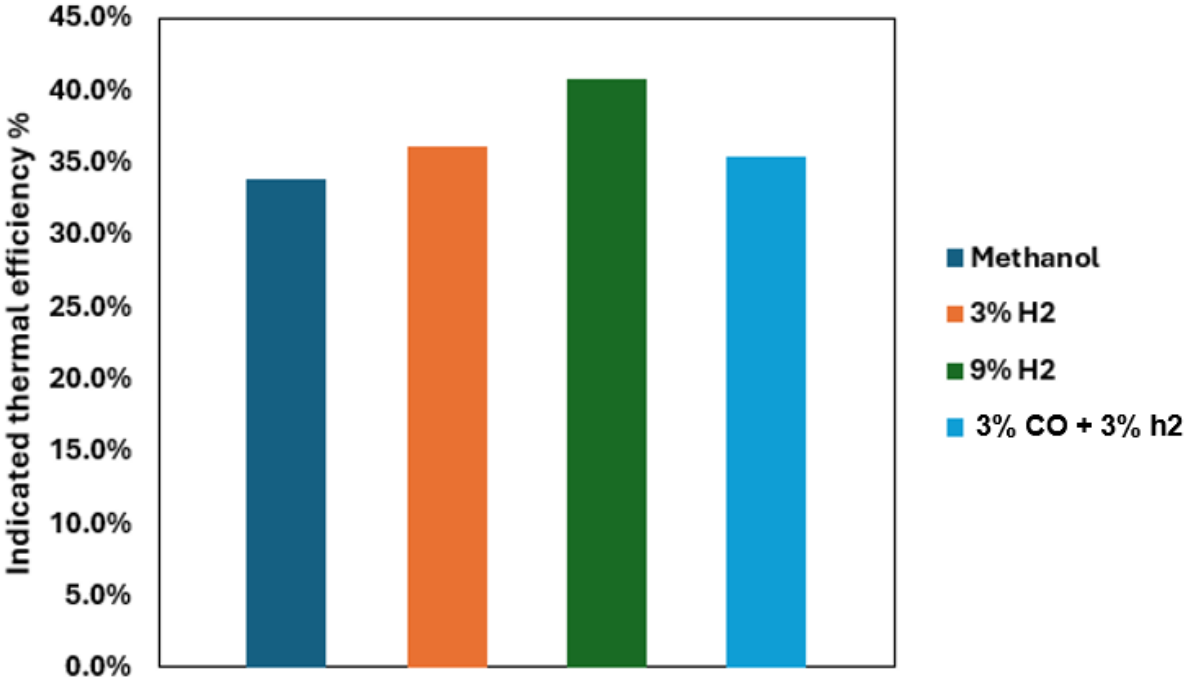

Figure 8.11: Indicated thermal efficiency(%) for neat methanol, 3% hydrogen addition, 9% hydrogen addition, and 3% CO + 3% H_2 addition

Indicated Thermal Efficiency reflects the effectiveness of converting the chemical energy of the fuel into useful work. Figure 8.11 compares the Indicated Thermal Efficiency of neat methanol operation with methanol enriched with 3% and 9% hydrogen, as well as methanol with the addition of 3% CO + 3% H_2, in a spark-ignition engine. As shown in the bar graph Figure 8.11, compared to neat methanol, the addition of 3% and 9% hydrogen resulted in a 6.8% and 20.5% increase in Indicated Thermal Efficiency, respectively. This improvement is likely due to hydrogen's higher flame speed compared to methanol, which enhances combustion efficiency by promoting more complete and faster burning of the fuel mixture. Additionally, the addition of 3% CO + 3% H_2 addition with methanol led to a 5% increase in Indicated Thermal Efficiency.

8.3 Summary

The study simulated the performance of a methanol-fueled spark-ignition engine at a fixed load of 11 bar IMEP to assess the effects of adding 3% CO + 3% H_2 and varying levels of hydrogen (3% and 9%) to methanol. The results showed that both hydrogen and 3% CO + 3% H_2 additions caused an earlier rise in in-cylinder pressure compared to neat methanol, with hydrogen alone resulting in a slightly earlier shift than the 3% CO + 3% H_2 blend. In terms of emissions, increasing hydrogen content significantly reduced carbon monoxide emissions but led to a rise in NOx emissions, whereas the 3% CO + 3% H_2 blend reduced both carbon monoxide and NOx emissions compared to neat methanol. Additionally, the indicated thermal efficiency improved with the addition of hydrogen (3% and 9%), while the 3% CO + 3% H_2 blend also enhanced thermal efficiency, though to a lesser extent than hydrogen addition alone.

Table 8.1: Outcome of Chapter

Operation	**CO Emission**	**NOx Emission**	**Indicated Thermal Efficiency**
Methanol + 3% H_2 addition	47% lower than neat methanol	1.4% higher than neat methanol	6.8% higher than neat methanol
Methanol + 9% H_2 addition	64% lower than neat methanol	7.9% higher than neat methanol	20.5% higher than neat methanol
Methanol + 3% CO + 3% H_2 addition	18% lower than neat methanol	12% lower than neat methanol	5% higher than neat methanol

Chapter 9

Conclusions and future work

9.1 Conclusions

Effect of boosting at high and low load condition

Low-power and high-power operating conditions on methanol spark-ignition engines with different levels of hydrogen addition was investigated. The effect of boosting at a constant power of 30 kW (low power rating) and 110 kW (high power rating) on neat methanol and methanol with 2% to 9% hydrogen addition was investigated at a fixed engine speed of 1800 RPM. Additionally, the effect of injection timing of methanol was examined. This investigation is carried out on a 50-litre genset diesel engine using the Ricardo engine database, modified to a spark-ignition methanol-fuelled single-cylinder engine. For the operating scenarios of pure methanol and methanol-hydrogen blend, a single wiebe function and a multi-wiebe function, two-zone combustion models, respectively, are used on the Ricardo wave solver to determine the start of combustion. The inputs for the single and multi-Wiebe functions are determined by using the laminar flame speed correlation function of methanol-hydrogen blends developed in [10] and by understanding the SI combustion model's laminar burning velocity correlation function developed in [11]. At high-power conditions, CO emissions were lower and NOx emissions were higher compared to low-power conditions for both neat methanol and methanol with varying hydrogen levels. Additionally, indicated thermal efficiency was higher at high-power conditions for both fuel types. Increased hydrogen enrichment reduced CO emissions under both low and high load conditions but led to a rise in NOx emissions, likely due to hydrogen's faster flame propagation properties. The increase in hydrogen addition also resulted in higher maximum in-cylinder pressure, heat release rate, and improved indicated thermal efficiency compared to neat methanol operation. Boosting under both low and high power

conditions further reduced CO emissions, likely due to improved air-fuel mixing before combustion. Increased boosting at high and low load conditions also led to reduced NOx emissions for both neat methanol and hydrogen-enriched methanol, likely due to the enhanced lean combustion process. Furthermore, boosting at both load conditions improved indicated thermal efficiency. The effect of injection timing was investigated under high and low-load operating conditions. Advancing the injection timing resulted in a reduction in CO and NOx emissions across all operating conditions. It was also observed that the one-dimensional numerical model lacked the ability to accurately predict in-cylinder fuel-air mixing and flame propagation structures. A three-dimensional numerical modelling approach was carried out to address this limitation.

Effect of injection timing of methanol during the compression stroke with different levels of hydrogen addition

The effect of injection timing in a methanol SI engine with 3%, 9%, and 12% hydrogen addition was investigated using a three-dimensional computational fluid dynamics model on the converge solver. The injection timing of methanol was investigated at 150,110,80 and 60°CA bTDC during the compression stroke. The SAGE solver, Reynolds-Averaged Navier Stokes (RANS) with the k- turbulence model, and the O'Rourke and Amsden heat transfer sub-model were employed to analyze in-cylinder characteristics. The Extended Zeldovich mechanism and the Hiroyasu-NSC model were used to evaluate NOx and soot emissions, respectively. The engine was simulated at a manifold pressure of 0.9 bar and equivalence ratio , with a fixed engine speed of 1200 RPM and a spark timing of 20° CA before top dead centre (bTDC). Increasing the percentage of hydrogen in the mixture resulted in an earlier rise of in-cylinder pressure as well as increased the maximum in-cylinder pressure compared to neat methanol operation and this effect was observed only up to 9% Hydrogen enrichment, beyond which the peak values of the in-cylinder pressure decreased due to reduction in the overall energy content of the charge. The magnitude of OH radicals formed during the combustion process also increased with hydrogen enrichment. For all the considered injection timings of methanol, the combustion duration reduced up to 9% enrichment of hydrogen beyond which it increased and a similar trend was observed for carbon monoxide, unburnt hydrocarbon and soot emissions but the overall magnitude of soot was insignificant. The NOx emissions increased with the addition of hydrogen of up to 9% in the mixture and thereafter it maintained a plateau. Enrichment of hydrogen favoured ignition under late injection of up to 60 °CA bTDC in neat methanol operation. The outcome of this study has shown that the enrichment of hydrogen in a methanol SI engine favours igni-

tion but the performance benefits are limited with higher percentages of hydrogen in this mode of operation.

Effect of injection timing of methanol during the intake stroke with different level of hydrogen addition

The effect of varying injection timing of methanol during the intake stroke, along with hydrogen enrichment, on performance and emissions was investigated. Methanol was injected at 240°, 260°, and 290° CA bTDC, with hydrogen concentrations of 3% and 9%. The investigation was conducted with a fixed manifold pressure of 0.9 bar, a methanol injection pressure of 110 bar, an engine speed of 1200 RPM, a compression ratio of 9.6, and an equivalence ratio of 0.71. The engine operated with a fixed spark timing of -20° CA bTDC. Advancing the injection timing of methanol during the intake stroke, along with increasing hydrogen addition, led to an earlier rise in in-cylinder pressure and an increase in peak in-cylinder pressure. This also improved the quality of fuel-air mixing, enhanced flame propagation after spark timing, reduced combustion duration, and increased OH radical formation. Moreover, advancing the injection timing of methanol during the intake stroke and adding hydrogen resulted in a decrease in carbon monoxide and soot emissions, but an increase in NOx emissions.

Lean burn investigation of methanol spark ignition engine with hydrogen addition

The lean burn investigation of the methanol spark-ignition engine was conducted with hydrogen additions ranging from 0% to 50%. The study was carried out at a fixed manifold pressure of 0.9 bar, a spark timing of 20° CA bTDC, and an engine speed of 1200 RPM. The engine was simulated across air-fuel ratios from stoichiometric (λ=1) to ultra-lean (λ=3.3) with varying levels of hydrogen addition. Lean burn operation of a methanol spark-ignition engine with varying levels of hydrogen addition resulted in a reduction in indicated mean effective pressure, lower in-cylinder pressure, increased combustion duration, and reduced OH radical formation. Under leaner conditions, indicated specific CO, NOx, soot, and HC emissions decreased compared to stoichiometric operation. However, further extending the lean burn operation of methanol spark ignition engine resulted to an increase in indicated specific CO, HC, and soot emissions, while NOx emissions decreased. Increasing hydrogen addition extended the lean burn limit of the methanol spark-ignition engine and increased indicated mean effective pressure (IMEP) under lean operation. Higher hydrogen levels also reduced indicated specific CO, soot,

and HC emissions from stoichiometric to extended lean operation compared to neat methanol. Furthermore, increased hydrogen addition led to shorter combustion duration, enhanced OH radical formation, and improved fuel-air mixing near the spark plug. However, increasing hydrogen addition beyond 3% had little effect on combustion efficiency.

Combined effect of CO+H_2 addition to methanol spark ignition engine

The combined effect of 3% CO + 3% H_2 addition and 3% and 9% hydrogen (H_2) enrichment on a methanol-fueled spark-ignition engine was investigated. The simulation was conducted at a fixed Indicated Mean Effective Pressure (IMEP) of 11 bar, with a fixed manifold pressure of 0.9 bar and an engine speed of 1200 RPM. Compared to neat methanol operation, the combined effect of 3% CO + 3% H_2 and hydrogen enrichment led to an earlier rise in in-cylinder pressure, enhanced flame propagation, increased OH radical formation during combustion and improved indicated thermal efficiency. However, hydrogen addition alone resulted in a higher indicated thermal efficiency than the combined effect of 3% CO + 3% H_2. The results showed that both hydrogen and the 3% CO + 3% H_2 blend reduced CO and NOx emissions compared to neat methanol operation. However, increasing the hydrogen concentration in methanol led to a greater reduction in CO emissions, but also caused an increase in NOx emissions compared to neat methanol

Summary of key Finding

The main aim of this thesis was to improve engine performance and reduce exhaust gas emissions in a methanol-fueled spark-ignition engine through hydrogen enrichment.This was achieved by optimizing methanol injection timing during both the compression and intake strokes, combined with hydrogen enrichment, enhances combustion efficiency by improving air-fuel mixing and flame propagation. This results in a significant reduction in CO emissions while maintaining high thermal efficiency and engine performance. Increasing boost pressure and operating under lean burn conditions extend the combustion stability of methanol-hydrogen blends, reducing NOx and CO emissions without having a negetive effect on indicated mean effective pressure (IMEP). Controlled hydrogen addition ensures efficient combustion while preventing excessive heat release that could negatively impact engine operation. The combined effect of 3% CO + 3% H_2 addition in a methanol-fueled spark-ignition engine leads to earlier pressure rise and enhanced flame propagation, lowering emissions while maintaining engine efficiency. However, hydrogen enrichment beyond 3% results in smaller performance improvements while benefit-

ing from reduced CO emissions. Balancing hydrogen addition and boost pressure optimization ensures sustainable emissions reduction without negatively affecting engine power and efficiency.

9.2 Future work

- In this study, a detailed investigation of in-cylinder characteristics of methanol with varying levels of hydrogen addition was conducted, while maintaining fixed spark timing, injection pressure, manifold pressure, and compression ratio settings. Future work could explore the effects of higher manifold pressure, variable spark timing, and different injection pressures to gain deeper insights into in-cylinder characteristics.
- Knocking in methanol-fueled spark-ignition engines with varying levels of hydrogen addition needs to be investigated under high compression ratios and higher load operating conditions.
- Long-term effects on engine components and the durability of methanol spark-ignition engines with hydrogen addition need to be investigated. The effects of spark timing and varying compression ratios on carbon monoxide and hydrogen addition in a methanol spark-ignition engine need to be investigated. Additionally, further studies should explore the combustion process with varying carbon monoxide and hydrogen addition ratios to methanol to fully understand the engine's performance.
- The feasibility and performance of integrating hydrogen and carbon monoxide addition in methanol spark-ignition engines need to be studied under real-world operating conditions to assess their practical applicability.

References

[1] A. K. Agarwal, D. K. Srivastava, A. Dhar, R. K. Maurya, P. C. Shukla, and A. P. Singh. Effect of fuel injection timing and pressure on combustion emissions and performance characteristics of a single cylinder diesel engine. *Fuel*, 111:374–383, September 2013.

[2] N. F. O. Al-Muhsen, Y. Huang, and G. Hong. Effects of direct injection timing associated with spark timing on a small spark ignition engine equipped with ethanol dual-injection. *Fuel*, 239:852–861, March 2019.

[3] B. Açıkgöz, C. Çelik, H. S. Soyhan, B. Gökalp, and B. Karabağ. Emission characteristics of a hydrogen–ch4 fuelled spark ignition engine. *Fuel*, 159:298–307, November 2015.

[4] V. Beschkov and Evgeniy Ganev. Perspectives on the development of technologies for hydrogen as a carrier of sustainable energy. *Energies*, 2023.

[5] Fanos Christodoulou and Athanasios Megaritis. The effect of reformer gas mixture on the performance and emissions of an hsdi diesel engine. *international journal of hydrogen energy*, 39(18):9798–9808, 2014.

[6] Murat Ciniviz, Hüseyin Köse, Eyüb Canli, and O Solmaz. An experimental investigation on effects of methanol blended diesel fuels to engine performance and emissions of a diesel engine. *Scientific Research and Essays*, 6(15):3189–3199, 2011.

[7] Convergent Science Inc. *CONVERGE CFD Manual*. Convergent Science Inc., Madison, WI, USA, 2023. Version 3.0.

[8] M. Crippa, D. Guizzardi, F. Pagani, M. Banja, M. Muntean, E. Schaaf, W. Becker, F. Monforti-Ferrario, R. Quadrelli, A. Risquez Martin, et al. Ghg emissions of all world countries, 2015.

[9] A. Demirci, H. Koten, and M. Gumus. The effects of small amount of hydrogen addition on performance and emissions of a direct injection compression ignition engine. *Thermal Science*, 22(3):1395–1404, 2018.

[10] B. Douailler, F. Ravet, V. Delpech, D. Soleri, B. Reveille, and R. Kumar. Direct injection of cng on high compression ratio spark ignition engine: Numerical and experimental investigation. In *SAE 2011 World Congress Exhibition*, pages 2011–01–0923, April 2011.

[11] Y. Du, X. Yu, J. Wang, H. Wu, W. Dong, and J. Gu. Research on combustion and emission characteristics of a lean burn gasoline engine with hydrogen direct-injection. *International Journal of Hydrogen Energy*, 41(4):3240–3248, January 2016.

[12] Indranil Dutta, Sudipta Chatterjee, Hongfei Cheng, R. K. Parsapur, Zhaolin Liu, Zibiao Li, E. Ye, H. Kawanami, J. Low, Z. Lai, X. Loh, and Kuo-Wei Huang. Formic acid to power towards low-carbon economy. *Advanced Energy Materials*, 2022.

[13] D. Feng, H. Wei, and M. Pan. Comparative study on combined effects of cooled egr with intake boosting and variable compression ratios on combustion and emissions improvement in a si engine. *Applied Thermal Engineering*, 131:192–200, February 2018.

[14] T. Ganapathy, R. P. Gakkhar, and K. Murugesan. Influence of injection timing on performance combustion and emission characteristics of jatropha biodiesel engine. *Applied Energy*, 88(12):4376–4386, December 2011.

[15] Irvin Glassman, Richard A Yetter, and Nick G Glumac. *Combustion*. Academic press, 2014.

[16] R. Golzari, H. Zhao, J. Hall, M. Bassett, J. Williams, and R. Pearson. Impact of intake port injection of water on boosted downsized gasoline direct injection engine combustion efficiency and emissions. *International Journal of Engine Research*, 22(1):295–315, January 2021.

[17] C. Gong, D. Li, Z. Li, and F. Liu. Numerical study on combustion and emission in a disi methanol engine with hydrogen addition. *International Journal of Hydrogen Energy*, 41(1):647–655, January 2016.

[18] C. Gong, Z. Li, Y. Chen, J. Liu, F. Liu, and Y. Han. Influence of ignition timing on combustion and emissions of a spark-ignition methanol engine with added hydrogen under lean-burn conditions. *Fuel*, 235:227–238, January 2019.

[19] C. Gong, Z. Li, lin Yi, K. Huang, and F. Liu. Research on the performance of a hydrogen/methanol dual-injection assisted spark-ignition engine using late-injection strategy for methanol. *Fuel*, 260:116403, January 2020.

[20] C. Gong, Z. Li, and F. Liu. Numerical study of the firing radicals and intermediates in the combustion process of a h2-assisted combustion disi methanol engine. *Fuel*, 348:128603, September 2023.

[21] C. Gong, Z. Li, J. Sun, and F. Liu. Evaluation on combustion and lean-burn limit of a medium compression ratio hydrogen/methanol dual-injection spark-ignition engine under methanol late-injection. *Applied Energy*, 277:115622, November 2020.

[22] C. Gong, Z. Li, L. Yi, and F. Liu. Experimental investigation of equivalence ratio effects on combustion and emissions characteristics of an h2/methanol dual-injection engine under different spark timings. *Fuel*, 262:116463, February 2020.

[23] C. Gong, J. Sun, and F. Liu. Numerical study of twin-spark plug arrangement effects on flame combustion and emissions of a medium compression ratio direct-injection methanol engine. *Fuel*, 279:118427, November 2020.

[24] C.-M. Gong, K. Huang, J.-L. Jia, Y. Su, Q. Gao, and X.-J. Liu. Regulated emissions from a direct-injection spark-ignition methanol engine. *Energy*, 36(5):3379–3387, May 2011.

[25] Jining Guo, Yuecheng Zhang, A. Zavabeti, Kaifei Chen, Yalou Guo, G. Hu, Xiaolei Fan, and G. Li. Hydrogen production from the air. *Nature Communications*, 2021.

[26] Habib Gürbüz and İsmail Hakkı Akçay. Evaluating the effects of boosting intake-air pressure on the performance and environmental-economic indicators in a hydrogen-fueled si engine. *International Journal of Hydrogen Energy*, 46(56):28801–28810, 2021.

[27] A. Güdden, S. Pischinger, J. Geiger, B. Heuser, and M. Müther. An experimental study on methanol as a fuel in large bore high speed engine applications – port fuel injected spark ignited combustion. *Fuel*, 303:121292, November 2021.

[28] T. Han, R. Singh, G. Lavoie, M. Wooldridge, and A. Boehman. Multiple injection for improving knock, gaseous, and particulate matter emissions in direct injection si engines. *Applied Energy*, 262:114578, March 2020.

[29] Ballapu Harshavardhan and JM Mallikarjuna. Effect of piston shape on in-cylinder flows and air–fuel interaction in a direct injection spark ignition engine–a cfd analysis. *Energy*, 81:361–372, 2015.

[30] S. S. Motallebi Hasankola, R. Shafaghat, O. Jahanian, and K. Nikzadfar. An experimental investigation of the injection timing effect on the combustion phasing and emissions in reactivity-controlled compression ignition (rcci) engine. *Journal of Thermal Analysis and Calorimetry*, 139(4):2509–2516, February 2020.

[31] Zhuoyao He, Zhan Gao, Lei Zhu, Shujing Li, Ang Li, Wugao Zhang, and Zhen Huang. Effects of h2 and co enrichment on the combustion, emission and performance characteristics of spark ignition natural gas engine. *Fuel*, 183:230–237, 2016.

[32] John B. Heywood. *Internal Combustion Engine Fundamentals*. McGraw-Hill, Inc., 1988.

[33] H. Hiroyasu and T. Kadota. Models for combustion and formation of nitric oxide and soot in direct injection diesel engines. In *1976 Automotive Engineering Congress and Exposition*, page 760129, February 1976.

[34] K. M. Holmgren, T. Berntsson, E. Andersson, and T. Rydberg. System aspects of biomass gasification with methanol synthesis – process concepts and energy analysis. *Energy*, 45(1):817–828, September 2012.

[35] F. Huang and W. Kong. Effects of hydrogen addition on combustion characteristics of a free-piston linear engine with glow-assisted ignition. *International Journal of Hydrogen Energy*, 46(44):23040–23052, June 2021.

[36] J. Hunicz, M. S. Geca, P. Kordos, and H. Komsta. An experimental study on a boosted gasoline hcci engine under different direct fuel injection strategies. *Experimental Thermal and Fluid Science*, 62:151–163, April 2015.

[37] N. Iafrate, M. Matrat, and J.-M. Zaccardi. Numerical investigations on hydrogen-enhanced combustion in ultra-lean gasoline spark-ignition engines. *International Journal of Engine Research*, 22(2):375–389, February 2021.

[38] SN Iyer, DN Rrustemi, LC Ganippa, and T Megaritis. Hydrogen enrichment in methanol si engine at varying injection timing during compression stroke. *International Journal of Hydrogen Energy*, 89:952–963, 2024.

[39] Mohammad Jafari, Puneet Verma, Ali Zare, Pietro Borghesani, Timothy A Bodisco, Zoran D Ristovski, and Richard J Brown. In-cylinder pressure reconstruction by engine acoustic emission. *Mechanical Systems and Signal Processing*, 152:107490, 2021.

[40] Y Jamal and ML Wyszynski. On-board generation of hydrogen-rich gaseous fuels—a review. *International journal of hydrogen energy*, 19(7):557–572, 1994.

[41] A. Jamrozik. The effect of the alcohol content in the fuel mixture on the performance and emissions of a direct injection diesel engine fueled with diesel-methanol and diesel-ethanol blends. *Energy Conversion and Management*, 148:461–476, September 2017.

[42] S.-R. Jhang, K.-S. Chen, S.-L. Lin, Y.-C. Lin, and W. L. Cheng. Reducing pollutant emissions from a heavy-duty diesel engine by using hydrogen additions. *Fuel*, 172:89–95, May 2016.

[43] C. Ji, B. Zhang, and S. Wang. Enhancing the performance of a spark-ignition methanol engine with hydrogen addition. *International Journal of Hydrogen Energy*, 38(18):7490–7498, June 2013.

[44] S. Jindal. Combustion performance and emissions of a di-ci engine running on karanj methyl ester: influence of injection timing. *International Journal of Sustainable Engineering*, 4(2):136–144, June 2011.

[45] J. Jose, A. Parsi, S. Shridhara, M. Mittal, and A. Ramesh. Effect of fuel injection timing on the mixture preparation in a small gasoline direct-injection engine. In *SAE/JSAE Small Engine Technology Conference*, pages 2018–32–0014, October 2018.

[46] C. Jung, J. Park, and S. Song. Performance and nox emissions of a biogas-fueled turbocharged internal combustion engine. *Energy*, 86:186–195, June 2015.

[47] S. Kaiser and S. Bringezu. Use of carbon dioxide as raw material to close the carbon cycle for the german chemical and polymer industries. *Journal of Cleaner Production*, 271:122775, October 2020.

[48] S. Kanth and S. Debbarma. Comparative performance analysis of diesel engine fuelled with hydrogen enriched edible and non-edible biodiesel. *International Journal of Hydrogen Energy*, 46(17):10478–10493, March 2021.

[49] Y. Karagöz, İ. Güler, T. Sandalcı, L. Yüksek, and A. S. Dalkılıç. Effect of hydrogen enrichment on combustion characteristics emissions and performance of a diesel engine. *International Journal of Hydrogen Energy*, 41(1):656–665, January 2016.

[50] U. Kesgin. Study on prediction of the effects of design and operating parameters on nox emissions from a leanburn natural gas engine. *Energy Conversion and Management*, 44(6):907–921, April 2003.

[51] J. Kim, K. M. Chun, S. Song, H.-K. Baek, and S. W. Lee. The effects of hydrogen on the combustion performance and emissions of a turbo gasoline direct-injection engine with exhaust gas recirculation. *International Journal of Hydrogen Energy*, 42(39):25074–25087, September 2017.

[52] J. Kim et al. Methanol production from co2 using solar-thermal energy: process development and techno-economic analysis. *Energy and Environmental Science*, 4(9):3122, 2011.

[53] J. Kim, H. Park, C. Bae, M. Choi, and Y. Kwak. Effects of water direct injection on the torque enhancement and fuel consumption reduction of a gasoline engine under high-load conditions. *International Journal of Engine Research*, 17(7):795–808, September 2016.

[54] K. Kim, Y. Jung, D. Kim, and C. Bae. Effect of injector configurations on combustion and emissions in a gasoline direct-injection compression ignition engine under low-load conditions. *International Journal of Engine Research*, 17(3):316–330, March 2016.

[55] T. Kim, J. Song, J. Park, and S. Park. Numerical and experimental study on effects of fuel injection timings on combustion and emission characteristics of a direct-injection spark-ignition gasoline engine with a 50 mpa fuel injection system. *Applied Thermal Engineering*, 144:890–900, November 2018.

[56] H. Koten. Hydrogen effects on the diesel engine performance and emissions. *International Journal of Hydrogen Energy*, 43(22):10511–10519, May 2018.

[57] J. Kotowicz, D. Wecel, and M. Brzeczek. Analysis of the work of a 'renewable' methanol production installation based on h2 from electrolysis and co2 from power plants. *Energy*, 221:119538, April 2021.

[58] H. Köse and M. Ciniviz. An experimental investigation of effect on diesel engine performance and exhaust emissions of addition at dual fuel mode of hydrogen. *Fuel Processing Technology*, 114:26–34, October 2013.

[59] B. E. Launder and D. B. Spalding. The numerical computation of turbulent flows. *Computer Methods in Applied Mechanics and Engineering*, 3(2):269–289, 1974.

[60] Felix Leach, Gautam Kalghatgi, Richard Stone, and Paul Miles. The scope for improving the efficiency and environmental impact of internal combustion engines. *Transportation Engineering*, 1:100005, 2020.

[61] C. Lhuillier, P. Brequigny, F. Contino, and C. Mounaïm-Rousselle. Experimental study on ammonia/hydrogen/air combustion in spark ignition engine conditions. *Fuel*, 269:117448, June 2020.

[62] H. Li et al. An investigation of the combustion process of a heavy-duty dual fuel engine supplemented with natural gas or hydrogen. *International Journal of Hydrogen Energy*, 42(5):3352–3362, February 2017.

[63] J. Li, C.-M. Gong, Y. Su, H.-L. Dou, and X.-J. Liu. Effect of injection and ignition timings on performance and emissions from a spark-ignition engine fueled with methanol. *Fuel*, 89(12):3919–3925, December 2010.

[64] Y. Li, X.-S. Bai, M. Tunér, H. G. Im, and B. Johansson. Investigation on a high-stratified direct injection spark ignition (disi) engine fueled with methanol under a high compression ratio. *Applied Thermal Engineering*, 148:352–362, February 2019.

[65] Y. Li, M. Jia, Y. Liu, and M. Xie. Numerical study on the combustion and emission characteristics of a methanol/diesel reactivity controlled compression ignition (rcci) engine. *Applied Energy*, 106:184–197, June 2013.

[66] F. Lindström, H.-E. Angstrom, G. Kalghatgi, and C. E. Möller. An empirical si combustion model using laminar burning velocity correlations. In *2005 SAE Brasil Fuels & Lubricants Meeting*, pages 2005–01–2106, May 2005.

[67] Changpeng Liu, Fubai Li, Heping Song, and Zhi Wang. Effects of h2/co addition on knock tendency and lean limit in a natural gas si engine. *Fuel*, 233:582–591, 2018.

[68] S. Liu, E. R. Cuty Clemente, T. Hu, and Y. Wei. Study of spark ignition engine fueled with methanol/gasoline fuel blends. *Applied Thermal Engineering*, 27(11–12):1904–1910, August 2007.

[69] X. Liu, C. Ji, B. Gao, S. Wang, C. Liang, and J. Yang. A laminar flame speed correlation of hydrogen–methanol blends valid at engine-like conditions. *International Journal of Hydrogen Energy*, 38(35):15500–15509, November 2013.

[70] D. Lou, Y. Ren, Y. Zhang, and X. Sun. Study on the effects of egr and spark timing on the combustion performance and emissions of a stoichiometric natural gas engine. *ACS Omega*, 5(41):26763–26775, October 2020.

[71] A. Montanaro, S. Malaguti, and S. Alfuso. Wall impingement process of a multi-hole gdi spray: Experimental and numerical investigation. In *SAE 2012 World Congress Exhibition*, pages 2012–01–1266, April 2012.

[72] Florian Nestler, AR Schütze, M Ouda, MJ Hadrich, A Schaadt, S Bajohr, and T Kolb. Kinetic modelling of methanol synthesis over commercial catalysts: A critical assessment. *Chemical Engineering Journal*, 394:124881, 2020.

[73] Mikkel Nielsen, Elisabetta Alberico, Walter Baumann, Hanno Drexler, Holger Junge, Sergio Gladiali, and Matthias Beller. Low-temperature aqueous-phase methanol dehydrogenation to hydrogen and carbon dioxide. *Nature*, 495:85–89, 2013.

[74] Peter J O'Rourke and Anthony A Amsden. The tab method for numerical calculation of spray droplet breakup. Technical report, SAE technical paper, 1987.

[75] İlker Örs, Halil Erdi Gülcan, Bahar Sayın Kul, Savaş Yelbey, and Murat Ciniviz. Evaluation of the effects of methanol and ethanol additions on performance and emissions in a spark plug ignition engine fueled with gasoline. *International Journal of Automotive Science and Technology*, 6(2):156–164, 2022.

[76] O. K. M. Ouda, S. A. Raza, A. S. Nizami, M. Rehan, R. Al-Waked, and N. E. Korres. Waste to energy potential: A case study of saudi arabia. *Renewable and Sustainable Energy Reviews*, 61:328–340, August 2016.

[77] M. Pan, G. Shu, H. Wei, T. Zhu, Y. Liang, and C. Liu. Effects of egr compression ratio and boost pressure on cyclic variation of pfi gasoline engine at wot operation. *Applied Thermal Engineering*, 64(1–2):491–498, March 2014.

[78] S. Pandey. A critical review: Application of methanol as a fuel for internal combustion engines and effects of blending methanol with diesel/biodiesel/ethanol on performance emission and combustion characteristics of engines. *Heat Transfer*, 51(4):3334–3352, June 2022.

[79] R. G. Papagiannakis, C. D. Rakopoulos, D. T. Hountalas, and D. C. Rakopoulos. Emission characteristics of high speed dual fuel compression ignition engine operating in a wide range of natural gas/diesel fuel proportions. *Fuel*, 89(7):1397–1406, July 2010.

[80] C. Park, G. Lim, S. Lee, C. Kim, and Y. Choi. Effects of the ignition timing retard and the compression ratio on the full-load performance and the emissions characteristics of a heavy-duty engine fuelled by hydrogen–natural-gas blends. *Proceedings of the Institution of Mechanical Engineers, Part J: Automobile Engineering*, 227(9):1295–1302, September 2013.

[81] Y. Park and C. Bae. Experimental study on the effects of high/low pressure egr proportion in a passenger car diesel engine. *Applied Energy*, 133:308–316, November 2014.

[82] Christoffer Pichler and Elna J. K. Nilsson. Reduced kinetic mechanism for methanol combustion in spark-ignition engines. *Energy & Fuels*, 32(12):12805–12813, 2018.

[83] E. Porpatham, A. Ramesh, and B. Nagalingam. Effect of hydrogen addition on the performance of a biogas fuelled spark ignition engine. *International Journal of Hydrogen Energy*, 32(12):2057–2065, August 2007.

[84] B. S. Nuthan Prasad, J. K. Pandey, and G. N. Kumar. Effect of hydrogen enrichment on performance combustion and emission of a methanol fueled si engine. *International Journal of Hydrogen Energy*, 46(49):25294–25307, July 2021.

[85] M. Pucilowski, M. Jangi, S. Shamun, C. Li, M. Tuner, and X.-S. Bai. Effect of start of injection on the combustion characteristics in a heavy-duty dici engine running on methanol. In *WCXTM 17: SAE World Congress Experience*, pages 2017–01–0560, March 2017.

[86] S. T. P. Purayil, M. O. Hamdan, S. A. B. Al-Omari, M. Y. E. Selim, and E. Elnajjar. Review of hydrogen–gasoline si dual fuel engines: Engine performance and emission. *Energy Reports*, 9:4547–4573, December 2023.

[87] A. A. Rai, N. K. Bailkeri, and S. Rao Br. Effect of injection timings on performance and emission characteristics of cng diesel dual fuel engine. *Materials Today: Proceedings*, 46:2758–2763, 2021.

[88] Royal IHC. Fuels and transition to zero emission vessels, 2023. Accessed: 2024-11-11.

[89] S. Sahu, P. Kumar, and A. Dhar. Effect of injection timing on combustion performance and emissions characteristics of methanol fuelled disi engine: A numerical study. *Fuel*, 322:124167, August 2022.

[90] N. Duarte Souza Alvarenga Santos, V. Rückert Roso, A. C. Teixeira Malaquias, and J. G. Coelho Baêta. Internal combustion engines and biofuels: Examining why this robust combination should not be ignored for future sustainable transportation. *Renewable and Sustainable Energy Reviews*, 148:111292, September 2021.

[91] R. O. D. Santos, L. D. S. Santos, and D. M. Prata. Simulation and optimization of a methanol synthesis process from different biogas sources. *Journal of Cleaner Production*, 186:821–830, June 2018.

[92] L. Schlapbach and A. Züttel. Hydrogen-storage materials for mobile applications. In *Materials for Sustainable Energy*, pages 265–270. Co-Published with Macmillan Publishers Ltd, UK, 2010.

[93] F. Schulz, J. Schmidt, A. Kufferath, and W. Samenfink. Gasoline wall films and spray/wall interaction analyzed by infrared thermography. *SAE International Journal of Engines*, 7(3):1165–1177, April 2014.

[94] P. K. Senecal et al. Multi-dimensional modeling of direct-injection diesel spray liquid length and flame lift-off length using cfd and parallel detailed chemistry. In *SAE 2003 World Congress Exhibition*, pages 2003–01–1043, March 2003.

[95] R. Senthil, R. Silambarasan, and G. Pranesh. The influence of injection timing on the performance and emission characteristics of an annona methyl ester operated diesel engine. *Biofuels*, 7(5):437–445, September 2016.

[96] H. Sharudin, N. R. Abdullah, G. Najafi, R. Mamat, and H. H. Masjuki. Investigation of the effects of iso-butanol additives on spark ignition engine fuelled with methanol-gasoline blends. *Applied Thermal Engineering*, 114:593–600, March 2017.

[97] X. Sun et al. Effect of hydrogen enrichment on the flame propagation emissions formation and energy balance of the natural gas spark ignition engine. *Fuel*, 307:121843, January 2022.

[98] J. Wang, P. Zhang, C. Zhang, and Z. Jing. Performance and emissions of a premixed combustion engine fueled by methanol–gasoline blends. June 2020.

[99] L. Wang, D. Liu, Z. Yang, H. Li, L. Wei, and Q. Li. Effect of h2 addition on combustion and exhaust emissions in a heavy-duty diesel engine with egr. *International Journal of Hydrogen Energy*, 43(50):22658–22668, December 2018.

[100] Yifan Wang, S. Vudata, P. Brooker, and J. Fenton. Electrochemical hydrogen compression: Modeling, internal states estimation and system control. *ECS Meeting Abstracts*, 2022.

[101] J. Wei et al. Impact of aluminium oxide nanoparticles as an additive in diesel-methanol blends on a modern di diesel engine. *Applied Thermal Engineering*, 185:116372, February 2021.

[102] M. Wei, S. Li, J. Liu, G. Guo, Z. Sun, and H. Xiao. Effects of injection timing on combustion and emissions in a diesel engine fueled with 25-dimethylfuran-diesel blends. *Fuel*, 192:208–217, March 2017.

[103] Christian Wouters, Patrick Burkardt, Marcus Fischer, Michael Blomberg, and Stefan Pischinger. Effects of stroke on spark-ignition combustion with gasoline and methanol. *International Journal of Engine Research*, 23(5):804–815, 2022.

[104] D. Xiang, P. Li, X. Yuan, P. Cui, and W. Huang. Highly efficient carbon utilization of coal-to-methanol process integrated with chemical looping hydrogen and air separation technology: Process modeling and parameter optimization. *Journal of Cleaner Production*, 258:120910, June 2020.

[105] P. Xiao, C. Lee, H. Wu, M. Z. Akram, and F. Liu. Impacts of hydrogen-addition on methanol-air laminar burning coupled with pressures variation effects. *Energy*, 187:115997, November 2019.

[106] C. Xu and H. Cho. Effect of methanol/water mixed fuel compound injection on engine combustion and emissions. *Energies*, 14(15):4491, July 2021.

[107] V. Yakhot and S. A. Orszag. Renormalization group analysis of turbulence. i. basic theory. *Journal of Scientific Computing*, 1(1):3–51, 1986.

[108] Y. Yan, R. Yang, X. Sun, R. Li, and Z. Liu. Numerical investigations of injection timing effects on a gasoline direct injection engine performance: Part a in-cylinder combustion process. *Frontiers in Energy Research*, 10:828167, February 2022.

[109] S. Yang, B. Li, J. Zheng, and R. K. Kankala. Biomass-to-methanol by dual-stage entrained flow gasification: Design and techno-economic analysis based on system modeling. *Journal of Cleaner Production*, 205:364–374, December 2018.

[110] H. L. Yip, Aleš Srna, A. Yuen, S. Kook, R. Taylor, G. Yeoh, P. Medwell, and Q. Chan. A review of hydrogen direct injection for internal combustion engines: Towards carbon-free combustion. *Applied Sciences*, 2019.

[111] A. Yousefi, H. Guo, and M. Birouk. Effect of diesel injection timing on the combustion of natural gas/diesel dual-fuel engine at low-high load and low-high speed conditions. *Fuel*, 235:838–846, January 2019.

[112] K. Zeng et al. Combustion characteristics of a direct-injection natural gas engine under various fuel injection timings. *Applied Thermal Engineering*, 26(8–9):806–813, June 2006.

[113] W. Zeng and M. Sjöberg. Utilizing boost and double injections for enhanced stratified-charge direct-injection spark-ignition engine operation with gasoline and e30 fuels. *International Journal of Engine Research*, 18(1–2):131–142, February 2017.

[114] B. Zhang, C. Ji, and S. Wang. Combustion analysis and emissions characteristics of a hydrogen-blended methanol engine at various spark timings. *International Journal of Hydrogen Energy*, 40(13):4707–4716, April 2015.

[115] B. Zhang, C. Ji, S. Wang, and Y. Xiao. Investigation on the cold start characteristics of a hydrogen-enriched methanol engine. *International Journal of Hydrogen Energy*, 39(26):14466–14471, September 2014.

[116] Y. Zhang, Q. Wang, R. Yang, Y. Yan, J. Fu, and Z. Liu. Numerical investigation of the effect of injection timing on the in-cylinder activity of a gasoline direct injection engine. *Advances in Mechanical Engineering*, 14(3):168781322210828, March 2022.

[117] L. Zhao, D. Wang, and W. Qi. Comparative study on air dilution and hydrogen-enriched air dilution employed in a si engine fueled with iso-butanol-gasoline. *International Journal of Hydrogen Energy*, 45(18):10895–10905, April 2020.

[118] Xudong Zhen, W. Yang, Shuaiqing Xu, and Yongsheng Zhu. Numerical analysis on knock for a high compression ratio spark-ignition methanol engine. *Fuel*, 103:892–898, 2013.

[119] J. H. Zhou, C. S. Cheung, and C. W. Leung. Combustion performance regulated and unregulated emissions of a diesel engine with hydrogen addition. *Applied Energy*, 126:1–12, August 2014.